

PRECISION TORQUE CONTROL FOR  
THREADED PART ASSEMBLY

by

BRIAN JAMES DUNNE

B.S., Worcester Polytechnic Institute  
(1982)

SUBMITTED TO THE DEPARTMENT OF  
MECHANICAL ENGINEERING  
IN PARTIAL FULFILLMENT OF  
THE REQUIREMENTS FOR THE DEGREE OF

MASTER OF SCIENCE IN MECHANICAL ENGINEERING

at the

MASSACHUSETTS INSTITUTE OF TECHNOLOGY

June 1986

© Brian James Dunne 1986

Signature redacted

Signature of author: \_\_\_\_\_

Department of Mechanical Engineering  
May 9, 1986

Signature redacted

Certified by: \_\_\_\_\_

Daniel E. Whitney  
Thesis Supervisor

Signature redacted

Accepted by: \_\_\_\_\_

Ain A. Sonin  
Chairman, Department Committee

MASSACHUSETTS INSTITUTE  
OF TECHNOLOGY

JUL 28 1986

LIBRARIES

Archives

PRECISION TORQUE CONTROL FOR  
THREADED PART ASSEMBLY

by

BRIAN JAMES DUNNE

Submitted to the Department of Mechanical Engineering  
on May 9, 1986 in partial fulfillment of the  
of the requirements for the Degree of Master of Science in  
Mechanical Engineering

ABSTRACT

The assembly of precision threaded parts in an automated assembly cell environment was examined. This task requires the application of torque to the parts at a precise level without overshoot. Piecewise linear and non-linear dynamic models for threaded part mating were developed based upon experimental data. A torque control method using DC motor current feedback was implemented. Process and controller models were combined to describe the closed loop dynamics. It was found that the process dynamics were not negligible. Experimental and simulated results using the non-linear model showed good agreement. The linear model was found to be of use to predict the transient dynamics of the system and was used to develop generalized controller design guidelines. The control method was found to be acceptable but had limitations due to friction in the motor. It also had degraded performance due to the low gain of the DC tachometer used to provide the required damping. An optical encoder-based tachometer was implemented to provide a velocity feedback device with a larger gain, and was shown to improve performance. Adding feedback from a mechanical torque sensor was investigated theoretically as a means of improving the control method by reducing the torque losses between the process and the device used to sense the actual torque being applied to the process.

Thesis Supervisor: Dr. Daniel E. Whitney  
Section Chief  
Charles Stark Draper Laboratory, Inc.  
Cambridge, MA

Title: Lecturer in Mechanical Engineering

## ACKNOWLEDGEMENTS

I thank Draper Laboratory for funding this research, and my education at M.I.T.; Vern Assarian for making my fellowship possible; and all the other members of Dept. 30 who assisted me in my efforts, particularly Ben Fudge for his guidance in fine measurements.

I thank Jon Rourke, the assembly cell task leader, who provided invaluable assistance in making this research topic possible; Don Seltzer, who performed the circuit designs; Tom Stepien and Alex Edsall, who provided software guidance; Ray Roderick, who provided much needed assistance with hardware; and to all the other members of Dept. 45Z who I learned and benefited from.

Special thanks go to Karen Sullivan for her painstaking efforts in typing this document; and to Joanne Crane for her support with getting it into its final form and printed.

Finally, I thank my advisor, Dr. Daniel E. Whitney, for his guidance and his patience throughout the course of this research; and for the base of learning that he has brought to the field of automation.

I hereby assign my copyright of this thesis to The Charles Stark Draper Laboratory, Inc., Cambridge, Massachusetts.

Signature redacted

  
Brian J. Dunne

Permission is hereby granted by The Charles Stark Draper Laboratory, Inc. to the Massachusetts Institute of Technology to reproduce and to distribute copies of this thesis document in whole or in part.

## TABLE OF CONTENTS

|   |    |
|---|----|
| Abstract.....   | 2  |
| Acknowledgements.....                                   | 3  |
| Table of Contents.....                                  | 4  |
| List of Symbols.....                                    | 7  |
| 1. Introduction.....                                    | 9  |
| 1.1 Overview.....                                       | 9  |
| 1.2 Threaded Part Assembly.....                         | 10 |
| 1.3 Thesis objectives.....                              | 12 |
| 1.4 Precedent for Research.....                         | 13 |
| 1.5 What Follows in This Thesis.....                    | 14 |
| 2. Background .....                                     | 15 |
| 2.1 Terminology.....                                    | 15 |
| 2.2 Class of Parts to be Considered.....                | 15 |
| 2.3 Gas Bearing Wheel Assembly.....                     | 17 |
| 2.4 Manual Threaded Part Assembly.....                  | 17 |
| 2.4.1 Torquing Methods.....                             | 17 |
| 2.4.2 Torquing Tools.....                               | 19 |
| 2.5 Assembly Cell Threaded Part mating.....             | 20 |
| 2.5.1 Torque Station (TS) Configuration.....            | 21 |
| 2.5.2 Arm/RCC/Collet/Tool Configuration.....            | 21 |
| 2.6 Automated Task Definition.....                      | 22 |
| 3. Mechanics of Threaded Part Mating.....               | 26 |
| 3.1 Cross-Threading.....                                | 26 |
| 3.2 Torque vs Angle Curve.....                          | 28 |
| 3.2.1 Experimental Torque vs Angle.....                 | 30 |
| 3.2.2 Velocity and Direction Dependency.....            | 33 |
| 3.2.3 Energy Absorption.....                            | 35 |
| 3.3 Wheel Assembly Parts vs Conventional fasteners..... | 35 |
| 3.4 Part Mating Models.....                             | 36 |
| 3.4.1 Piecewise Linear Model.....                       | 38 |
| 3.4.2 Non-Linear Model.....                             | 41 |
| 3.4.3 Generalized Model.....                            | 45 |
| 3.5 Considerations for Process Control.....             | 49 |



|  |     |
|--|-----|
| 4. Methods of Threaded Part Mating Control.....            | 50  |
| 4.1 Mechanical Configuration.....                          | 50  |
| 4.1.1 Choice of Actuator/DC Motor.....                     | 50  |
| 4.1.2 Direct Drive.....                                    | 52  |
| 4.1.3 Sensing Devices.....                                 | 53  |
| 4.1.4 System Configuration.....                            | 56  |
| 4.2 Torque Control and Measurement.....                    | 56  |
| 4.2.1 DC Motor Current Feedback.....                       | 57  |
| 4.2.2 Torque Sensor Feedback.....                          | 57  |
| 4.2.3 Need for Compliance.....                             | 58  |
| 4.3 Control System Concepts.....                           | 59  |
| 4.3.1 Current Feedback Concepts.....                       | 59  |
| 4.3.2 Torque Sensor Feedback Concepts.....                 | 63  |
| <br>   |     |
| 5. DC Motor Current Feedback Torque Control.....           | 67  |
| 5.1 Existing Torque Station.....                           | 67  |
| 5.1.1 Principle and Sequence of Operation.....             | 67  |
| 5.1.2 Controller Circuit and Hardware.....                 | 68  |
| 5.1.3 Torque Station Parameters.....                       | 72  |
| 5.2 Modeling/Analysis.....                                 | 72  |
| 5.2.1 Performance/Calibration Model.....                   | 74  |
| a) Free Running Model.....                                 | 74  |
| b) Torque Watch Windup Model.....                          | 78  |
| c) Effects of Controller Parameters.....                   | 80  |
| 5.2.2 Models for Threaded Part Mating.....                 | 81  |
| a) Piecewise Linear Model.....                             | 82  |
| b) Coulomb Friction Spring Model.....                      | 85  |
| 5.3 Simulation.....  | 87  |
| 5.3.1 Free Running Model Simulation.....                   | 88  |
| 5.3.2 Torque Watch Windup Simulation.....                  | 88  |
| 5.3.3 Piecewise Linear Part Mating Model Simulation.....   | 88  |
| 5.3.4 Coulomb Friction Spring Model Simulation.....        | 92  |
| 5.4 Experimental Results.....                              | 95  |
| 5.4.1 Steady-state speed test.....                         | 97  |
| 5.4.2 Torque Watch Stall Torque Test.....                  | 97  |
| 5.4.3 Motor Torque Test.....                               | 99  |
| 5.4.4 RCC Stiffness Test/Deflection Sensor Apparatus....   | 101 |
| 5.4.5 Threaded Part Mating Tests.....                      | 105 |
| 5.4.5 Comparison to Simulated Results.....                 | 109 |
| 5.5 Evaluation of Performance.....                         | 109 |
| 5.5.1 General Performance.....                             | 109 |
| 5.5.2 Investigation of Control Circuit Deficiency.....     | 113 |
| 5.5.3 Improved Performance.....                            | 117 |
| 5.6 Variation of Parameters/Generalized Design Issues..... | 117 |
| 5.6.1 Review of Performance Model Variations.....          | 117 |
| 5.6.2 Variations Using Piecewise Linear Model.....         | 119 |
| 5.6.3 Variation Using CFS Model.....                       | 127 |
| 5.6.4 Experimental Variation of Parameters.....            | 138 |

|  |     |
|--|-----|
| 6. Improved Current Feedback Torque Control.....                       | 142 |
| 6.1 Implementation of Encoder-Based Velocity Signal<br>Generation..... | 142 |
| 6.1.1 Method Used.....   | 143 |
| 6.1.2 Objectives for Torque Control.....                               | 144 |
| 6.1.3 Hardware Set-Up.....   | 144 |
| 6.1.4 Steady-State Speed Tests.....                                    | 146 |
| 6.1.5 Torque Watch Stall Torque Tests.....                             | 149 |
| 6.1.6 Torque Watch Windup Transients.....                              | 152 |
| 6.1.7 Use of Motor/Encoder for Threaded Part Mating.....               | 152 |
| 6.2 Alteration of Control Scheme.....                                  | 156 |
| <br>   |     |
| 7. Torque Sensor Feedback Torque Control.....                          | 159 |
| 7.1 Torque Feedback Objectives.....                                    | 159 |
| 7.2 Torque Sensor Design and Placement.....                            | 160 |
| 7.2.1 Design Principles.....   | 161 |
| 7.2.2 In-line Torque Sensor Design.....                                | 161 |
| 7.2.3 Use of the RCC as a Torque Sensor.....                           | 164 |
| 7.3 Torque Feedback Control Concepts.....                              | 164 |
| 7.3.1 Sensor Parameters.....   | 165 |
| 7.3.2 Influence of Torque Feedback on System Dynamics...               | 166 |
| 7.3.3 In-Line Torque Sensor Use.....                                   | 170 |
| 7.3.4 RCC Torque Sensor Use.....                                       | 171 |
| 7.4 Evaluation of the Torque Feedback Method.....                      | 172 |
| <br>   |     |
| 8. Conclusion and Recommendations.....                                 | 173 |
| 8.1 Threaded Part Mating Model.....                                    | 174 |
| 8.2 Current Feedback Torque Control.....                               | 175 |
| 8.3 Part Mating Controller Design Guidelines.....                      | 177 |
| 8.4 Further Recommendations.....                                       | 181 |
| <br>   |     |
| Appendix A- Hardware Models.....                                       | 182 |
| A.1 DC Permanent Magnet Motors.....                                    | 182 |
| A.1.1 Motor Construction and Operation.....                            | 182 |
| A.1.2 Model.....   | 184 |
| A.1.3 Torque Output.....   | 188 |
| A.1.4 Variations from the Ideal Model.....                             | 189 |
| A.1.5 Choice of DC PM Motor Type.....                                  | 191 |
| A.2 Power Operational Amplifiers.....                                  | 192 |
| A.3 Motor/Amp Interaction.....   | 194 |
| A.4 DC PM Tachometers.....   | 198 |
| A.5 Friction Modeling.....   | 200 |
| <br>   |     |
| Appendix B- Optical Encoder-Based Velocity Signal Generation.....      | 203 |
| B.1 Objectives.....  | 203 |
| B.2 Incremental Optical Encoders.....                                  | 204 |
| B.3 Methods of Velocity Signal Generation.....                         | 204 |
| B.4 Low Pass Filtering of a Pulse Train Method.....                    | 205 |
| References .....   | 210 |

## LIST OF SYMBOLS

### Acronyms

|      |                          |
|------|--------------------------|
| ARCT | Arm/RCC/Collet/Tool      |
| CFS  | Coulomb Friction Spring  |
| M/E  | Motor/Encoder            |
| M/T  | Motor/Tachometer         |
| RCC  | Remote Center Compliance |
| TS   | Torque Station           |

### Variables

|            |   |                           |
|------------|---|---------------------------|
| $B_m$      | Motor viscous damping                       | [in-oz-sec]               |
| $B_{mf}$   | Motor/TS viscous damping                    | [in-oz-sec]               |
| $C_{tv}$   | Torque to voltage conversion                | [v/in-oz]                 |
| $C_{vt}$   | Voltage to torque conversion                | [in-oz/v]                 |
| $G_a$      | Current gain of amplifier                   | [amps/amp]                |
| $G_c$      | Gain of command voltage(1/Rc)               | [amps/volt]               |
| $G_e$      | Gain of encoder-based tach                  | [amps/volt]               |
| $G_t$      | Gain of feedback voltage(1/Rt)              | [amps/volt]               |
| $i_c$      | Command signal current                      | [amps]                    |
| $i_m$      | Motor armature current                      | [amps]                    |
| $i_t$      | Feedback current(tach)                      | [amps]                    |
| $J_m$      | Motor inertia                               | [in-oz-sec <sup>2</sup> ] |
| $J_{mf}$   | Motor/TS inertia                            | [in-oz-sec <sup>2</sup> ] |
| $J_{tc}$   | Tool/collet inertia                         | [in-oz-sec <sup>2</sup> ] |
| $J_{tot}$  | Total inertia( $J_{mf}+J_{tc}$ )            | in-oz-sec <sup>2</sup>    |
| $K_c$      | Torsional stiffness of RCC                  | [in-oz/rad]               |
| $K_{eq}$   | Equivalent series spring constant           | [in-oz/rad]               |
| $K_p$      | Instantaneous stiffness of threaded parts.. | [in-oz/rad]               |
| $K_s$      | Torque Sensor stiffness                     |                           |
| $K_t$      | Motor torque constant                       | [in-oz/amp]               |
| $K_{tach}$ | DC Tachometer constant                      | [v-sec/rad]               |
| $K_{tot}$  | Total parallel spring constant              | [in-oz/rad]               |
| $R_1$      | Current feedback resistance                 | [Ohms]                    |
| $R_2$      | Current ground resistance                   | [Ohms]                    |
| $R_c$      | Command input resistance                    | [Ohms]                    |
| $R_t$      | Tachometer feedback resistance              | [Ohms]                    |

|                |   |               |
|----------------|---|---------------|
| $T_c$          | Torque command                              | [in-oz]       |
| $T_f$          | Friction torque                             | [in-oz]       |
| $T_m$          | Motor torque                                | [in-oz]       |
| $T_{rcc}$      | Torque due to RCC windup                    | [in-oz]       |
| $T_n$          | Net output torque of motor                  | [in-oz]       |
| $V_c$          | Voltage input command                       | [volts]       |
| $V_n$          | Electrical Noise voltage                    | [volts]       |
| $V_t$          | Velocity Feedback voltage( $V_{tach}+V_n$ ) | [volts]       |
| $V_{tach}$     | Nominal Tachometer output voltage           | [volts]       |
| $\theta_m$     | Angular position of motor/TS                | [rad;deg]     |
| $\theta_t$     | Angular position of tool/collet             | [rad;deg]     |
| $\Delta\theta$ | $\theta_m - \theta_t$                       | [rad;deg]     |
| $\omega_m$     | Angular velocity of motor/TS                | [rad/sec;rpm] |
| $\omega_{ss}$  | Steady state angular velocity               | [rad/sec;rpm] |
| $\omega_t$     | Angular velocity of tool/collet             | [rad/sec;rpm] |
| $\Delta\omega$ | $\omega_m - \omega_t$                       | [rad/sec;rpm] |

## CHAPTER 1

### INTRODUCTION

#### 1.1 Overview

Automation has become a necessary ingredient of present-day manufacturing. Past breakthroughs in manufacturing research have resulted in the application of automation to tasks of ever-increasing precision and complexity. Systems are being developed not only for mass production processes, but also for applications that require accuracy, repeatability, and environmental conditions that humans cannot always provide. Precision assembly is one of these applications. As real systems are being developed, it is becoming evident that efforts must be made to extend the capabilities of automation to the more stringent requirements of low production/high quality precision assembly.

The requirements of precision assembly are centered around size, cleanliness, and exacting specifications. Assemblies involved normally include small parts that have tight tolerances. The parts are often fragile. Forces and torques required for assembly are much smaller than those encountered in many automated processes, and must be closely monitored. The assemblies must also be protected from contaminants encountered in normal working environments. Examples of precision assemblies include fine measuring devices with instrument-grade parts.

These requirements do not allow "standard" automation systems to be used, even if such systems exist. The tools used to perform precision assembly are often highly specialized. The measurement of small assembly forces and torques requires sensors with fine resolution that can be used in an automated system. Scaling down previously developed hardware is not always possible. Encompassing all of the requirements is the need for a clean environment. This must be considered in the design of all hardware and the implementation of all assembly sequences.

An effort is presently underway at The Charles Stark Draper Laboratory to address the issues of automated precision part assembly. The assembly of small instrument-grade devices in a clean room environment is being performed by a cartesian robot in a self-contained assembly cell<sup>[15]</sup>.

The prototype cell is shown in Figure 1.1. It contains an assembly base capable of X and Y axis motion, and an arm/tool holder capable of Z axis motion. A fourth degree of freedom -- rotation about the Z axis -- is provided by a subassembly known as the torque station (TS). It is located on the assembly base. A Remote Center Compliance (RCC) device is located at the end of the arm. It provides additional limited degrees of freedom in the form of engineered compliance to make precision assembly possible. Four tools are employed as end effectors for the various assembly tasks. Each of these tools has compliance along the Z axis so that interaction forces along this axis can be passively controlled. The housing of the cell acts as a barrier to contamination. A blower recirculates the air in the cell through a High Efficiency Particulate Air (HEPA) filter to remove contamination. Development and testing of this cell has included the work of this thesis. Detailed descriptions of the parts of the cell critical to this research will be described in later sections.

## 1.2 Threaded Part Assembly

Two major tasks accomplished by the robot are peg-in-hole insertions and threaded part assembly. This thesis addresses issues pertaining to the latter. Nevins and Whitney have reported that the task of inserting screws is the second most common assembly task<sup>[12]</sup>. It is often the final task in an assembly after a series of peg-in-hole tasks.

In the automated assembly cell utilized for this work, the torque station has the responsibility for threaded part assembly. It provides the torque necessary to properly mate the threaded parts. The existing design of the torque station followed from that of assembly cells built in the past for other tasks. These cells did not perform instrument-grade assemblies. Higher torque levels and looser tolerances were present. The

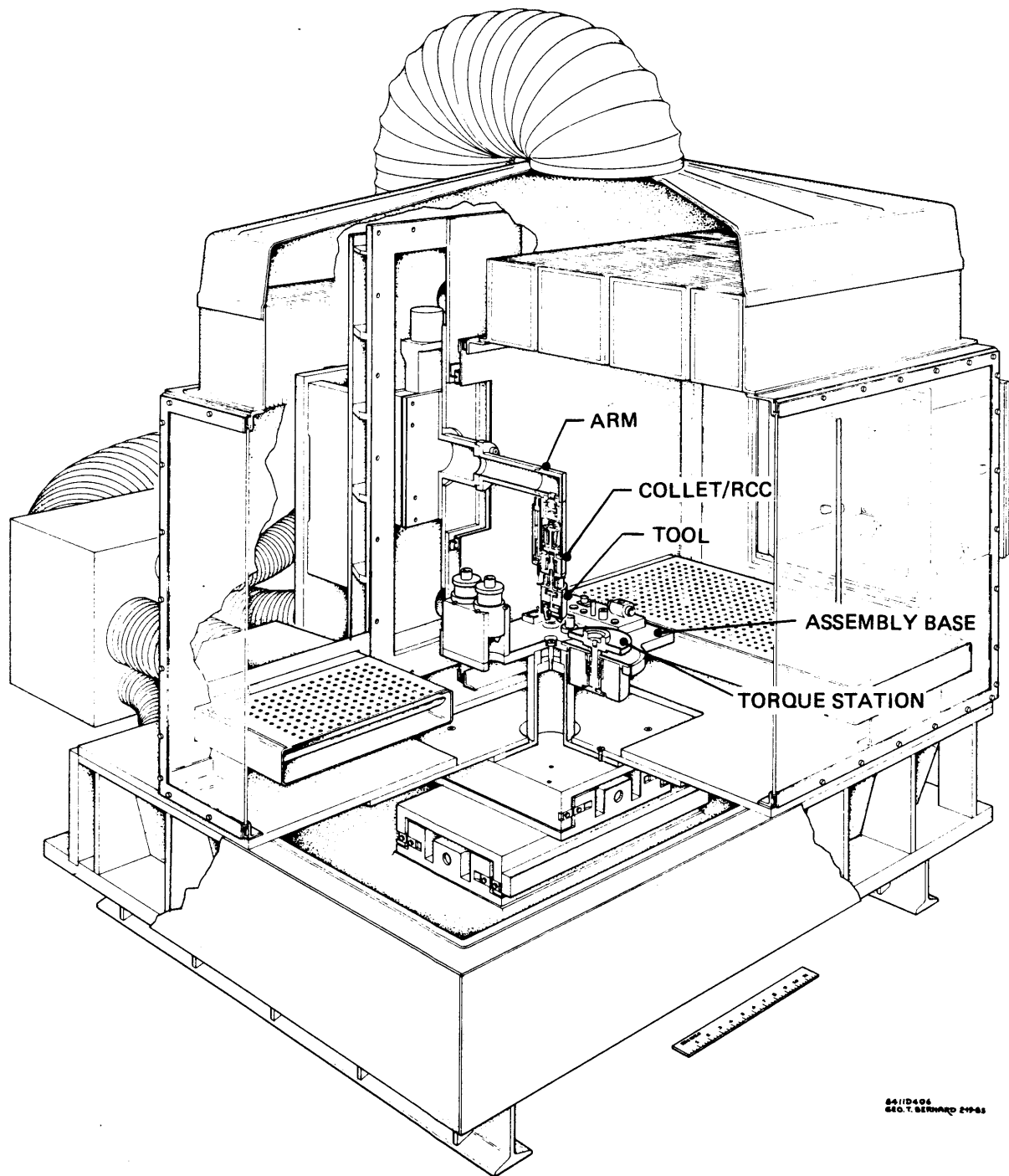


Figure 1.1 Automated Assembly Cell

operation of the torque station depends on its mechanical configuration, its controller, the arm/tool holder/RCC assembly that it acts in conjunction with, and the parts that it assembles. It is the author's opinion that examination of all of these must be made to evaluate the torque station performance.

### 1.3 Thesis Objectives

This thesis attempts to further understand threaded part mating and its control in an automated assembly system for instrument-grade assemblies. Application of torque to the parts is the action necessary to satisfy the assembly specification. This is a relatively straightforward task for a human operator skilled in instrument assembly. This is not the case for a basic robotic control system. This is especially true for the size of parts and specifications common in precision assembly.

Simons and Van Brussel distinguish between force/ torque control tasks of two types<sup>[16]</sup>. One type includes applications where the contact forces are used as a source of information to aid control of the process. Passive peg-in-hole insertions are an example. The second type includes those processes where the magnitude of the applied force/ torque is an essential part of the process specification. This type includes grinding, polishing, deburring, threaded part mating, and others. Critical to success in this type is some understanding of the process. A model that represents the process is necessary. Representing the process as a rigid entity without its own dynamics may cause undesired results.

Although hardware already exists, it is first necessary to take a step back and examine the threading process itself. A model of the process can then be formulated and combined with a model of the torque station and its controller. The process model can also be used for any other control scheme that is proposed. With this analytical understanding, experimentation and evaluation can yield more meaningful results. Extension of the results to new designs can then be made.



#### 1.4 Precedent for Research

The assembly of threaded parts is a common task and is one that has been successfully implemented in automated manufacturing. So, why study it? The answer is that it has been taken for granted in many cases and is not fully understood. The small size, fragility of parts, and more stringent specifications common to instrument-grade assembly preclude the use of readily available devices.

Examination of prior work in the field of automation reveals that a detailed analysis of threaded part mating dynamics and a torque station controller design methodology has not been presented. Although static models for threaded joints do exist, an extension of the results to the dynamics of an automated assembly system is lacking. Dean<sup>[3]</sup> examined an automated bolting but concentrated on end effector design. Precise torque control was not addressed. He also worked with much larger parts.

Much has been published in the area of force/torque control, but the author is aware of none that utilizes precision threaded part mating as an application. Mason<sup>[11]</sup> mentions that certain constraints must be imposed on the parts to perform the task, but does not provide the detail. Motor current control is recommended for screwing/threading operations by Koren<sup>[9]</sup>. However, the process is not modelled, and the controller design not discussed. Hartley<sup>[6]</sup> describes the control of fastener tightening as a two-stage process. He describes a combination of velocity and torque control to accomplish the task. However, the sensors and actuators used to do this are not mentioned. The torque levels involved are quite large and the method seems to depend on this fact.

Products described as nut runners and automatic screwdrivers are available from vendors in the automation products industry. Often, though, these are geared for mass production assembly lines. Once again, torque levels and precision are larger than the levels mandated by precision assembly. Cleanliness is a major problem since pneumatic actuators are usually employed.

## 1.5 What Follows in This Thesis

Presented in this document is a description of the issues addressed in the course of conducting research into the area of precision torque control for threaded part mating. Chapter 2 contains background information. Terminology is presented. Manual assembly techniques are discussed. The parts used in this thesis are described. Chapter 3 presents the mechanics of threaded part mating. Experimental data from actual parts is used to define a model to be used for the threading process. Chapter 4 introduces the methods of controlling threaded part mating. DC motor current feedback and torque sensor feedback are identified. Hardware implementation is discussed. Chapter 5 discusses modeling and experimentation utilizing the existing torque station of the automated assembly cell. The DC motor current feedback method of torque control is utilized. Its performance and limitations are discussed as well as the validity of the model developed in Chapter 3. Proposed and implemented improvements to the torque station are discussed in Chapter 6. New actuator and feedback hardware for the control scheme is introduced as an alternative to that of the existing configuration. Chapter 7 discusses the torque sensor feedback method of torque control and its implementation for the application of threaded part mating. A summary of ideas is presented in Chapter 8 with recommendations for further research. Included in the two appendices is a discussion of specific hardware modeling issues.

## CHAPTER 2

### BACKGROUND

#### 2.1 Terminology

The terms used in the following discussions are now defined. A generic pair of threaded parts is shown in Figure 2.1. Screwing parts together consists of several phases. First, initial placement and part mating must occur. This requires that the thread axes of the two parts be aligned so that cross-threading will not occur when the parts are screwed together. Some axial force is required to keep the parts in contact. Rundown occurs when the parts are rotated in opposite directions about the thread axis. Normally one part remains stationary while the other is rotated with respect to it. Sufficient torque is required to overcome the friction of the contacting threads. This will be referred to as the rundown torque ( $T_r$ ). Bottoming is the point where non-threaded surfaces of the parts first come into contact. Tightening is the phase of threading after bottoming occurs. The torque required increases as this phase progresses. The final torque to be delivered is obtained from the assembly specifications of the parts involved.

By convention, the threading axis will be considered the Z axis. Thus, tightening the parts implies torque about this axis.

#### 2.2 Class of Parts to be Considered

It was stated above that an objective of this research is to extend the results to assembly cells and parts other than those available and under present consideration. To qualify this, it is stated that instrument-grade parts will be emphasized. This is the type of parts assembled by the automated assembly cell. Properties of this class of parts tend to include: 1) relatively fine threads; 2) a high degree of cleanliness; 3) 100 per cent dimensional inspection; 4) no burrs; and

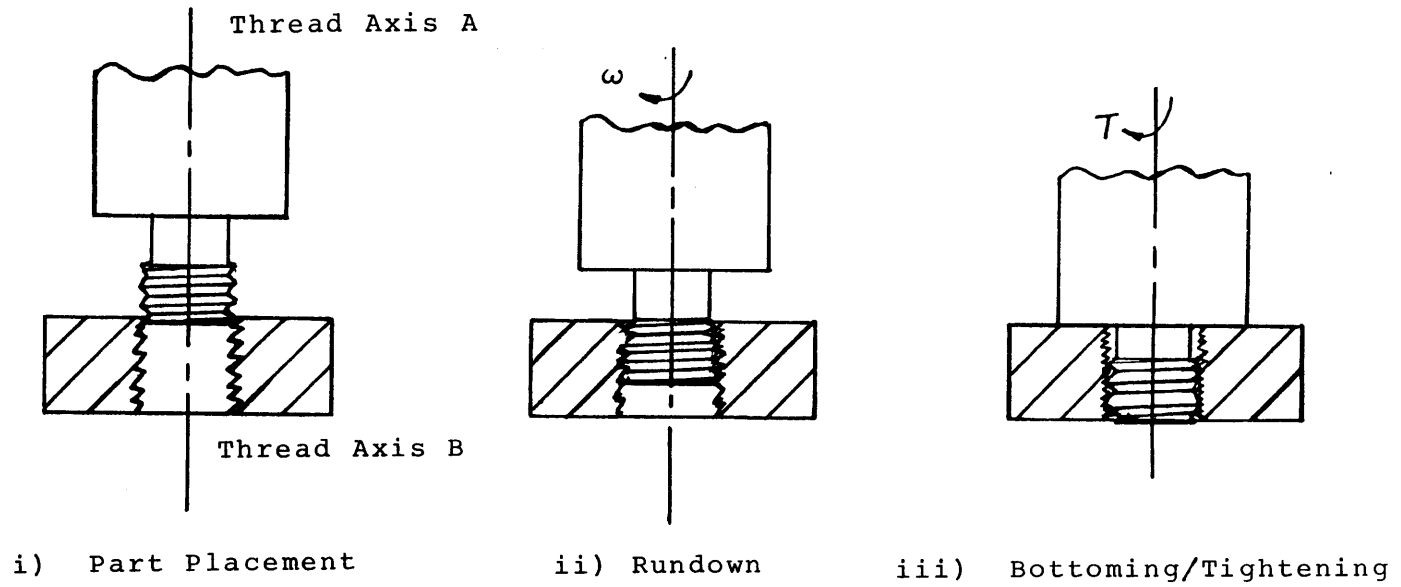


Figure 2.1 Phases of Threaded Part Mating

5) pre-assembly by hand. The threads are normally single lead. Tight fit is not necessarily the case. The threaded joint formed by the assembled parts is not normally used for structural or high load bearing service.

### 2.3 Gas Bearing Wheel Assembly

The parts used for modeling and experimentation in this thesis are the threaded components of a gas bearing wheel assembly. These parts are representative of those to be assembled by the torque station of the automated assembly cell. The components and assembly are shown in Figure 2.2. The threaded parts are the shaft and two thrust plates. The parts are made of anodized beryllium. The threads are no. 7-72-UNS (0.151 in. major diameter). Note that this is a very fine thread. The class of threads is 2A (shaft) and 2B (thrust plates). Note that these are class 2 threads, and not class 3, which calls for tighter tolerances and fit. Bottoming occurs in these parts after approximately five and one-half turns.

The manual assembly specification calls for the parts to be torqued to a preliminary value of 2 in.-oz and a final value of  $10 \pm 1$  in.-oz. No specification is put on axial or radial load, or allowable torque about the x and y axes during rundown. Although not yet finalized, the automated assembly sequence calls for continuous torquing to the final value.

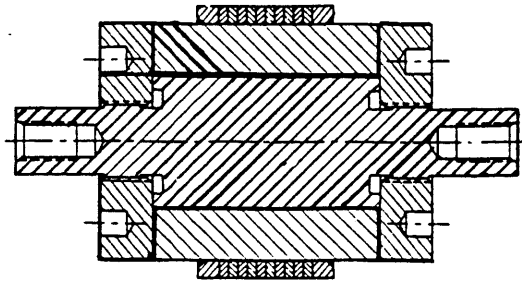
### 2.4 Manual Threaded Part Assembly

In order to achieve an understanding of automated assembly of threaded parts, it is useful to examine manual assembly. Both the methods and tools used are now examined.

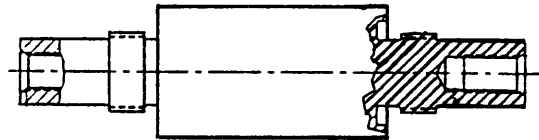
#### 2.4.1 Torquing Methods

Various schemes used to meet assembly torque specifications are employed in industry<sup>[18]</sup>. They include:

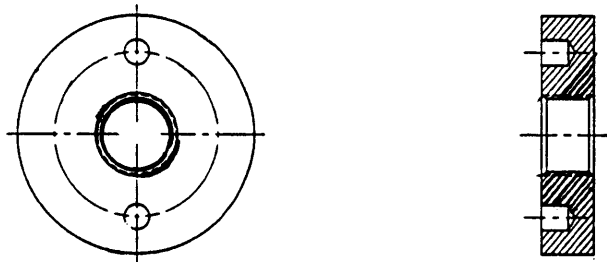
1. Direct torquing
2. Snug and turn-of-nut
3. Impact and stall methods
4. Tension monitoring



a) Assembly- Shaft, Thrust Plates(2), Rotor



b) Shaft



c) Thrust Plate

Figure 2.2 Gas Bearing Wheel Assembly

The first method, direct torquing, is the most common method used for precision assemblies. The parts are usually run down and bottomed by hand or other means. Then a torque measuring device is used to perform tightening until the desired torque level is reached. The human operator provides the power necessary to do this. The speed at which torque is applied depends on the operator. Skilled operators maintain that smooth turning at a low speed should be used. This method is used in manual gas bearing wheel assembly.

The snug and turn-of-nut approach consists of running the parts down, bottoming, and achieving a "snug tight" condition. This is normally hand tight. One of the parts (usually a nut) is then turned relative to the other by a prescribed angle. This angle is usually determined experimentally and relates to some torque level. This method is common in high quantity/low accuracy assembly. The snug tight condition is an operator-dependent source of error. The method is not desirable if the amount of turn for necessary tightening is small.

Impact and stall methods are also common in high quantity and repetitious assembly. A powered device such as an impact wrench is used. Normally rundown is performed at a high angular velocity. The torquing device is designed to stall when a desired torque level is reached. Often this is done with some form of mechanical slip clutch. A common problem with this method is overtightening.

A method seeing increased use is tension monitoring. The reason for torque specification in most structural or load bearing fastener joints is to achieve a certain preload, or tension, in the fastener. Since this is the quantity desired to be controlled rather than torque, methods are used to measure it during assembly. Although high accuracy and precision can be achieved with this method, the size and torque levels involved make it difficult for application to instrument-grade assembly.

#### 2.4.2 Torquing Tools

All sorts of devices to measure torque while applying it to parts have been marketed. Most have some form of indicator that shows the elastic deflection of a linear spring under load. Common to all precision devices is a small range. Measurement traversing only one order of magnitude is normally a maximum.

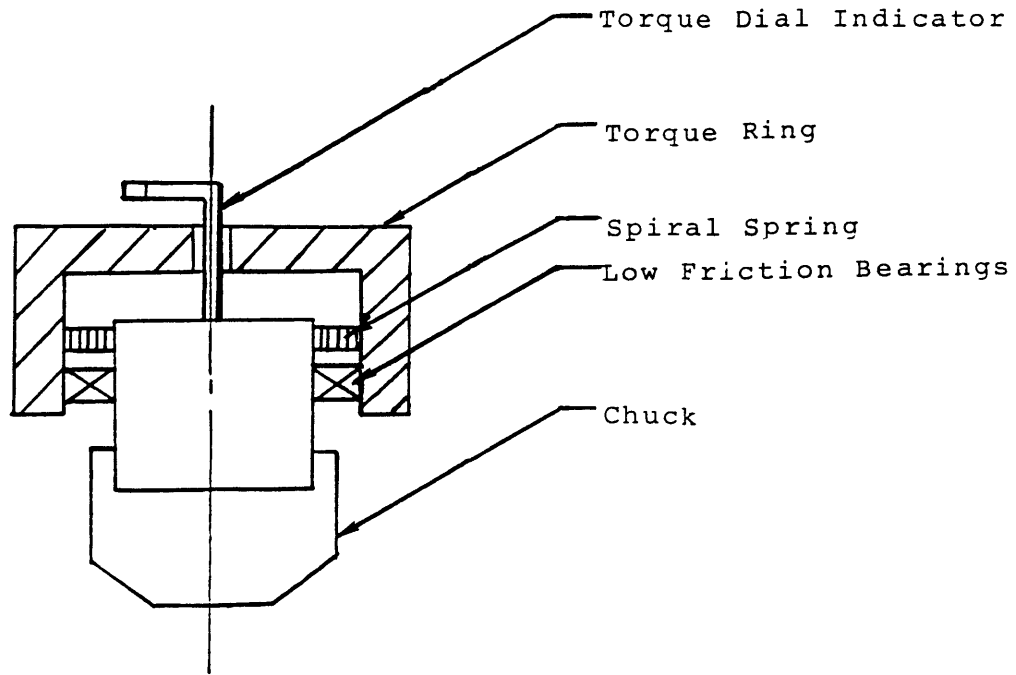


Figure 2.3. Torque watch schematic.

Torque watches are commonly used for low level torque applications. This is the device used for manual assembly of the gas bearing wheel assembly. A schematic of this device is shown in Figure 2.3. The strain element is a spiral torsion spring specially designed to exhibit linearity in the torque range of interest. Midrange deflection is normally about 180°. This is quite large compared to force/torque sensors described in the robotic force/torque control literature. Friction in the bearings is kept to a small fraction of the desired torque measurement.

## 2.5 Assembly Cell Threaded Part Mating

This subsection provides more detail about the hardware in the assembly cell used for automated threaded part mating. To perform the task, all four degrees of freedom of the cell are used. The gripper in the tool holds one part which we call the stationary part, and the torque station holds the other which we call the rotating part.



Initial part placement is accomplished by placing the parts in the torque station and tool, and manipulating the X-Y-Z degrees of freedom. The accuracy required for this task is inherent to the design of the robot and is not of concern to this thesis. This includes alignment of the threading axis of one part with respect to that of the other.

Threading operations are performed by turning the rotating part with respect to the stationary part using the torque station. This configuration was chosen for reasons of contamination control and hardware complexity. Electric power does not have to be transmitted through the interface to the tool. All rotating members which can generate particulate contamination are kept below the assembly base.

The two critical assemblies of the assembly cell for threading operations are the torque station and arm/RCC/collet/tool.

#### 2.5.1 Torque Station (TS) Configuration

The mechanical configuration of the torque station is shown in Figure 2.4. The major components are:

1. DC Motor/Tachometer (M/T)
2. Drive shaft housed in duplex bearings
3. Torque adapter
4. Pair of solenoid-actuated air cylinder pistons

The torque adapter accepts the fixtures that hold the parts for assembly. The air cylinders are used to provide mechanical stops for holding the torque adapter in a "home" position. The motor is the source of torque and rotation. It is connected directly to the drive shaft. Gearing is not employed. The M/T, drive shaft, and torque adapter are capable of continuous rotation. The merits of this configuration will be discussed in Chapter 4.

#### 2.5.2 Arm/RCC/Collet/Tool (ARCT) Configuration

The tool used to hold the stationary part during threading is held in a collet which is housed in the base of the RCC. The RCC is connected to the robot arm. The assembly is shown in Figure 2.5.

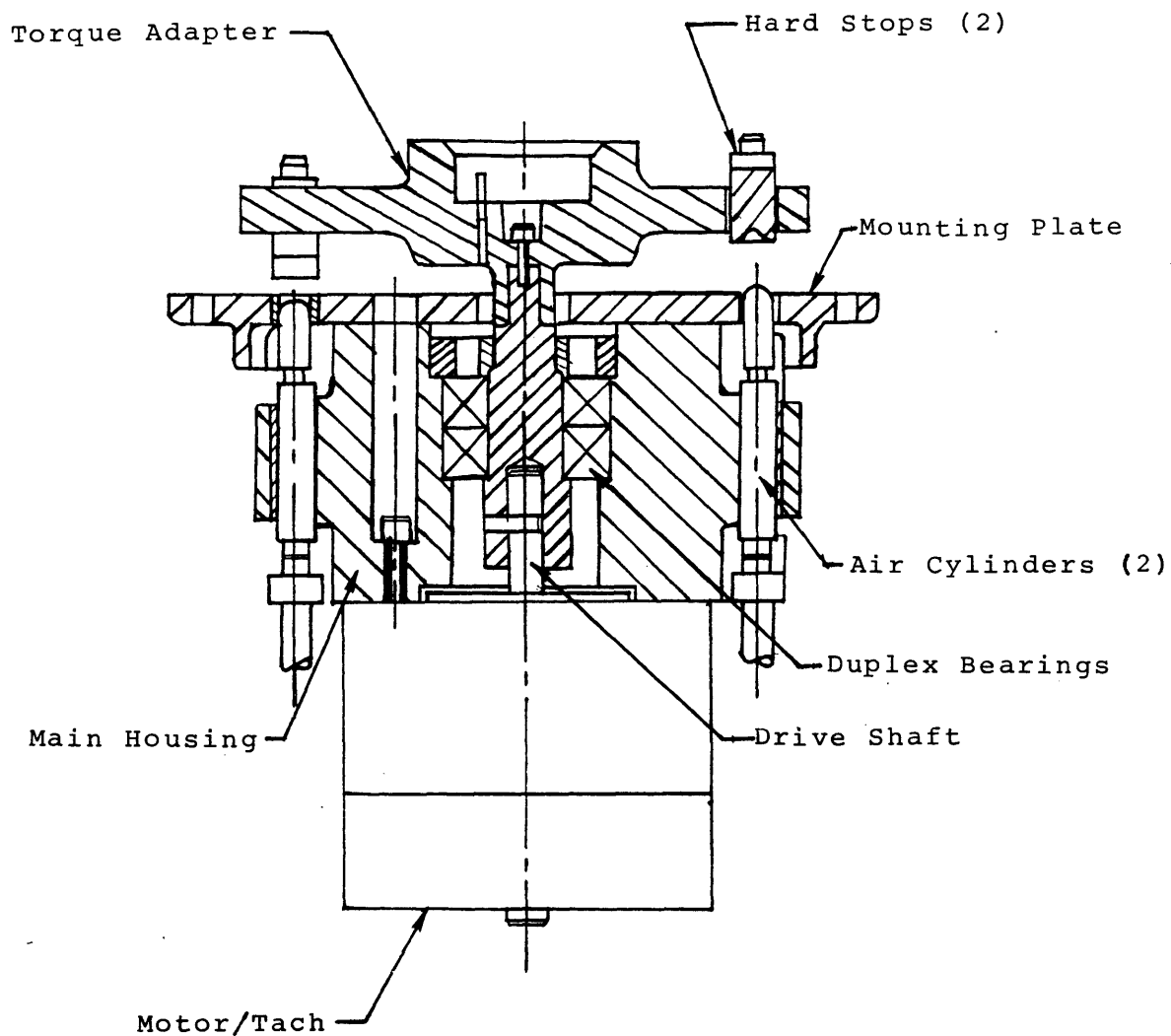


Figure 2.4 Torque Station Assembly

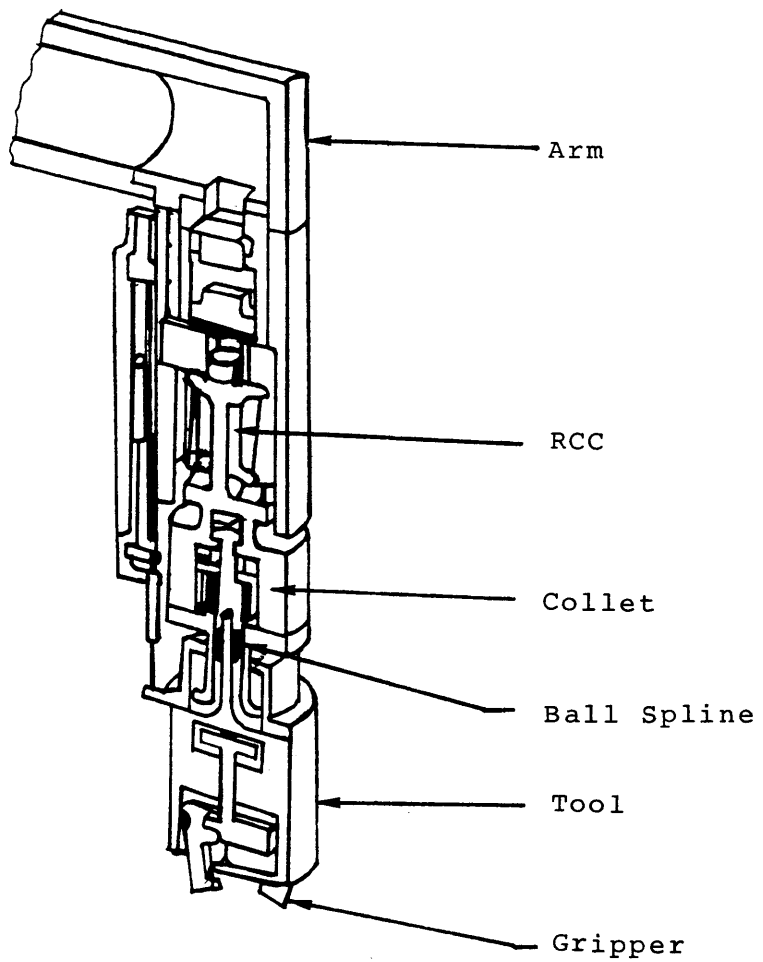


Figure 2.5 Arm/Tool/Collet/Tool Assembly

The assembly cell RCC has a wire construction. It is compliant for all degrees of freedom except for Z-axis translation. This degree of freedom is added by the tool described below. An optical sensor is employed in the RCC but only measures X and Y translation. The RCC was designed so that the low diametral clearance peg-in-hole assembly required for instrument assemblies can be performed. It also aids in fixture placement and tool changing. Readers not familiar with RCC operation are referred to references<sup>[5,20]</sup>.

The tool used for threading consists of a pneumatic gripper attached to a Z-axis ball spline. The weight of the tool is counterbalanced with a compression spring attached to the spline. This allows contact forces during assembly operations to be passively controlled. For threading, this is important during initial part mating and alignment. When the parts are initially put into contact by Z-axis motion of the arm, enough travel in the ball spline is taken up to allow rundown and tightening to occur. This frees the robot from having to coordinate Z-axis feed with Z-axis rotation.

An LVDT is attached to the tool to monitor the tool travel along the spline. The resolution of this device is 0.001 in. The discussion in Chapter 4 will show that this resolution is of only minimal use for threaded part mating control. Its primary purpose is for protection of the robot and parts from solid collisions.

## 2.6 Automated Task Definition

Now that the capabilities of the assembly cell utilized for this work have been described, the specific tasks necessary for automation of the threading operations can be listed. Since the assembly cell has the capability to properly place the parts to begin part mating, the task begins at the rundown phase.

The goal of the automated assembly sequence is to achieve controlled speed rundown and controlled torque tightening. It is desired to do this with a smooth transition between control phases. Torque must be applied without overshoot. The final torque in the parts may be higher than the steady-state applied torque if overshoot occurs.

During the rundown phase, the primary variable to be controlled is rundown velocity,  $\omega_r$ . The kinetic energy during rundown and at the point of bottoming is

$$KE_r = 1/2 J\omega_r^2 \quad (2-1)$$

In this formula, J represents the total inertia of the rotating parts of the torque station. The torque station controller must dissipate this energy and stop rotation at the proper torque level. Note that applying torque without speed control during the rundown phase would result in continued acceleration of the inertia and thus a very large angular velocity.

The most important phases to be controlled are the bottoming and tightening phases. This is where the torque specification of the parts must be met. The torque delivered by the torque station in this phase must result in the proper final torque delivered to the parts themselves. Since the RCC is only instrumented for X-Y motion, the ARCT assembly cannot provide torque information in its present form. The TS assembly must gather this information in one form or another. Chapter 3 shows that dynamics associated with the mating parts and ARCT assembly make this task more complicated than delivering a static torque.

## CHAPTER 3

### MECHANICS OF THREADED PART MATING

This chapter examines the issues related to the process of threaded part mating. It is necessary to characterize the process so that it can be modelled. This model is used to represent the process in the design of a torque station controller.

#### 3.1 Cross-Threading

Although this work concentrates on torque control of threaded part mating, it is useful to consider the aspects of cross-threading. This is an undesirable condition and results in failure of part mating. Cross-threading includes an angular form and a parallel form.

The usual form encountered is angular cross-threading. This results from angular misalignment of the thread axes of the two parts to be assembled. Figure 3.1a shows proper alignment and part mating<sup>[8]</sup>. If the two parts are misaligned such that point A is rotated to point A', cross-threading will occur. This is shown in Figure 3.1b. A cross-threading angle,  $\theta_{ct}$ , can be defined as

$$\theta_{ct} = \tan^{-1} (p/d) \quad (3-1)$$

where  $p$  is the pitch and  $d$  is the major diameter of the threads. For the shaft and thrust plate of the wheel assembly,  $\theta_{ct} = 5.3^\circ$ . Note that for a given thread diameter, decreasing the pitch decreases the cross-threading angle. The calibration of the assembly cell assures that  $\theta_{ct}$  is not exceeded for the wheel assembly.

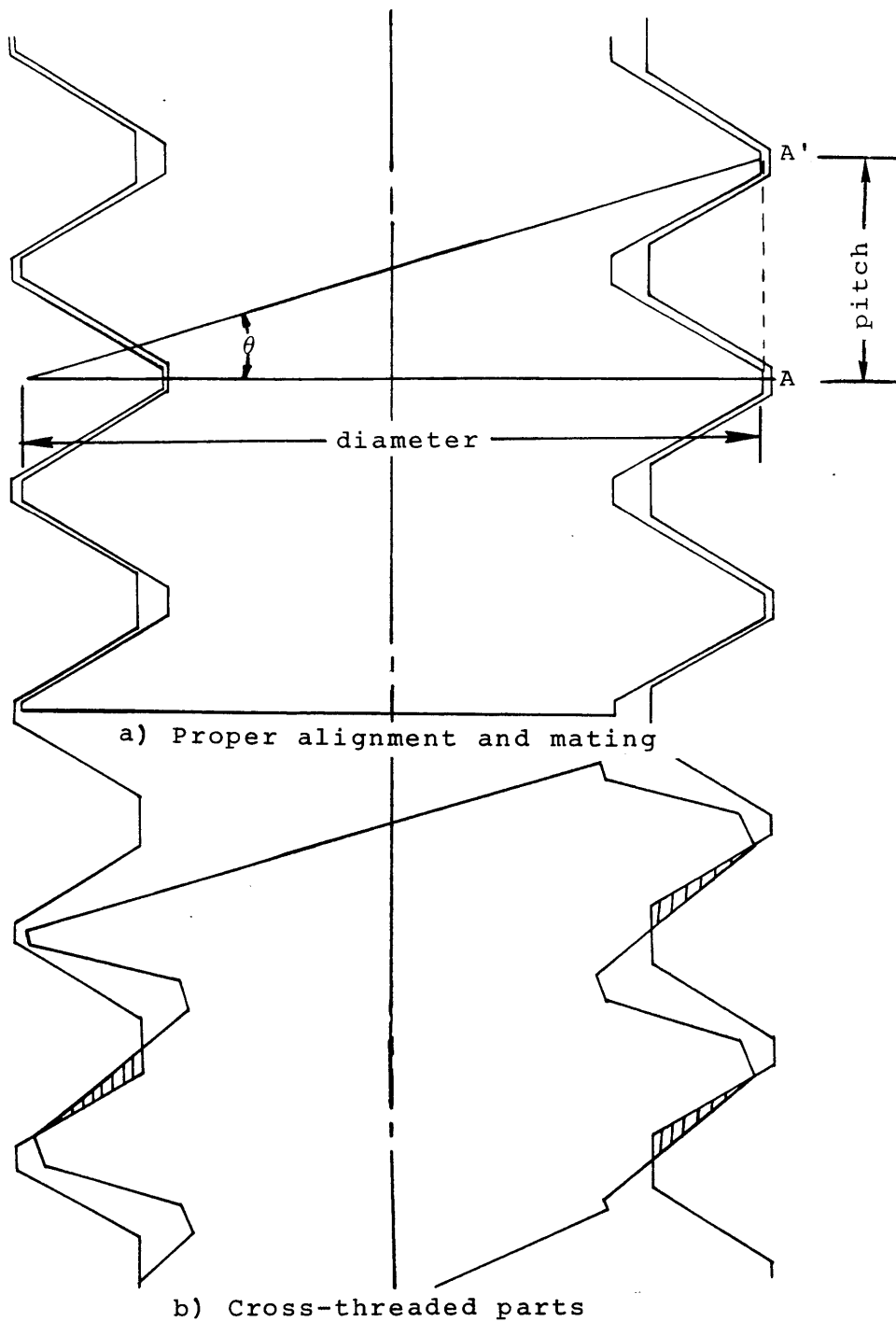


Figure 3.1 Angular Cross-Threading

Parallel cross-threading is a more subtle form. It is mentioned by Blaer<sup>[1]</sup> and was a concern in the research of Dean<sup>[3]</sup>. It occurs when the beginning threads of the two parts overlap when initial part mating occurs. The first threads are tapered and not fully developed. Their weaker sections are twisted together when rotation to initiate threading occurs. This problem can happen even if the parts are perfectly aligned. Mentioned of parallel cross-threading by Blaer was for experiences with coarse threads. Dean did not observe the problem.

Cross-threading has not been a problem with the automated assembly cell. The threading operation has been successfully performed several hundred times on several sets of parts with no observation of the problem. The ability to teach the robot to position the parts repeatably to 0.001 inch in X and Y, maintain proper angular alignment, and palletize the parts correctly prevents the occurrence of angular cross-threading. Also, the RCC plays a role in correcting lateral and angular misalignments, and the ball spline allows motion along the Z axis. The latter may be beneficial to the prevention of parallel cross-threading. Initial part mating and placement is similar to the initial phase of a peg-in-hole insertion.

### 3.2 Torque vs Angle Curve

Since starting the threads properly was not a major problem, this research concentrated on characterizing the remaining phases of part mating. During the process of assembling threaded parts, the two parts involved are rotated with respect to each other about the thread axis. The amount of torque required to produce this relative rotation depends upon which phase of threading is involved. Two variables which can describe the process are the torque applied and difference in angle that results. The Torque vs Angle Curve (TVA) is defined as the representation of the threading process using these two variables. It is similar to a force versus deflection curve for a spring element. A generic torque vs angle curve is shown in Figure 3.2.



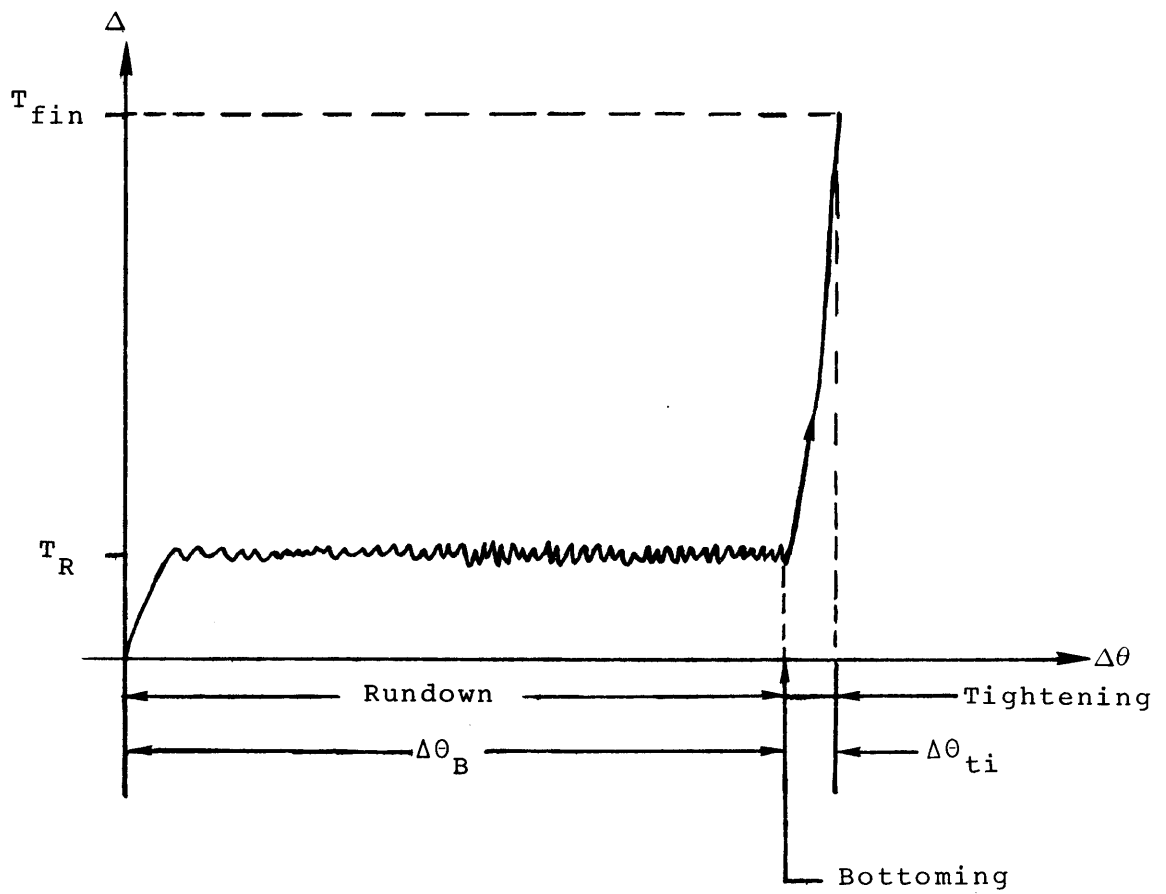


Figure 3.2. Torque vs Angle Curve

The rundown phase is characterized by a fairly constant level of torque. The average level is the rundown torque,  $T_r$ . Variations in this torque are caused by changes in friction between the two parts. This can be caused by axial or radial loads, and variations in surface finish and thread dimensions. For precision parts and assembly procedures, these variations are kept to a minimum. In the assembly cell, the axial load is minimized by the counterbalanced tool. The change in angle from the start of threading to bottoming is the bottoming angle,  $\Delta\theta_B$ . The magnitude of this angle is dependent on the initial angular position ( $\omega_z$ ) of the parts. A fraction of a turn may be required before the screwing action of the threads begins. This variation makes it difficult to predict the exact magnitude of  $\Delta\theta_B$ .

At the point of bottoming, the torque level increases and the curve develops a slope. The shape of the curve during the tightening phase depends upon the parts involved. The angular travel between bottoming and the final applied torque,  $T_{fin}$ , is the tightening angle,  $\Delta\theta_{ti}$ . The magnitude of this quantity is also dependent upon the parts involved.

The characteristics of the TVA curve show that the threading process is not at all linear. It cannot be described by a simple element and transfer function like a linear spring. Analytical methods can be used to predict the parameters of the curve. However, these methods depend heavily upon friction coefficients and the stiffnesses of the parts. A broad range of values can result from estimating these quantities. It was decided that finding the curve experimentally would provide more sound results.

### 3.2.1 Experimental Torque vs Angle

To determine the TVA curve of the wheel assembly, the first step was to observe the manual assembly procedure. In this procedure, one end of the shaft is held in a fixture. It becomes the stationary part. Initial part mating and rundown are performed by hand. The average bottoming angle observed was 5.5 revolutions ( $1980^\circ$ ). The value varied with the relative starting position of the parts. An attempt to measure the rundown torque was made using a torque watch and the fixture used to transmit torque to the thrust plate. The fixturing holding the shaft was held in a vise so that only the torque watch needed to be held and aligned. The value of  $T_r$

varied from 0.25 in.-oz to 1.0 in.-oz depending on the amount of axial load. An operator has difficulty controlling the exact value of this load. The average value with the weight of the torque watch, fixture, and thrust plate as the axial load was 0.75 in.-oz. Tightening of the parts from the bottoming point revealed that  $\Delta\theta_{ti}$  was very small -- not visually apparent.

An experiment was designed to measure the tightening angle. The thrust plate was fitted with a teflon ring as shown in Figure 3.3. A set screw was assembled into this ring to provide a lever arm to measure the angle as a linear deflection at a known radius. An Indiac measuring device was used to measure the deflection. Since this involved a contacting type of measurement, the torque that the stylus of the device imparted on the thrust plate had to be considered. This torque was reduced to a level that could be ignored by adjusting the force required to deflect the stylus and achieve a reading. The experimental procedure was as follows:

1. Mount the shaft and its holding fixture in a vise to prevent it from rotating.
2. Rundown the thrust plate/ring to the bottoming point.
3. Apply increasing amounts of torque to the thrust plate to tighten the joint, and measure the resulting deflection.
4. Calculate the angle travelled.

A summary of the experimental data for several runs is shown in Figure 3.4. Since the same torque levels were used for each run, some of the data points overlap. The biggest difficulty with the procedure was finding a zero point for the beginning of the tightening phase. Torque levels between 0.75 and 1.0 in.-oz show varying deflections. Data above torque levels of 1.0 in.-oz were more stable and showed a definite development of slope to the curve. It was decided to choose this point as the zero. The highest torque level applied was greater than the specified 10 in.-oz level to observe data past the final point of interest. Examination of the data reveals a nearly linear trend. The slope of the curve shows a slight increase as the torque increases.

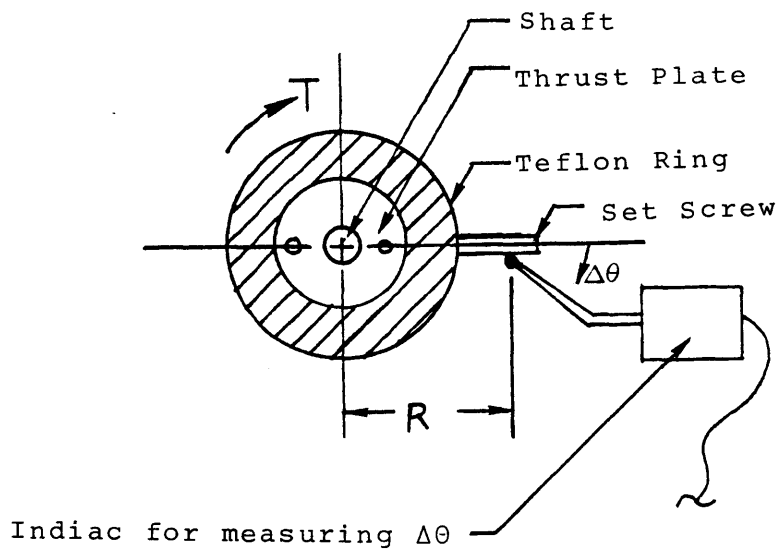


Figure 3.3 Experimental set-up.

For modeling purposes, it was decided that the slope of the TVA curve was the most important parameter. A linear fit of the data is shown by the solid line in Figure 3.4. The slope of this line is 8.04 in.-oz/deg (480 in.-oz/rad). For the models used in this thesis, this linear fit is employed. If the data points are connected with straight lines, slopes vary from 6.7 to 13.4 in.-oz/deg (382 to 764 in.-oz/rad). Of course the maximum slope is found between  $T = 10$  and 12 in.-oz.

The data indicate a tightening angle for  $T_{fin} = 10$  in.-oz of between 1.1 and 1.2 degrees. This is a rather abrupt stop and is a small portion of a revolution. Due to the difficulty in measuring this angle, some error is expected, but the results do give a good indication of the magnitude of the parameters of the TVA curve.

### 3.2.2 Velocity and Direction Dependency

To this point, discussion of the TVA curve has neglected any dependency on the relative velocity of the parts during tightening. The experimental results were from a static procedure. Whether or not the parameters of the curve change when the parts are tightened at various velocities is not known. The mating of the parts is essentially an increase in the friction torque as the joint is tightened. It is known that the friction coefficient has some dependency on velocity. Manual precision assembly with a torque watch is normally performed at a low angular velocity. Therefore, it may be beneficial to control the tightening speed with a torque station controller.

What happens when the parts are reversed or disassembled has also not been discussed. Several attempts were made to measure the torque required to disassemble the parts once tightened. A range of 9.5 to 12.5 in.-oz was found for parts that were assembled with a final torque of 10 in.-oz. This points out two factors in process modeling and control. First, the magnitude of the assembly torque cannot be exactly monitored by that of the disassembly torque of the parts. Second, a complete reversal in torque is required to decrease the relative angle between the parts  $\Delta\theta$ . The parts remain together when the torque is reduced to zero.

# Wheel Assembly Torque vs Angle

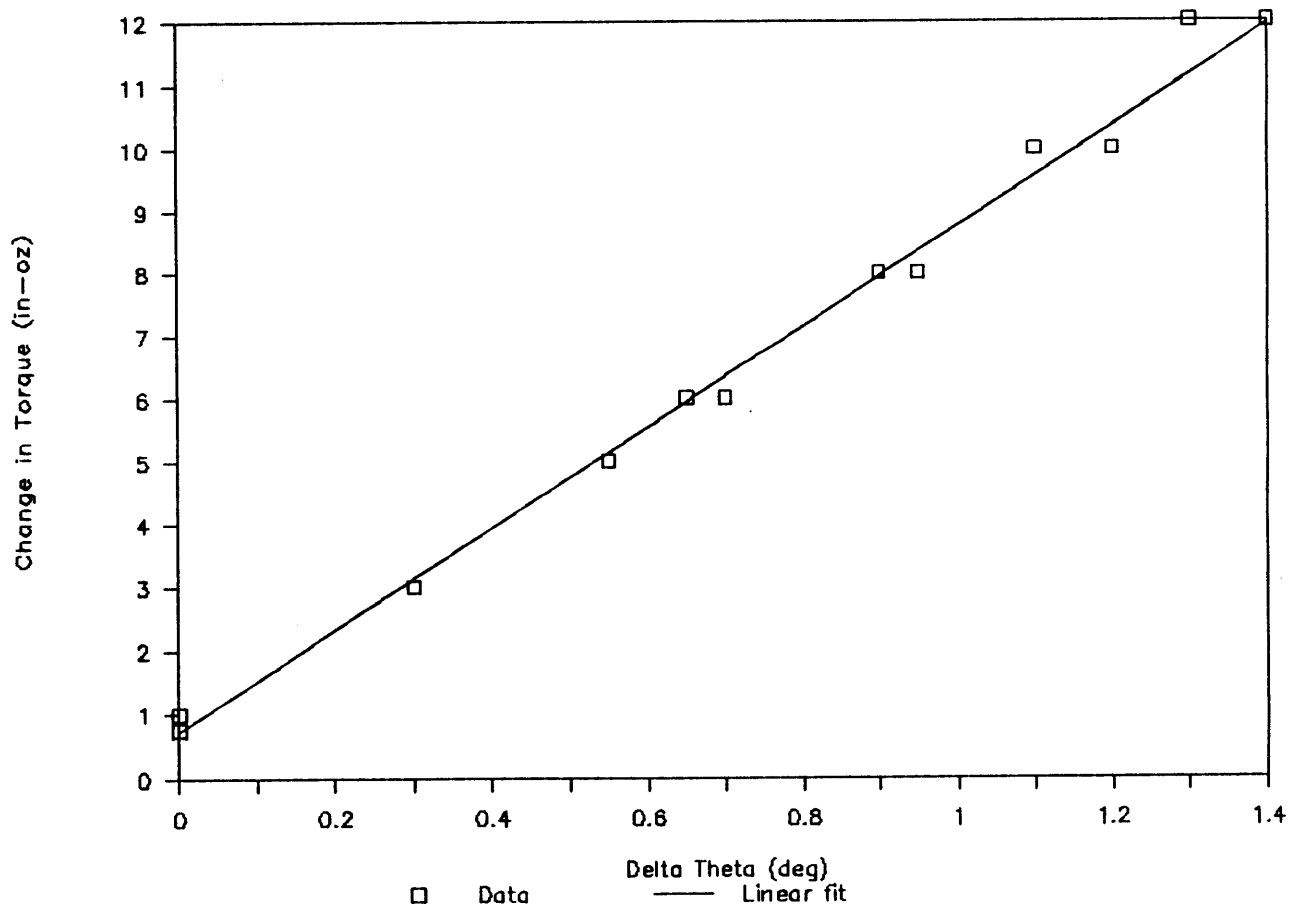


Figure 3.4 Experimental TVA Results

### 3.2.3 Energy Absorption

Another piece of information that can be obtained from the TVA curve is the energy that is dissipated in part assembly. This energy is equal to the area under the positive portion of the curve. If  $f_{ti}(\Delta\theta)$  describes the curve, then the energy is

$$E_{\text{thread}} = E_{\text{run}} + E_{\text{ti}} \quad (3-2)$$

$$E_{\text{run}} = T_R \Delta\theta_B \quad (3-3)$$

$$E_{\text{ti}} = \int_{\Delta\theta_B}^{\Delta\theta_{\text{ti}}} f_{\text{ti}}(\Delta\theta) d(\Delta\theta) + T_R[\Delta\theta_{\text{ti}}] \quad (3-4)$$

where the subscripts run and ti correspond to rundown and tightening, respectively.

From the linear fit of Figure 3.3, the values from the experimental data are

$$E_{\text{run}} = 0.015 \text{ in.-oz-rad} \quad (3-5)$$

$$E_{\text{ti}} = 0.186 \text{ in.oz-rad} \quad (3-6)$$

Note that this value can be compared to the kinetic energy of the rotating torque station shown in Equation (2-1). The torque station controller must take care of the dissipation of any energy not dissipated by the parts.

### 3.3 Wheel Assembly Parts vs Conventional Fasteners

Since the wheel assembly is only one in many that could be encountered in automated assembly, it is necessary to compare it with other threaded parts. First of all, the purpose of the torque specification and torque levels for threaded joints varies from assembly to assembly. In the case

of the shaft and thrust plate, the joint is used to position the parts very precisely with respect to each other. It is desired to keep the stresses and deflections in the parts low enough so that creep and microyield are not a problem. The torque level is very low compared with a typical fastener of comparable diameter.

Conventional fasteners are normally tightened to develop a tension in a bolt and compression in a nut. A standard rule of thumb in threaded joint design is to torque the fastener so that a tension level of 90% of the yield stress in tension is developed. For a thread diameter similar to that of the shaft and thrust plate, a torque level of about 500 in.-oz would be used. Clearly this is much larger than the 10 in.-oz employed. A consequence of this comparison is that the experimental torque vs angle curve may only show the beginning of the tightening process. The TVA curve may show different characteristics if higher torques are used. The slope of the curve may increase with further tightening since more work is being put into deflecting the parts. The maximum value of the slope would be the torsional stiffness of the parts themselves. Failure in threads probably occurs before this point, though.

The shaft and thrust plate is also an example of hard stop threaded part assembly. The TVA curve shows an abrupt change at the point of bottoming. The tightening angle is a small fraction of one revolution. Assemblies employing a soft gasket or parts are referred to as soft stop assemblies. In this case tightening occurs over a much larger angle. Note that these are actually just relative terms. Variations in each category can exist. The main point is that some assemblies are more stiff than others. The effect of this on automated assembly will be discussed in the modeling and simulation sections that follow.

### 3.4 Part Mating Models

In order to simulate the threaded part mating process and develop guidelines to control it, a mathematical representation of the TVA curve is used. The experimentally obtained TVA curve was essentially a static measurement. However, in an automated assembly situation, a dynamic situation must be described. Before this is done, several terms must be defined.



The elements of a model are shown in Figure 3.5. Using variables of rotational dynamics, the parts and the fixtures which hold them are lumped into two inertias,  $J_{mf}$  and  $J_{tc}$ . The former represents the inertia of one threaded part and the rotating parts of the torque station. The latter represents the inertia of the other threaded part and the tool/collet assembly suspended in the RCC. The angular position and velocity of the two inertias are represented by  $\theta_m$  and  $\omega_m$ , and  $\theta_t$  and  $\omega_t$ , respectively.

The RCC is modeled as a torsional spring with stiffness  $K_c$ . It is assumed to be linear. Measurement of this stiffness will be described in Chapter 5. Viscous damping of the RCC is considered negligible. For situations where elastomeric pad RCCs are employed, the damping may not be negligible. Assembly configurations not containing a RCC, or other form of compliance, as the base for the stationary part must be modeled differently. For a rigid mount,  $K_c$  would go to infinity,  $J_{tc}$  would have no dynamics, and the stationary part would become ground. This was the case in the TVA curve experiment.

The input torque from the actuator to the system is  $T_m$ . The friction in the actuator and drive is represented by  $T_f$ . Viscous damping is indicated by  $B_{mf}$ . The reaction torque of the RCC is  $T_{rcc}$ . Its magnitude is

$$T_{rcc} = K_c \theta_t \quad (3-7)$$

where  $\theta_t = 0$  is the free angular position of the tool/collet.

The interaction between the two parts is an equal and opposite reaction torque,  $T_p$ . The magnitude of the torque is defined by the TVA curve.

Two models were developed. The first is a linear model which breaks the process up into a series of linear models. Since this linear model has limitations which compromise the complete description of the process, a more complicated non-linear model was also developed.

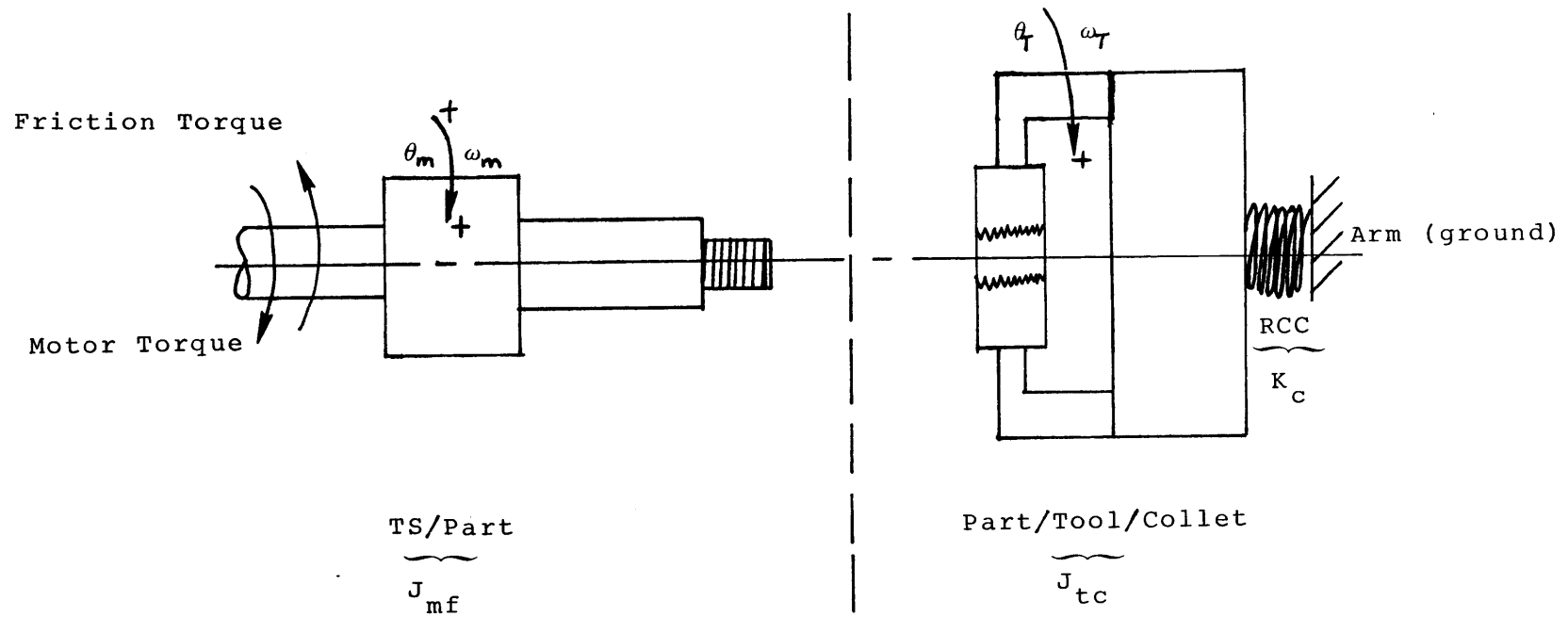


Figure 3.5 Part Mating Model Elements

### 3.4.1 Piecewise Linear Model

The first model developed separates the part mating dynamics into separate models for the rundown and tightening phases (pre-bottoming and post-bottoming).

During rundown the parts are separate identities. The torque exerted on one part by the other is the rundown torque. Figure 3.6a shows the free-body diagram for this phase. The equations of motion can be derived by summing the torques on each inertia.

$$\Sigma T_{mf} = J_{mc} \alpha_m \quad (3-8)$$

$$J_{mf} \frac{d\omega_{mf}}{dt} = T_m - T_f - T_R - B_{mf} \omega_m \quad (3-9)$$

for  $\omega_m > \omega_t$

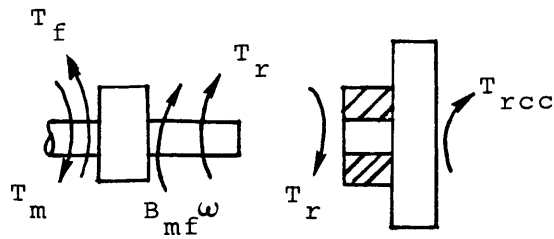
Note the condition imposed upon Equation (3-9). For  $\omega_m < \omega_t$ , the direction of  $T_R$  changes sign. For  $\omega_m < 0$ , the direction of  $T_f$  changes sign.

$$\Sigma T_{tc} = J_{tc} \alpha_t \quad (3-10)$$

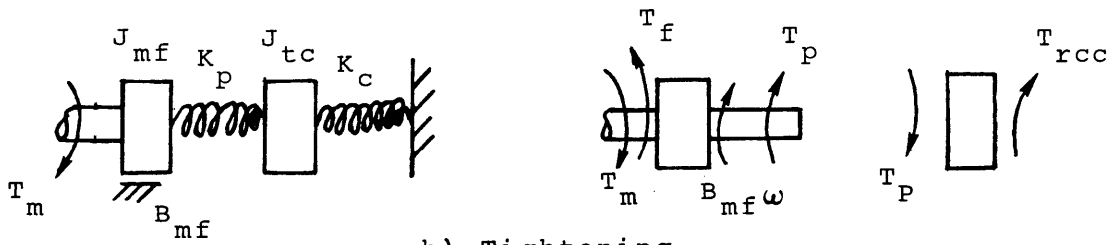
$$J_{tc} \frac{d\omega_t}{dt} = T_r - K_c \theta_t \quad (3-11)$$

For the tightening phase, the part mating process is considered a linear spring with stiffness  $K_p$ . This stiffness is found using the linear fit of the TVA curve. The part torque becomes, from the free-body diagram in Figure 3.6b,

$$\begin{aligned} T_p &= K_p \Delta\theta \\ &= K_p (\theta_m - \theta_t) \end{aligned} \quad (3-12)$$



a) Rundown



b) Tightening

Figure 3.6 Piecewise Linear Model

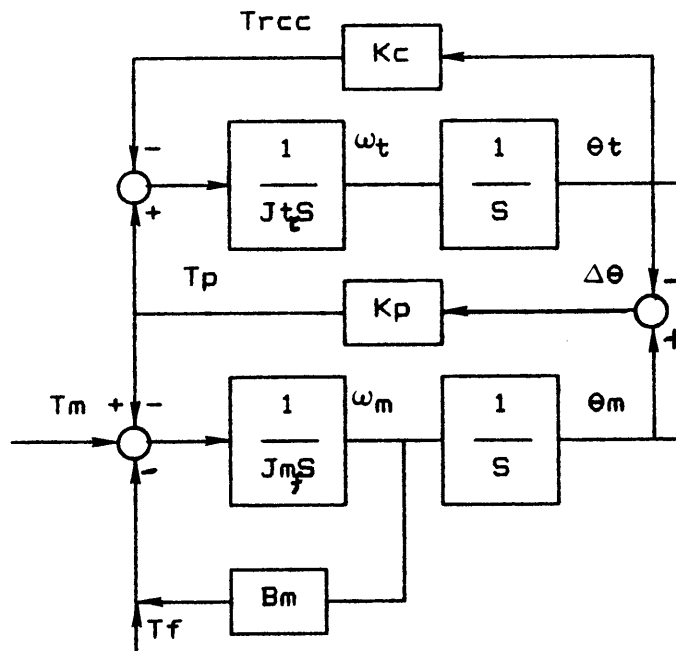


Figure 3.7 Piecewise Linear Block Diagram Tightening Phase

For this phase  $\theta_m = \theta_t = 0$  is defined as the angle of the parts at bottoming. All other initial conditions are the final conditions from the rundown phase.

The equations of motion become

$$J_{mf} \frac{d\omega_m}{dt} = T_m - T_f - B_{mf}\omega_m - K_p(\theta_m - \theta_t) \quad \text{for } \omega_m > \omega_t \quad (3-13)$$

$$J_{mf} \frac{d\omega_m}{dt} = K_p(\theta_m - \theta_t) - K_c\theta_t \quad (3-14)$$

A block diagram of the linear model is shown in Figure 3.7. It represents the equations of motion and can be combined with other models to form a complete torque station assembly model.

The equations derived for the linear model are an extreme simplification of the process. Considering the parts as a spring does describe the torque/deflection relationship of the parts. However, if an initial condition were presented such that the parts were tightened, they would then attempt to unwind themselves like a spring. Clearly this does not happen. Therefore, the model is only valid for increasing  $\Delta\theta$  or  $\Delta\omega > 0$ . The model is convenient since linear analysis methods can be utilized with it. Its merit is shown in the torque station controller analysis of Chapter 5.

### 3.4.2 Nonlinear Model

A nonlinear model was developed by combining the spring and coulomb friction characteristics of the part mating process. A model of coulomb friction is presented with the hardware modeling of Appendix A. Examination of the rundown phase shows striking similarity to coulomb friction. The torque exerted by part 'A' on part 'B' always opposes the motion of part 'B' with respect to part 'A', and vice-versa. For example, in Figure 3.8a, if  $\omega_m > \omega_t$ , then  $\Delta\omega = \omega_m - \omega_t$  is positive and the part reaction torque,  $T_p$ , is in the direction shown. If the relative motion is reversed as in Figure 3.8b, then the part reaction torque is reversed. Mathematically, this can be described as

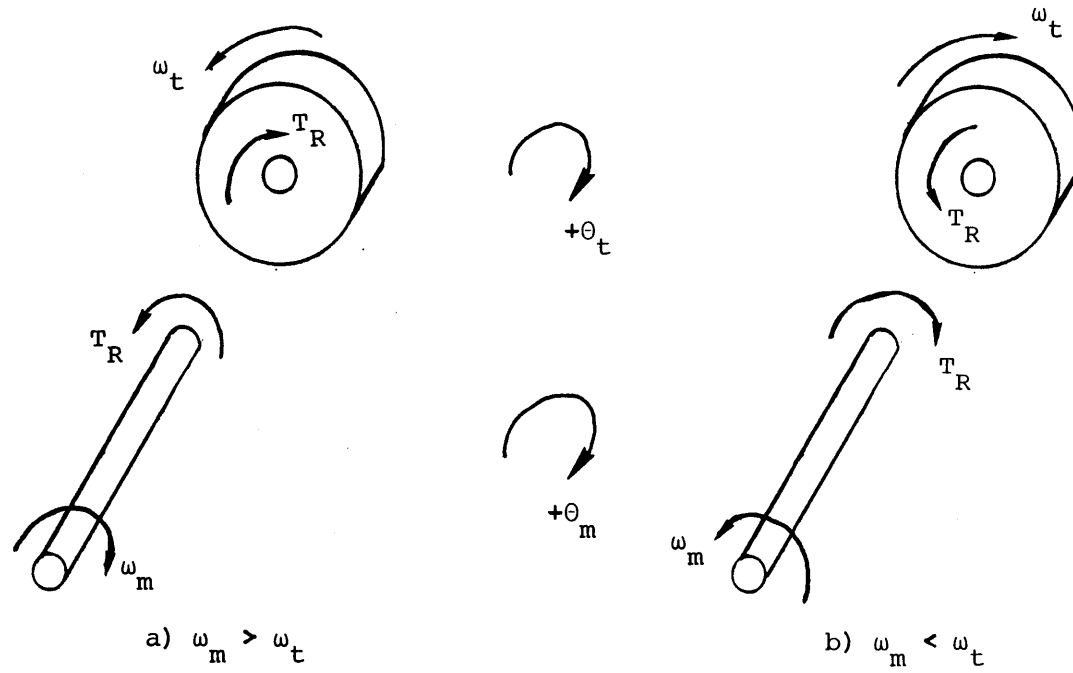


Figure 3.8 Part Torque During Rundown

$$T_{PR} = T_r \operatorname{sgn}(\Delta\omega) \quad (3-15)$$

The sign function,  $\operatorname{sgn}$ , is defined as

$$\operatorname{sgn}(a) = \begin{cases} 1 & a > 0 \\ 0 & a = 0 \\ -1 & a < 0 \end{cases} \quad (3-16)$$

Completion of the model extends the flat section of the TVA curve during rundown into the section with a slope during tightening. If the same sign condition is applied to this section, the relationship for the part torque due to tightening becomes

$$T_{PT} = K_p (\Delta\theta - \Delta\theta_B) \operatorname{sgn}(\Delta\omega) \quad (3-17)$$

The total part torque is

$$T_P = T_{PR} + T_{PT} \quad (3-18)$$

Equations (3-16) through (3-18) are more clearly illustrated by Figure 3.9. If  $\Delta\omega$  changes sign, then  $T_P$  does also. If tightening has progressed to, say, point A, and is stopped, then a reversal in direction of the applied torque must occur to cause a decrease in  $\Delta\theta$ , and vice-versa. The part torque is now direction-dependent as well as position-dependent.

$$T_p = f(\Delta\theta, \Delta\omega) \quad (3-19)$$

The equations of motion for this model can now be derived. They are as follows

$$\begin{aligned} J_{mf} \frac{d\omega_m}{dt} = & T_m - |T_f| \operatorname{sgn}(\omega_m) - B_{mf}\omega_m \\ & - T_r \operatorname{sgn}(\Delta\omega) - K_p (\theta_m - \theta_t - \Delta\theta_B) \operatorname{sgn}(\Delta\omega) \end{aligned} \quad (3-20)$$

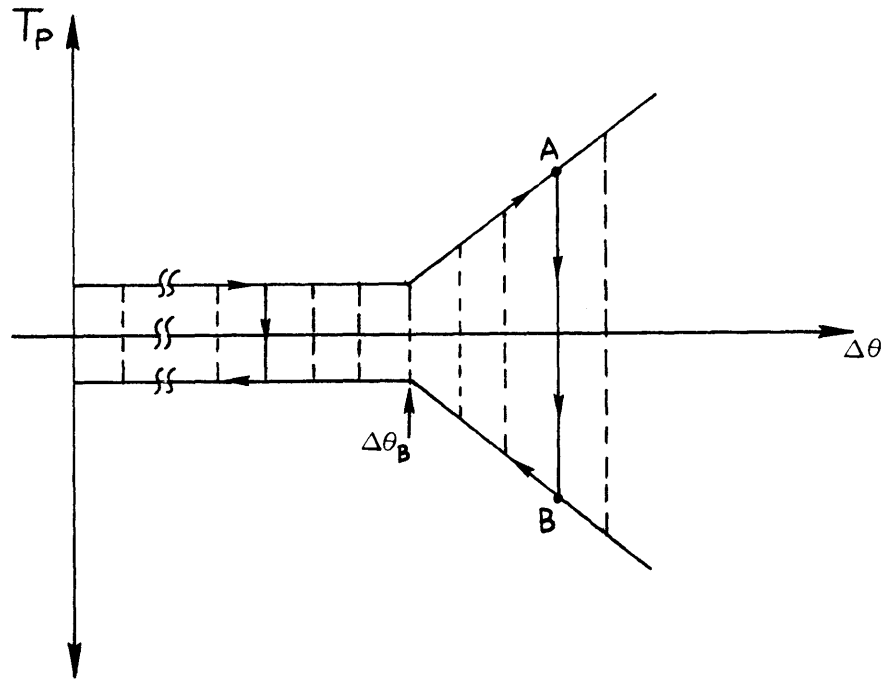


Figure 3.9 Illustration of Non-linear Model



$$J_{tc} \frac{d\omega_t}{dt} = T_r \operatorname{sgn}(\Delta\omega) + K_p (\theta_m - \theta_t - \Delta\theta_B) \operatorname{sgn}(\Delta\omega) - K_c \theta_t \quad (3-21)$$

A block diagram of Equations (3-20) and (3-21) is shown in Figure 3.10.

### 3.4.3 Generalized Model

The development of the nonlinear model described by Equations (3-17) through (3-21) was for a linear fit to the experimental TVA data. This fit sufficed for the purposes of this thesis. However, different TVA curves may require a more sophisticated description. Figure 3.11 shows representations of a general TVA curve. Only the portion of the curve past the bottoming point is shown. The symbol X represents an experimental data point. The data are finite in number, but information is needed between the points. The information can be estimated with curve fitting techniques, or straight lines between each point.

A continuous fit to the data is shown in Figure 3.11a. Using the notation of Equation (3-18)

$$T_p = T_r + f_c [\Delta\theta, \operatorname{sgn}(\Delta\omega)] \quad (3-22)$$

where  $f_c$  is a continuous function. In order to fit the data, some estimate of the increase in slope beyond the last datum is needed. The instantaneous slope of the curve is the instantaneous stiffness of the threaded joint.

The second method of fitting the data is to connect the points with straight lines. The TVA curve becomes a piecewise continuous linear function of the points as shown in Figure 3.11b. The curve can be described by

$$T_p = T_r + f_p [\Delta\theta, \operatorname{sgn}(\Delta\omega)] \quad (3-23)$$

where the piecewise function,  $f_p$ , is

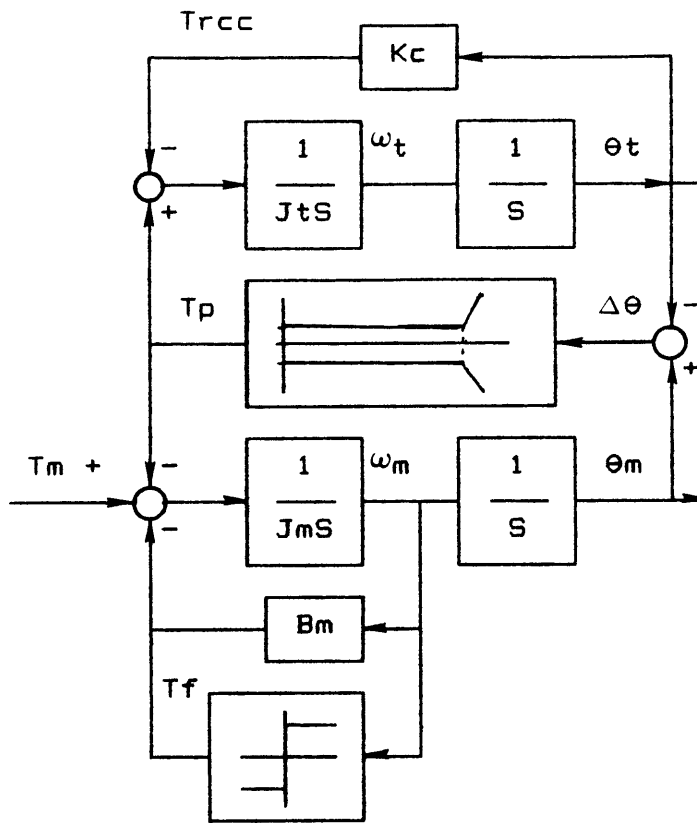


Figure 3.10 Non-linear Model

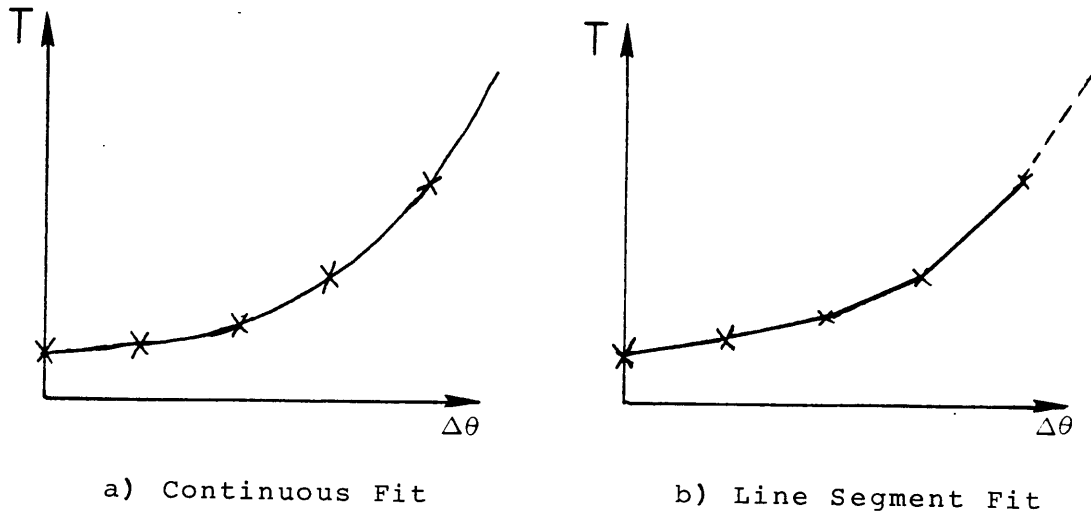


Figure 3.11. Generalized TVA curve.

$$\begin{aligned}
 |f_p(\Delta\theta)| &= (K_{p1})(\Delta\theta_2 - \Delta\theta_1) & \Delta\theta_1 < \Delta\theta < \Delta\theta_2 \\
 & (K_{p2})(\Delta\theta_3 - \Delta\theta_2) & \Delta\theta_2 < \Delta\theta < \Delta\theta_3 \\
 & \vdots \\
 & (K_{pi})(\Delta\theta_{i+1} - \Delta\theta_i) & \Delta\theta_i < \Delta\theta < \Delta\theta_{i+1}
 \end{aligned}$$

(3-24)

The piecewise part stiffnesses,  $K_{p_i}$ , are constant between the data points

$$K_{p_i} = \frac{T_p(\Delta\theta_{i+1}) - T_p(\Delta\theta_i)}{\Delta\theta_{i+1} - \Delta\theta_i} \quad i = 1, \dots, n \quad (3-25)$$

where  $n$  = number of data points.

If this method is used, the decision for the slope to be used past the last datum is more critical. Some estimate must be made from a stress analysis of the threaded joint.

The assumption of complete reversal of direction of torque needed to decrease  $\Delta\theta$  may also need some improvement. Depending on the torque levels involved, that path back to zero torque may include a small decrease in  $\Delta\theta$ . This is shown by path 1 versus path 2 in Figure 3.12.

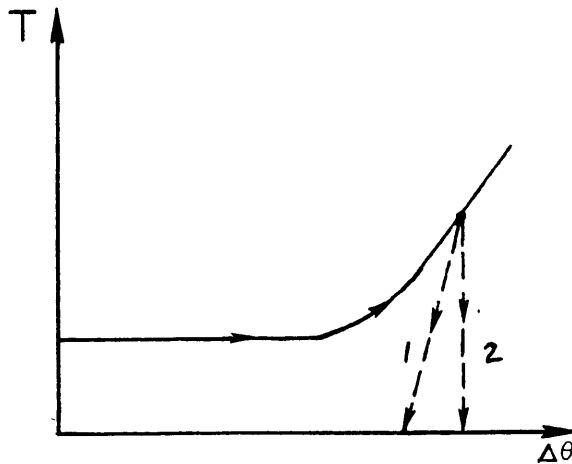


Figure 3.12. Alternate TVA paths.

Assuming the positive TVA curve can be reflected about the  $\Delta\theta$  axis to form a path for decreasing  $\Delta\theta$  is also a simplification. Better instrumentation is required to provide a more accurate experimentally-based model. Dynamic threaded part mating has the characteristics of a stick-slip type of system. Systems such as this make it difficult to provide an exact model. Experimental data is required. For precision hard stop assemblies, this data is difficult to obtain due to the small tightening angle. A smoother curve than that of a typical fastener is expected since the parts are clean, free of burrs, and have a better surface finish.

### 3.5 Considerations for Process Control

Characterization of the threaded part mating process reveals areas that are necessary to consider in torque station controller design. Since the process consists of different phases, the controller must be able to adapt to quickly changing conditions. The speed at which rundown is performed affects both the kinetic energy at the bottoming point and the time required to stop the  $J_{mf}$  inertia before  $\Delta\theta_{ti}$  is exceeded for the desired torque level. Unlike other processes, no overshoot in torque applied to the threaded joint can be tolerated since the final torque in the parts is the greatest torque applied rather than the final steady-state value.

The existence of dynamics due to the tool/collet inertia and the RCC complicates matters. However, it will be shown that this compliance is valuable to the control problem.

Noting that three different torques exist --  $T_m$ ,  $T_p$ , and  $T_{RCC}$ , one asks which is the one necessary to control. The answer is all three. The torque in the parts is equal to the others for a static situation. However, transient dynamics could cause the parts to be overtightened.

An exact measurement of  $T_p$  would require exact experimental or analytical data for  $\Delta\theta_B$  and  $\Delta\theta_{ti}$ . The difficulties in the determination of these quantities has already been discussed. The next chapter explores methods of controlling  $T_m$ ,  $T_{RCC}$ , and the system dynamics so that the proper  $T_p$  is achieved.

## CHAPTER 4

### METHODS OF THREADED PART MATING CONTROL

With the threaded part mating process having been described, methods of controlling the process are now presented. In order that the torque station assemble the parts and meet the torque specification, design of the electro-mechanical configuration and the electrical controller are critical. A description of the torque station configuration utilized in this research was presented in Chapter 1. This chapter first examines the reasons for choosing the hardware configuration. Then several methods of controlling the hardware and the torque applied to the threaded parts are presented. Modeling of specific hardware components is discussed in Appendix A.

#### 4.1 Mechanical Configuration

Necessary and desired features of the torque station actuation, power transmission, and sensing elements are now discussed.

##### 4.1.1 Choice of Actuator/DC Motor

Since torque is the primary variable to be controlled in threaded part mating, the actuator which delivers the applied torque is perhaps the most critical component in the system. This thesis only considers precision permanent magnet DC motors for torque station actuation. Pneumatic actuators are common in assembly line nutrunners and automatic screwdrivers. As was discussed earlier, they are rejected for use in the automatic assembly cell since they suffer from cleanliness problems and cannot be adapted to a size and configuration that is necessary. It is also questionable whether or not the necessary degree of accuracy can be provided with this type of actuator. AC and stepper motors were also investigated,

but were rejected for the more versatile DC motor. Stepper motors are normally utilized for positioning applications rather than torque control. A separate torque sensor is necessary with this type of motor. New AC motors are becoming available that have desirable torque characteristics. However, they require more sophisticated power supplies and amplifiers than DC motors. Overall, DC motors are more compatible with the rather simple assembly cell control hardware and supervisory computer that is utilized.

A mathematical model of a permanent magnet (PM) DC motor is presented in Appendix A. Readers not familiar with these mathematics are referred to that discussion. The particular features which make a DC motor a good choice for the automated assembly cell torque station are as follows:

1. Torque output proportional to electric current input.
2. Linear speed vs. torque at a constant voltage.
3. Fast response time.
4. Clean room compatibility.
5. Size compatible with assembly cell.

The first item above is particularly important for precision torque control.

The particular motor chosen for the torque station was a PMI Model 6M4H DC motor. This motor is of the "printed circuit" type. Its particular features are listed below:

1. Good low speed performance.
2. Very low armature inductance (electrical time constant = 0.075 msec)
3. Low inertia.
4. An ironless, disc-type "printed circuit" armature.
5. No cogging torque (consequence of an ironless armature).
6. Brush-type commutation.
7. Less than 5% variation in the torque constant about one motor revolution.

The motor is also attached to a DC tachometer used for velocity feedback for speed control and damping. The pancake construction of the pair was particularly ideal for the tight envelope along the Z-axis that is available in the assembly cell. An integral tachometer also reduces any dynamic coupling between the motor and tach.

Success with this type of motor has been reported in the robotic force/torque control literature. Low speed precision torque control is mentioned in Luh, Fisher, and Paul [10] using a larger model of the PMI motor.

Brushless PM DC motors appear to be the choice of the future. Brush friction is the main contribution to internal friction in a small precision DC motor. With brushes eliminated, the designer can minimize friction with a judicious choice of bearings. Brushless motors can be incorporated as piece parts directly into the TS drive housing. An entire set of bearings could be eliminated. The biggest drawback of brushless motors is the complexity of their drive electronics. Switching of the armature current from one electromagnetic circuit to another must be done using information from position sensors. Designs which produce the very linear torque-vs-current characteristic of brush commutated motors are just being realized.

#### 4.1.2 Direct Drive

The torque station design employs a direct drive transmission of power from the motor to the torque adapter, fixtures, and parts. The primary reason for this choice is that with the low torque levels involved (0-15 in.-oz) no multiplication of torque is needed for available motors which are compatible with the assembly cell design. Chapter 5 will point out that a speed reducer may be beneficial in terms of required speed control. However, the losses and design difficulties associated with the addition of a gear ratio outweigh the benefits.

If a speed reducer were employed, the output torque of the motor would be multiplied, but so would the output torque error. Therefore, a torque sensor on the output side of the gear ratio would be necessary. For torque control methods utilizing the motor as a torque sensor, this is undesirable.



A gear ratio large enough to produce the required speed reduction may preclude the use of low loss gearing such as positive-drive belts or O-ring drives. High gear ratio devices often are plagued by large losses due to friction and cannot be driven backwards. The latter is necessary for torque station fixture position calibration. A gearhead employed in conjunction with the motor also suffers problems of efficiency and inaccuracies in torque conversion.

A final argument against speed reduction is the lack of precision DC motors in the sub 1 in.-oz output torque range. This is the range that would be required for the torque station. Measuring torque below 0.5 in.-oz is difficult and controlling it is even harder. Motor manufacturers hesitate to release tight specifications on motors in this range. Internal friction in the motor is the primary reason. This is especially true for brush-type motors. Applications that require a larger torque level may be forced to employ gearing if compatible motors cannot deliver enough torque.

Overall, the transmission of power in the torque station should avoid losses and inaccuracies due to inexact torque transmitted through a high gear ratio. Backlash should also not be present. In a direct drive transmission this is possible. The stiffness of the drive must be high enough so that no uncontrollable dynamics are created.

#### 4.1.3 Sensing Devices

To control the threaded part mating process, sensors are required to provide information to a controller. A process can only be controlled as well as it can be measured, or as well as a controller can utilize the sensor data to reconstruct the states of the process. The variables of interest in threading are torque, position, and velocity. The following sensors are discussed as candidates to measure these variables:

1. DC torque motor with ammeter.
2. DC tachometer.
3. Incremental optical encoder.
4. Linear variable displacement transducer (LVDT).
5. Torque sensor.

These electro-mechanical devices are those considered by this research; others do exist. Discussion of the mathematical representation of the devices is presented in Appendix A. Use of these devices in a threading control application is discussed here.

Since the motor has been presented as the chosen actuator, it may be a surprise to include it in a list of sensors. However, a precision DC motor can be utilized to provide torque information as well as to deliver it. This is due to the proportionality between the current through its armature and the torque that it delivers. Creating an ammeter to measure the current constitutes the sensor. A major disadvantage of the motor/ammeter as a sensor is that it indicates only the motor torque, not necessarily the net torque delivered to the threaded parts. This is due to friction in the motor and drive. The electrical noise associated with current measurement is also a factor.

A DC tachometer is utilized by the existing assembly cell torque station. It provides velocity feedback information as an analog voltage proportional to angular velocity. It is a valuable device in that it provides a continuous output signal and does not require a power supply. Its bandwidth is higher than that of the motor since it has less inductance. However, for small velocities (<10 rpm) it suffers from a small signal to noise ratio. Because of this, some filtering and amplification of the signal may be necessary which may compromise response time. Appendix A shows that the load impedance should be much larger than the output impedance of the tach. This may not be possible in some feedback control systems. Position information can also be obtained from the tach by integrating the signal, but better devices are available.

One of these devices is an incremental optical encoder. Very high resolution is available with an encoder. The device is readily adaptable to integral mounting to a DC motor. The device is also compact and has no contacting parts. It does not add friction to the system nor generate debris. The latter is critical to clean room operation. An encoder is a digital device. Interfacing it with an analog control system requires additional hardware. Obviously it is the sensor of choice in a digital system.

Velocity information can also be generated from the output of an encoder. Methods for doing this are outlined in Appendix B. One of these methods forms the basis for hardware developed by this research to create an improved torque station. Operation and performance of this hardware is presented in Chapter 6.

Since the design of the tooling employed by the assembly cell incorporates an LVDT to measure displacement of the gripper in the ball spline, the LVDT can be utilized to monitor position information during the threading process. For each revolution of the parts relative to each other during rundown, the gripper is displaced along the Z-axis by one pitch of the threads. If the resolution of the LVDT is  $r_z$ , then the amount of rotation that can be resolved is

$$\begin{aligned} d\theta &= 360 \cdot n \cdot r_z \quad (\text{deg}) \\ &= 2\pi \cdot n \cdot r_z \quad (\text{radians}) \end{aligned} \quad (4-1)$$

where  $n = 1/\text{PITCH}$  is the number of threads per inch for the parts being assembled. The LVDT used in the tool has a resolution of 0.001 in. For the shaft and thrust plate parts,  $d\theta = 25.9^\circ$ . This value is too large to allow use of the LVDT signal during tightening. The LVDT was used to show variations in  $\Delta\theta_B$  for the wheel assembly. It can be employed in a position loop for rundown, but a safety factor to account for uncertainty in  $\Delta\theta_B$  must be employed. Therefore, some other means must be used to smooth the transition between rundown and tightening. The LVDT is very valuable in detecting whether or not Z-axis displacement of the gripper has stopped. This information can be used to signal the completion of the assembly task or jamming of the parts.

The final sensing device to be discussed is a mechanical torque sensor. This device normally senses the deflection of a compliant member, and provides a signal proportional to the torque causing the displacement. The advantage of this device is the ability to calibrate it independently of the actuator. Critical to the success of this device is the ability to remove friction and other losses between the sensing element and the process. Particular aspects of torque sensor design are presented in Chapter 7 in conjunction with the control method utilizing the sensor.

#### 4.1.4 System Configuration

As mentioned in Chapter 1, the assembly cell performs threading with the motor in the assembly base rather than in the arm assembly. All rotating parts which can generate debris are kept below the surface of the assembly base. This configuration is particularly convenient for cartesian assembly cells. It allows the ARCT assembly to be optimized for tool changing, peg-in-hole insertions, and precise gripping of palletized parts. This is the only type of general configuration considered in this thesis. Other types of robots may employ the rotational Z-axis degree-of-freedom in the arm. It is hoped that the principles and results presented in this document can be extended to those situations.

Although the primary purpose of the torque station is threading, it is beneficial to keep in mind that any controller design should not preclude the use of the torque station for other uses. In the operation of the assembly cell, several fixtures and subassemblies must be located with dowel pins. This requires that the torque station be positioned very accurately. With the present design, the positioning is done with the air cylinders since only one "home" position is required. This scheme works well but is limited to a single position. In future assembly requirements, more positions may be required. The scheme also requires hard stops on the torque adapter resulting in a large radius and unnecessary inertia. It will be shown that the magnitude of this inertia is a parameter of controller design and should not be fixed by the need for hard stops.

#### 4.2 Torque Control and Measurement

In order to successfully control the threaded part mating process, it is necessary to propose, model, and evaluate methods of closed loop torque control. This section addresses the first of these tasks. Two methods of closed loop control were identified. They are:

1. DC motor current feedback.
2. Torque sensor feedback.

Each method has its advantages, disadvantages, and unique features. Common to both is the generation of a feedback signal which measures a torque in the system. Neither can directly measure the torque in the threaded joint itself so each must incorporate the part mating model of Chapter 3 into the design of a closed loop controller.

#### 4.2.1 DC Motor Current Feedback

The first method is to utilize the magnitude of the current through the armature of a precision DC PM motor as the torque feedback signal. Thus the sensor is actually an ammeter setup to measure the current. This is normally implemented in hardware by sensing the voltage drop across a small resistor to ground. The sensed voltage is compared with the torque command voltage to produce an error signal.

The principle advantage of this method is that the motor can be utilized for two functions, and the system hardware is simpler and more compact. The method does not rely on a compliant member, so the dynamics of the system are less complex and more easily observed.

The biggest disadvantage of the method is that once a motor is chosen, the configuration must live with its parameters and internal friction. Several design options are eliminated and tight restrictions are put on motor precision and parameter stability. It can also be argued that the sensing of torque information across the energy transformation of a power transducer is not as desirable as sensing across that of a signal transducer.

#### 4.2.2 Torque Sensor Feedback

A second method of torque control is to utilize the output signal of a torque sensor as the feedback signal. This signal is summed with the torque command to produce an error signal for the TS controller. Torque sensors normally measure the deflection of a spring or shaft of known stiffness. For the torque levels and resolution required by the assembly cell, a custom-designed sensor is probably necessary.

The principle advantage of this method is the ability to attach the sensor to the process such that no losses between the sensed torque and process torque exist. The compliance of the device can also be used as a design parameter to help achieve desirable closed loop dynamics. This method also puts less restrictions on the actuator that is used. A final advantage is that the torque sensing and torque application can be calibrated independently.

This method is more versatile, but puts more demands on the configuration and controller designs. Small design envelopes may not allow an additional sensor assembly. Additional dynamics are added to the system. These dynamics must be modeled and controlled unless the sensor compliance is much larger than that of the RCC and parts. In order to meet this requirement, the natural frequency of the torque station may be too low to enable it to perform precise positioning tasks such as fixture installation.

#### 4.2.3 Need for Compliance

Before control system configuration concepts are discussed, it is necessary to point out the value of torsional compliance in a torque control system. During the rundown phase of threading, the TS must turn one part relative to the other at some velocity. It must then pass the bottoming point and stop when the desired torque level in the parts is reached. This implies that the instantaneous position of the torque station, the parts, and the RCC/collet determines the torque level in the threaded joint. The basic equation describing torque in the TS, torque sensor, parts, ART chain is

$$T = K_{EQ} \Delta\theta \quad (4-2)$$

where  $K_{EQ}$  is the equivalent series stiffness of the chain and  $\Delta\theta$  is the overall deflection of the chain. If each of the elements of the chain had zero compliance, then any error in  $\Delta\theta$  would result in infinite torque error. Obviously, this is not the case with real assemblies since everything has some compliance. That the threaded joint and RCC have torsional compliance has already been presented. The point to be made is

that the amount of overall compliance in a torque control system determines the amount of positional error that can be tolerated. Added compliance allows greater error and results in a slower, more easily observed system.

#### 4.3 Control System Concepts

Each torque feedback method can be utilized in a closed loop control system in several different configurations. The control law utilized depends on the sensors and method of feedback that is employed. This section presents some of the possibilities. The concepts are presented in the figures below in schematic form according to the symbols shown in Table 4-1. All configurations conform to the fixed placement of the motor and arm/RCC/collet/tool assembly in the assembly cell. For situations where an RCC is not present, or the actuator is in the arm, other schemes are possible.

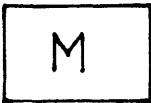








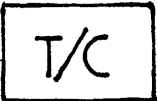



In each scheme, the motor is the actuator and delivers a torque,  $T_m$ . Friction torque is represented by  $T_f$ . Torque, position, and velocity commands are signified by  $T_c$ ,  $\theta_c$ , and  $\omega_c$ , respectively. A constant  $K$  is used to represent a control gain. Measured quantities are signified by a prime attached to the variable. Only concepts are presented here. Implementation, modeling, and experimentation are discussed in Chapters 5, 6, and 7.

##### 4.3.1 Current Feedback Concepts

A method of utilizing current feedback torque control is shown in Figure 4.1. The motor acts as actuator and torque sensor, and is rigidly attached to the TS torque adapter which holds the rotating part during threading. A tachometer is attached to the motor to provide velocity feedback. No position sensing is employed except for the LVDT, which is used only for gross monitoring.

The principle of this method is to command a torque to the motor and feed back a signal proportional to the current in the motor such that the output is assured. Velocity feedback must also be added to limit the angular velocity during rundown, and add damping to the system during

Table 4-1  
Schematic Symbols for Control Configurations

|   |                         |   |                                       |
|---|-------------------------|---|---------------------------------------|
|    | Motor                   |    | Controller/<br>Signal Amplifier       |
|    | Tachometer              |    | Position to<br>Velocity Converter     |
|    | Encoder                 |    | Transfer of Electrical<br>Information |
|  | Threaded Parts          |   |                                       |
|  | Part Holding Fixture    |  | Torque Sensor                         |
|  | Tool/Collet             |  | Arm/Ground                            |
|  | RCC<br>Torsional Spring |  | LVDT                                  |



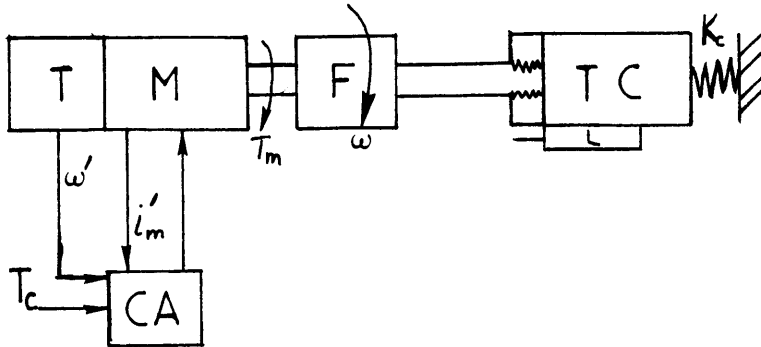


Figure 4.1 M/T Current Feedback

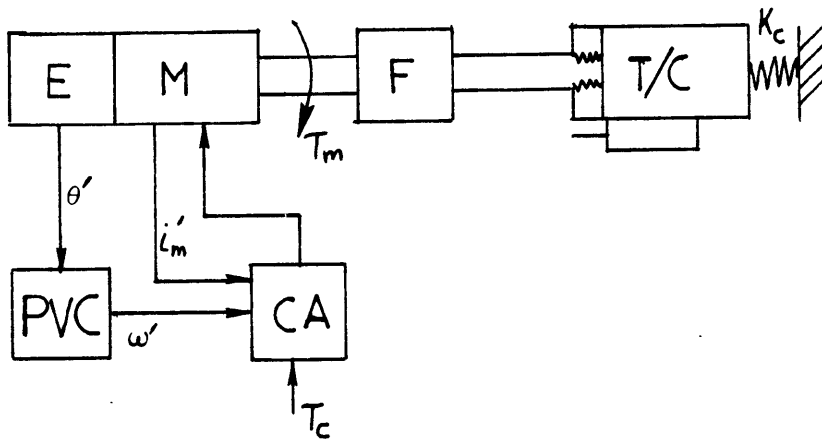


Figure 4.2 M/E Current Feedback

tightening. If this is not done, the speed of the motor and torque station will become very large since torque will be continually delivered to the inertia of the torque station. The control law is in the form

$$T_m \propto T_c - K\omega' \quad (4-3)$$

when  $\omega = 0$ ,  $T_m < T_c$ . When  $\omega > 0$ , the torque delivered by the motor is limited to control speed.

The advantage of this scheme is that rather simple control hardware can be employed. No position sensing is required. A direct-drive link can be achieved between the motor and the torque adaptor. No modification of the ARCT side of the process is required.

The biggest disadvantage is that once the torque loop between motor and amplifier is created, the only control gain available is the velocity feedback gain. The designer must rely on this gain and the part mating and RCC compliances to achieve desired dynamics.

The torque measured is that of the motor itself. Any losses such as motor brush friction and drive friction result in loss of some of this torque. The net torque delivered to the parts by the motor is

$$T_n = T_m - T_{fm} - T_{fd} \quad (4-4)$$

The latter terms are the friction and brush losses in the motor and drive. Calibration of the system must take this into account.

This scheme is the one employed in the existing assembly cell TS controller. It is extensively discussed, modelled, simulated, and experimentally evaluated in Chapter 5.

A variation on this concept is shown in Figure 4.2. In this variation, the tachometer is replaced by an encoder. The encoder signal is used to generate a velocity signal for feedback and is also available for position information.

This variation also utilizes the control law of Equation (4-3). It is operationally identical to the M/T implementation, and has the same advantages as well as disadvantages. The encoder does provide more versatility since a position loop could also be easily added to the TS controller.

Because of performance problems with the M/T version, this variation was also implemented by this research. The implementation is described in Chapter 6. Design and simulation of the position to velocity converter hardware is presented in Appendix B.

A further variation of the general current feedback scheme of Figure 4.1 is shown in Figures 4.3a and 4.3b. These variations utilize the addition of extra engineered torsional compliance. One employs the compliance in the TS drive and the other in conjunction with the ARCT assembly. The added compliance does not change the control law, but allows the designer additional freedom in the choice of controller gains since the system natural frequency and damping are altered. Neither of these variations was implemented.

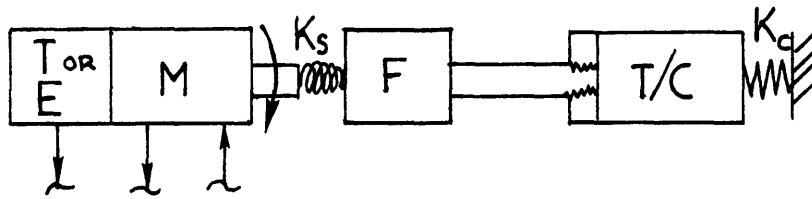
#### 4.3.2 Torque Sensor Feedback Concepts

The concepts shown in Figure 4.3 form the basis for torque sensor feedback implementations. A torque sensor is just an engineered compliance with instrumentation to detect its deflection. Figure 4.4 shows placement of a torque sensor on either side of the threaded joint. The control laws for this concept are in the form

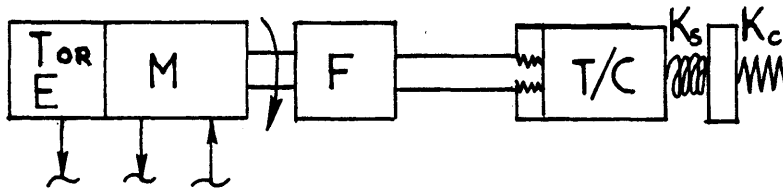
$$T_m \propto (T_c - T_s) H_T(s) \quad (4-5)$$

where  $H_T(s)$  is the controller transfer function for torque control.  $T_s$  is the sensed torque.

Addition of the torque sensor to the control loop adds additional dynamics and requires a more complex controller. The controller will probably require multi-mode operation. During rundown the torque required is much less than that required for tightening. The control law that is

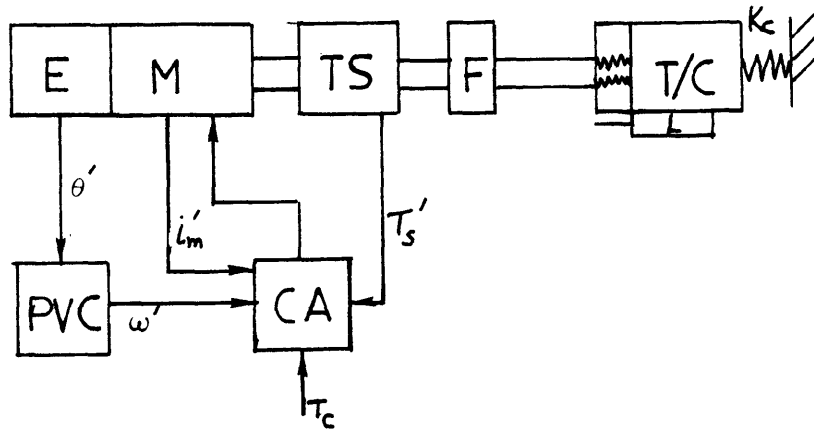


a) Compliance in Torque Station

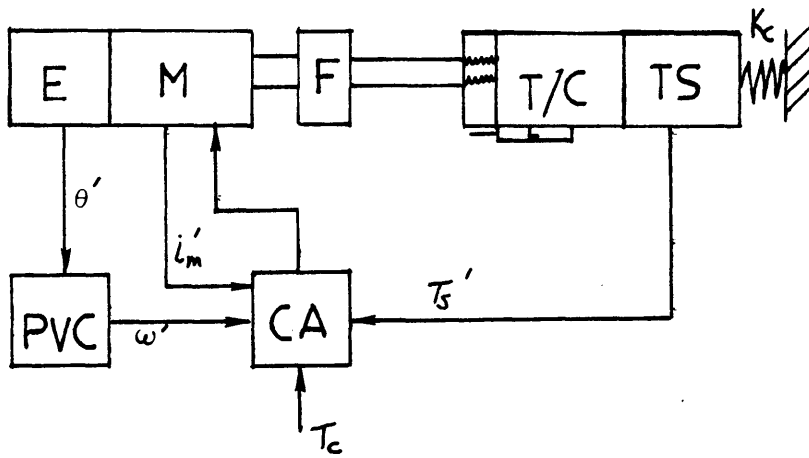


b) Compliance in Tool/Collet

Figure 4.3 Adding Engineered Compliance



a) Sensor in Torque Station



b) Sensor in Tool/Collet/RCC

Figure 4.4 Torque Sensor Feedback Concepts

optimal for tightening may not be so for rundown. Wherever the torque sensor is placed, an uncontrollable mode of oscillation due to inertia suspended from the torque sensor is present.

Torque sensor feedback control was not implemented in this thesis. Adapting a torque sensor to the existing assembly would be difficult due to the volume available. Chapter 7 examines the issues of implementing a torque sensor for torque control of threaded part mating. Design of the sensor itself is a formidable task.

Placing a torque sensor on the arm/RCC/collet/tool side of the threaded joint is probably not feasible for the assembly cell. The ARCT assembly is specially designed for very small diametral clearance peg-in-hole insertions. Adding a torsional compliance specifically designed for torque sensing may adversely affect these insertions. Use of the RCC with additional instrumentation as a torque sensor is also addressed in Chapter 7.

## CHAPTER 5

### DC MOTOR CURRENT FEEDBACK TORQUE CONTROL

The method of torque control by DC motor current feedback is utilized by the existing torque station of the automated assembly cell. This section utilizes the hardware models presented in Chapter 3 and Appendix A to model and simulate the operation of the torque station. This analysis is compared to experimental results with the actual hardware performing threaded part assembly. The actual performance is evaluated. Variations in the parameters are discussed to show their influence on the system dynamics. The results are used to evaluate changes in the nominal analysis to provide for parameter estimation error and alternate designs for different torque stations and parts.

#### 5.1 Existing Torque Station

##### 5.1.1 Principle and Sequence of Operation

Threaded part mating is one of the precision assembly operations performed by the assembly cell. The torque station acts in conjunction with the ARCT assembly to perform the threading operations as part of an automated sequence.

The control principle of the existing torque station is to control part mating torque by controlling the torque of the motor in the TS. This is done by closing a current feedback loop. The current is proportional to the motor torque, so in effect, the torque is controlled. The controlled torque applied to the parts is only the final phase of the part mating process, though. During rundown the torque required is less than the final torque. Applying torque to the inertia of the torque station without equal

resistance from the parts would cause a constant acceleration, and excessive speeds would result. Therefore it is also necessary to control the motor speed during rundown until the final torque level in the parts is reached. This is done in the torque station control scheme by feeding back the DC tachometer output to provide closed loop speed control.

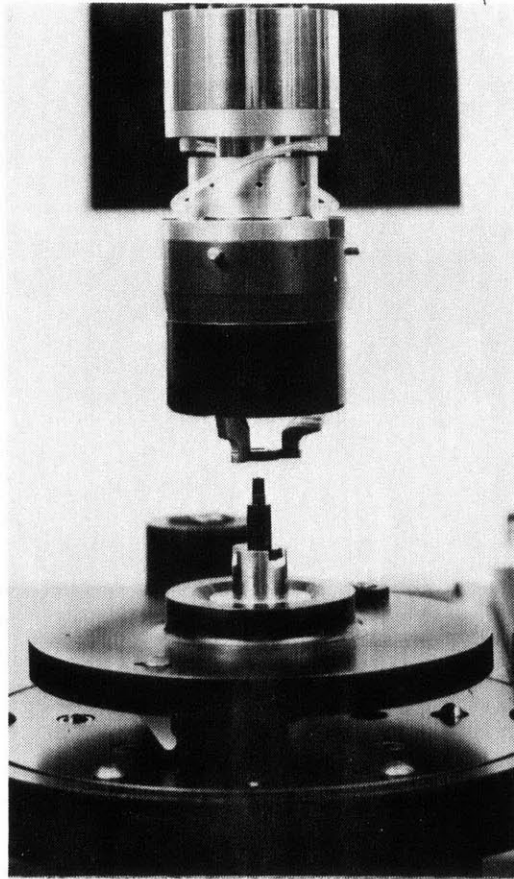
In the assembly sequence of the assembly cell, it is desired to operate the torque station by issuing a command to torque the parts with controlled speed rundown and smooth transition through bottoming and tightening to the final torque. This must be done without torque overshoot. The torque station must also have the capability to run independently of part mating so that it can be locked in position to accept parts and fixtures by the air cylinders and hard stops. It must also be very stable due to the fragility of the parts, tools, and RCC. Since the TS is normally sealed inside the clean environment of the cell, it is desirable that calibration not have to be done often, and that some indication of the performance be supplied remotely.

The sequence of operation for threaded part assembly is shown in Figure 5.1. One part is placed in a fixture in the torque station. The other is picked up by the gripper and positioned in the proper XY position. The arm then feeds the part held in the tool along the thread or Z axis until the parts contact and enough travel in the tool's ball spline is taken up to account for translation along the Z axis during rundown. Then a command is given to assemble the parts. The phases of part mating are performed and tightening is stopped when the torque station stalls. The output of the LVDT is monitored to signal the controller to stop applying torque when no travel in the ball spline has occurred for a given period.

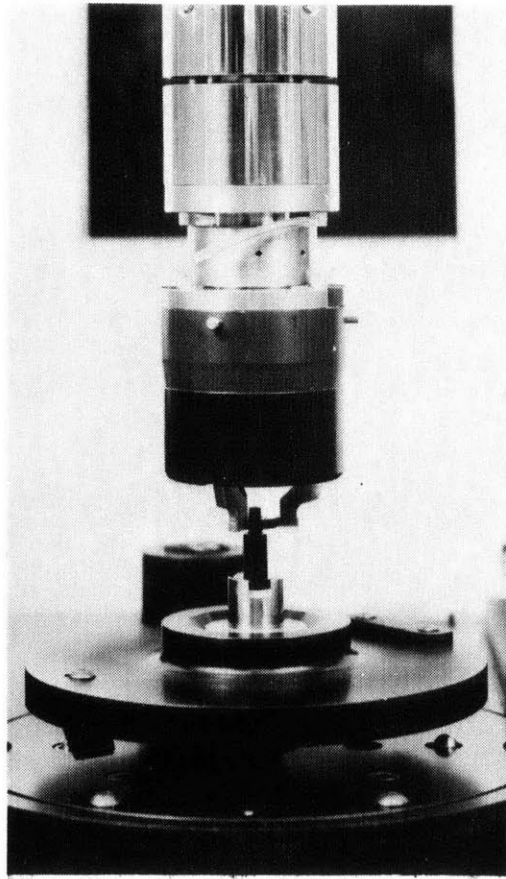
#### 5.1.2 Controller Circuit and Hardware

The control circuit used to implement the control strategy described above is shown in Figure 5.2. It is identical to the current control amp/motor configuration presented in Appendix A except for the addition of the tach feedback signal summed at the input of the amplifier. If the following "gains" are defined

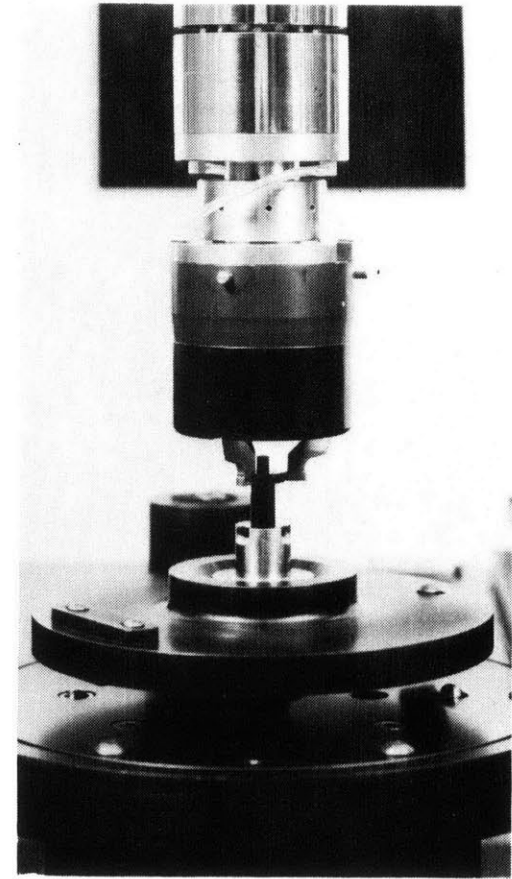




1) XY Alignment



2) Part Placement/Rundown



3) Bottoming/Tightening

Figure 5.1. Threaded Part Mating Sequence.

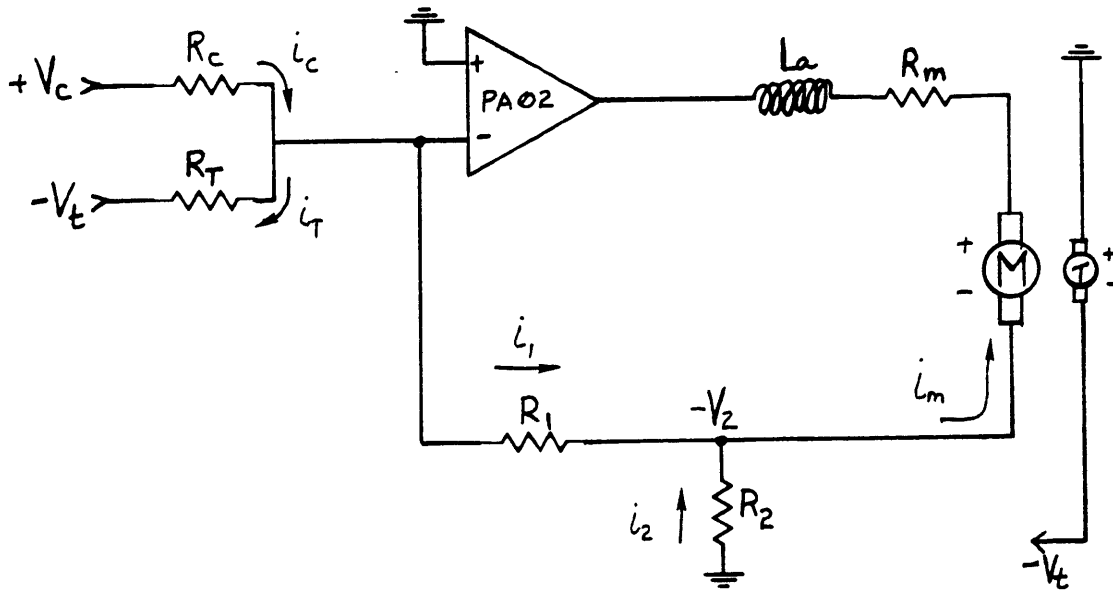


Figure 5.2 Control Circuit

$$G_C = 1/R_C \quad (5-1)$$

$$G_T = 1/R_T \quad (5-2)$$

then the current in the motor is

$$i_m = G_A [G_C V_C - G_T V_{TACH}] \quad (5-3)$$

The amplifier current gain is

$$G_A = \frac{R_1 + R_2}{R_2} \approx \frac{R_1}{R_2} \quad (5-4)$$

for  $R_1 \gg R_2$ . The motor and tachometer have the following output relations

$$T_m = K_T i_m \quad (5-5)$$

$$V_{TACH} = K_{TACH} \omega_m \quad (5-6)$$

Assuming that the tach is contaminated by electrical noise, the actual feedback shown in the circuit schematic is

$$V_t = V_{TACH} + V_n \quad (5-7)$$

The torque of the motor can now be described as

$$T_m = G_A K_T [G_c V_c - (K_{TACH} \omega + V_n)] \quad (5-8)$$

for  $\omega > 0$ , and

$$T_m = G_A K_T [G_c V_c - G_T V_n] \quad (5-9)$$

when the motor is stopped. This illustrates the basic principle of the control loop. When  $\omega > 0$  the torque is reduced to control speed, and when  $\omega = 0$  the torque is equal to that commanded with some modification due to noise.

The actual operation of the circuit depends on the dynamics of the load connected to the motor. Part of this load is always the internal friction of the motor and torque station,  $T_f$ . Since this torque always opposes the motor torque, the net torque output of the torque station is

$$T_n = T_m - T_f \quad (5-10)$$

This is the torque delivered to the parts during assembly.

In addition to the control circuit, the assembly cell also has provisions for issuing voltage commands as well as recording voltage signals. The software written for the cell is the Draper Automation Programming Language (DAPL). This is a general purpose language for cartesian robotic assembly written in the C language and implemented on an IBM PC/XT. The software and computer are interfaced to the torque station

controller and sensors through a multichannel data acquisition system. The original setup for the cell only provided for the monitoring of the LVDT and tach outputs since normal torque station operation did not require any others. As part of the ongoing cell development, sensing of the current feedback voltage,  $V_2$ , and the output of a sensor used to measure RCC deflection have been added for the purposes of this research. The control computer is only used for issuing commands and reading sensors and has limited real-time control capabilities.

For ease of use, the torque command,  $T_C$ , is issued in units of in.-oz in software and converted to the required voltage output by a conversion factor,  $V_C = C_{TV}T_C$ , where  $C_{TV}$  has units of V/in.-oz.

### 5.1.3 Torque Station Parameters

The actual parameters of the torque station, its controller, the RCC, and the parts are given in Table 5-1. The values shown for the motor, tach, and amp are those from the respective vendors and verified by experimentation. The inertias were calculated from piece part drawings. The values of the resistances were checked by instrumentation. Viscous damping was estimated from that of the motor. Both values are actually negligible. The friction of the motor and TS drive was measured with a torque watch. The range shown covers starting and running friction. A value for the stiffness of the RCC is given which was determined experimentally applying torque from the torque station and instrumentation to measure the deflection. The procedure and apparatus will be described with the experimental results. Definitions of the parameters are given in the List of Symbols. The reader is also referred to the modeling discussions in Chapter 3 and Appendix A.

## 5.2 Modeling/Analysis

Combining the process model of Chapter 3 with the torque station controller relationships allows several models of the closed loop control system to be formulated. Two models were formulated. First, a basic performance and calibration model was chosen to illustrate the general nature of the controller dynamics. Once this was done, the model of the part mating dynamics was added to show the response of the controller to threaded part mating.

Table 5.1 Torque Station Parameters

Motor/Tachometer (PMI Model 6M4HT)

$$\begin{aligned}R_m &= 1.32\Omega \\L_a &= <100 \mu\text{H} \\K_T &= 4.06 \text{ in.oz/amp} \\K_B &= 3.00 \text{ V/Krpm (0.02865 V-sec/rad)} \\K_{\text{TACH}} &= 0.75 \text{ v/Krpm (0.007162 v-sec/rad)} \\J_m &= 8.5 \times 10^{-4} \text{ in.-oz-sec}^2 \\B_m &= 1.24 \times 10^{-3} \text{ in.-oz-sec}\end{aligned}$$

Total Torque Station (including motor/tach)

$$\begin{aligned}J_{mf} &= 7.31 \times 10^{-2} \text{ in.-oz-sec}^2 \\B_{mf} &= 2.48 \times 10^{-3} \text{ in.-oz-sec} \\T_f &= 1.0 - 1.25 \text{ in.-oz}\end{aligned}$$

Tool/Collet/RCC

$$\begin{aligned}J_{TC} &= 2.48 \times 10^{-2} \text{ in.-oz-sec}^2 \\K_C &= 180 \text{ in.-oz/rad (3.14 in.-oz/deg)}\end{aligned}$$

Control Circuit

$$\begin{aligned}R_1 &= 3.9 \text{ K}\Omega \\R_2 &= 0.5 \Omega \\R_C &= 10 \text{ K}\Omega\end{aligned}$$

Amp (APEX Microtechnology Model PA02)

Saturation Voltage - 11 V (15 V supply)  
Maximum Current - 5A  
Response Time - 0.6  $\mu\text{sec}$

### 5.2.1 Performance/Calibration Model

The first model shows the system dynamics independent of the threaded parts. It is actually two models. One is a "free running" model which shows the speed control dynamics of the system when the torque station has no load except for its own friction. The other involves the existing method of measuring torque output and calibrating the torque station. In this case, a torque watch is attached to a fixture in the torque adapter and allowed to rotate freely when a torque/velocity command is given. Then the housing of the torque watch is restrained causing the device to "wind up" to a final torque value and stall the torque station. The output of the torque watch is then recorded and compared to the torque command.

#### a) Free Running Model

The most basic model of the TS system dynamics is shown in Figure 5.3. The block diagram illustrates the equations of motion for the torque station with only a disturbance torque load,  $T_D$ . This load includes the friction torque. From the block diagram, the transfer functions are as follows:

For  $T_D = V_n = 0$

$$G_1(s) = \frac{\omega_m(s)}{T_c(s)} = \frac{C_{TV}G_C G_A K_T}{J_{MF}s + (B_{MF} + G_A K_T G_T K_{TACH})} \quad (5-11)$$

For  $T_c = V_n = 0$

$$G_2(s) = \frac{\omega_m(s)}{T_D(s)} = \frac{-1}{J_{MF}s + (B_{MF} + G_A K_T G_T K_{TACH})} \quad (5-12)$$

For  $T_c = T_D = 0$

$$G_3(s) = \frac{\omega_m(s)}{V_n(s)} = \frac{-G_T G_A K_T}{J_{MF}s + (B_{MF} + G_A K_T G_T K_{TACH})} \quad (5-13)$$

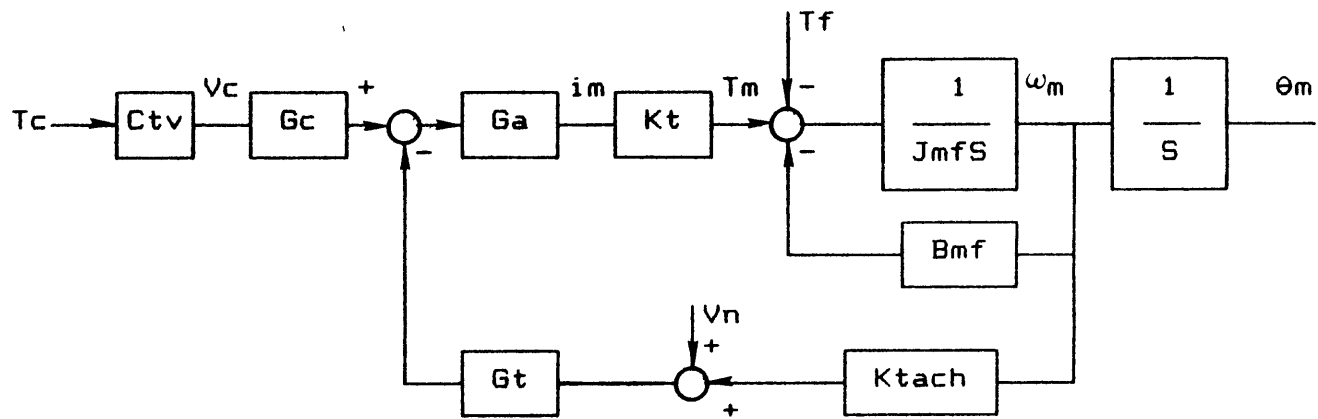


Figure 5.3 Free Running Model

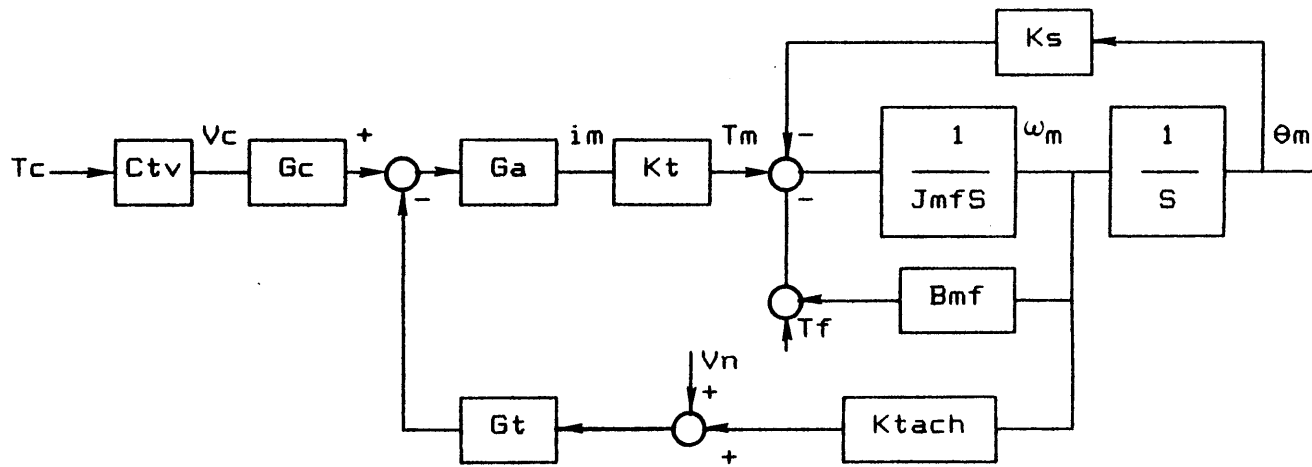


Figure 5.4 Torque Watch Windup Model

Adding a position state

$$\frac{\theta_m(s)}{\omega_m(s)} = \frac{1}{S} \quad (5-14)$$

The characteristic equation is

$$S[J_{MF}S + (B_{MF} + B_E)] = 0$$

where  $B_E = G_A K_T G_T K_{TACH}$ . The poles are

$$S_1 = 0 \quad (5-15)$$

$$S_2 = -B_T/J_{MF}$$

Here  $B_T = B_{MF} + B_E$  is the total system damping -- a sum of its "mechanical" and "electrical" parts. In the case of the torque station, the mechanical damping is negligible, which is why tach feedback is necessary.

These equations describe a proportional velocity controller. The system is inherently stable, of first order in velocity response, and has the time constant

$$\tau_m = \frac{1}{S_2} \quad (5-16)$$

Steady-state relationships are described by the following equations. The stall torque is defined as that necessary to cause the motor to stall. At stall,  $\omega=0$ , and  $T_D = T_m = T_{STALL}$ . For  $V_n = 0$

$$T_{STALL} = (C_{TV} G_C G_A K_T) T_C \quad (5-17)$$

It is desired that the motor torque be equal to the torque that is commanded. Therefore the conversion factor is chosen as



$$C_{TV} = 1/G_C G_A K_T \quad (5-18)$$

For a running condition with noise,

$$T_m = T_D = T_C - B_T \omega_m - (G_A K_T G_T) V_n \quad (5-19)$$

The steady-state velocity is

$$\omega_{ss} = \frac{1}{B_T} (T_C - T_D) - \frac{1}{K_{TACH}} V_n \quad (5-20)$$

The last term ignores the mechanical damping.

Table 5-1 shows the values for the controller gains used by the existing torque station. The first gains chosen were  $G_C$  and  $G_A$ . The available input  $V_C$  is +10 V. A maximum current of 5 amps is available. It was desired to control torque to +16 in.-oz. The following values were chosen to meet these limitations and are found from the resistance values.

$$\begin{aligned} G_A &= 7801 \text{ amps/amp} \\ G_C &= 1/10,000 \text{ amps/V} \\ C_{TV} &= 0.316 \text{ in.-oz/V} \end{aligned}$$

Once these gains are chosen, the tach feedback gain,  $G_T$ , determines the system dynamics. The existing tach feedback gain was chosen to produce a low free running speed and thus a low rundown speed during threading. The value used was

$$\begin{aligned} G_T &= 1/22.5 \text{ amps/volt} \\ (R_T &= 22.1 \Omega) \end{aligned}$$

which produces

$$|\omega_{ss}| \approx |T_C| \quad (\text{rpm, in.-oz})$$

for  $T_D = V_n = 0$ . Employing numerical values, Equations (5-17) and (5-20) become

$$T_{\text{STALL}} = T_c - 1407 V_n \quad (5-21)$$

$$\omega_{\text{SS}} = 0.947 (T_c - T_D) - 1333 V_n \quad (5-22)$$

where torque is in in.-oz, velocity in rpm and noise in volts.

The poles are located at

$$s_1 = 0$$

$$s_2 = 137.95 \text{ sec}^{-1}$$

and the time constant is  $\tau_m = 0.007 \text{ sec}$ .

#### b) Torque Watch Windup Model

The free running model can be easily extended to show the system dynamics when a torque watch is used to measure the stall torque. Windup of the torque watch causes a disturbance torque which is proportional to the angular position of the torque station. Figure 5.4 shows the modified block diagram. Writing the system equations in state space form

$$\frac{d}{dt} \begin{bmatrix} \theta_m \\ \omega_m \end{bmatrix} = \begin{bmatrix} 0 & 1 \\ -\frac{K_s}{J_{MF}} & -\frac{B_T}{J_{MF}} \end{bmatrix} \begin{bmatrix} \theta_m \\ \omega_m \end{bmatrix} + \begin{bmatrix} 0 & 0 & 0 \\ \frac{C_{TV} G_C G_A K_T}{J_{MF}} & -\frac{1}{J_{MF}} & \frac{G_A K_T G_T}{J_{MF}} \end{bmatrix} \begin{bmatrix} T_c \\ T_f \\ V_n \end{bmatrix} \quad (5-23)$$

The system now has second-order dynamics due to the "mechanical" position feedback. The stiffness of the torque watch is  $K_S$  and assumed to be linear. A torque watch with a 0-20 in.-oz range was used for torque station calibration with a stiffness of  $K_S = 3.66$  in.-z/rad (0.064 in.-oz/deg).

The characteristic equation becomes

$$s^2 + \frac{B_T}{J_{MF}} s + \frac{K_S}{J_{MF}} = 0 \quad (5-24)$$

The natural frequency is

$$\omega_n = (K_S/J_{MF})^{1/2} \quad (5-25)$$

and the damping ratio is

$$\zeta = B_T/2(K_S J_{MF})^{1/2} \quad (5-26)$$

The poles are

$$s_{1,2} = -\frac{B_T}{2J_{MF}} \pm \frac{1}{2} \left( \frac{B_T^2}{J_{MF}^2} - 4 \frac{K_S}{J_{MF}} \right)^{1/2} \quad (5-27)$$

Applying numerical values, the following quantities are found

$$\begin{aligned} s_{1,2} &= -0.36, -137.6 \quad \text{sec}^{-1} \\ \omega_n &= 7.1 \text{ rad/sec} \\ \zeta &> 1 \end{aligned}$$

The system is overdamped with a slowest time constant of  $\tau_m = 2.75$  sec. Comparison to the free running model shows that the poles have moved slightly toward each other on the real axis, but the time constant has changed a great amount.

The stall torque relation of equations (5-17) and (5-21) remains unchanged. However, the motor torque and torque watch torque differ by the magnitude of the friction torque

$$T_n = T_m - T_f \quad (5-28)$$

Calibration of the torque station for a desired net torque must include the effects of friction. Another variable that can be monitored during torque watch calibration and, more importantly, during threading is the voltage  $V_2$  in the control circuit. This voltage can be converted to motor torque,  $T_m$ , by the following conversion

$$T_m = C_{VT} V_2 \quad (5-29)$$

where  $C_{VT} = K_T/R_2$ .

#### c) Effects of Controller Parameters

A brief look back at the performance model is needed to explain the effects of the controller parameters. Threaded part mating has not yet been introduced but basic principles of TS operation can be formulated before a more complicated and nonlinear model is considered.

First, the velocity feedback gain has the most profound effect on the system dynamics. In the existing torque station it is the only gain that can be used to alter threading dynamics since all other parameters are fixed. For free running and the rundown phase of part mating, the gain controls the steady-state velocity and the time constant. A simple root locus shows that increasing the gain results in a slower steady-state velocity and a faster response, and vice-versa. However, a larger gain also makes the system more susceptible to noise. Appendix A discusses the lower limitation on tach signal reliability. To achieve a smaller velocity for a given stall torque, a poorer signal-to-noise ratio of the tach signal and a higher system noise sensitivity are necessary. In other words, performance is degraded.

For processes which produce a position-dependent load torque on the torque station, the feedback gain controls the damping and can determine whether or not overshoot occurs. The torque watch dynamics show that the system is definitely overdamped, but this may not be the case for a stiffer threaded parts system.

Another variable to consider is the torque station inertia. The magnitude of the inertia does not affect the steady-state velocity nor the stall torque, but it does determine the transient response of the velocity controller. It can also affect the damping and natural frequency in the mechanical position feedback case. A larger inertia reduces the damping and the natural frequency, and vice-versa.

A final variable to be considered is the spring constant, or "mechanical feedback gain". Increasing this constant also reduces the damping but increases the natural frequency.

Thinking of the threaded part mating process in an extremely elementary way, a controller designer could estimate the "stiffness" of the parts to be assembled, combine it in series with the estimated RCC or other device stiffness, and use this equivalent stiffness of the process in place of the torque watch stiffness to estimate the system dynamics and choose gains. Various root loci could be used to ensure that the system was overdamped. A preliminary design could be generated in this way allowing long lead-time hardware to be chosen. Then more careful modeling and simulation could be performed. This forms the first of several guidelines for generalized TS controller design guidelines presented by this thesis.

### 5.2.2 Models for Threaded Part Mating

Now that the basic operation of the controller has been discussed, the dynamics of the threaded parts are added. Both the piecewise linear and "coulomb friction spring" models presented in Chapter 3 are used. Simulation of the models is presented after both are discussed.

a) Piecewise Linear Model

Incorporation of the piecewise linear part mating model into the basic controller model is shown in Figure 5.5. The first block diagram shows rundown, and the second tightening. One set of state equations can be used to represent each phase. They are

$$\frac{d}{dt} \begin{bmatrix} \theta_m \\ \theta_t \\ \omega_m \\ \omega_t \end{bmatrix} = \begin{bmatrix} 0 & 0 & 1 & 0 \\ 0 & 0 & 0 & 1 \\ -\frac{K_p}{J_{MF}} & \frac{K_p}{J_{MF}} & -\frac{B_T}{J_{MF}} & 0 \\ \frac{K_p}{J_{TC}} & -\frac{(K_p + K_c)}{J_{TC}} & 0 & 0 \end{bmatrix} \begin{bmatrix} \theta_m \\ \theta_t \\ \omega_m \\ \omega_t \end{bmatrix} + \begin{bmatrix} 0 & 0 & 0 & 0 \\ 0 & 0 & 0 & 0 \\ \frac{C_{TV} G_C G_A K_T}{J_{MF}} & -\frac{1}{J_{MF}} & -\frac{1}{J_{MF}} & -\frac{K_T G_A G_T}{J_{MF}} \\ 0 & 0 & \frac{1}{J_{TC}} & 0 \end{bmatrix} \begin{bmatrix} T_c \\ T_f \\ T_r \\ V_n \end{bmatrix} \quad (5-30)$$

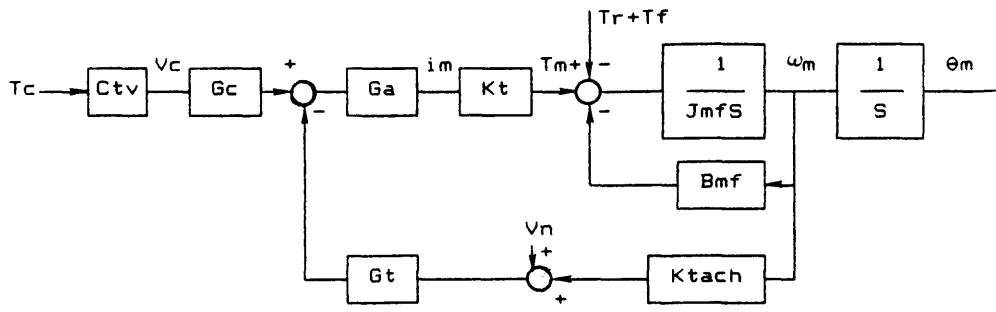
For rundown  $K_p = 0$ . For tightening,  $\theta_m = \theta_t = 0$  is at the bottoming point, and the steady-state velocity from rundown is used as an initial condition.

The output equations for motor torque, part torque, and RCC torque are

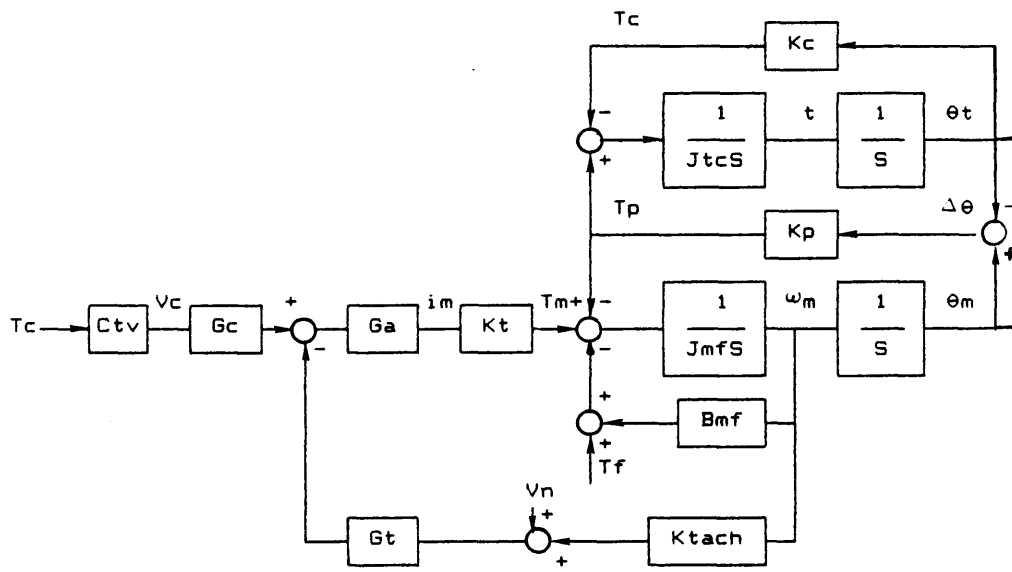
$$T_m = G_A K_T [C_{TV} G_C T_c - G_T (V_n + K_{TACH} \omega_m)] \quad (5-31)$$

$$T_p = K_p (\omega_m - \omega_T) + T_r \quad (5-32)$$

$$T_{RCC} = K_C \theta_T \quad (5-33)$$



a) Rundown Phase



b) Tightening Phase

Figure 5.5 Piecewise Linear Model

The characteristic equation is

$$s^4 + \left(\frac{B_T}{J_{MF}}\right) s^3 + \left(\frac{K_p}{J_{MF}} + \frac{K_p + K_c}{J_{TC}}\right) s^2 + \left(\frac{K_p + K_c}{J_{TC}}\right) \left(\frac{B_T}{J_{MF}}\right) s + \left(\frac{K_p K_c}{J_{MF} J_{TC}}\right) = 0 \quad (5-34)$$

Using numerical values, the poles are

$$\begin{aligned} s_1 &= -14.9 \quad ; \quad \tau_1 = 0.067 \text{ sec} \\ s_2 &= -108 \\ s_{3,4} &= -7.6 \pm 172j \end{aligned}$$

Examination of the eigenvectors and several rounds of multivariable root locus changing the stiffnesses, inertias and damping shows some insight into the nature of the dynamics. Considering the TS/parts/ARCT chain as a generalized vibratory system with damping, the dynamics consist of two modes. The first is represented by the almost undamped complex pair above. It is the oscillation of the tool/collet inertia between the RCC and "part spring". Obviously this does not happen with real parts except during rundown. The undamped mode is a consequence of the linearized model. The second mode is that represented by the two real poles above. It is the oscillation or deflection of the entire chain in series. If enough is provided, the electrical damping damps out any oscillation of this mode.

Consideration of the dynamics with this model is admittedly a gross simplification. However, as will be shown in comparison to the nonlinear model, the piecewise linear model does provide a good picture of the nature of the dynamics. The "part oscillation mode" which is an artifact of the model is shown to be unimportant. Of prime importance is the entire "chain mode", which is both observable and controllable by the TS controller. It is desired to keep this mode overdamped so that overshoot in torque in the parts will not occur.



b) Coulomb Friction Spring Model

Incorporation of the nonlinear "coulomb friction spring" (CFS) part mating model into the controller model is shown in Figure 5.6. The equations of motion become

$$\frac{d\theta_m}{dt} = \omega_m \quad (5-35)$$

$$\frac{d\theta_t}{dt} = \omega_t \quad (5-36)$$

$$\frac{d\omega_m}{dt} = \frac{1}{J_{MF}} [-A_{33}\omega_m + B_{31}T_c - T_f \operatorname{sgn}(\omega_m) - B_{34}V_n - T_p] \quad (5-37)$$

$$\frac{d\omega_t}{dt} = \frac{1}{J_{TC}} (T_p - T_{RCC}) \quad (5-38)$$

where

$$A_{33} = B_T \quad (5-39)$$

$$B_{31} = C_{TV}G_C G_A K_t \quad (5-40)$$

$$B_{34} = K_T G_A G_T \quad (5-41)$$

$$T_p = [T_r + K_p(\Delta\theta - \Delta\theta_B)] \operatorname{sgn}(\Delta\omega) \quad (5-42)$$

$$T_{RCC} = K_c \theta_t \quad (5-43)$$

$$\Delta\theta = \theta_m - \theta_t \quad (5-44)$$



$$\Delta\omega = \omega_m - \omega_t \quad (5-45)$$

The output equations for motor torque, part torque, and RCC torque are given by Equations (5-31), (5-42), and (5-43), respectively. Equations (5-35) through (5-38) are written as a series of nonlinear first order differential equations to put them in the form necessary for numerical integration. This is used for the simulations to follow.

Due to the complex nature of the nonlinear model, standard analysis methods cannot be employed. Simulations were used to evaluate the model, and show trends in parameter changes. These trends are combined with the results of the linear model to formulate a second set of controller design guidelines.

### 5.3 Simulation

Four models of TS controller operation have been formulated. These models are now simulated using the numerical values for the torque station. The three linear models were simulated using CTRL-C, a linear systems analysis software package. This software accepts linear system descriptions in the standard state space form

$$\begin{aligned} \underline{\dot{X}} &= \underline{A}\underline{X} + \underline{B}\underline{u} \\ \underline{Y} &= \underline{C}\underline{X} + \underline{D}\underline{u} \end{aligned}$$

where

$\underline{X}$  = state vector  
 $\underline{u}$  = input vector  
 $\underline{Y}$  = output vector

The time history of the input vector must be supplied along with the initial state vector. A time step must also be chosen with enough resolution to show the system dynamics, and not cause numerical integration errors. The nonlinear equations were simulated using SIMNON, a software package which accepts systems described as a series of nonlinear first order differential equations. The inputs, initial states, and time must also be chosen.

All simulations use a torque command of  $T_c = 10$  in.-oz, which is the nominal value of the wheel assembly torque.

### 5.3.1 Free Running Model Simulation

Shown in Figure 5.7 is the response to a step input in torque command. The initial conditions are all zero. A first order response is seen with a time constant of 7 msec. The effect of the disturbance torque is shown. The response time is not altered but the steady-state speed is reduced. The steady-state motor torque,  $T_m$ , is equal to the disturbance torque,  $T_D$ , which includes friction and any load. Addition of electrical noise decreases the steady-state speed if it adds to the tach voltage, and vice-versa. For different torque commands, the steady-state velocity varies according to equation (5-22).

### 5.3.2 Torque Watch Windup Simulation

Figure 5.8 shows the system response for the torque watch windup model. A friction torque of 1.25 in.-oz is used. The initial conditions are  $\theta = 0$  and  $\omega = \omega_{ss}$ . The latter is the steady-state free running velocity with the given torque command and friction torque. Note that the final torque applied to the torque watch is the net output torque of the TS. Although the final internal torque of the motor is equal to the command, friction subtracts from this torque to produce the net output. Therefore, an amount equal to the friction torque must be added to the desired output torque to form the torque command.

### 5.3.3 Piecewise Linear Threading Model Simulation

Shown in Figure 5.9 is the result of a rundown simulation using the piecewise linear model. The initial conditions were all zero. A step input in torque command was applied. The disturbance torques used were 1.0 in.-oz for friction torque and 0.25 in.-oz for rundown torque. The figure shows that a steady-state TS velocity is achieved. Oscillation of the tool/collet inertia is shown. Note that this oscillation has a frequency and magnitude that make it difficult to observe visually. It does not have an appreciable

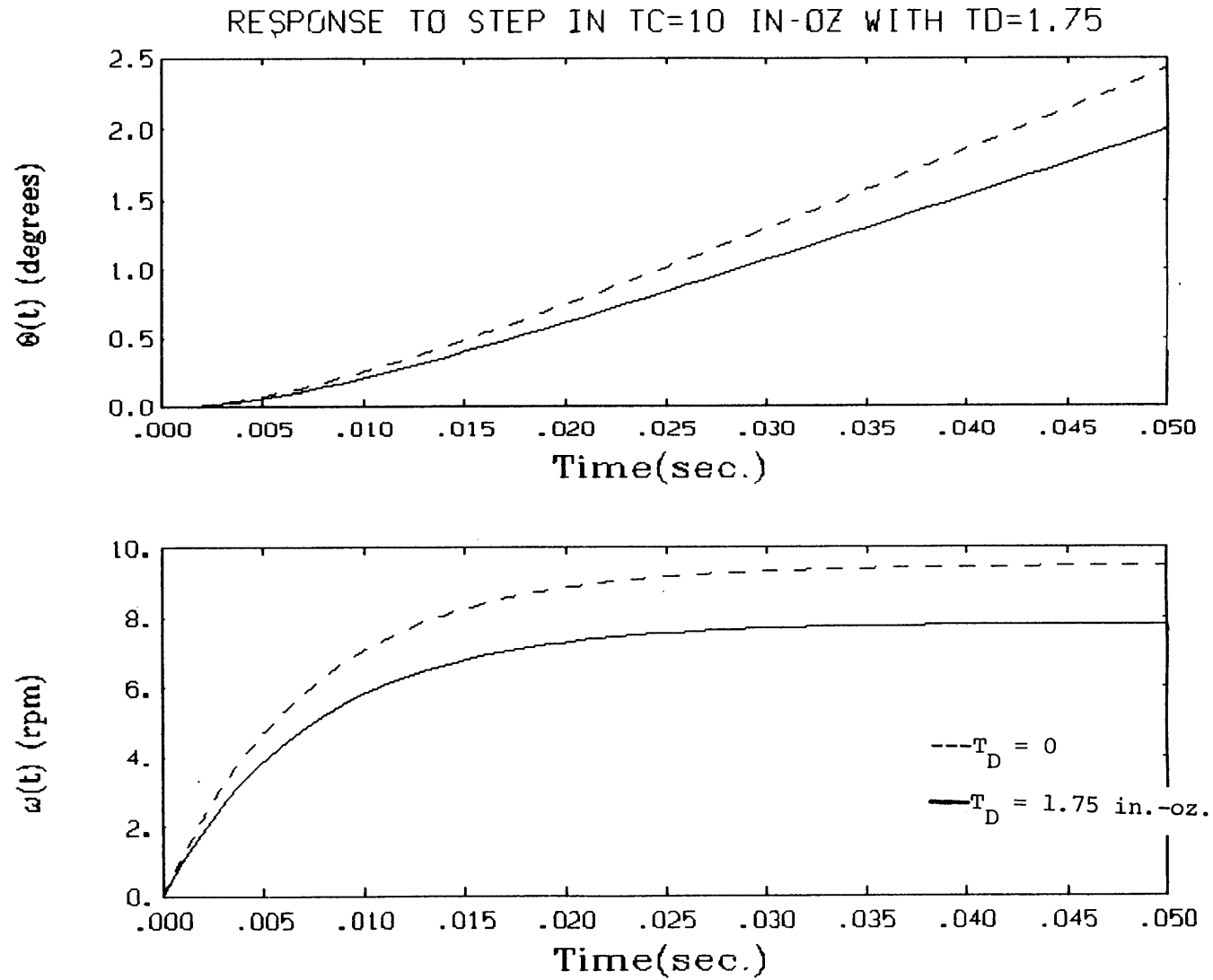


Figure 5.7 Free Running Simulation

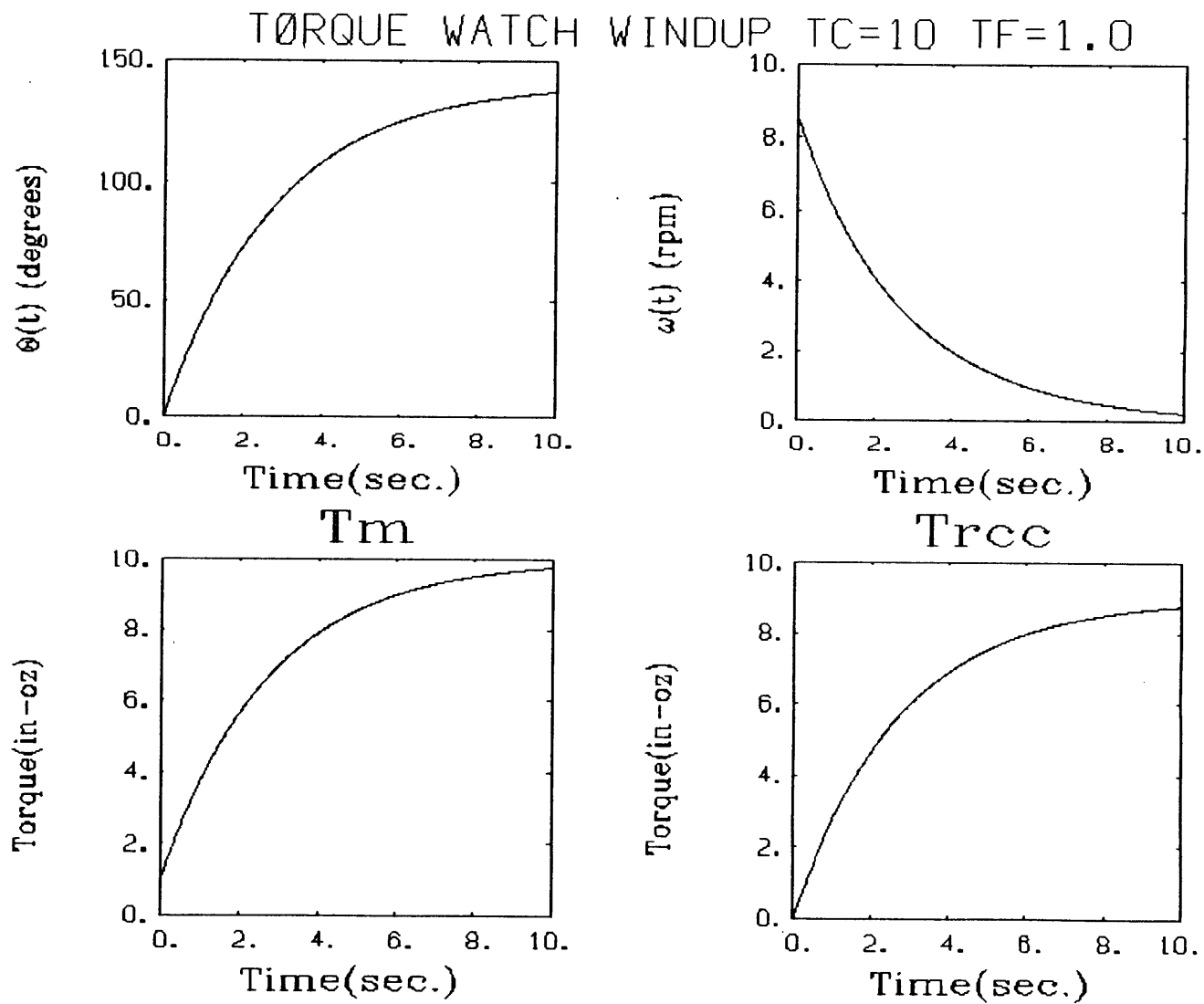


Figure 5.8 Torque Watch Windup Simulation

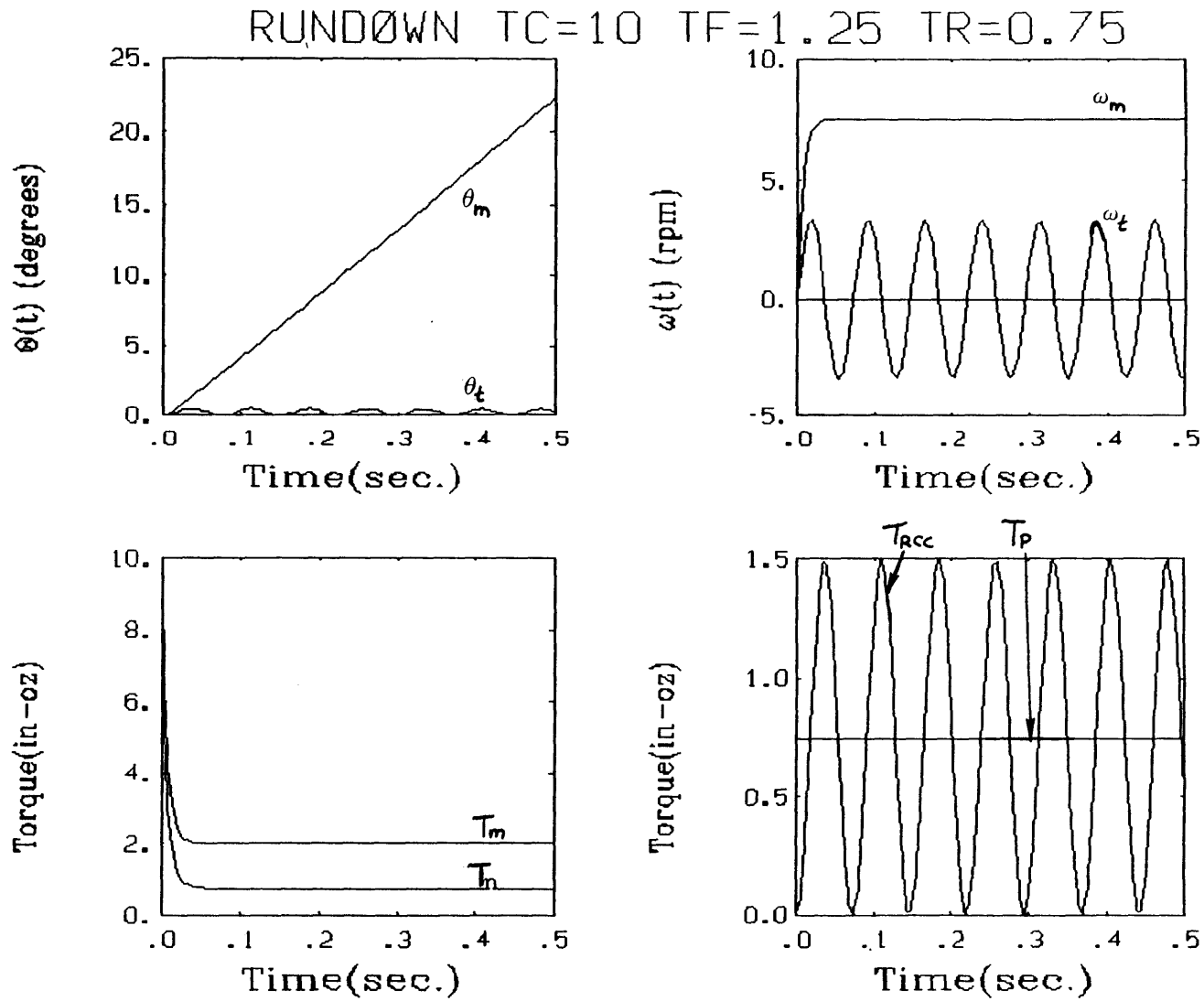


Figure 5.9 Rundown Simulation- Linear Model

effect on the motion of the torque station inertia. The part torque is equal to the rundown torque and the RCC torque oscillates about this value. Its peak-to-peak magnitude is twice that of the rundown torque. The steady-state motor torque is equal to the sum of the friction and rundown torque. The net output torque is equal to the part torque.

Figure 5.10 shows the result of a tightening simulation. The same values of friction and rundown torque were used. Examination of the response of the system shows an overdamped second-order response with oscillatory dynamics superimposed upon it. This is the result indicated by the system poles from Equation (5-34). Of most interest is the general form of the response.

The superimposed oscillation is a result of the simplification of the model. In the simulation, periods of relative separation of the parts ( $\Delta\omega < 0$ ) are shown. This is due to the parts acting as a spring. For real parts this does not happen. The parts stick together as they are tightened and a reversal of applied torque is required to separate them. This may not be the complete reversal of the CFS model, though.

#### 5.3.4 Coulomb Friction Spring Model Simulation

Equations (5-35) through (5-45) were used to perform a simulation of the nonlinear CFS part mating model. Figure 5.11 shows the results for the tightening phase. This phase is where the model differs from the linear models and is of prime importance to this thesis. Examination of the results shows that the response is similar to the piecewise linear simulation without the superimposed oscillation of the tool/collet inertia. The plot of the part torque shows negative spikes. These spikes correspond to instances of the parts attempting to separate. Occurrence of these spikes is lessened by using a smaller time step in the simulation. For an extremely small time increment with a high precision machine, these spikes may disappear. They do point out, though, that the system dynamics can cause a net torque which would attempt to decrease instead of increase  $\Delta\theta$ . In static manual assembly, only an increase is seen. Also, there are no dynamics of the stationary part. Thus the assumption that the TVA curve can be reflected about the  $\Delta\theta$  axis should be investigated further.



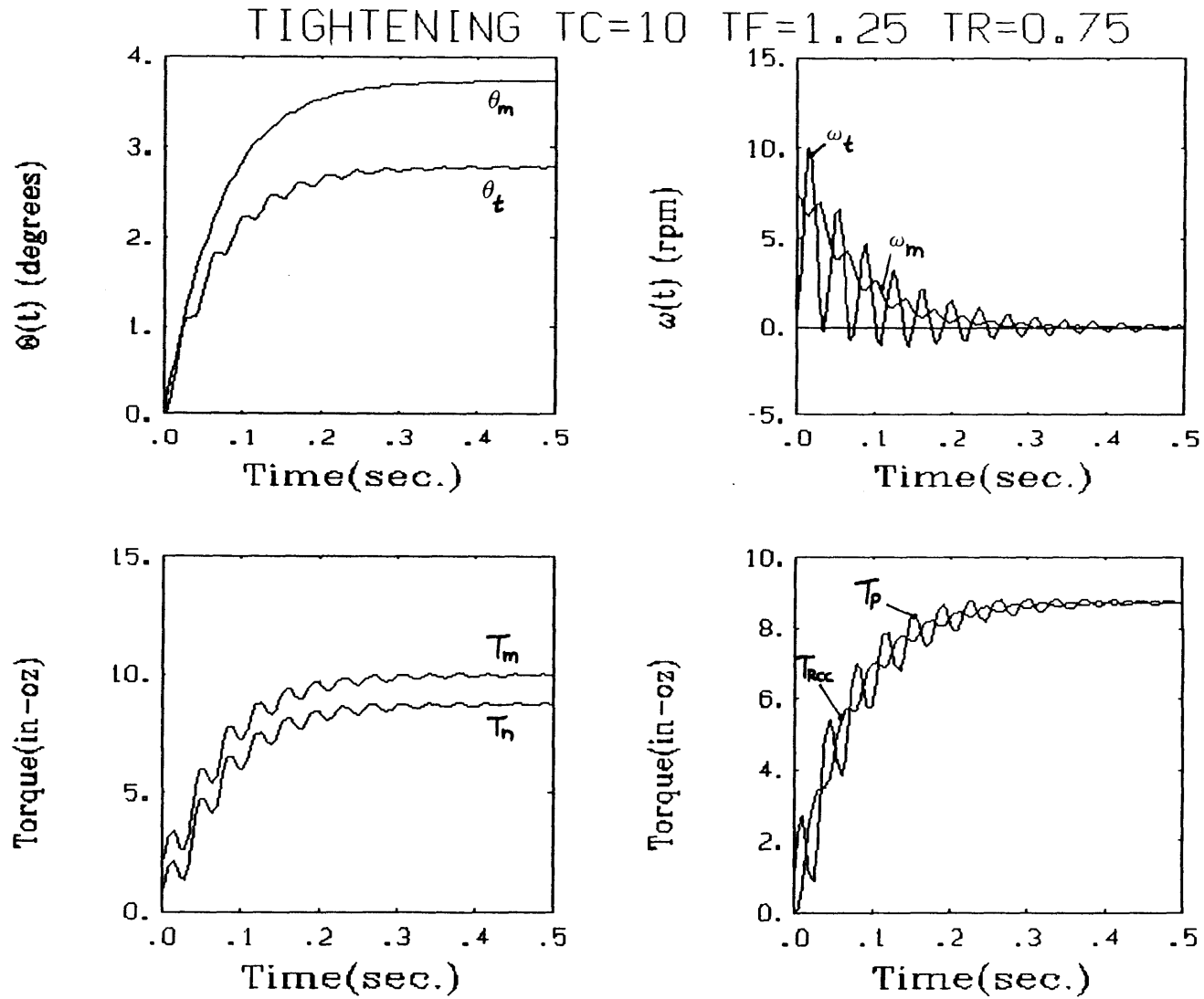


Figure 5.10 Tightening Simulation- Linear Model

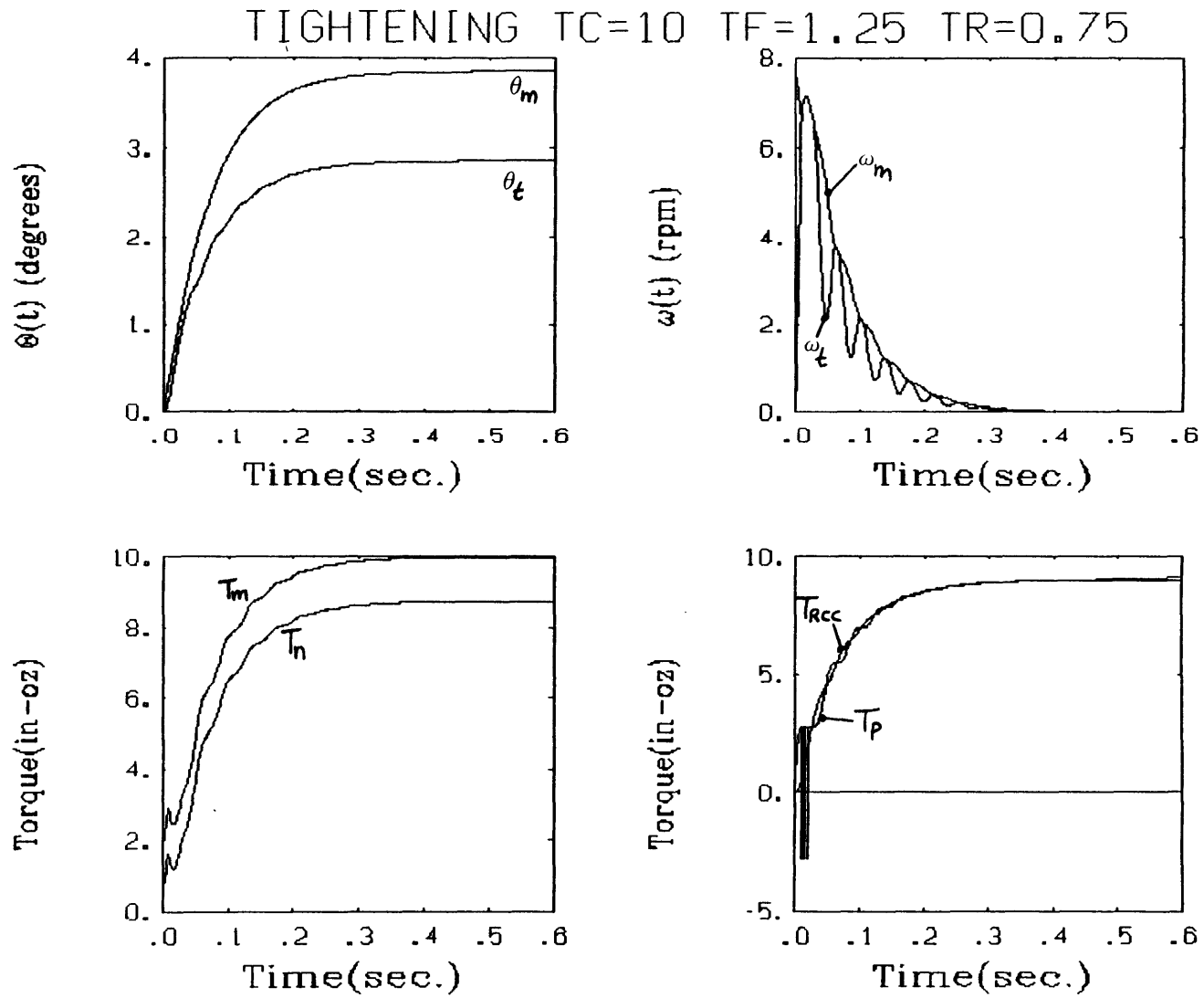


Figure 5.11 Tightening Simulation- Nonlinear Model

Figure 5.12 shows a comparison of the linear and nonlinear part mating models. The plot of the motor torque is shown for both simulations. The plot is enlarged from Figures 5.10 and 5.11 to show the details of the curves more clearly. Note that the linear model has a general shape that corresponds to that of the nonlinear model. The CFS model does not exhibit oscillations but its response is also not as smooth as a typical overdamped second order response. Several transitions or bumps are seen. These correspond to the beginning of periods where the inertias are traveling together ( $\Delta\omega = 0$ ).

The same net torque result as the torque watch simulation is also shown. The torque delivered to the parts is that of the motor minus the friction torque. For the linear model, the final torque in the parts and the RCC is equal to the final net torque, or the torque in all the elements of the system series chain is equal. Thus the steady-state values from this model do not show torque overshoot in the parts. The transient dynamics could include overshoot, through, and should be examined. The non-linear model does show steady-state overshoot in part torque as well as transient overshoot. This is shown in the later section on variations in parameters.

#### 5.4 Experimental Results

Several tests were performed that paralleled the modeling and simulation that has been presented. The speed control and output torque control performance was tested for the entire range of operation of the torque station. These tests were to measure the performance of the torque controller for various torque commands, and to find out whether or not the hardware performs as designed and modeled. It was also desired to evaluate the torque watch windup test as a viable calibration for the hardware. Once these performance tests were completed, data were collected during actual threaded part assembly operations. These experiments were used to evaluate the performance of the torque station for threaded part assembly and to make a comparison of experimental and simulated results.

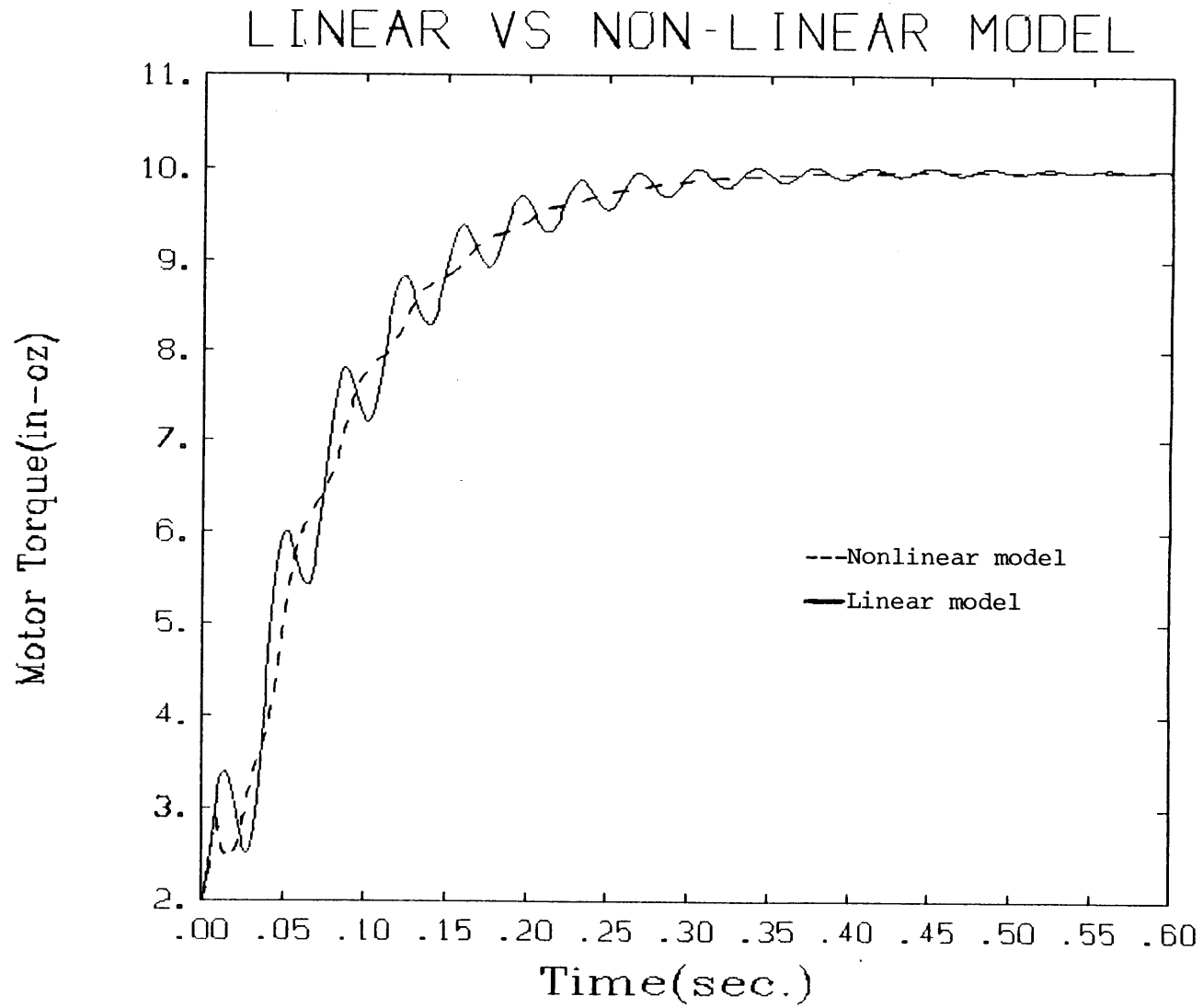


Figure 5.12 Comparison of Simulated Results.

#### 5.4.1 Steady-State Speed Test

The free running steady-state speed of the torque station was measured by sampling the output of the tachometer. This was performed without any load on the torque station except for its internal friction. Sampling was performed using software written to be compatible to the assembly cell's DAPL software. Sampling was performed at 20 Hz for 25 seconds. The test was performed for torque commands of  $T_c = 0-20$  in.-oz in 2 in.-oz increments.

The corresponding steady-state velocity range is 0-19 rpm, and the tach output voltage that corresponds to this range is 0-15 mV. Since this is such a small signal and the resolution of the A/D converter used is 4.8 mV (12 bits), the tach signal must be amplified and filtered. The latter was found to be desirable when the assembly cell was originally constructed. A low pass filter with a gain of 100 and a 50 msec time constant was used. From the tach gain, filter gain, and D/A resolution, a resolution of 0.1 rpm was found.

Figure 5.13 shows the result of averaging the data for each torque command and converting to units of velocity. Also shown (by the solid line) is the calculated value for the steady-state velocity with a friction torque of 1.25 in.-oz. The results show good correlation for torque commands above 6 in.-oz. Below this level the performance is degraded. This is due primarily to friction which is variable at low speeds. Since the purpose of the speed control function of the controller is to limit the rundown speed during threading, and not maintain an exact value, the measured performance is considered to be satisfactory. Some improvement is necessary for lower torque commands but this is limited by the internal friction of the torque station.

#### 5.4.2 Torque Watch Stall Torque Test

The torque watch windup test that was described in the modeling section was used to measure the torque station output torque for various torque commands. Measurements were made for torque commands of 0-20 in.-oz in 1 in.-oz increments. A torque watch with a 0-5 in.-oz range was used for  $T_c = 0$  to 9 in.-oz to improve low torque measurement. The torque watch described in the model (0-20 in.-oz range) was used for  $T_c = 5-20$  in.-oz. The overlap of data was used to compare results with different spring rates, and to compare the torque watches. Several measurements were made for each torque command and the values averaged. Figure 5.14 shows the plotted data. The solid line is the calculated value for a friction torque of 1.25 in.-oz.

Measured Velocity vs Torque Command  
 $M/T \ Gt=1/22.5$

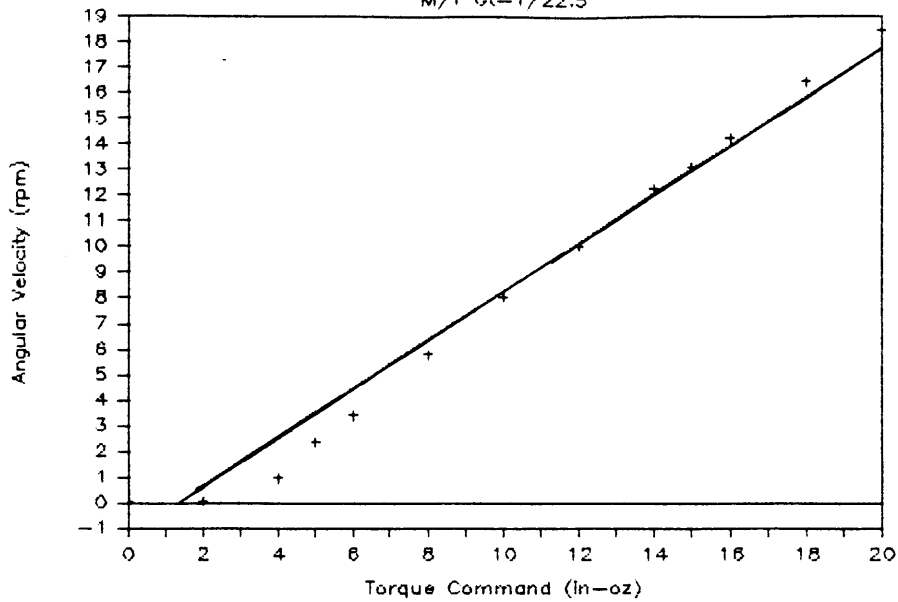


Figure 5.13 Free Running Velocity Test Results

Actual Torque vs Commanded Torque  
 $M/T \ Gt=1/22.5$

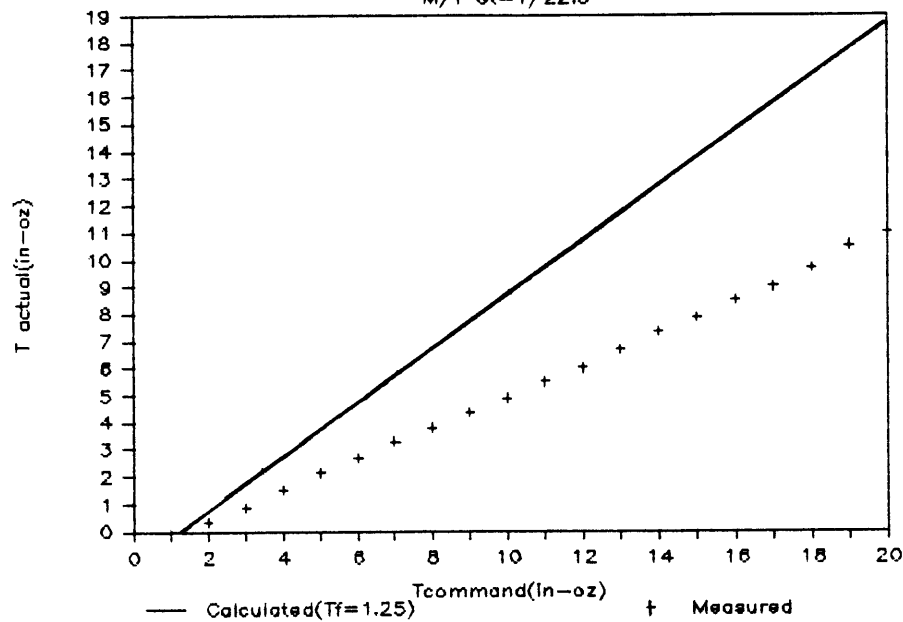


Figure 5.14 Stall Torque Test Results

It is obvious that the desired output torque is not achieved. The experimental data is reasonably linear, though. A slope of 0.59 in.-oz/ in.-oz is found for a linear fit to the data. This compares to the calculated slope of 1.0 in.-oz/in.-oz. Clearly something is wrong. The next experiment is used to eliminate one possibility for why this is so.

#### 5.4.3 Motor Torque Test

Since the stall torque test revealed undesirable TS performance, the test was repeated measuring the motor torque,  $T_m$ , as well as the output torque. The motor torque is measured by measuring the current feedback voltage,  $V_2$ , and the current,  $i_m$ , through the motor. Equation (5-29) shows the proportionality between  $V_2$ ,  $i_m$ , and  $T_m$ . Before the experiment was performed the conversion from  $V_2$  to  $i_m$  was calibrated using an ammeter to measure the current. Conversion from  $i_m$  to the motor torque used the vendor's quoted torque constant of the motor. For static tests, the ammeter was used to measure current and for dynamic tests,  $V_2$  was read by the assembly cell computer and A/D converter.

The results of the test are shown in Figure 5.15. Both the motor and output torques are shown. The offset between the torques is that lost in the torque station, the friction torque. The figure shows that there is a good correlation between the motor torque measured with  $i_m$ , or  $V_2$ , and the actual output torque. A linear fit to the motor torque curve gives a slope of 0.55 in.-oz/in.-oz. This shows that the proper current is not being maintained by the current feedback loop and amplifier, and that the conversion of current to torque by the motor is not the reason for the undesirable output torque vs torque command that was observed.

The test also reveals that measurement of  $V_2$  allows the output torque of the torque station to be estimated at least to within the level of uncertainty in friction torque. This is important in remotely monitoring the motor and output torques during the threading process when a torque watch cannot be used. The feedback voltage also monitors the performance of the control circuit. Since the assembly cell is sealed off from the outside environment during normal operation, the viability of measurements such as this are critical to process monitoring.

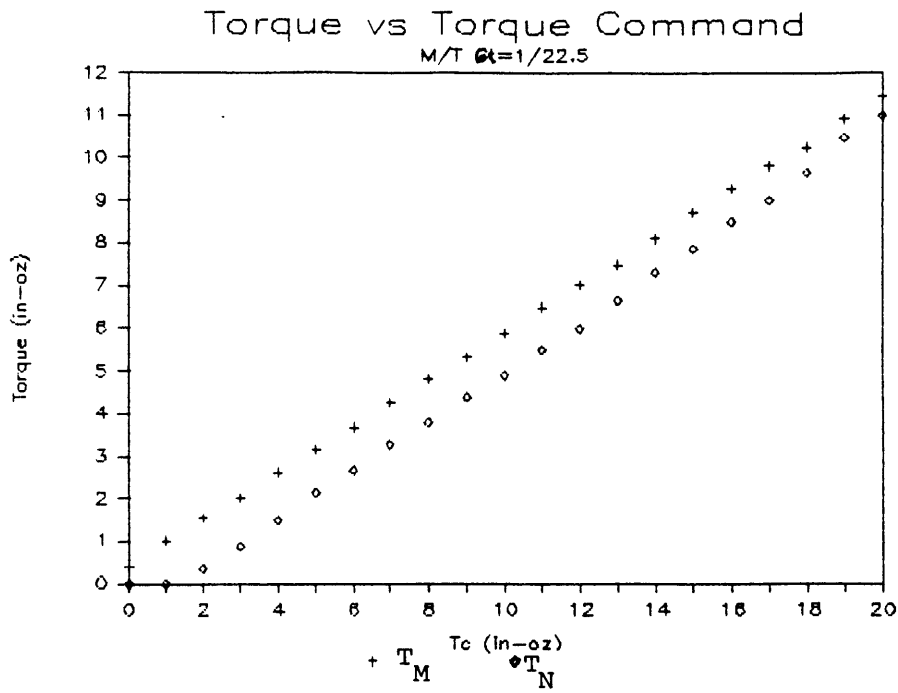


Figure 5.15 Motor Torque and Net Torque

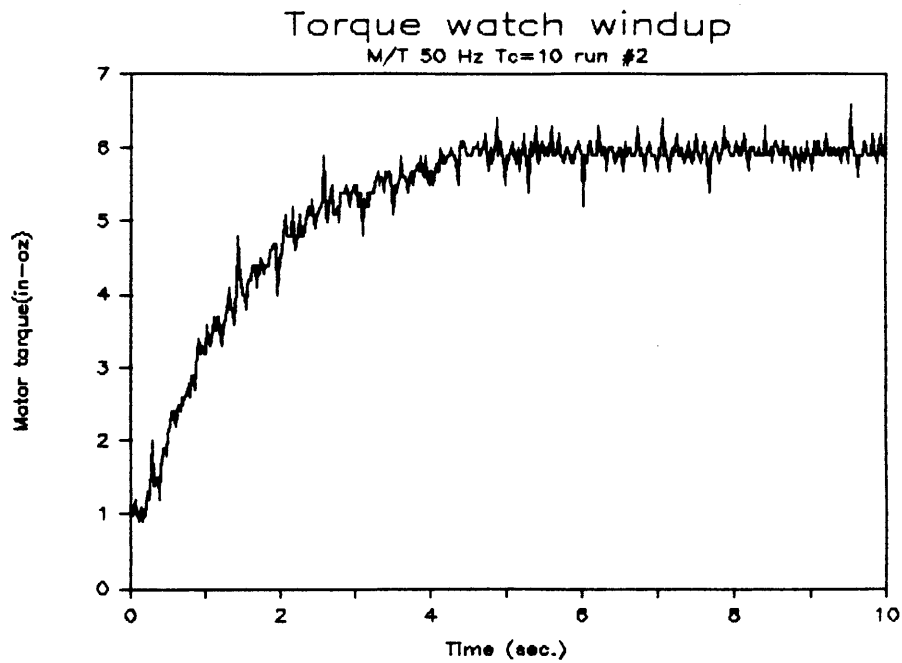


Figure 5.16 Torque Watch Windup Transient Response-  $T_m$



Figure 5.16 shows data collected for  $T_m$  during the torque watch windup test. Data were collected at a 50 Hz sampling rate, and converted to motor torque in software. Torque commands of 10 and 16 in.-oz were used. The latter was used to compare the dynamics for different torque commands and to produce a motor torque closer to the desired 10 in.-oz value. This larger command was also employed in the threading experiments that follow.

#### 5.4.4 RCC Stiffness Test/Deflection Sensor Apparatus

The assembly cell RCC has five degrees of freedom -- X and Y translation, and  $\theta_x$ ,  $\theta_y$ , and  $\theta_z$  rotation. It is rigid along the sixth degree of freedom -- Z translation. To measure the stiffness of the RCC in torsion about the Z or thread axis, a relationship must be defined between deflection and applied torque. Since the RCC is only instrumented for X and Y translation measurements, a sensor apparatus was designed to measure angular deflection of the RCC. The apparatus is shown in Figure 5.17. A Kaman Sciences Corp. displacement measurement transducer was installed in a plexiglass housing which was fixed to the robot arm above the RCC. This was the stationary or ground side of the apparatus. The transducer is a noncontacting eddy current proximity sensor. It requires a nonmagnetic target for operation. This target was made from a 1" x 1" x 0.25" block of aluminum. The target was fixed to the outside of the tool changing collet assembly, and was the moving, or deflecting, side of the apparatus. Adjustments were provided so that the gap between the sensor and the target could be properly adjusted. It is necessary to keep the faces parallel to within 15°. The width of the gap was approximately 0.080" for the free state of the RCC.

The principle of operation of the apparatus is to measure the angular deflection of the RCC as a linear displacement at a known radius. The angle involved is less than 3° so that the errors introduced by this approach are small. A noncontacting sensor was chosen so that the dynamics of the RCC were not altered and that no torque was exerted by the measurement itself. Another advantage was that the sensor output, once calibrated, provides a voltage signal proportional to the gap between the sensor and target. Thus, dynamic measurements of deflection could be made during the threading process.

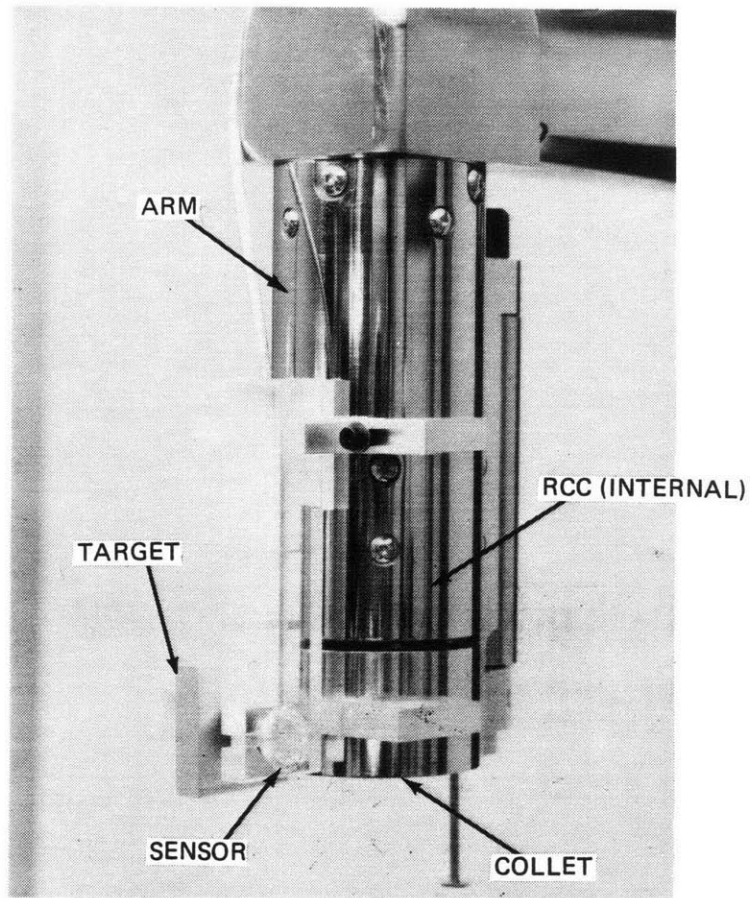


Figure 5.17. RCC Deflection Apparatus.

Measurement of the stiffness proved to be a difficult task. The sensor apparatus requires that a pure torque be delivered to the collet assembly to deflect the RCC. Attaching a torque watch or other torque measuring device to the collet is not feasible because there is no way to apply only torque and no translation by hand. The only feasible way of applying a pure moment was to put a tool in the collet and grip a fixture in the torque station. This provided a rigid link between the torque station and the RCC so that only RCC angular deflection would result from applied torque. A drawback of this approach is that the motor must be used to apply the torque and the motor torque is contaminated by friction. It was not possible to disassemble the motor from the TS and apply torque with a torque watch through the motor bearings.

The procedure used was to grip a fixture in the torque station and apply torque using a torque command from the TS controller. Since overshoot and friction were of concern, torque was applied starting from a zero torque command and increasing in 1 in.-oz increments. Once the final torque was reached, the torque command was decreased in 1 in.-oz increments back to zero. This reversal was necessary to remove any direction dependency on friction. The results of one run are shown in Figure 5.18. The arrows indicate the direction of the test. A hysteresis effect due to friction is seen. The torque axis of the plot was formed by converting the torque commands to actual torque using the data from the stall torque test (Figure 5.14).

Several runs were performed. The stiffness was found by applying a linear fit to the deflection vs torque data. The slopes for the forward and reverse directions were averaged for each run, and the result averaged with that of the other runs. An average value of  $K_C = 180$  in.-oz/rad (3.14 in.-oz/deg) was found. Variations in the slopes from 161 to 206 in.-oz/rad were found. The average value was used in the previous simulations that were shown.

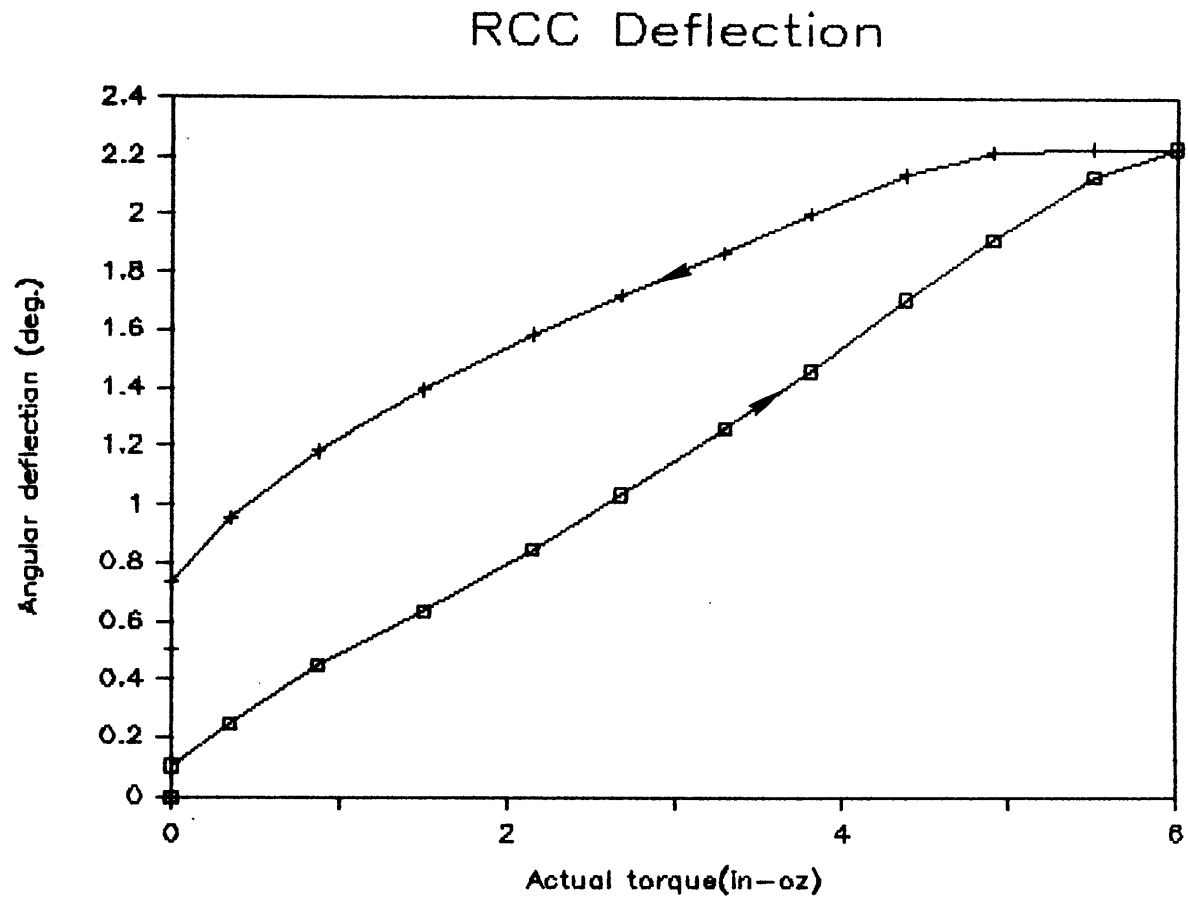


Figure 5.18 Results of RCC Stiffness Test

#### 5.4.5 Threaded Part Mating Tests

The test of most interest to this thesis was a measurement of the threaded part mating process controlled by the TS control system. Data was collected during actual shaft and thrust plate assembly using the assembly procedure described earlier. The simulated results showed plots for all the torque, position, and velocity variables involved. Unfortunately, sensors to provide experimental results for all of these variables were not available. A good representation of the process was found, though, by measuring the motor torque,  $T_m$ , and the deflection of the RCC,  $\Delta\theta_t$ . Since  $\Delta\theta_t$  is proportional to RCC torque, an indication of torque on either side of the part mating process is provided. The output of the tach was unsuitable for velocity data since its required filtering masked the part mating transient.

Software compatible with the DAPL software was written to simultaneously sample the motor torque and RCC deflection sensors. A sampling rate of 100 Hz for each channel was used. Results were found using the torque command of  $T_c = 10$  in.-oz. An input of  $T_c = 16$  in.-oz was also used to compare the dynamics of different torque commands and to provide a motor torque closer to the desired value. Data was collected during the rundown phase as well as during the tightening transient.

Figure 5.19 shows the results for a torque command of 10 in.-oz. Rundown and tightening are plotted for the motor torque and RCC deflection. The tightening transient also includes the final portion of rundown and the steady-state torque level and deflection when the motor stalls. Note that oscillation during rundown varies.

The final rundown portion and deflection transient are shown for two different sets of parts in Figure 5.20. Note that the deflection transient is similar but that one set of parts has more oscillation of the tool/collet during rundown than the other. The parts used in the greater oscillation case were those used for assembly cell testing and robot teaching, and may have been somewhat worn. The second set of parts was closer in quality to those used for actual assemblies.

Figure 5.21 shows a plot of both the measured variables, with a grid to compare the time correlation of the transients. Note that there appears to be a small increase in motor torque and then a brief plateau as bottoming occurs. The steady-state values of the motor torque and RCC deflection are reached at approximately the same time.

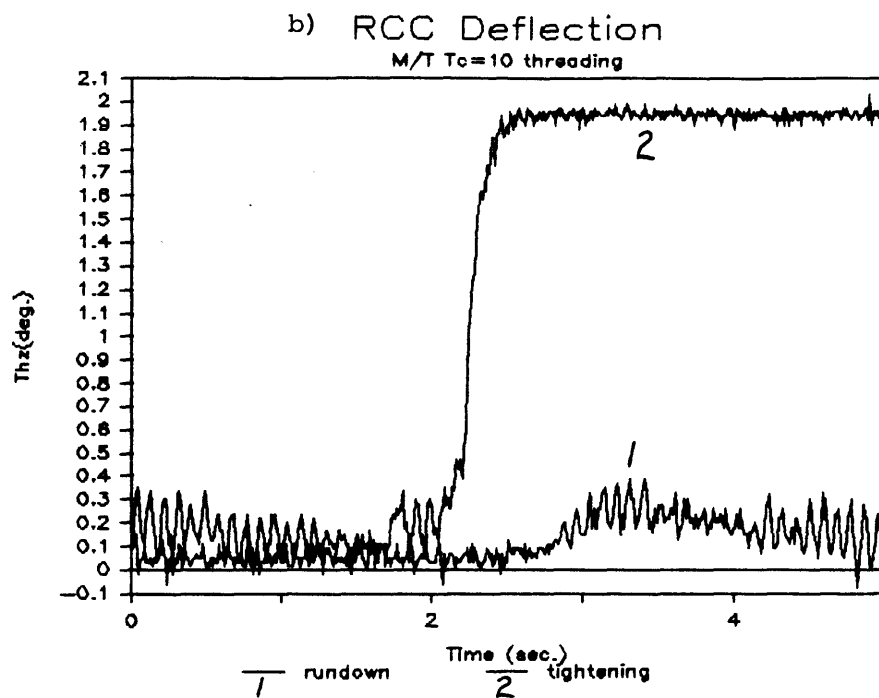
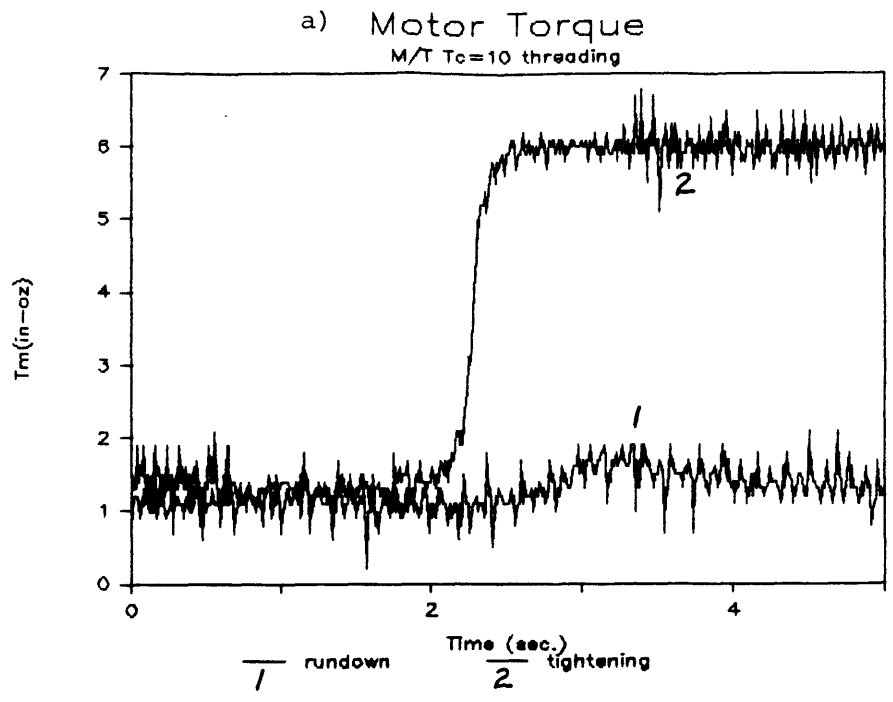
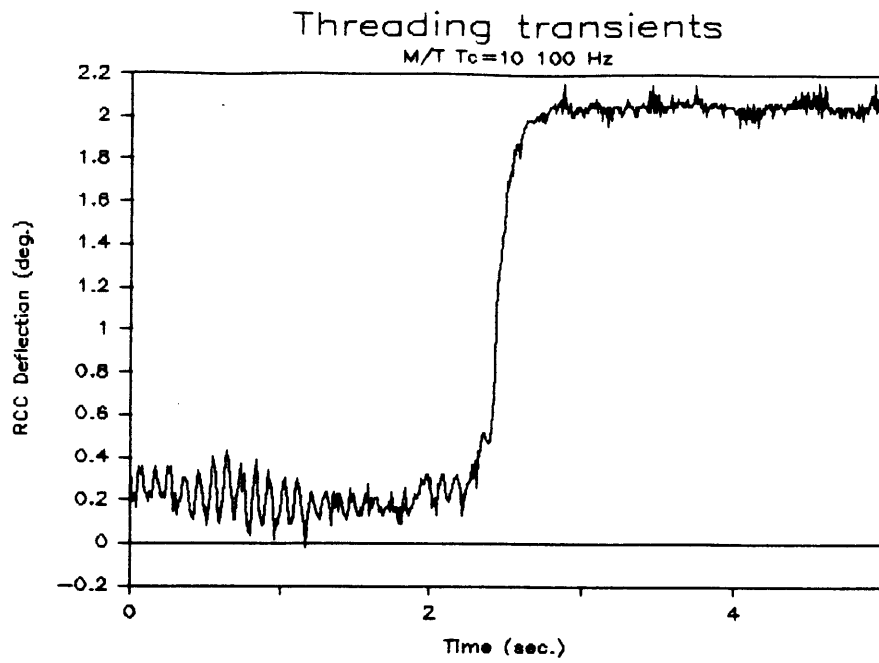
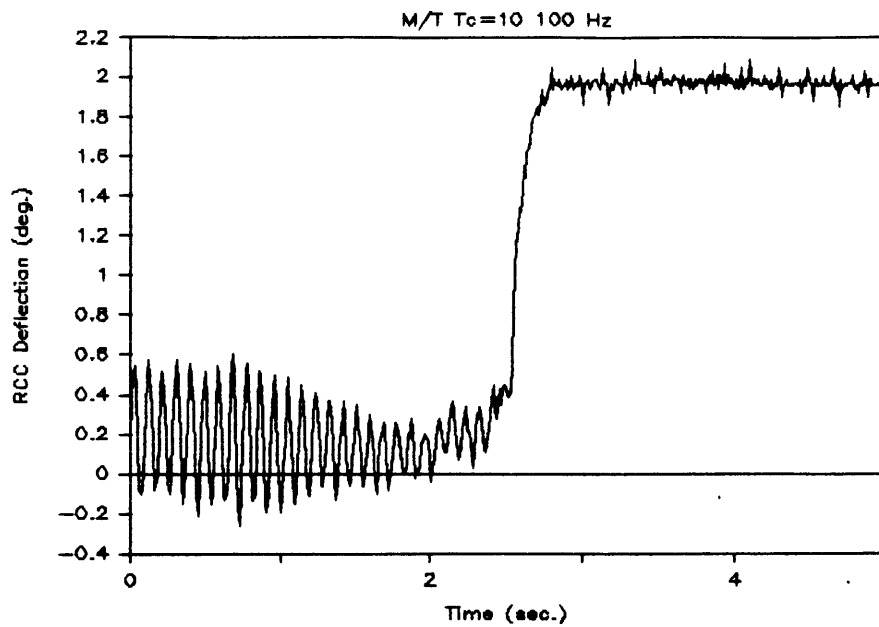


Figure 5.19 Measured Transients for Threading Test



a) New Parts



b) Old Parts

Figure 5.20 Comparison of RCC/Tool/Collet Oscillation for Different Sets of Parts

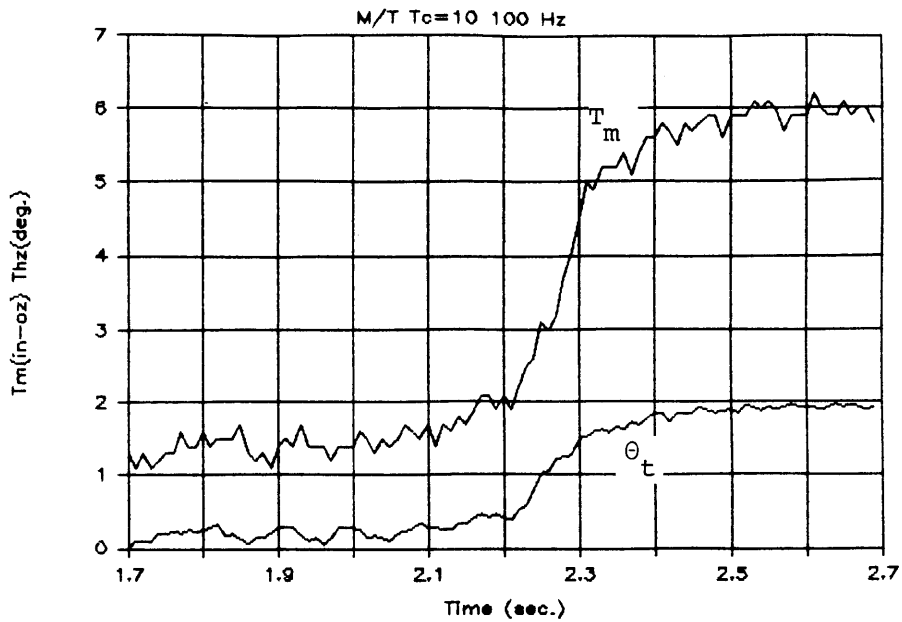


Figure 5.21 Time Correlation of Motor Torque and RCC Deflection during Tightening

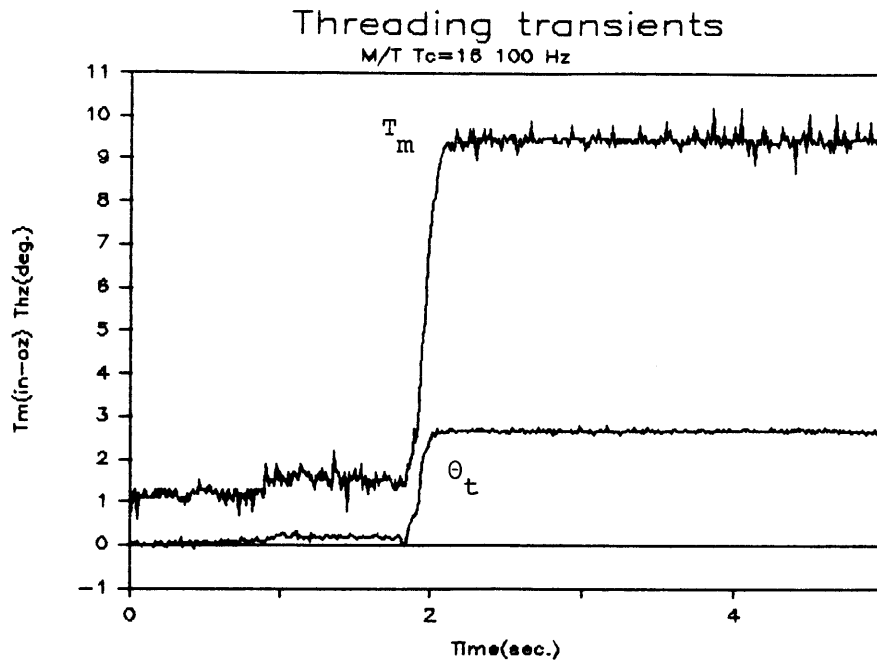


Figure 5.22 Measured Transients for Threading Test with increased command of T<sub>c</sub> = 16 in.-oz



The test was also run for a torque command of  $T_c = 16$  in.-oz. The results are shown in Figure 5.22. In several runs that were done, there appeared to be less oscillation of the tool/collet during rundown.

The results for the two different torque commands are shown in Figure 5.23. An increased torque command yields similar dynamics but a higher torque level and deflection, which is expected. The higher torque levels show a slightly sharper rise but not by much.

#### 5.4.6 Comparison to Simulated Results

To evaluate the modeling, analysis, and simulation that was done, a comparison was made between the simulated and measured results. Figure 5.24 shows a comparison between the motor torque variable for the nonlinear simulation, and measured results for 10 and 16 in.-oz torque commands. The sample comparison is made for the deflection variable and is shown in Figure 5.25.

The results correlate fairly well. The rise times of the transients are close and some of the curve details are seen. This is especially true for the motor torque for  $T_c = 16$ , and the nonlinear  $T_c = 10$ . Because of this correlation, the nonlinear model was judged to be reasonably accurate for the parts and torque controller hardware used in this thesis. The discrepancy between torque command and final output torque is a fault of the control hardware and is the subject of the next section.

### 5.5 Evaluation of Performance

The performance of the torque station with regard to threaded part assembly is now evaluated using the simulated and experimental results.

#### 5.5.1 General Performance

All of the phases of threaded part mating are performed by the assembly cell. The accuracy of the XYZ positioning of the robot and the alignment capabilities of the RCC ensure that initial placement of the parts is made and that the threads are started properly. Rundown speed is controlled by the torque station. A smooth transition is made between rundown and tightening at

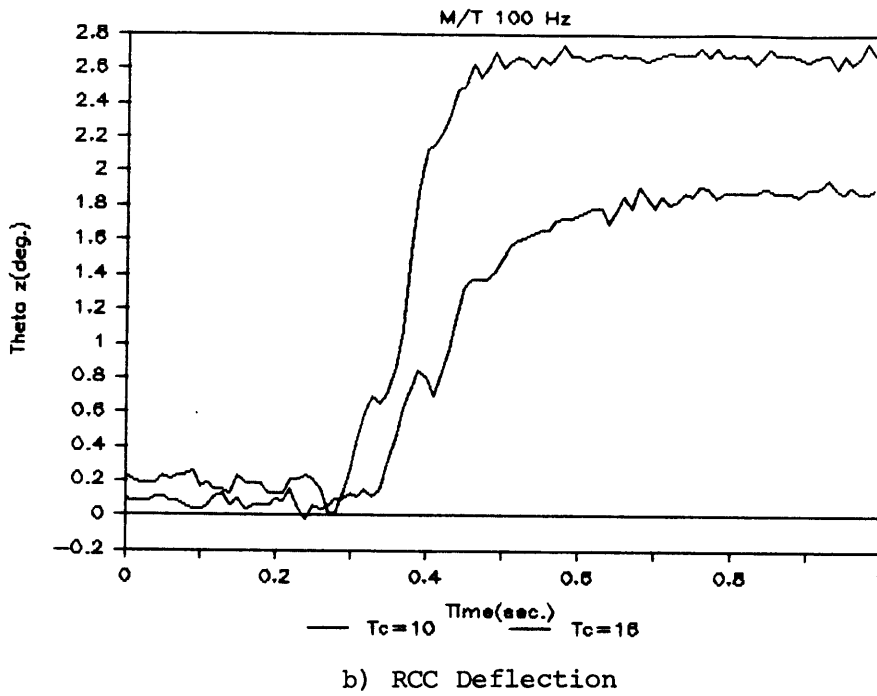
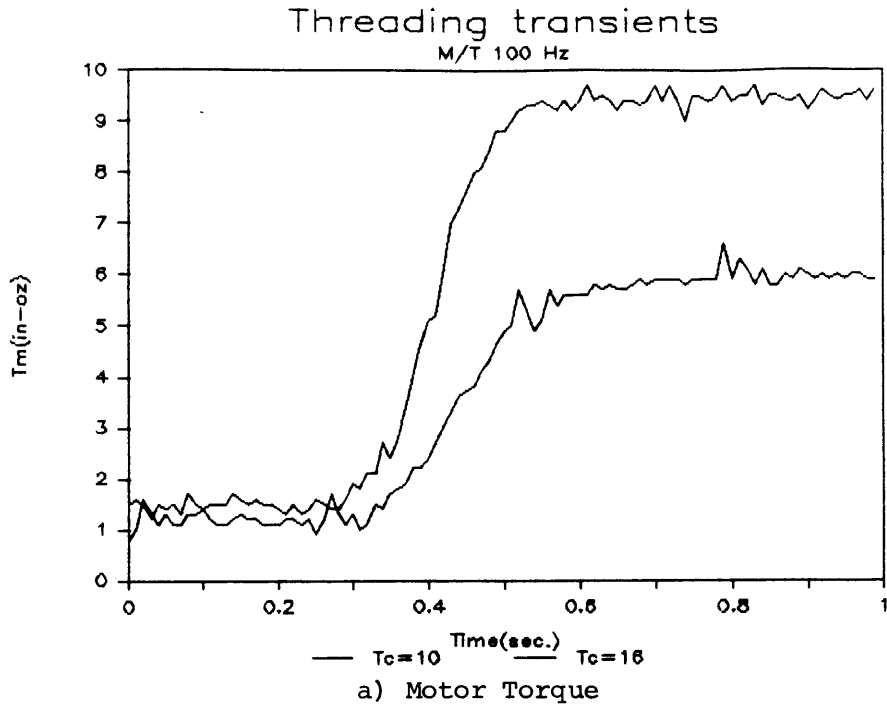


Figure 5.23 Comparison of Measured Tightening Responses for  $T_c = 10$  in.-oz and  $T_c = 16$  in.-oz

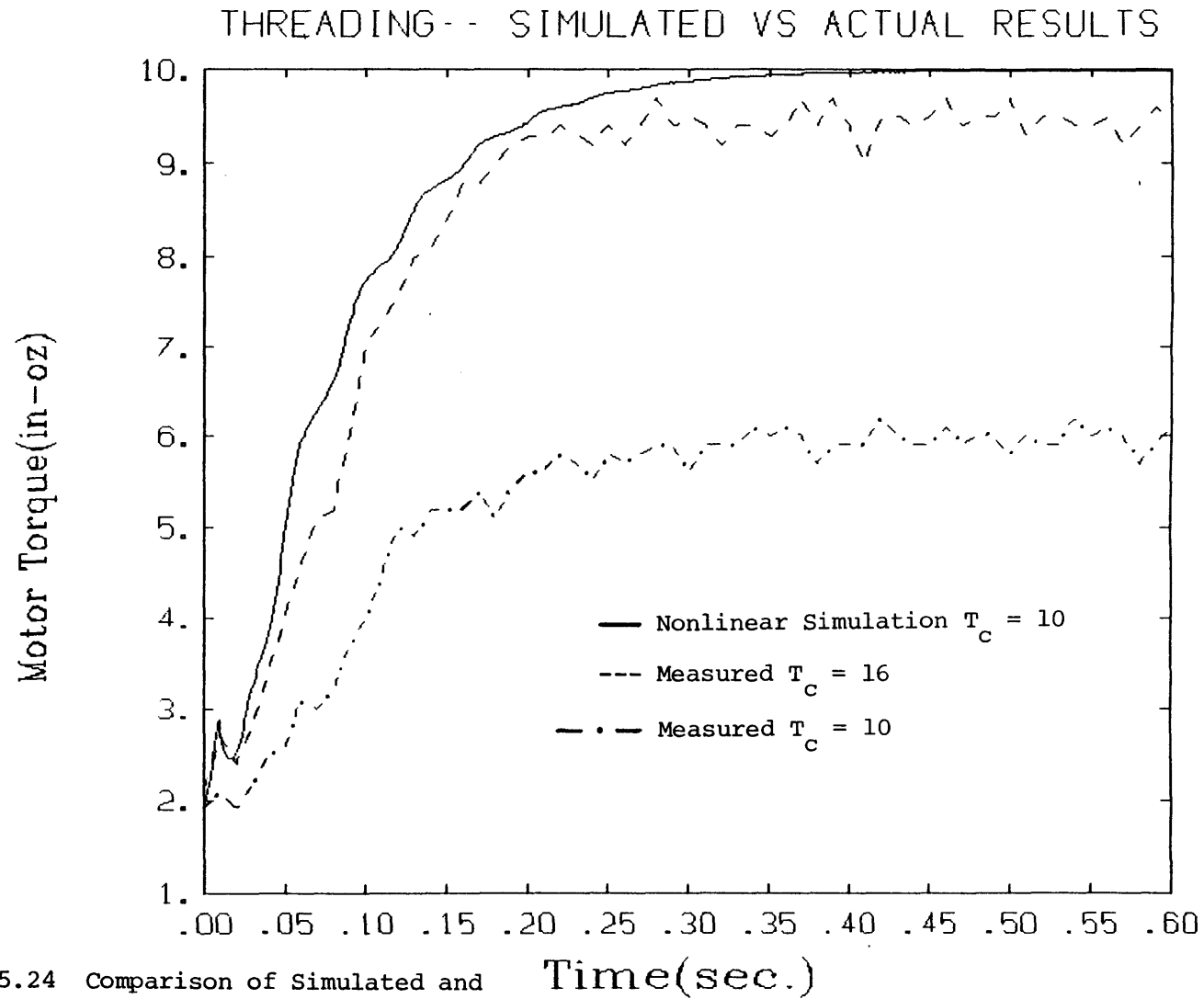


Figure 5.24 Comparison of Simulated and Measured Results  
Motor Torque

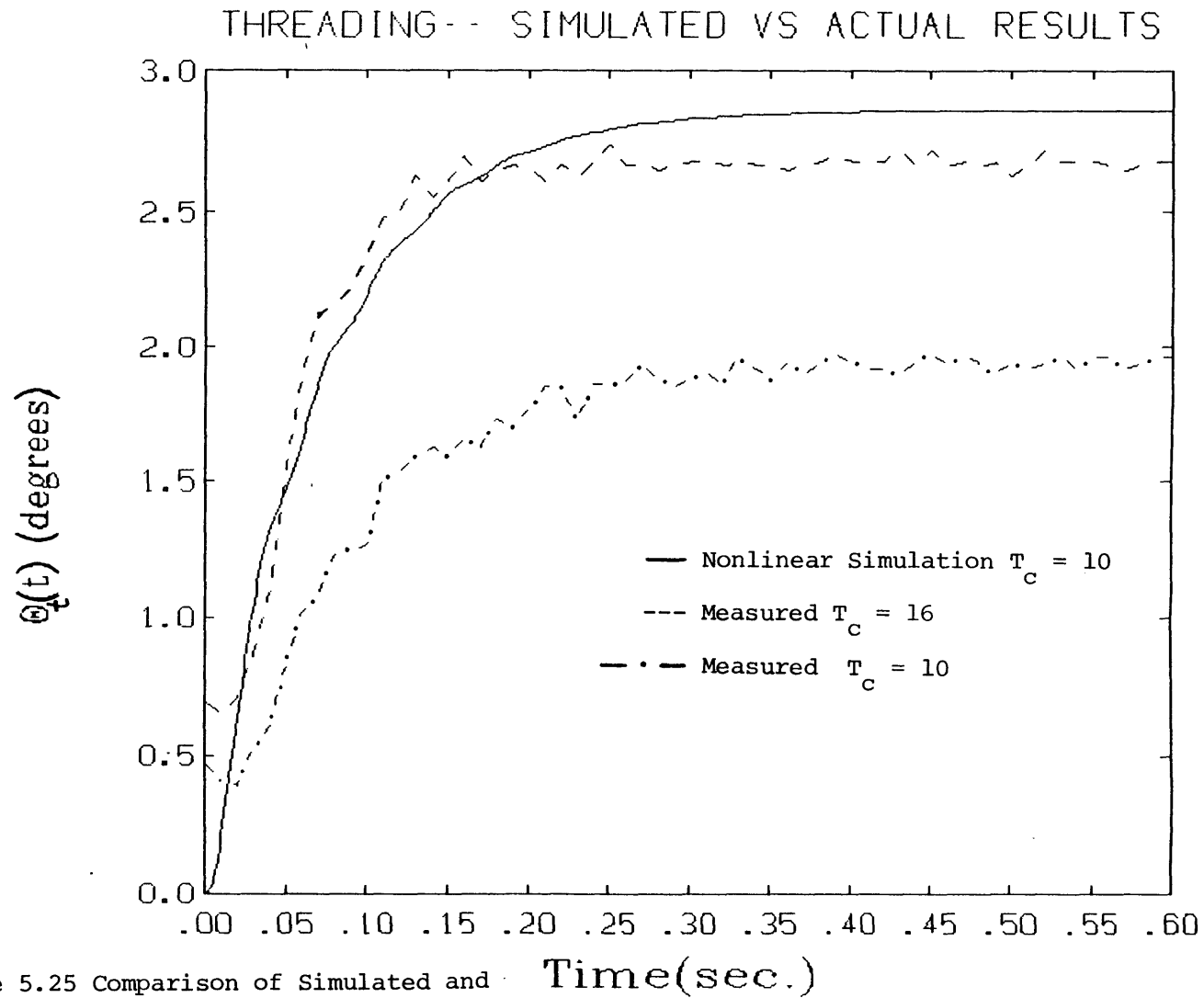


Figure 5.25 Comparison of Simulated and Measured Results  
RCC Deflection

the bottoming point. The applied torque rises as the motor stalls and no overshoot is seen with the amount of damping used. Of greatest importance, though, is whether or not the proper amount of torque is applied to the parts.

Examination of the data from the motor and net stall torque tests shown in Figures 5.14 and 5.15 shows that there is a discrepancy between the desired and actual torques. Conversion of current to torque by the motor is not the problem. The problem is due to an insufficient amount of current through the motor being supplied by the control circuit.

One solution to the problem is to use a larger input -- one great enough to achieve the desired current and thus desired output torque. This is somewhat feasible as shown by the comparison of torque commands of 10 and 16 in.-oz. The transient dynamics are not greatly affected for tightening even though a higher rundown speed results. This solution is somewhat marginal because the real cause of the control circuit problem is not fixed nor known.

The presence of friction also limits the current feedback torque control method since the controlled value,  $T_m$ , is not the same as the desired output value,  $T_n$ . However, with careful calibration, the amount of torque lost due to friction at each desired output torque level can be found. Since other methods of torque control also require careful calibration for precision torquing of +1 in.-oz tolerances, this does not appear to be a problem.

Most important to the current feedback torque control method is achieving the proper level of motor torque vs torque command and utilizing a set of parameters that guarantees an overdamped torque output response. These two topics are now addressed by investigations into the assembly cell controller deficiency, and the effect of varying the parameters which determine the dynamics of the control system.

### 5.5.2 Investigation of Control Circuit Deficiency

In order to find the cause of the actual controlled current vs desired current problem, several tests were performed. First the torque station was locked with the air cylinders and hard stops, and the tach disconnected. This was to show the effect of the tach feedback summed with the input command on the current feedback loop. Data was collected using 1 in.-oz increments in the torque command. Figure 5.26 shows the results for the measured current vs

### Measured current vs Torque Command

M/T  $G_t=1/22.5$

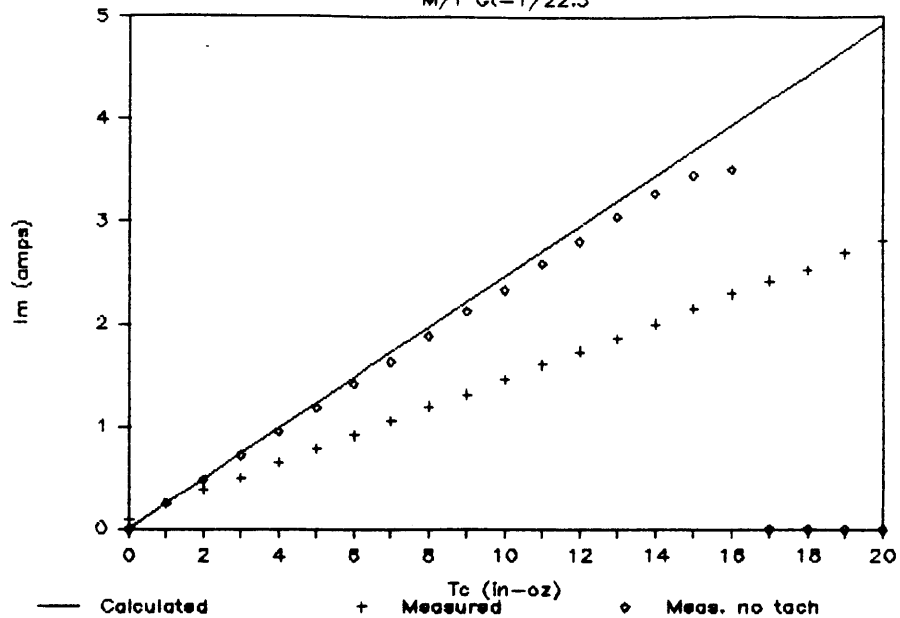


Figure 5.26 Comparison of Current Feedback Loop Performance with and without Tach Feedback

### Motor current Test

Varying  $G_t=1/R_t$   $T_c=10$

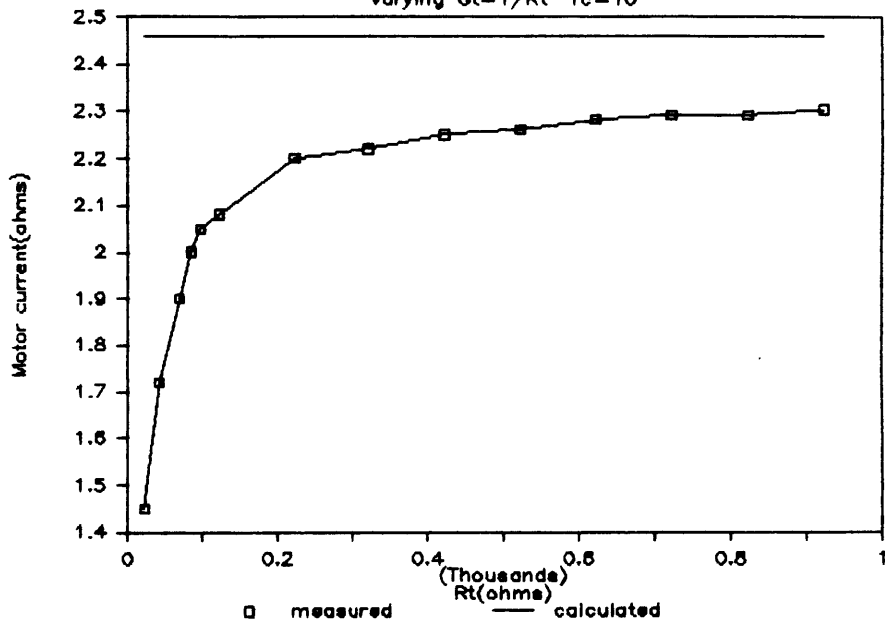


Figure 5.27 Results of test showing dependence of Current Feedback Loop on velocity feedback gain resistor

torque command with the tach feedback disconnected. Also shown is the same test with the tach feedback connected with the gain of  $G_T = 1/22.5$  amps/volt used in torque station operation. The latter is the same test as the motor torque of Figure 5.14.

Clearly the results are much closer to the desired results when the tach feedback is disconnected. Since the tach itself has no output when it is not moving, it was decided that the feedback gain could be the cause. In order to achieve the high amount of damping and low speed control, a very small amount of resistance ( $R_t = 22.5 \Omega$ ) in the feedback path is needed compared to that of the input resistance ( $R_c = 10 \text{ K}\Omega$ ) and the current feedback resistance ( $R_2 = 3.9 \text{ K}\Omega$ ) (Figure 5.2). The locked TS current test was repeated for  $T_c = 10$  and various decreased feedback gains (increased resistance). The results are shown in Figure 5.27. It is shown that the controlled current varies with velocity feedback gain. For resistances above  $1 \text{ K}\Omega$  (or gains below  $0.001$  amps/V) the effect is minimized. It is assumed that this relationship holds for all torque commands.

No specific reason is given here for these results. More review of the control circuit design is needed. It is believed by this author that the low resistance of the velocity feedback path for high velocity feedback gains allows current to leak into the path from the current control loop. To support this hypothesis, the torque watch windup test was repeated and data were collected for the tach output signal. The results are shown in Figure 5.28. Three curves are shown. It is seen that when the motor and tach stop, the tach voltage does not return to zero as it should. The steady-state level is a positive voltage that depends on the torque command, or current level in the control loop. Since the velocity signal subtracts from the torque command, a lower value of current, and thus torque, exists.

A solution to the problem would seem to be decreasing the velocity feedback gain so that the  $1 \text{ K}\Omega$  resistance level was reached. This is undesirable, however, because a steady-state free speed above  $421 \text{ rpm}$  would result, and the lowered system damping for the tightening phase of part mating would cause torque overshoot. This last fact shows the need for an analysis of the effects of choosing system parameters different from those employed in the existing TS design.

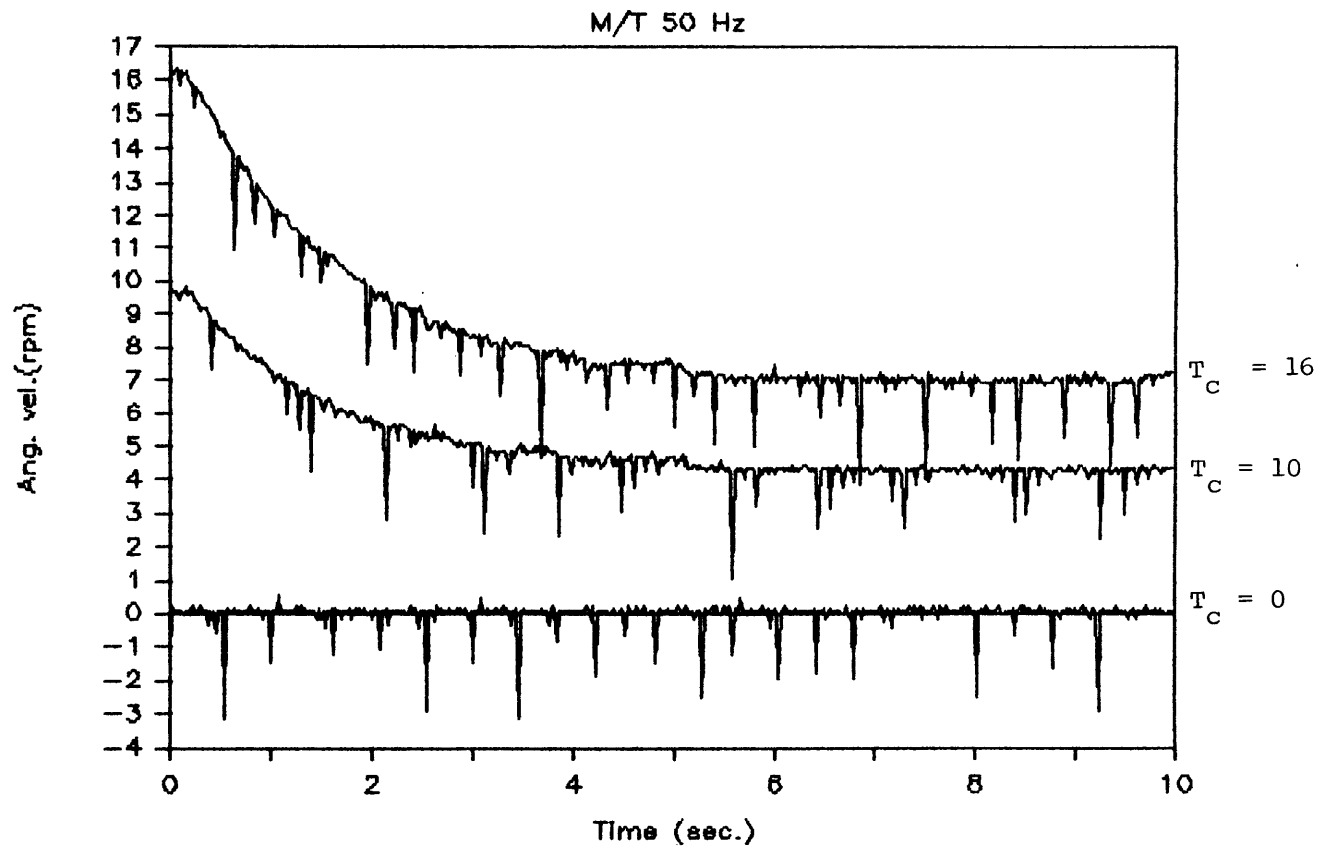


Figure 5.28 Measured Velocity Signal during Torque Watch Windup for various torque commands



### 5.5.3 Improved Performance

From the above investigation, several areas of improvement to the torque station design can be identified. The first, which has been alluded to, is to decrease the friction in the TS drive. Uncertainty in this parameter is the limiting factor in resolution of torque control. A brushless motor/tach was suggested earlier. Second, a control circuit design which decouples the summing junctions of the current and velocity feedback could be investigated. A design is needed for which the tach feedback gain has no effect on the current loop performance. Third, the low gain of the tachometer is the main reason for the small velocity feedback resistor that is needed. Employing a tach with a larger gain is possible. However, the gain would have to be increased by a factor of 44 in the case of the existing torque station circuit to achieve the same damping and speed control. This is impractical due to increased device size, friction, and output impedance. The latter is discussed in Appendix A. Chapter 6 shows the implementation of an optical encoder-based tachometer which lessens some of the problems experienced with the DC PM tachometer.

### 5.6 Variation of Parameters/Generalized Design Issues

The simulations and experimental results presented so far have dealt with the specific parameters of the existing torque station and the specific parts considered by this thesis. A variation in  $G_T$  was used in the motor current dependence on feedback test but the effect of this gain on the system dynamics was not discussed. An objective of this thesis is to extend the results so that general guidelines for torque station controller design for precision threaded part mating can be proposed.

#### 5.6.1 Review of Performance Model Variations

In the discussion of the general performance model in Section 5.2.1, the effects of changes in parameters were described for the torque station being connected to a generic process which exerted a position-dependent disturbance torque. The torque watch windup process is a specialized case which produces standard second order dynamics described by a characteristic equation in the form  $S^2 + 2\zeta\omega_n S + \omega_n^2$ . For this process and a generalized process which can be put in this form by estimating an equivalent stiffness  $K_s$  and equivalent contributions to  $J_{MF}$  and  $B_T$ , it is necessary that

$$B_T > 2(K_S J_{MF})^{1/2} \quad (5-45)$$

for an overdamped response. Remembering that  $B_T = B_{MF} + G_T K_{TACH} G_A K_T$ , and that in general  $B_{MF} = 0$ , it is seen that the overall feedback gain,  $G_T K_{TACH}$ , has the most profound effect on the damping ratio and response. It appears as a term in Equation (5-45). The amp current gain and motor torque constant are fixed when a configuration and current control gain are chosen.

Threaded part mating is a more complicated process than torque watch windup, but it is also a position-dependent disturbance torque generator, and will now be shown to exhibit some of the same general characteristics with respect to current feedback torque control with tach velocity feedback control system. The tightening phase will be emphasized since it has more complicated dynamics. The rundown phase is easily characterized by the performance and linear rundown models.

#### 5.6.2 Variations Using Piecewise Linear Model

Comparison of the piecewise linear and nonlinear coulomb friction models was shown briefly in the simulations of Chapter 5.3.4. It was shown that the overall system dynamics for threading during tightening could be estimated from the piecewise linear model by ignoring the oscillatory "part mode". It is assumed that this is true when the mode has a much higher frequency than the overall "chain" mode and remains lightly damped. This assumption was made by comparing simulated results for several excursions from the values of  $J_{MF}$ ,  $J_{TC}$ ,  $K_p$ ,  $K_c$ , and  $G_T$  used for the torque station. The magnitudes of these excursions were what this author felt were reasonable. Extreme variations of several orders of magnitude were not investigated. The ability to utilize the linear tightening model to predict the nonlinear model and actual system dynamics forms the basis for a second set of generalized guidelines for torque station design.

The tool used to examine the effects of variations in the control parameters is a root locus analysis of the roots of the characteristic equation of the piecewise linear model of tightening. The characteristic equation is repeated below

$$s^4 + \left(\frac{B_T}{J_{MF}}\right)s^3 + \left(\frac{K_p}{J_{MF}} + \frac{K_p + K_c}{J_{TC}}\right)s^2 + \left(\frac{K_p + K_c}{J_{TC}}\right)\left(\frac{B_T}{J_{MF}}\right)s + \left(\frac{K_p K_c}{J_{MF} J_{TC}}\right) = 0 \quad (5-46)$$

To achieve an overdamped response for tightening of the parts, it is necessary to have enough electrical damping so that the "dominant" pair of poles, corresponding to the chain mode, be real. A closed form solution for Equation (5-46) which illustrates this requirement is difficult to obtain due to the large number of parameters involved. A root locus or equation simplification approach is more practical.

The parameters chosen for variation analysis were  $J_{MF}$ ,  $J_{TC}$ ,  $K_p$ ,  $K_c$ , and  $G_T$ . These variables are considered by this author to be those which would differ for other assembly cell designs and parts. Other parameters also have an effect but are actuator, sensor, and amplifier dependent and are fixed when hardware is chosen. For example, only so many motor torque constants are available to the designer. The designer also cannot change the part stiffness, but it is conceivable that several different threaded part assemblies could be assembled by the same torque station. There are countless numbers of variations possible with the many variables of the control system. For a specific torque station, designers must analyze the specific variables that they can change. Several examples of these variations are now presented using numerical values. They present the general nature of variation of parameters.

The first variation to be considered is variation of  $G_T$  which also represents the total damping. Using larger values for the part and RCC stiffnesses to more clearly illustrate the effect,  $G_T$  was varied from 0.0444 to 0.0014 amps/volt, while holding other parameters constant. Note that this corresponds to values of  $R_t$  from 22.5 to 714  $\Omega$ . A value of 614 in.-oz/rad was used for  $K_p$  and  $K_c$ . The resulting root locus is shown in Figure 5.29. The closely bunched pair of complex poles correspond to the part oscillation mode

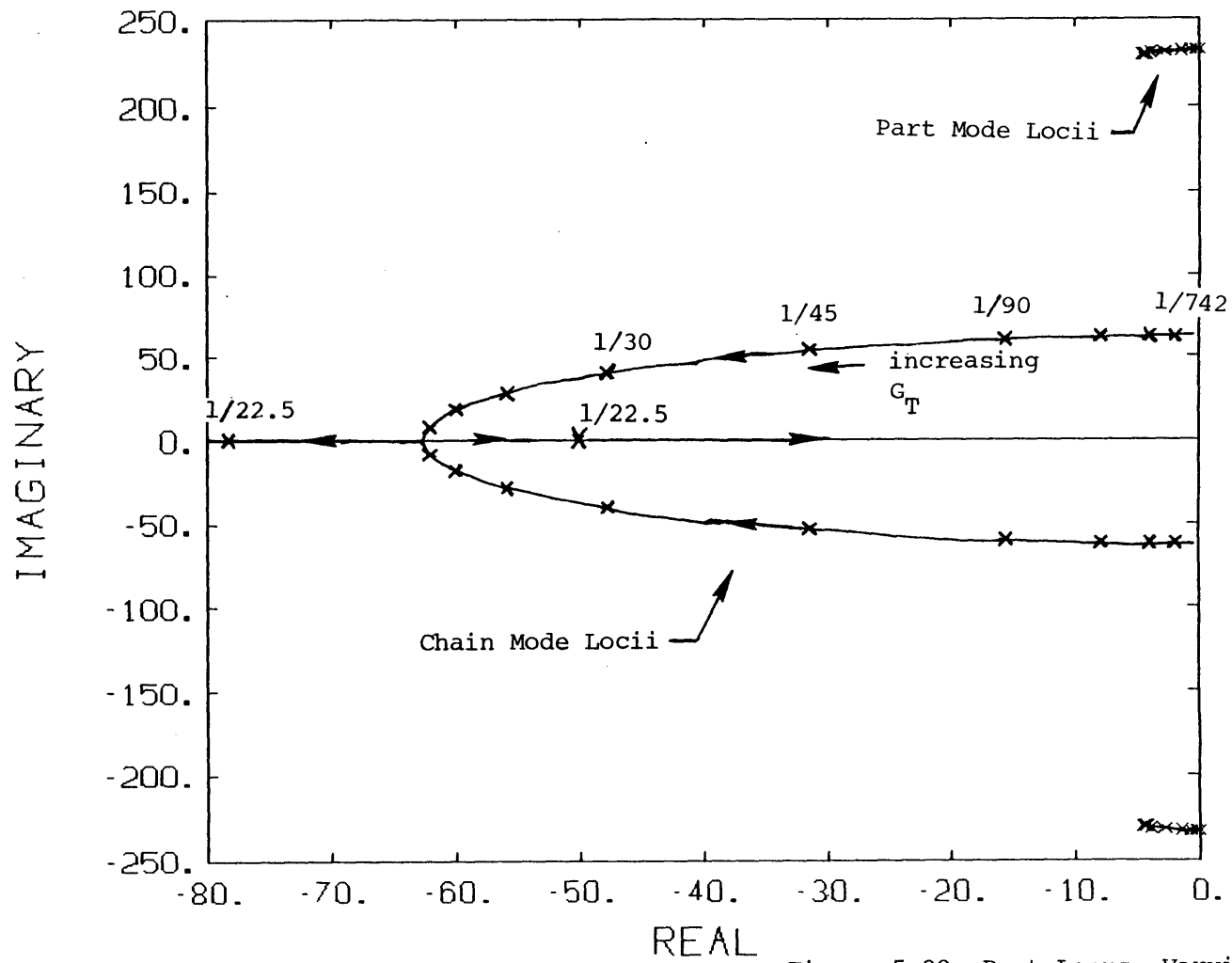


Figure 5.29 Root Locus Varying  $G_T$   
 $K_P = 614$   $K_C = 614$

which is ignored. The other locus which departs from the real axis corresponds to the chain mode, which is of interest. It is seen that the damping must be increased to ensure that two real poles result. In this case a gain of above 0.043 amps/volt should be used.

Another variation considered was the variation of  $J_{MF}$  for several values of  $G_T$ . Four values of  $G_T$  were used -- 1/22.5, 1/50, 1/75, and 1/100. The value of  $J_{MF}$  was varied from 0.073 to 0.005 in.-oz-sec<sup>2</sup>. The values of  $K_C$  and  $K_D$  used in the previous variation were also used. Motivation for this came from a desire of the designers of the prototype assembly cell to utilize a torque station with decreased inertia for the second generation design. The results are shown in Figures 5.30 through 5.33. For each of the loci, a "break inertia",  $J_B$ , can be defined. This is the inertia above which the chain mode poles,  $S_1$  and  $S_2$ , become underdamped. At the critical damping point a pair of repeated poles results. Table 5-2 summarizes the value of the break inertia for each value of  $G_T$ .

Table 5-2. Break inertias.

| $G_T$ (A/V) | $J_B$ (in.-oz-sec <sup>2</sup> ) | $S_{1,2}$ (sec <sup>-1</sup> ) |
|-------------|----------------------------------|--------------------------------|
| 1/22.5      | 0.0775                           | -60.9                          |
| 1/50        | 0.0125                           | -146                           |
| 1/75        | 0.00475                          | -280                           |
| 1/100       | 0.0024                           | -430 ( $S_{3,4}$ )             |

The loci show that decreased inertia allows smaller velocity feedback gains to be used and vice-versa. Also illustrated is that greater changes in inertia have to be made than feedback gain to influence the overall damping. Maybe the most important result of the variation is shown in Figure 5.33. For a smaller feedback gain of 1/100, the chain mode converges to a pair of complex poles instead of overdamped poles, and is closer in frequency to the part mode. In this case, the assumption that the linear model predicts the actual dynamics may not be valid, and a nonlinear simulation should be performed.

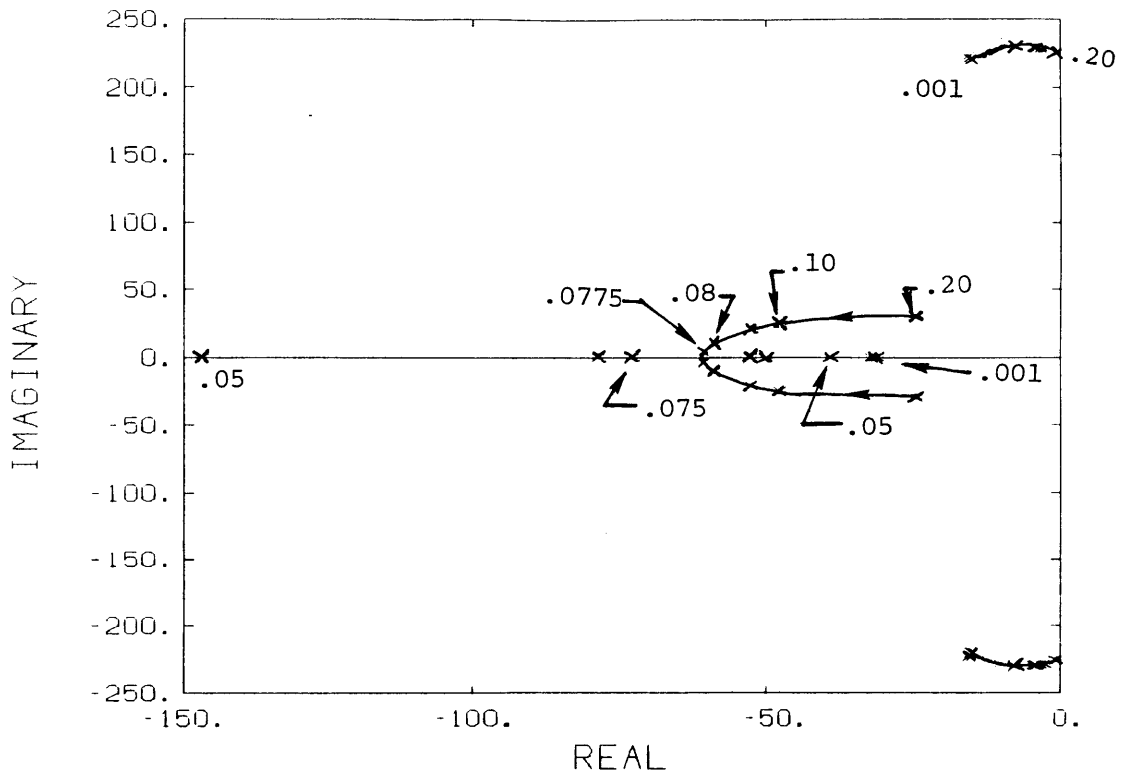


Figure 5.30 Root Locus Varying  $J_{MF}$ ;  $G_T = 1/22.5$

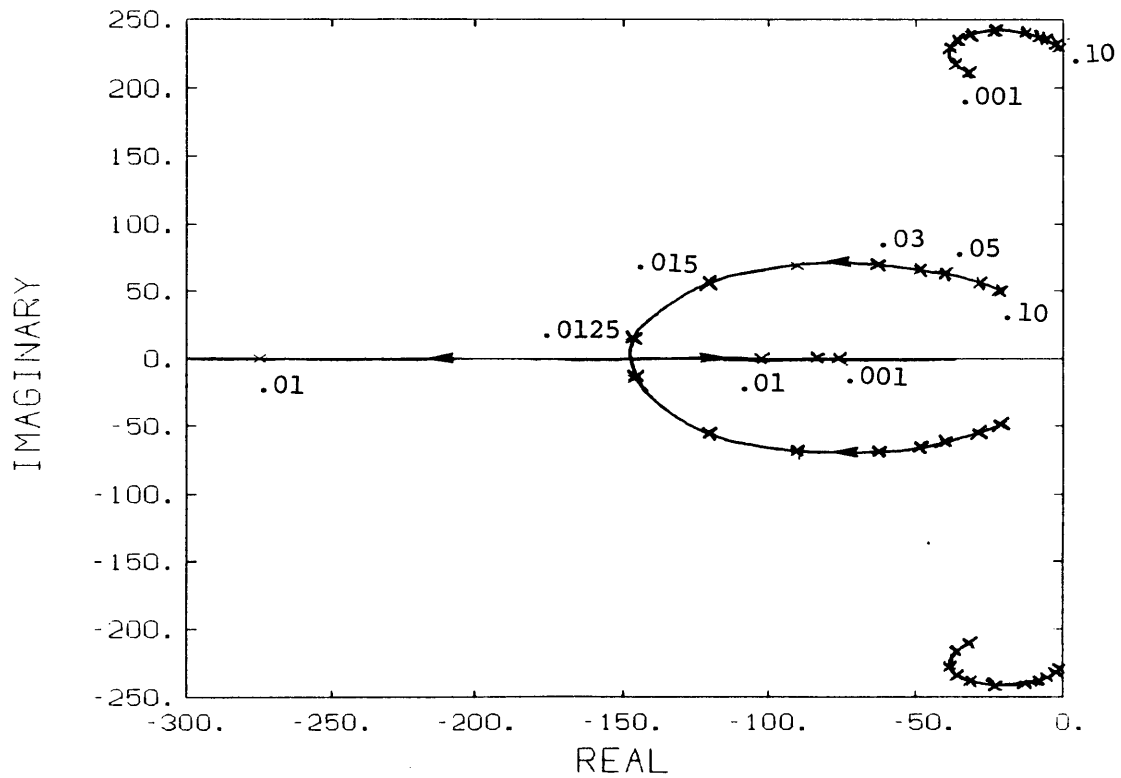


Figure 5.31 Root Locus Varying  $J_{MF}$ ;  $G_T = 1/50$

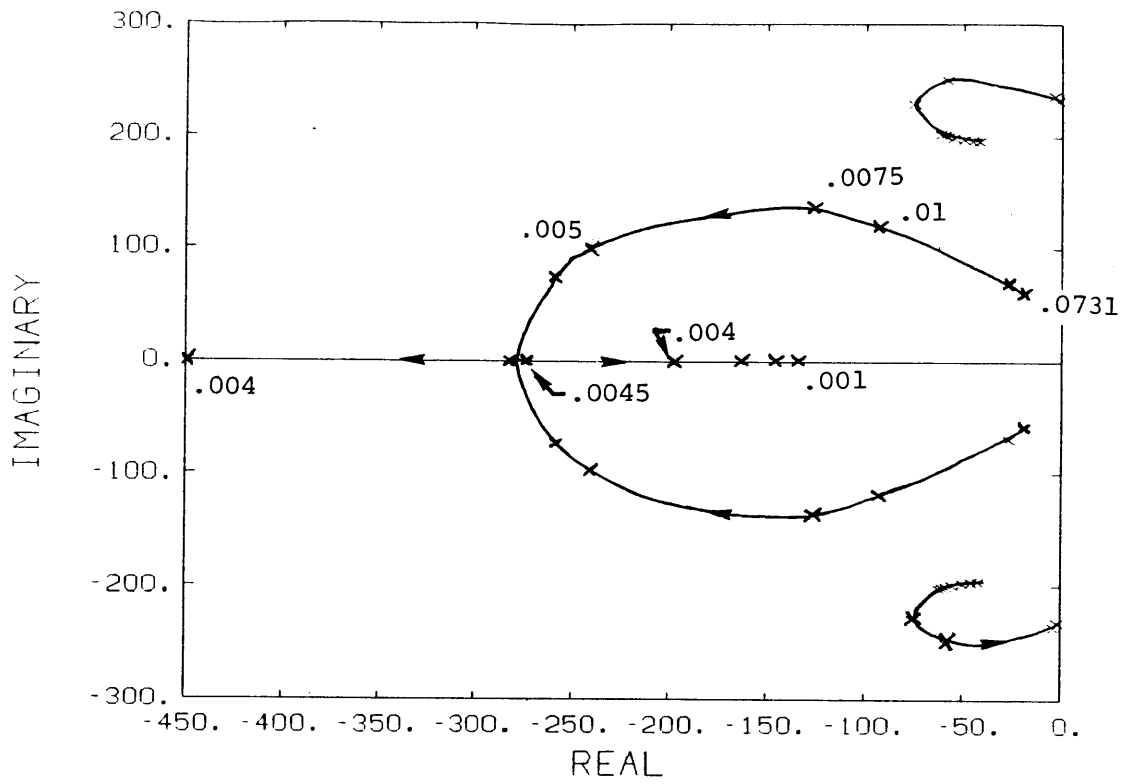


Figure 5.32 Root Locus Varying  $J_{MF}$ ;  $G_T = 1/75$

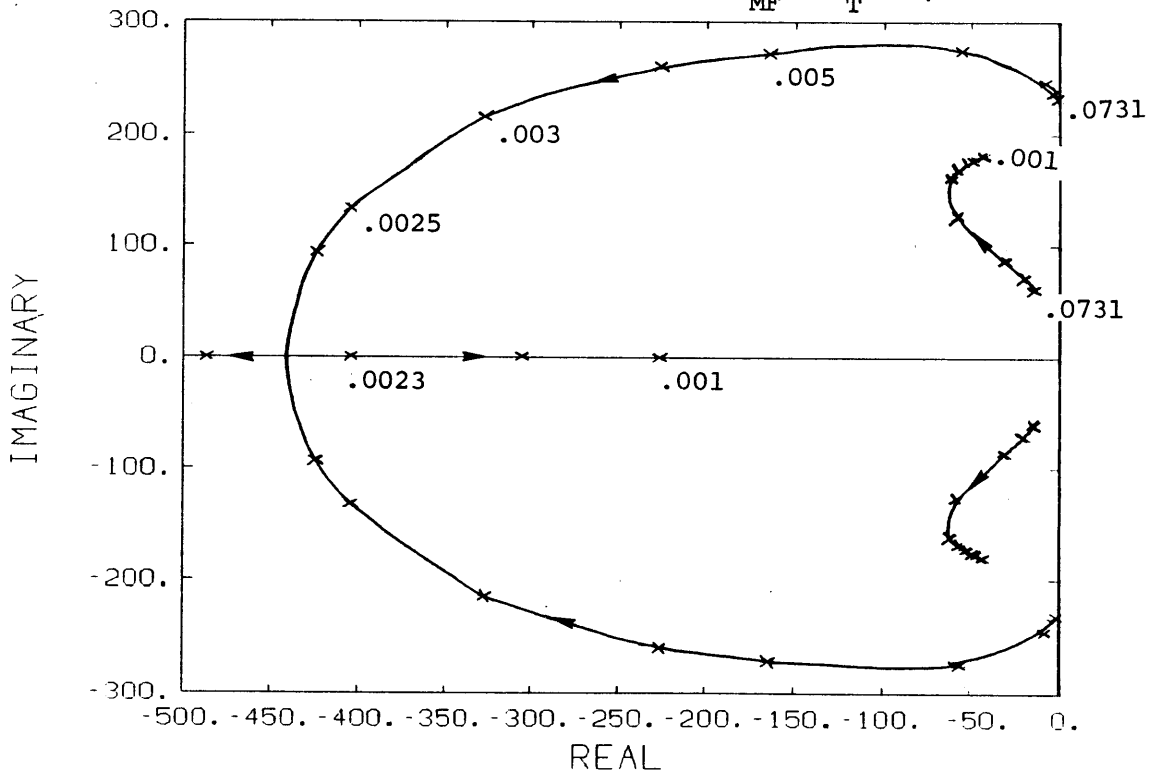


Figure 5.33 Root Locus Varying  $J_{MF}$ ;  $G_T = 1/100$

A final variation to consider is the variation of the part torque,  $K_p$ . Figure 5.34 shows root loci for  $K_c = 300$ ,  $J_{MF} = 0.0731$ , and  $G_T = 1/22.5$  and  $1/50$ . The direction of the arrows shows increasing  $K_p$ . The same range of values from 0 to 5000 in.-oz/rad was used for each locus. For  $G_T = 1/22.5$  the poles remain real until  $K_p = 5000$ , but for  $G_T = 1/50$ , the poles become complex above  $K_p = 85$ . Thus one feedback gain could handle a much larger range of parts than the other.

Many other cases could be considered. In general, increasing  $G_T$  causes the poles to become more damped. Decreasing  $J_{MF}$  and  $K_p$  causes the poles to become more damped. Although not shown, the latter is also true for  $J_{TC}$ ,  $K_c$ ,  $K_1$ , and  $K_2$  where

$$K_1 = K_p + K_c \quad (5-47)$$

$$K_2 = K_p K_c / (K_p + K_c) \quad (5-48)$$

These two stiffnesses correspond to the total and series stiffness of the parts and RCC. The total stiffness corresponds to the part mode while the series stiffness corresponds to the chain mode.

The root locus approach is fairly powerful but somewhat involved. A quicker approach is to try to reduce Equation (5-45) to second order by combining the part mating parameters  $K_p$ ,  $K_c$ ,  $J_{MF}$ , and  $J_{TC}$  into a set of equivalent parameters that approximate the system. Since the chain mode is used to describe the transient response during tightening, an equivalent stiffness of the process can be estimated using  $K_2$ . This leaves the choice of an equivalent inertia. If one of the part or RCC stiffnesses was much greater than the other, then the choice would be simple. However, so would the process model. If  $K_p \gg K_c$ , then  $K_2 \approx K_c$  and the inertias would move together. The equivalent inertia would be  $J_{MF} + J_{TC}$ . If  $K_p \ll K_c$ , then  $K_2 \approx K_p$ , and the tool, collet inertia, would have only a small contribution to the dynamics. In this case the equivalent inertia would be  $J_{MF}$ .

If an equivalent stiffness and inertia are chosen for the process, the characteristic equation reduces to the form

$$J_{EQ} s^2 + B_T s + K_{EQ} = 0 \quad (5-49)$$



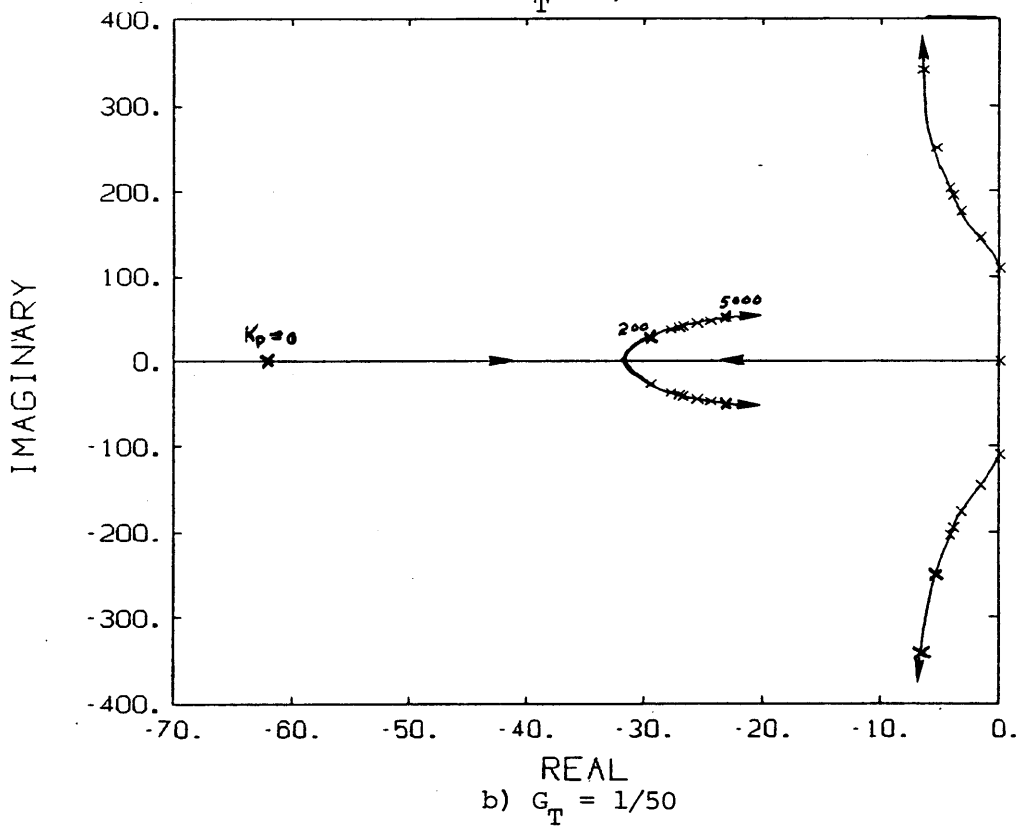
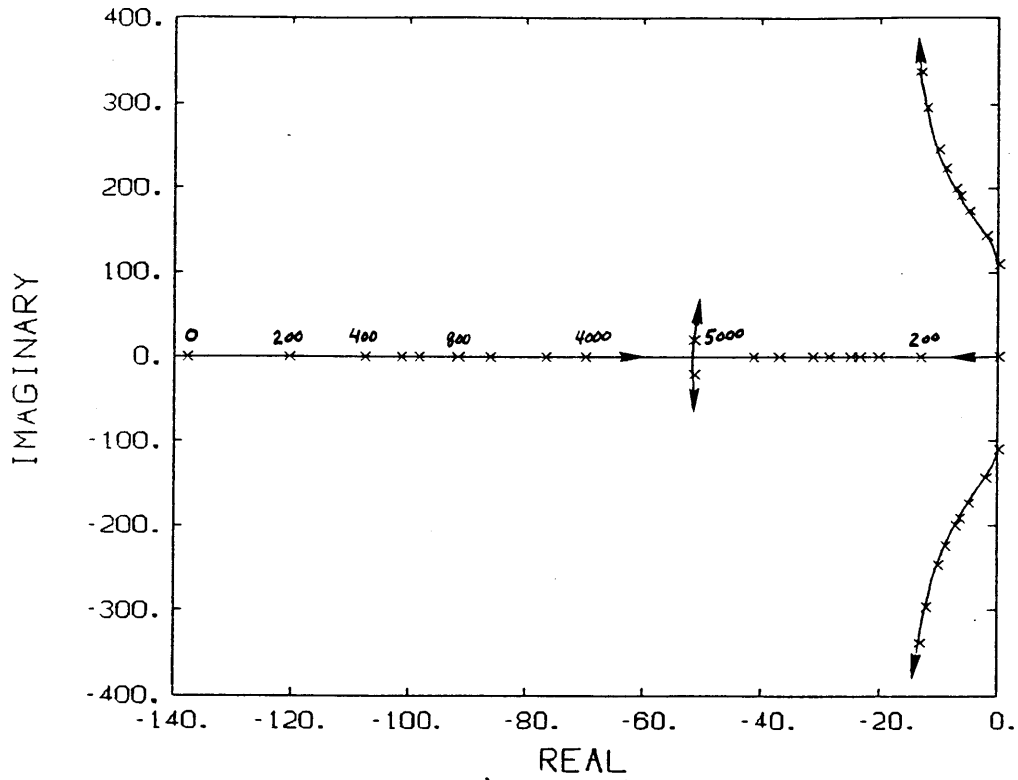


Figure 5.34 Varying  $K_p$ ;  $K_C = 300$

where  $J_{EQ}$  and  $K_{EQ}$  are the equivalent process parameters. In order to produce an overdamped system, the damping ratio,  $\zeta_{EQ}$ , must be greater than one.

$$\zeta_{EQ} = \frac{B_T}{2(J_{EQ} K_{EQ})^{1/2}} > 1 \quad (5-50)$$

For the two extremes described above

$$\zeta_{EQ} = \frac{B_T}{2 [K_c (J_{MF} + J_{TC})]^{1/2}} \quad \text{for } K_p \gg K_c \quad (5-51)$$

$$\zeta_{EQ} = \frac{B_T}{2(K_p J_{MF})^{1/2}} \quad \text{for } K_p \ll K_c \quad (5-52)$$

In many situations, and this is shown in the existing assembly cell parameters, this author expects that neither of these two situations exist. In this case, an equivalent inertia must be chosen between the two extremes based on some ratio of the two stiffnesses, and two inertias, or

$$J_{MF} < J_{EQ} < (J_{MF} + J_{TC}) \quad (5-53)$$

or

$$J_{EQ} = J_{MF} + \Delta J$$

where  $\Delta J = f(K_p/K_c; J_{MF}/J_{TC})$  and  $0 \leq f \leq 1$ . One such function could be

$$\Delta J = 1 - \exp(-K_p/K_c) \quad (5-54)$$

This is also somewhat cumbersome. An approach which is very conservative is to assume the worst case, and use the damping ratio in Equation (5-51). This allows any uncertainty in the part model to be accounted for. However, this conservative approach may require large amounts of electrical damping which can cause the control circuit problems experienced in this thesis.

Use of the piecewise linear model as a design tool is judged to be acceptable for the range of values considered in this thesis. The damping ratios of Equations (5-50) through (5-52), and the use of root locus can be used as guidelines in controller design. Several assumptions have been made in the approach, to the subtleties of each torque station and parts that it assembles should be considered on an individual basis.

A summarizing thought is that compliance in the robot is beneficial to torque control. If the RCC or other compliant device is much softer than the process, and the inertia between the robot compliance and process is small, then the performance of the control system is less sensitive to process modeling errors. Unfortunately, this cannot always be done.

### 5.6.3 Variations Using CFS Model

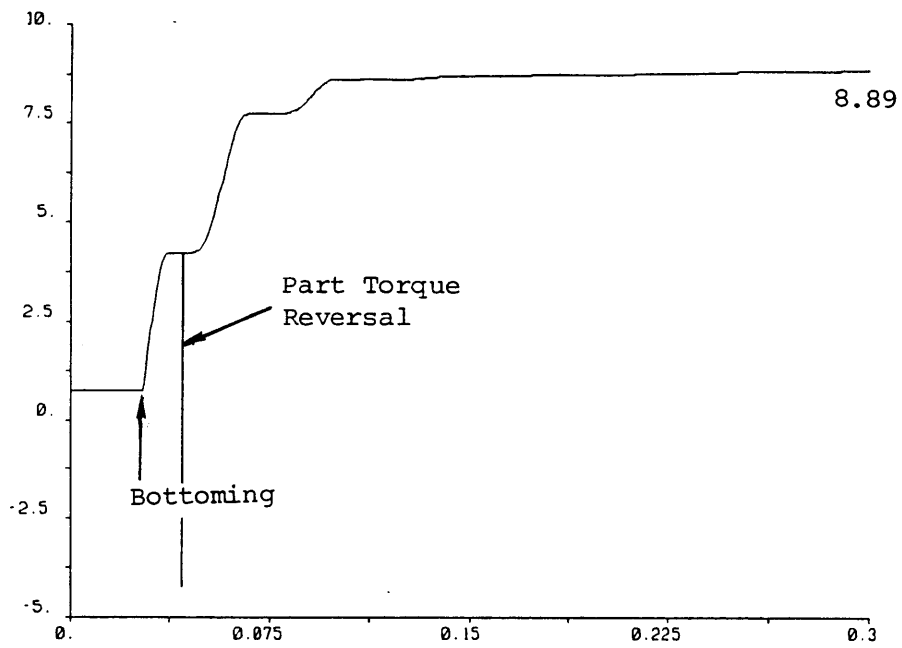
Use of the methods presented in the previous discussion was tested with several nonlinear simulations. The case of varying  $G_T$  and its effects on the system dynamics are now shown in the results of a simulation using the CFS model. The parameters used were the values shown in Table 5-1. The same values of  $K_p$  and  $K_c$  given in the root locus for varying  $G_T$  were used. Simulations were run for  $G_T = 1/22.5, 1/50, \text{ and } 1/100$ . The parameters used result in the piecewise linear model poles shown in Table 5-3.

Table 5-3. Poles versus  $G_T$ .

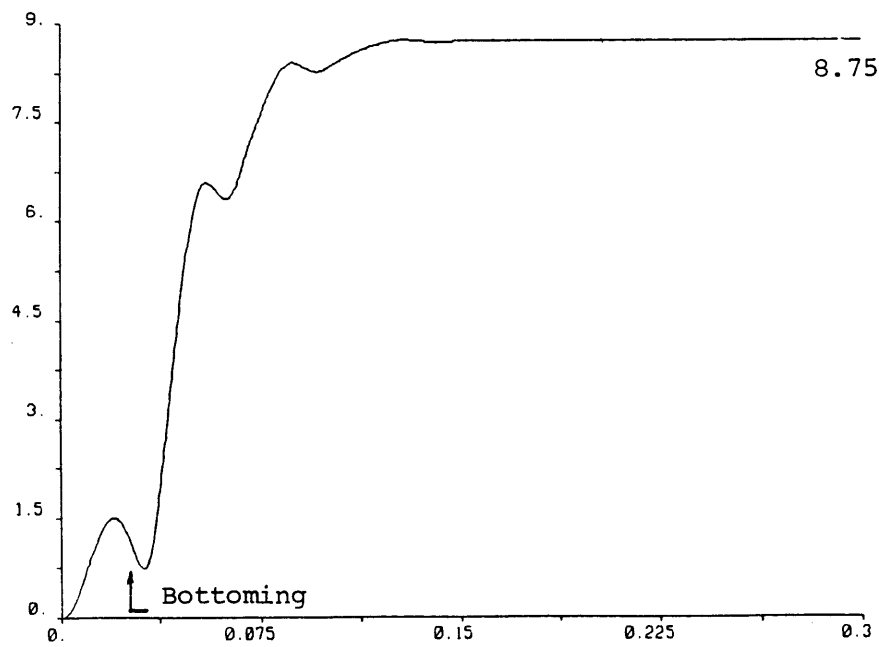
| $G_T$  | $S_{1,2}$     | $\zeta_{1,2}$ |
|--------|---------------|---------------|
| 1/22.5 | -50, -78      | >1            |
| 1/50   | -28.4 ± 55.3j | 0.46          |
| 1/100  | -14.2 ± 60.4j | 0.23          |

Note:  $\zeta_{1,2}$  corresponds to  $S_{1,2}$ , not  $\zeta_{EQ}$ .

Figures 5.35, 5.36, and 5.37 show the results. In all of the plots, the abscissa is time in seconds. The torques are in in.-oz, the velocities in rpm, and the positions in degrees. The bottoming point is indicated. A torque command of 10 in.-oz was used.

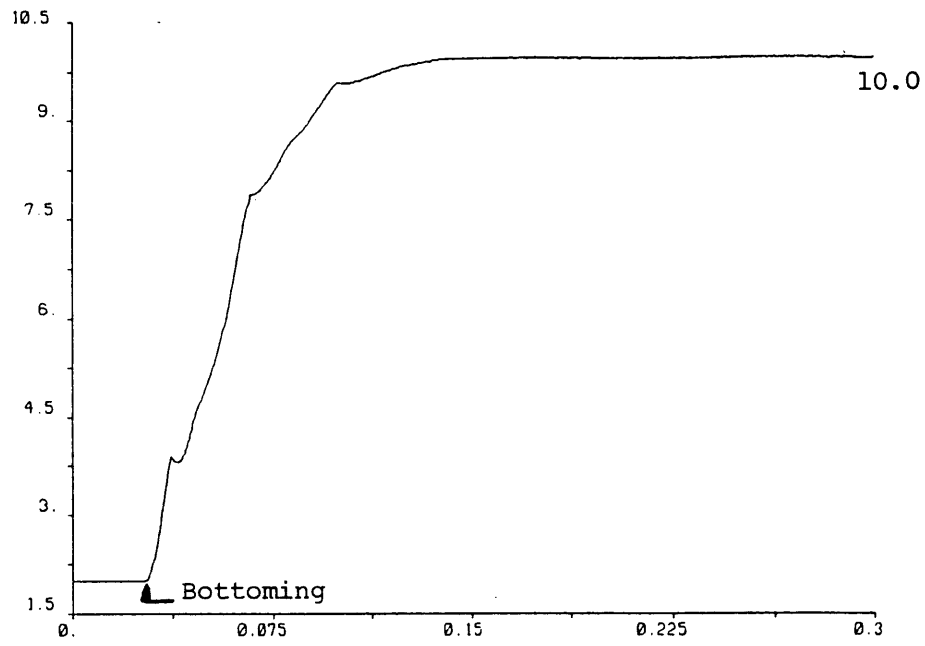


a) Part Torque,  $T_p$

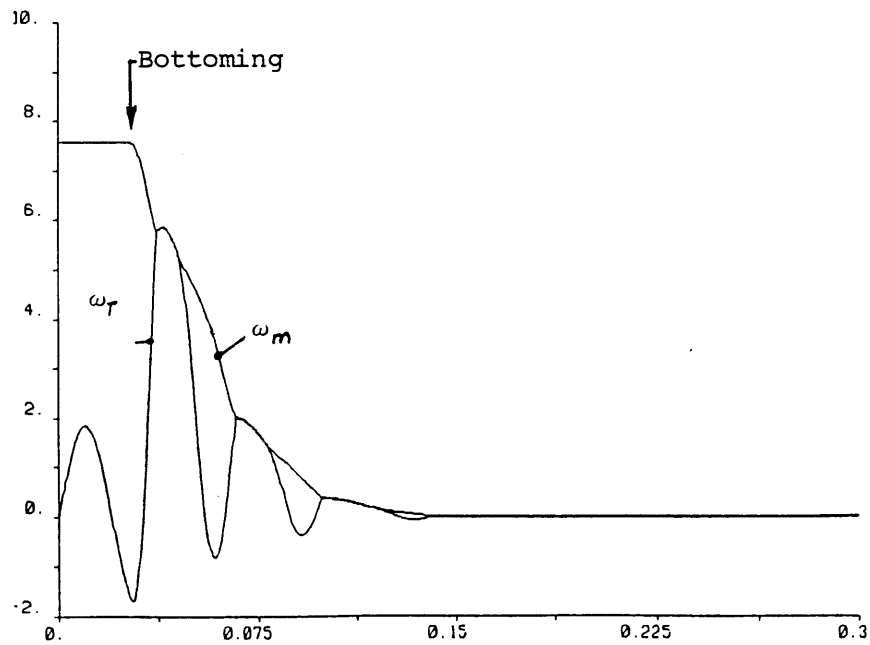


b) RCC Torque,  $T_{RCC}$

Figure 5.35 Nonlinear Simulation  $G_r = 1/22.5$   
 $T_c = 10$   $T_f = 1.25$   $T_r = 0.75$

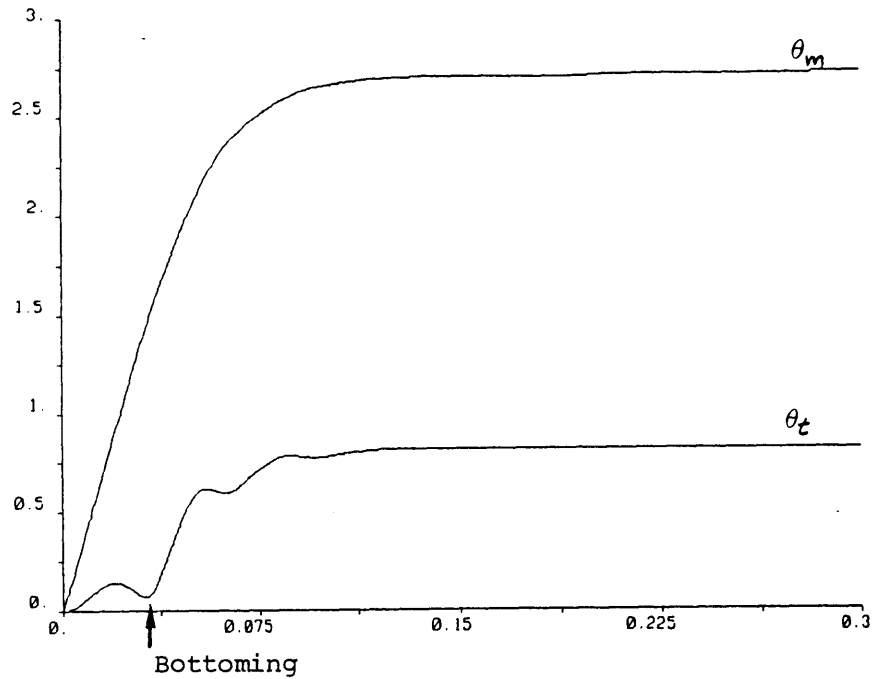


c) Motor Torque,  $T_m$

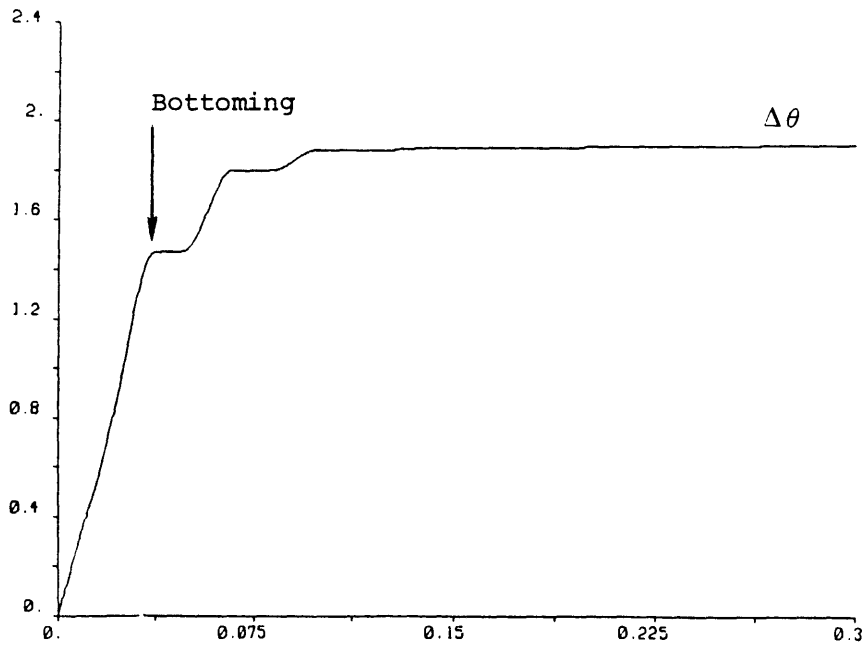


d) Angular Velocities

Figure 5.35 (ctd.)

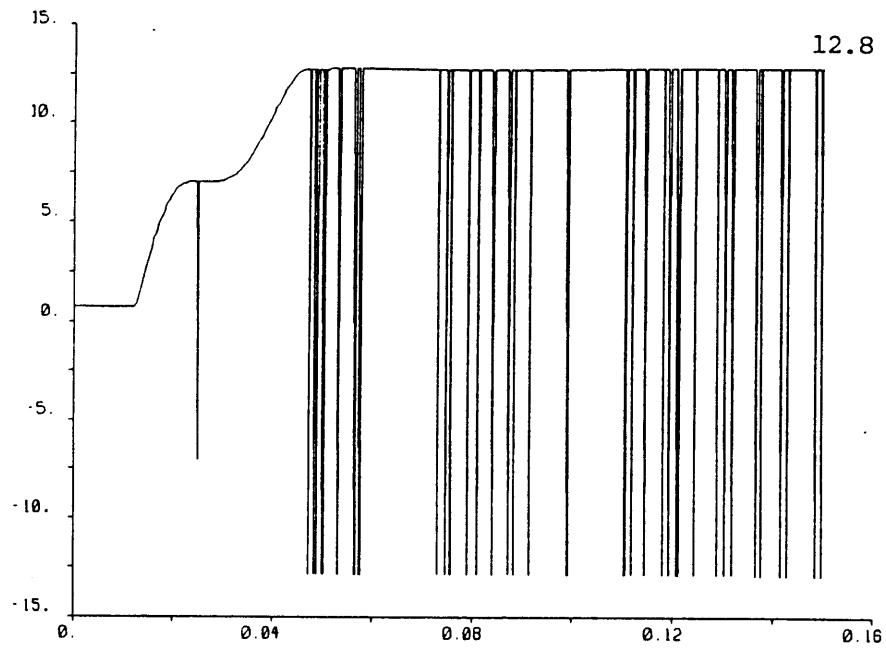


e) Angular Positions

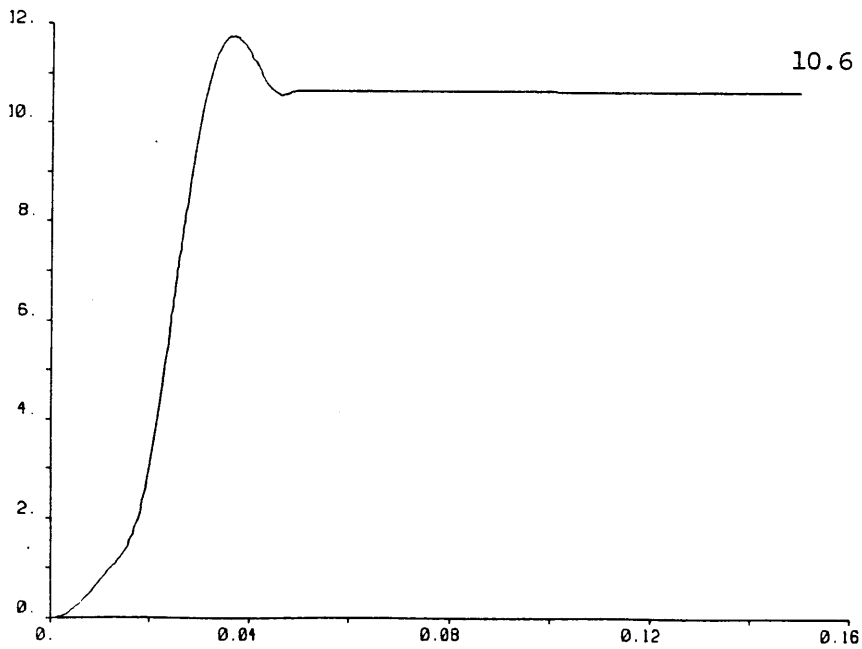


f) Difference in Positions

Figure 5.35 (ctd.)

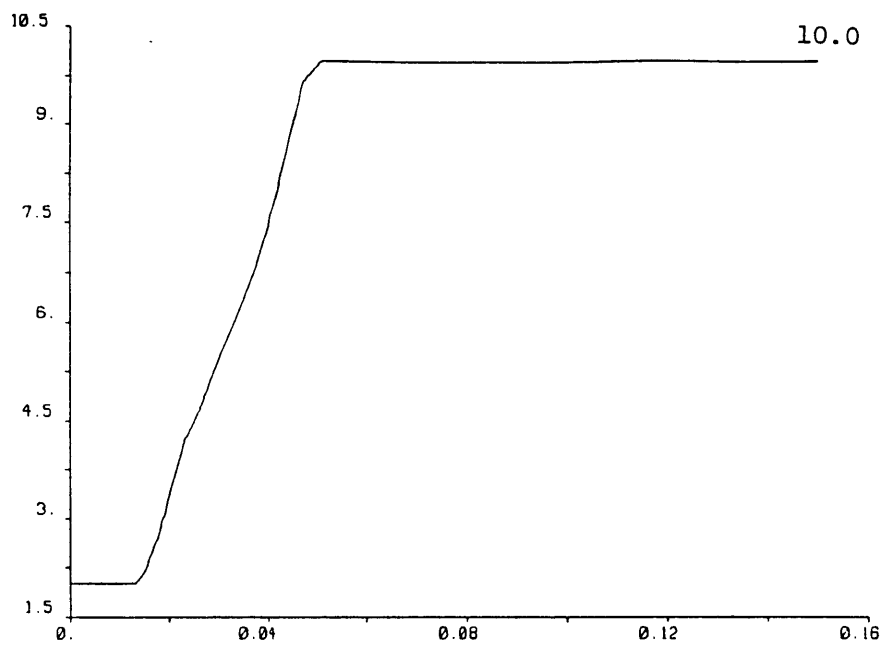


a) Part Torque,  $T_P$

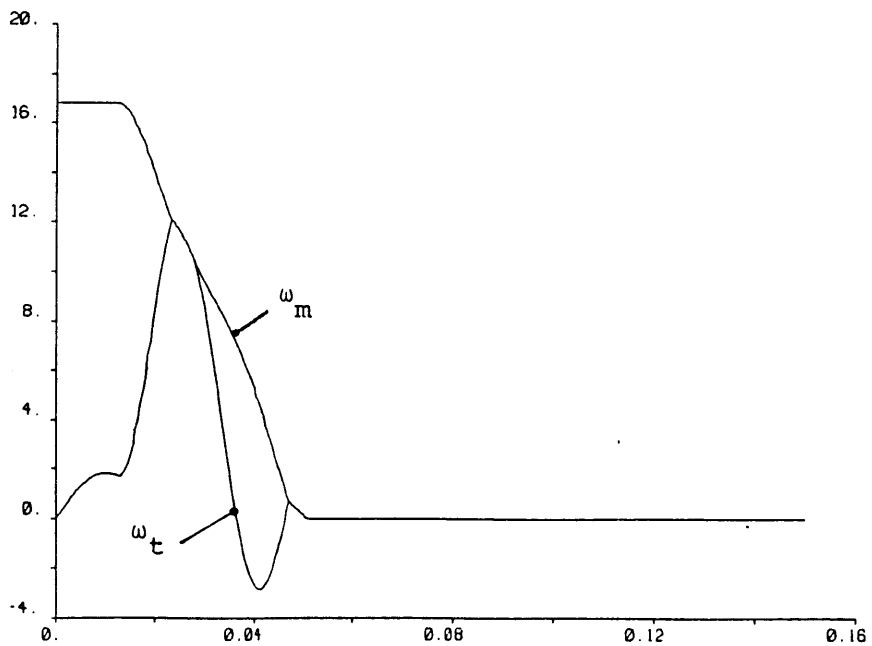


b) RCC Torque,  $T_{RCC}$

Figure 5.36 Nonlinear Simulation  $G_m = 1/50$   
 $T_c = 10$   $T_f = 1.25$   $T_r = 0.75$



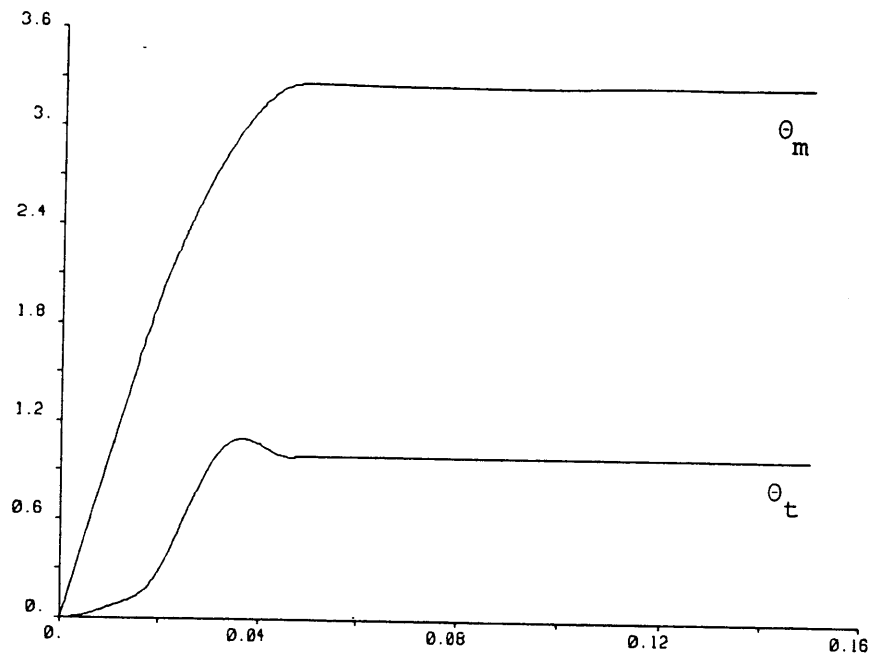
c) Motor Torque,  $T_m$



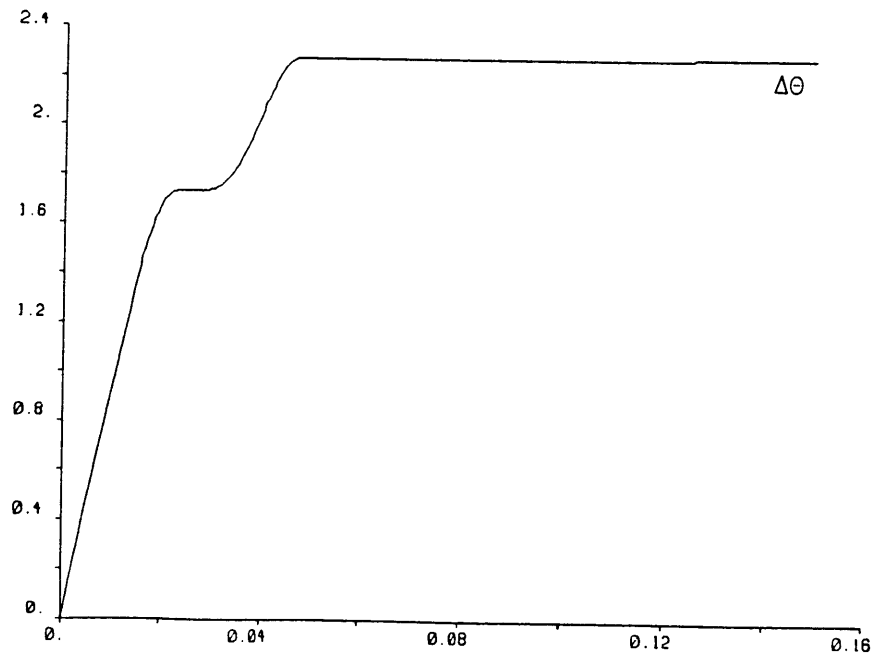
d) Angular Velocities

Figure 5.36 (ctd.)



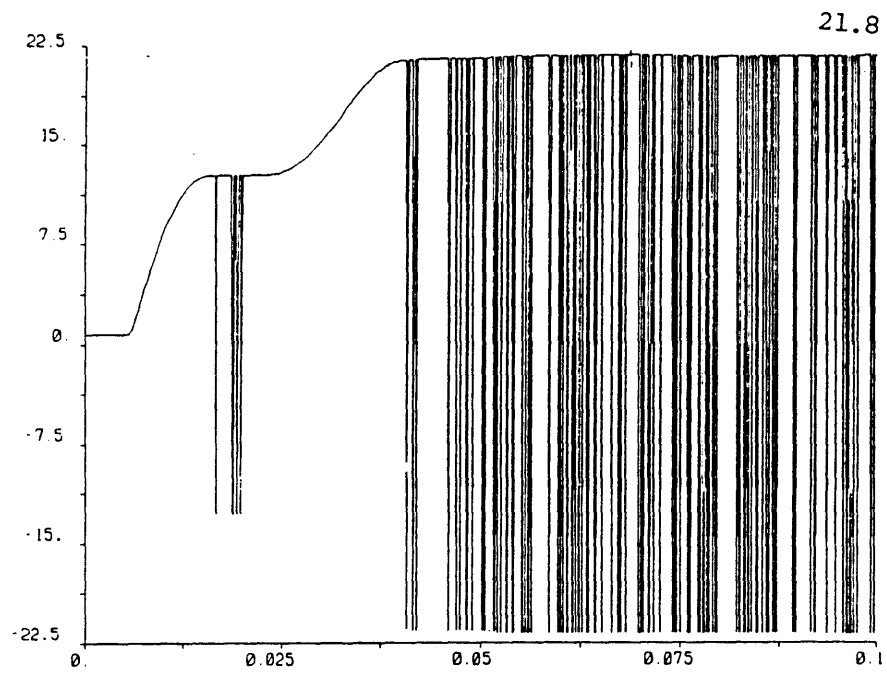


e) Angular Positions

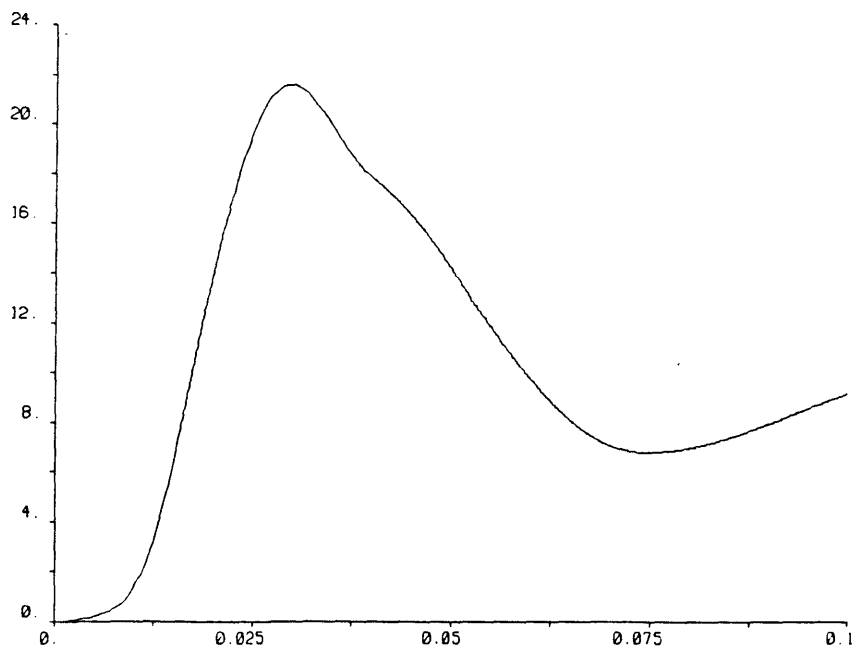


f) Difference in angles

Figure 5.36 (ctd.)

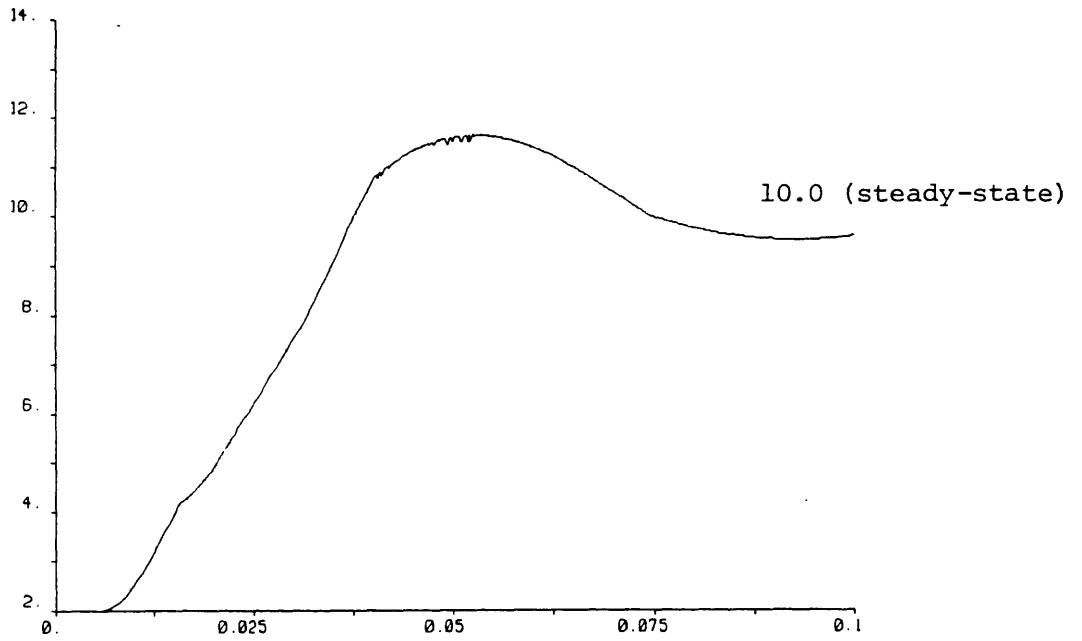


a) Part Torque,  $T_p$

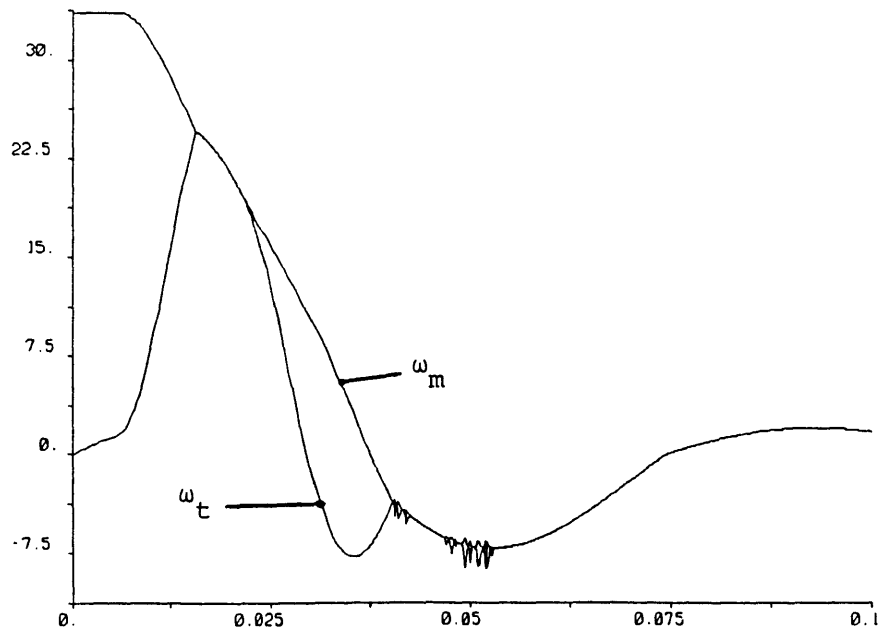


b) RCC Torque,  $T_{RCC}$

Figure 5.37 Nonlinear Simulation  $G_c = 1/100$   
 $T_c = 10$   $T_f = 1.25$   $T_r = 0.75$

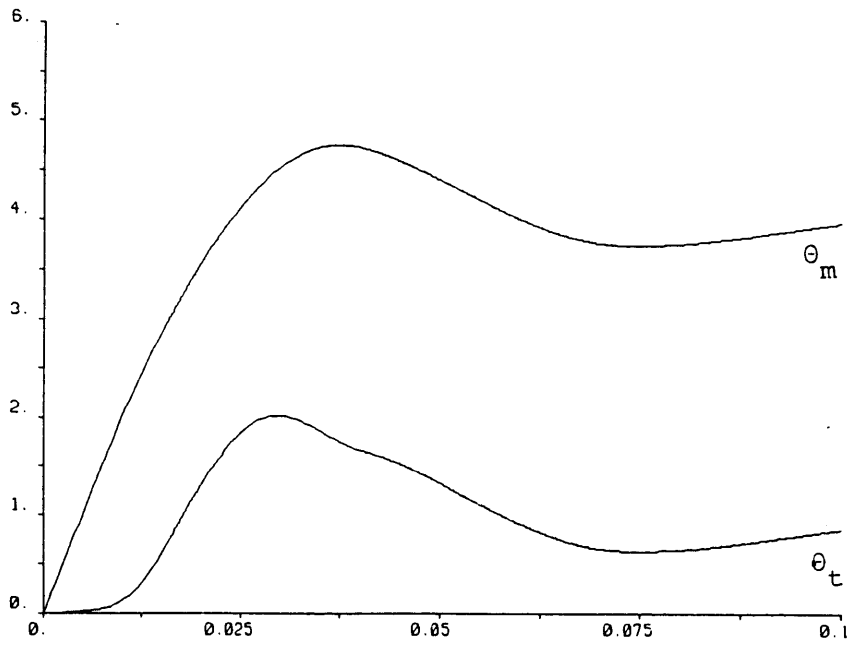


c) Motor Torque,  $T_m$

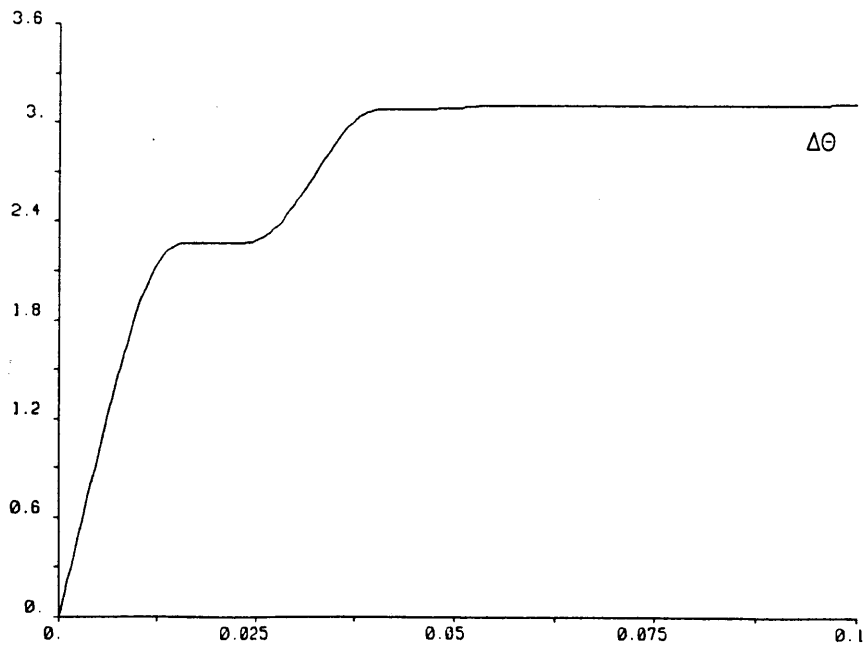


d) Angular Velocities

Figure 5.37 (ctd.)



e) Angular Positions



f) Difference in angles

Figure 5.37 (ctd.)

In the first case, the poles of the linear model predict an overdamped response. The nonlinear simulation agrees with this prediction. The final motor torque is 10 in.-oz, but because of the friction torque of 1.25 in.-oz, the final part torque and RCC torque is less.

For the second case, an underdamped response is predicted by the linear model. Examination of the nonlinear results in Figure 5.36 shows the same prediction. Notice that the model only allows continued tightening in the joint due to the requirement for complete reversal in torque to separate the parts. In this simulation higher final values for the part and RCC torques are found even though the final motor torque is still 10 in.-oz as commanded. Note that the tool/collet remains in a position that produces a higher torque on the parts than the motor. Equilibrium is maintained due to the presence of friction. The motor torque exhibits no overshoot. This points out the need to model the entire process and not just the input.

The "part torque",  $T_p$ , is not a torque in the normal sense of the term. It is really an indication of the position of the threaded parts relative to one another, and of the applied torque that is required to put them in that position. Therefore equilibrium in this CFS model can show overtightened parts at equilibrium.

Figure 5.37 shows the results for an extreme case of overshoot. Again, the part and RCC torques are higher than the input motor torque. More oscillation is present. Note the increased number of negative spikes on the part torque plot. The dynamics of this case are more oscillatory causing a greater tendency to decrease  $\Delta\theta$  of the parts.

An even more extreme case of separation may be seen in real parts. It is this author's opinion that the model is valid for moderate amounts of overshoot and torque reversals.

In the prototype assembly cell, the RCC is less stiff than the value used here and also has mechanical stops which limit excessive deflection. Thus in actual hardware there are limits to the amount of overshoot in the tool/collet inertia. Another factor which limits the overshoot is the limit on torque that the motor can apply due to amplifier saturation. Note that overshoot in motor torque can only result when  $\omega_m < 0$  even though much greater overshoot is present in the RCC due to inertial overrun.

These simulations present a case of providing enough damping in the control circuit. Even if it were possible to perform rundown, stop at the bottoming point to reduce the kinetic energy of the rotating inertia, and start tightening at zero velocity, overshoot could still occur due to a lack of damping. Thus the velocity feedback is just as important for tightening control as it is for rundown speed control.

#### 5.6.4 Experimental Variation of Parameters

Since the existing torque station could not be physically altered, only the effects of variations in  $G_T$  could be examined experimentally. The threaded part tightening experiment was repeated using decreased feedback gains to examine differences in the measured results. Use of the same feedback gains used in the experiment to determine the dependence of the current loop on  $G_T$  were planned. The motor and output torques for these gains were known so results could be compared. The first four gains were  $G_T = 1/22.5, 1/42.5, 1/69.5, \text{ and } 1/84.5$ . Unfortunately, all of these gains could not be investigated because the tightening experiment caused the RCC to bang into its hard stops during the tightening transient for gains below  $1/42.5$ . This was due to excessive deflection, and is highly undesirable since damage to the RCC is caused. Therefore data was only available for the first two gains.

The increased deflection was the result of two factors. First, decreased damping causes overshoot in the RCC torque. Second, an increased level of motor torque is present due to the higher feedback resistor. The RCC has a travel of approximately  $\pm 4.5^\circ$  between stops. This corresponds to an RCC torque of 14-16 in.-oz based on the stiffness data. Therefore, overshoot is limited.

Getting back to the experiment, the results are shown in Figure 5.38 for the two gains that were used. The motor torque and RCC deflection measurements are compared for the two gains. The plot of the motor torque shows a slightly faster rise time. The increased torque is due to the dependence of the current feedback loop on the gain. A greater difference in response is seen in the plot of the RCC deflection. The response with the higher is definitely more damped. These results roughly correspond to those of Figures 5.35 and 5.36, although the same stiffnesses are not represented.

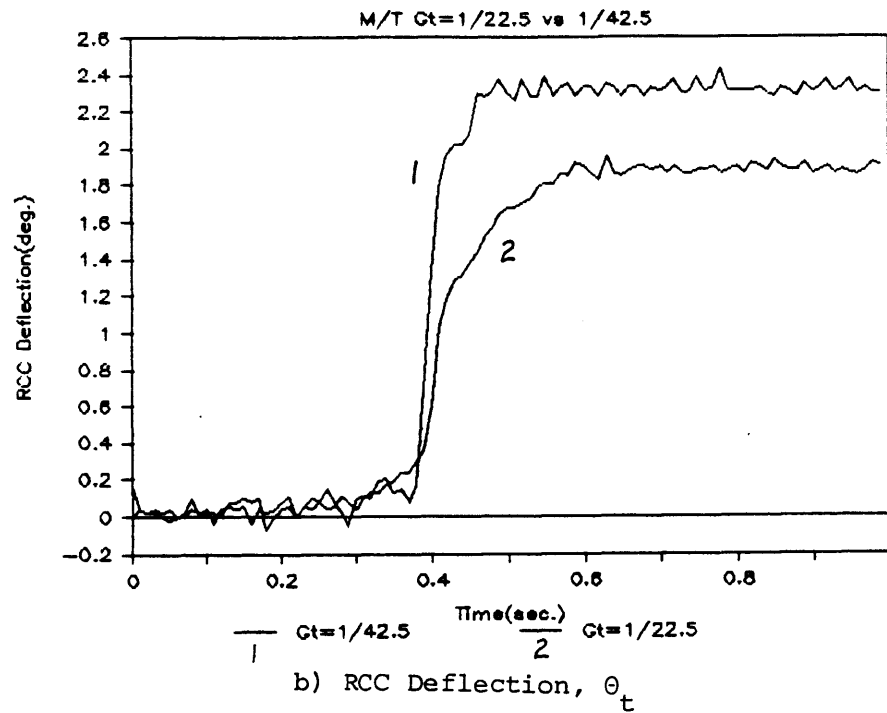
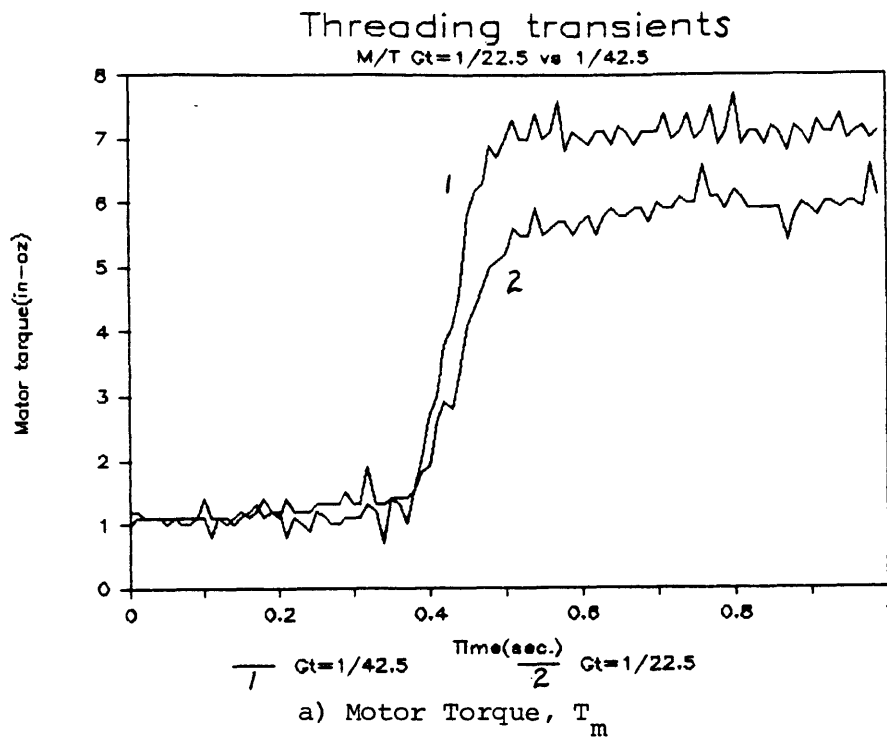


Figure 5.38 Measured Motor Torque and RCC Deflection Transients during Threading showing effect of change in  $G_T$

Another experiment using varied  $G_T$  in the torque watch windup test was performed. This test did not shed further light on the threading problem, but did allow a broader range of feedback gains to be investigated. A comparison of the results for gains of 1/22.5, 1/42.5, and 1/97.5 is shown in Figure 5.39. Evaluation of the results is complicated by the difference in final torque levels due to gain, but the response is definitely less damped as  $G_T$  is decreased.



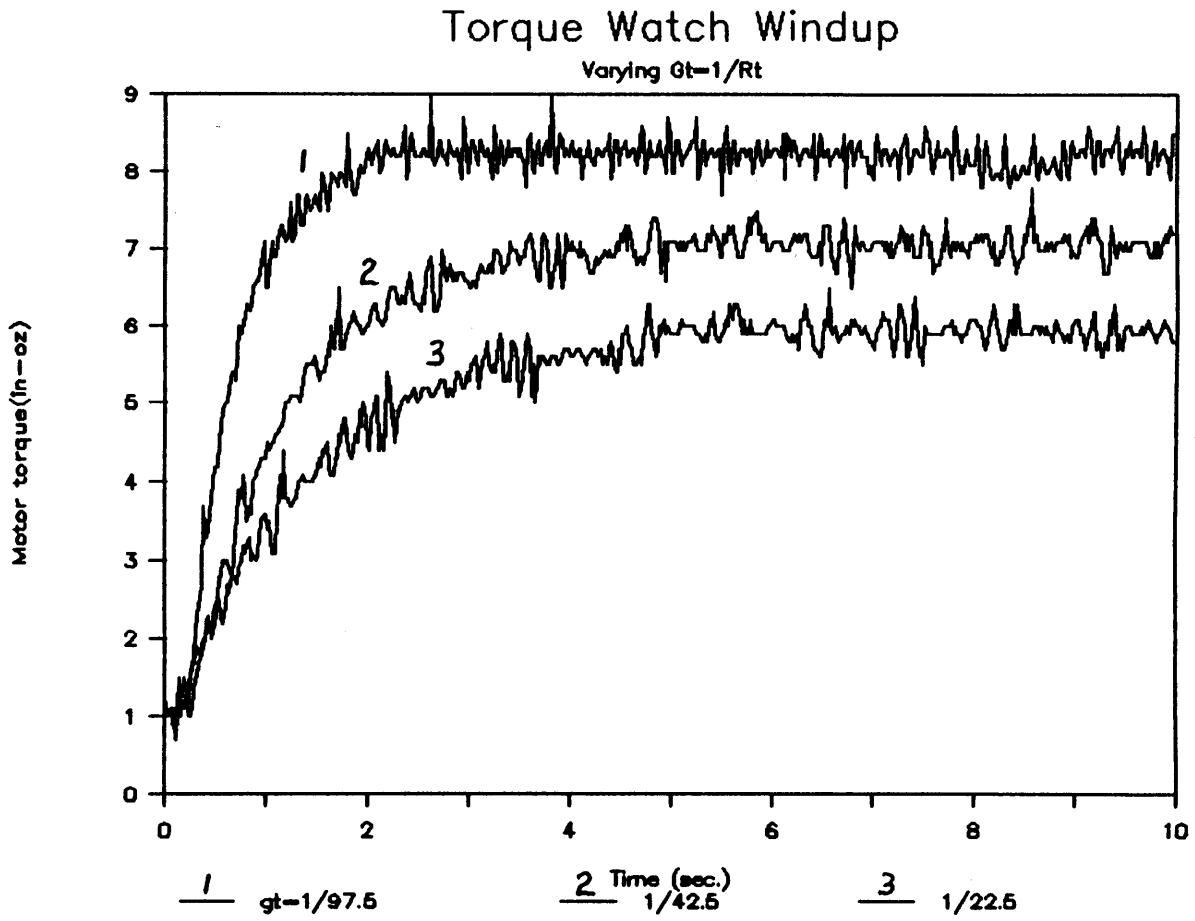


Figure 5.39 Measured Motor Torque during Torque Watch Windup for various Velocity Feedback Gains--  $G_T$  using  $T_C = 10$  in.-oz

## CHAPTER 6

### IMPROVED CURRENT FEEDBACK TORQUE CONTROL

This chapter examines implementations which can be used to improve upon the performance of the existing torque station for torque control. The shortcomings of the performance were identified in Section 5.5. The current feedback torque control scheme with added damping from velocity feedback was judged to be acceptable. The experimental results show that enough damping can be added to produce the desired results in the case of the wheel assembly parts. However, the experimental results were clouded by the dependence of the control circuit on the size of the feedback resistor that controls the overall velocity feedback gain. Comparing the part tightening response for different amounts of damping results in different torque levels applied as well as different damping in the transient. It is this problem that the following implementations seek to alleviate. It is desired that the input command only be adjusted for friction loss, and not leakage of the current control signal into the velocity feedback path. Precision assembly requires exacting performance from the assembly cell and any sources of degraded performance should be eliminated. A replacement of the DC tachometer by an optical encoder based tachometer is now presented as well as a modification to the procedure for using the existing controller to perform threaded part mating.

#### 6.1 Implementation of Encoder-Based Velocity Signal Generation

Future assembly cell needs require the addition of position control to the torque station. An investigation into the use of an incremental optical encoder for this task revealed that the device could also be used in conjunction with converting electronics to generate a velocity feedback

signal. It was also found that the resulting configuration could provide a larger signal than the DC tachometer so the velocity feedback resistor could be increased, and torque station performance enhanced.

#### 6.1.1 Method Used

Various methods can be used to generate the effect of velocity feedback with an encoder signal. These methods are listed in Appendix B. The method used by this research is also detailed in that appendix. It basically consists of the generation of an analog pulse train of prescribed magnitude and pulse width whose frequency is directly proportional to the angular velocity. The average value of this pulse train is also proportional to the velocity. The pulse train is used as the velocity feedback signal. Since this signal is not smooth it is desired to low pass filter the pulse train. This provides an averaging action on the signal but also introduces a lag when the angular velocity changes, and increases or decreases the frequency of the pulse train. Thus there is a trade off between smoothing the signal and introducing additional dynamics in the velocity feedback that can cause oscillations and stability problems with the velocity control loop.

From the performance model it was seen that a time constant was associated with the free speed control. Repeating Equation (5-16), this was

$$\tau_m = J_{MF}/B_T \quad (6-1)$$

To minimize the effect of the pulse train filtering on the velocity and torque control system, the following relationship should be observed

$$\tau_f \ll \tau_m \quad (6-2)$$

where  $\tau_f$  is the time constant of the first order low pass filter. For small angular velocities where the pulse width of the pulse train is much less than the period of the pulse train, a rough signal results from the utilization of Equation (6-2). However, experimentation proved that a rough signal produced better results than employing enough filtering to provide a smooth signal. It was found that the closed loop controller itself smooths out the effects of a rough feedback signal which produces a rough error

signal. Note that the average value of the rough signal vs velocity determines the "gain" of the encoder/electronics which corresponds to the gain of the DC tachometer,  $K_{TACH}$ . However, note also that the signal of this encoder-based tachometer, or "Entach," must still be filtered if a smooth signal for data collection purposes is desired. This filtering can be done with analog hardware, or a digital filter after collection of the data in sampled form.

### 6.1.2 Objectives for Torque Control

That the low pass filtering of a pulse train method is acceptable for speed control is all fine and good, but it must also be acceptable for torque control and, more specifically, the tightening of threaded parts. The main objective of this implementation of an Entach was to find out if it provided better performance in the control circuit than a DC tachometer. Experimentation proved more valuable than simulation because real hardware was utilized and the Entach velocity feedback signal required extensive modeling.

The major area of improvement offered by the Entach is that the magnitude of its average output signal is not totally dependent on the sensor itself as is the case with a DC tach. Thus the equivalent gain of the Entach,  $G_E$ , can be made to be much higher than  $K_{TACH}$  by the electronics that generate the pulse train. Therefore a larger feedback resistor,  $R_t$ , can be used to achieve the same overall velocity feedback gain,  $G_T K_{TACH}$  or  $G_T G_E$ . Since small values of this resistor were shown to adversely affect the performance of the current feedback loop, use of the Entach improves torque station operation. The encoder also reduces the friction in the drive by a small amount since it is a noncontacting device.

### 6.1.3 Hardware Set-Up

The experimental hardware used for the Entach implementation is shown in Figure 6.1. An optical encoder was installed on another MPI model 6M4H motor as shown. The encoder has a resolution of  $N = 1024$  counts/revolution. The motor/encoder (M/E) assembly was attached to a stand. A "dummy" inertia disc was attached to the motor output shaft using an adapter. This was to approximate the inertia of the torque station. The adapter also allowed the apparatus to be interfaced with a torque watch for stall torque tests. The

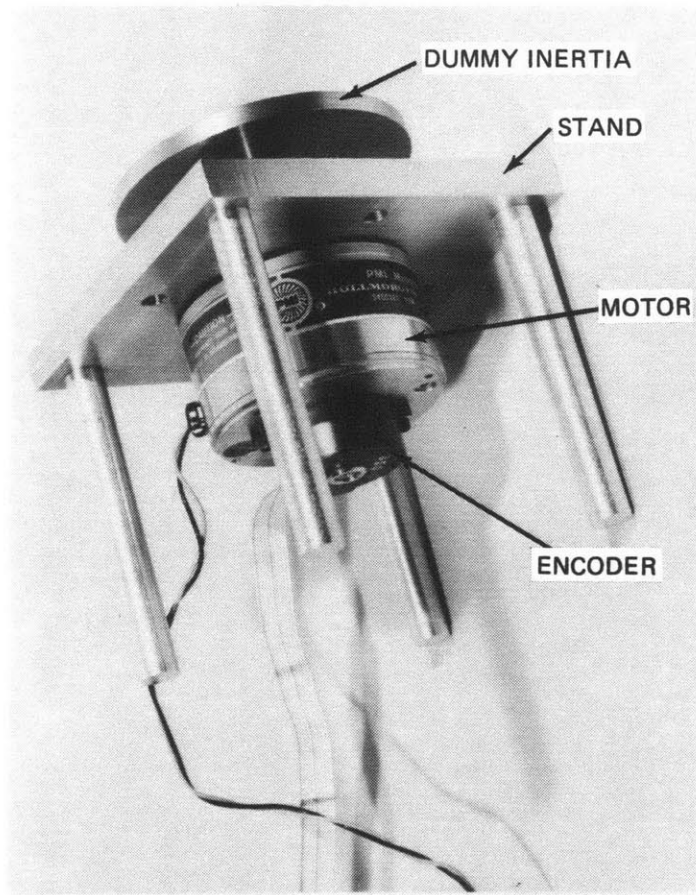


Figure 6.1. Motor/Encoder Apparatus

M/E assembly was chosen to allow it to be installed in the torque station. This installation was not carried out due to the development schedule of the assembly cell. Plans are being made to utilize it in the next generation of the assembly cell.

The experimental apparatus was connected to the assembly cell TS controller for testing. The encoder output was connected to the converting electronics (see Appendix B) which were connected to the velocity signal summing point in the control circuit. The same assembly cell computer, data acquisition system, and experimental software used for M/T testing was utilized.

Since actual part tightening experiments couldn't be performed, a series of experiments was to evaluate performance by other means. From preliminary experiments, a feedback resistor of  $1\text{ k}\Omega$  was chosen (this produces  $G_T = 1/1000$ ). Several pulse train filter time constants were tried with varied results. A time constant of  $\tau_f = 1\text{ msec}$  was chosen to keep the filter faster than the speed control loop (7-15 msec depending on gain). This value produced smooth speed control to near 1 rpm. In the following results, these values were used unless specified otherwise.

#### 6.1.4 Steady-State Speed Tests

The steady-state speed vs torque command test was performed using the motor/encoder. The results are shown in Figure 6.2. Since the feedback signal was not smooth, a calibration had to be performed between the output of a 50 msec low pass filter used to smooth the collected signal, and hand timed velocity using a stopwatch. This method was acceptable for speeds less than 30 rpm. The results show that the desired linearity between torque command and speed was achieved. This shows that the Entach provides an average signal that is proportional to the speed in the range tested. A linear fit to the data is shown by the solid line in the figure. From the slope of this line an equivalent gain can be found for the Entach. Ignoring measurement noise,  $V_n$ , and assuming that the mechanical damping,  $B_{mf}$ , is negligible, Equation (5-20) for steady-state velocity becomes

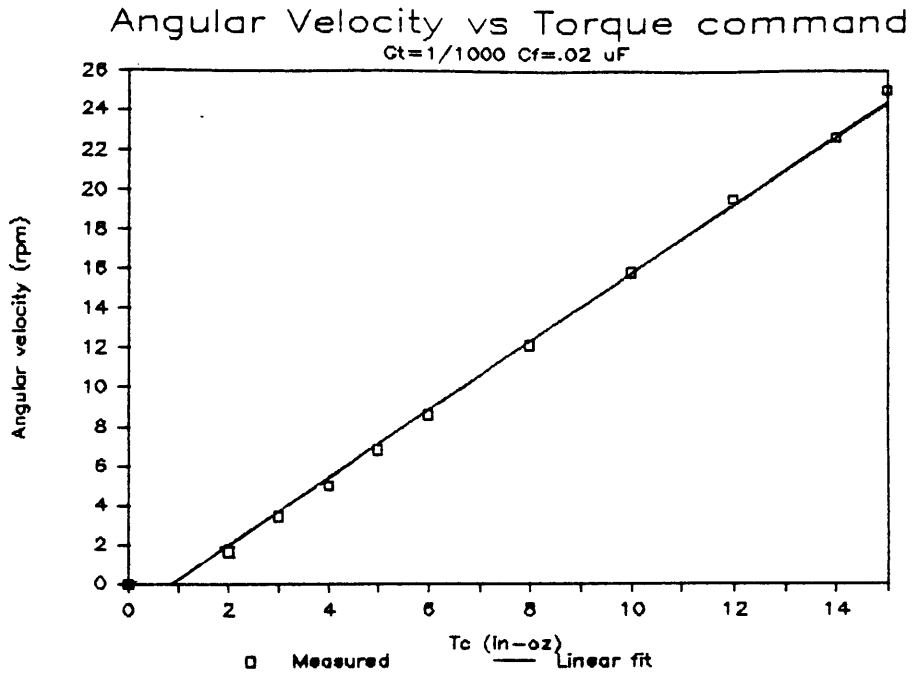


Figure 6.2 Free Running Tests for Motor/Encoder with Entach;  $G_T = 1/1000$   $C_f = .02 \mu F$

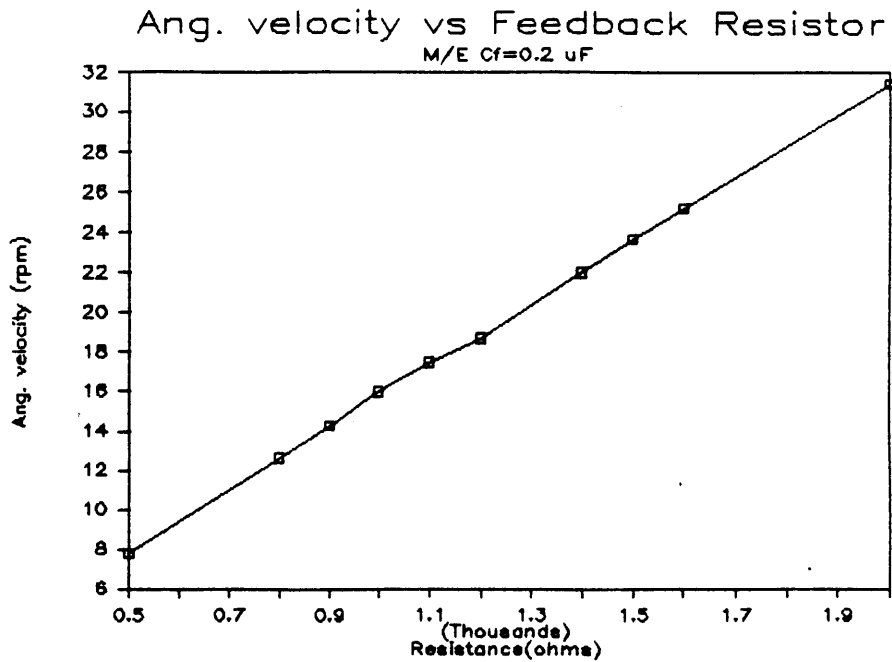


Figure 6.3 Measured Steady-state Velocity for M/E for varying  $G_T$  at  $T_c = 10$

$$\omega_{ss} = \frac{1}{G_A K_T G_T G_E} (T_c - T_f) \quad (6-3)$$

where  $G_E$  replaces  $K_{TACH}$  as the gain of the velocity measuring device. Solving for  $G_E$ ,

$$G_E = \frac{1}{G_A K_T G_T \omega_{ss}} (T_c - T_f) \quad (6-4)$$

Since the friction torque just produces an offset in the speed, Equation (6-4) can be rewritten in the form

$$G_E = \frac{1}{G_A K_T G_T} \frac{T_c}{\omega_{ss}} \quad (6-5)$$

The quantities  $G_A$ ,  $K_T$ , and  $G_T$  are known, and the quantity  $T_c/\omega_{ss}$  is the inverse of the slope of the linear fit to the experimental data. The linear fit produced a slope of 1.72 rpm/in.-oz. Using this quantity and the parameter values

$$G_E = 0.0183 \quad \text{V/rpm} \quad (0.175 \text{ V-sec/rad})$$

Comparing this to  $K_{TACH}$

$$\frac{G_E}{K_{TACH}} = 24.4$$

Therefore the Entach has a much larger gain than the DC tach and a larger  $R_T$  can be used to produce the same electrical damping in the control circuit.

The same test was repeated for  $T_c = 10$  and various values of  $R_T$  to show any dependency on the feedback resistor. Figure 6.3 shows the results. The solid line connects the data points. Rewriting Equation (6-4) in terms of  $R_T$

$$G_E = \frac{R_T}{G_A K_T} \frac{T_c - T_f}{\omega_{ss}} \quad (6-6)$$



Thus for  $T_c$  and  $T_f$  constant, the velocity should be proportional to  $R_T$ . Using a measured value of  $T_f = 1.25$  in.-oz, values ranging from 0.0178 to 0.0183 V/rpm were calculated for  $G_E$ , and no trend was shown. This compares favorably with the last result.

Note that the value of  $G_E$  is not truly a linear gain. It is only a representation for the equivalent gain of the Entach compared to a smooth output device such as a DC tach. The actual signal has variations which depend on the frequency and pulse width of the pulse train, and the amount of filtering that is done. The filter time constant does not significantly change the average value but does influence the smoothness.

From the experimentally determined gain of  $G_E = 0.0183$  V/rpm for the M/E, and a chosen feedback gain of  $G_T = 1/1000$ , a comparison can be made to the equivalent M/T system. The corresponding gain for the M/T would be  $G_T = 1/40$  to produce the same overall damping. This gain is slightly above the minimum gain needed to assure an overdamped response for threading using the guidelines in Chapter 5. Therefore,  $G_T = 1/1000$  was used for the M/E torque performance tests.

#### 6.1.5 Torque Watch Stall Torque Tests

The torque watch stall torque test was repeated for the M/E apparatus using the gains mentioned above. Actual output torque,  $T_n$ , and motor torque,  $T_m$ , were measured for values of  $T_c$  from 0 to 15 in.-oz. Actual torque results are shown in Figure 6.4. The solid line indicates the calculated values for  $T_f = 1.25$  in.-oz. Compared to the results of the M/T using  $G_T = 1/22.5$ , great improvement is shown. The desired torque is delivered for the 0-15 in.-oz range. Figure 6.5 shows the results for the measured motor torque. Again, the solid line indicates the calculated values. Correlation of this variable with the desired levels is also very good. Note that this was expected due to the larger feedback resistor and impedance of the Entach electronics. A plot of the two variables together is shown in Figure 6.6. As was the case with the M/T, the motor torque can be used to predict the net output torque.

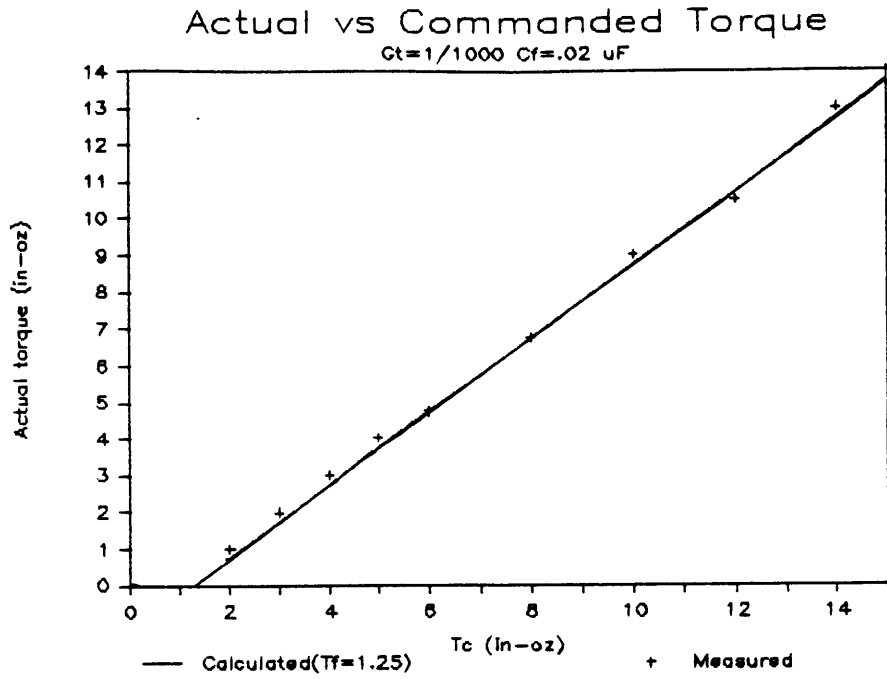


Figure 6.4 Stall torque test results for M/E with  $G_T = 1/1000$  and  $C_f = .02 \mu F$

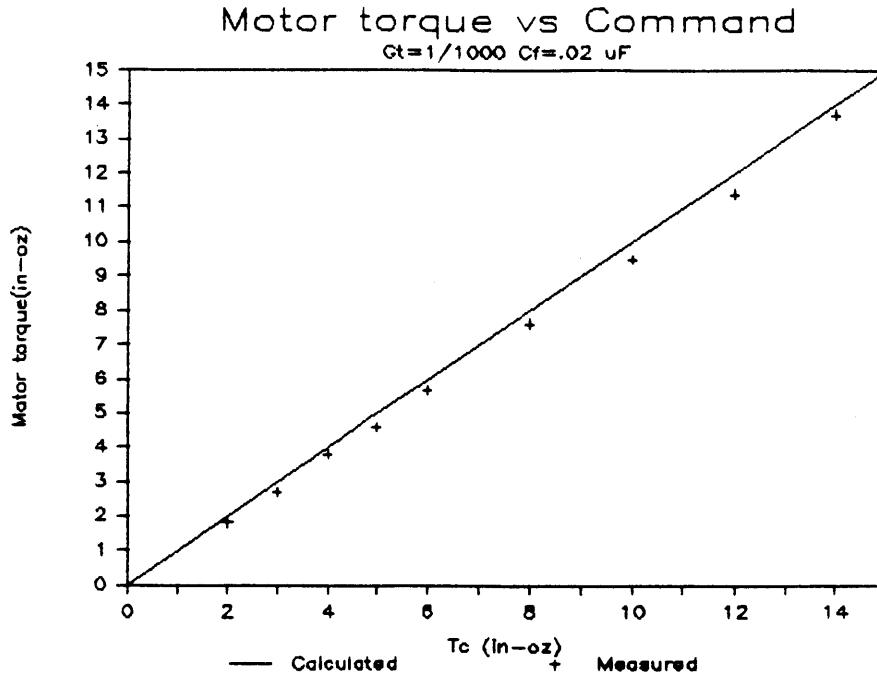


Figure 6.5 Measured Motor Torque for M/E with  $G_T = 1/1000$  and  $C_f = .02 \mu F$

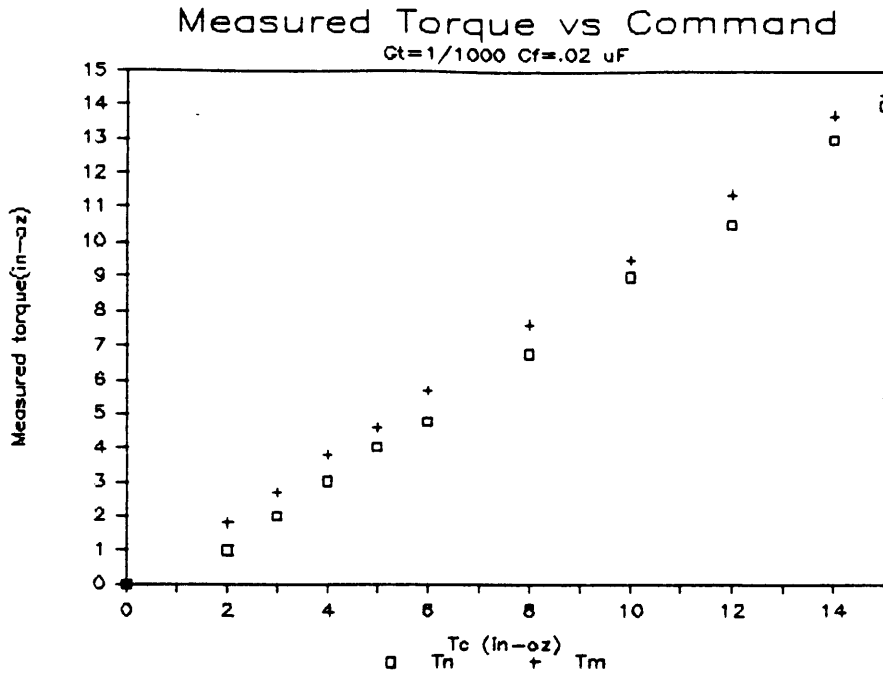


Figure 6.6 Correlation of Motor Torque and Net Output Torque for M/E

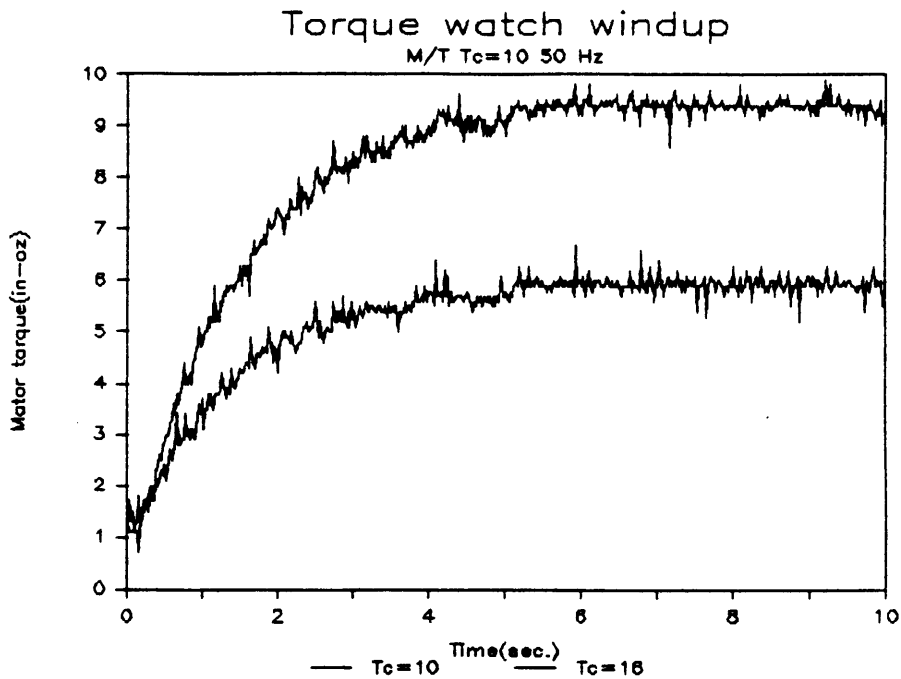


Figure 6.7 Comparison of Torque Watch Windup Motor Torque transients for M/T and M/E with similar damping.

### 6.1.6 Torque Watch Windup Transients

A third test performed on the M/E was the collection of motor torque and velocity signal data during torque watch windup. Figure 6.7 shows the comparison between M/T and M/E results for a torque command of 10 in.-oz. It is seen that for roughly the same dynamic response, the M/E delivers a final motor torque very close to the desired value while the M/T does not. Thus the M/E implementation delivers the correct level of torque, and the proper damping to achieve an overdamped response. Figure 6.8 shows the averaged velocity signal during torquing for the torque watch test. The units are not rpm, but normalized from 0 to 10. The upper trace shows the signal during free running, the lower trace is at  $T_c = 0$  or zero velocity, and the transient is the decrease in velocity as the motor stalls. Note that in this case the velocity signal goes back to zero at motor stall which was not the case in the M/T results. Therefore no (or very little) leakage of the input command to the velocity feedback path took place, and the proper amount of current was delivered by the circuit to the motor.

### 6.1.7 Use of Motor/Encoder for Threaded Part Mating

All of the results shown so far indicate that the motor/encoder with Entach has superior performance for the same amount of overall damping compared to that of the motor/tachometer. However, the torque watch windup process is a much slower and less stiff system than threaded part mating. Full judgement cannot be made until further testing using the M/E in the torque station is performed. Since this could not be part of this research, another experiment was devised to show the response of the control system with the Entach for a very stiff system.

The dummy inertia disk was fitted with a bolt that protruded through the disk toward the stand of the apparatus shown in Figure 6.1. A block was attached to the stand. The block and bolt were adjusted so that they would impact when the motor and disk were rotated. Thus a stiff impact test could be performed on the M/E. For the test, the motor/disk was driven to a steady-state speed, and motor torque data was collected as the bolt and block collided. Sampling was performed at 200 Hz. It was found that varying the time constant of the Entach's pulse train filter affected the motor torque

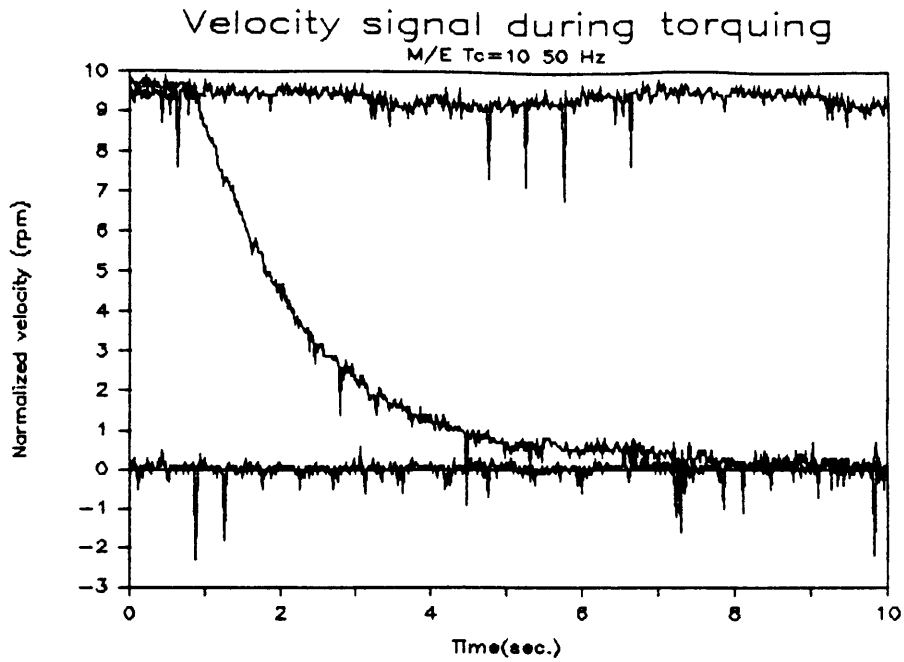


Figure 6.8 Measured Velocity Signal during Torque Watch windup for M/E at  $T_c = 10$  in.-oz. Compare to M/T results in fig. 5.28.

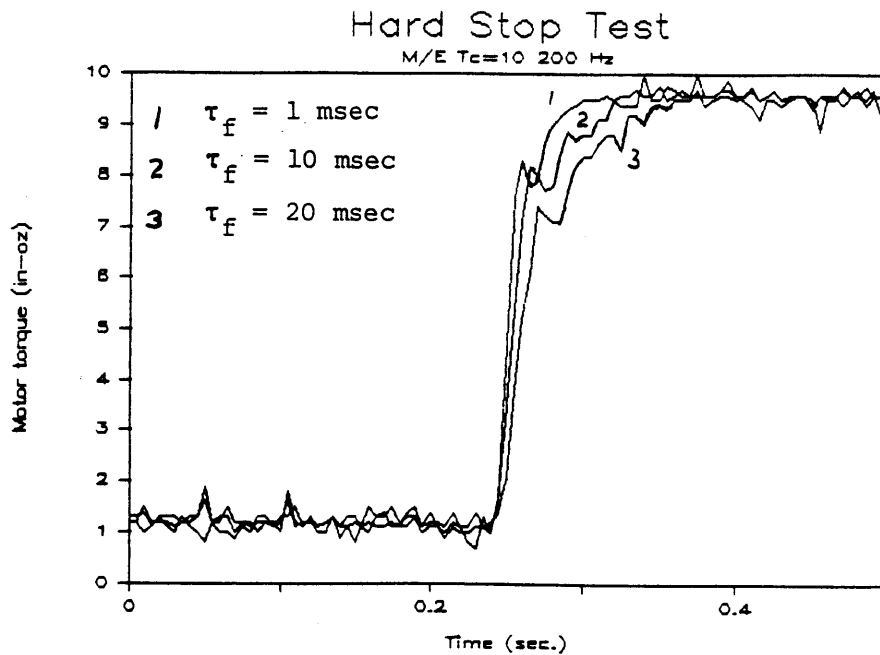


Figure 6.9 Measured Motor Torque for M/E Impact Test with varying  $G_T$

response. Results are shown in Figure 6.9 for time constants of 1, 10, and 40 msec. It is seen that increasing the time constant of the filter slows down the torque rise in the motor. This is due to the increased decay time of the filter output. This filter output provides the velocity feedback signal. Since the filter takes longer to go to zero output, the negative velocity feedback causes the same result in the motor torque. Thus the filter can also be used to alter the system dynamics as well as the feedback gain,  $G_T$ . This can aid the threaded part mating process by adding a form of damping.

Note that this filtering cannot be used in excess, though. This is because an increased time constant has adverse effects on free running and rundown speed control. If the filter's time constant is not less than that of the desired speed control loop, then large oscillations in speed can result when the motor/inertia is started from rest. An example of this is shown in Figure 6.10. In this case the time constant of the filter was increased to 50 msec, and a command given for free running speed. This compares to the intended velocity loop time constant calculated from Equation (6-1) of 12 msec. The results show that the motor torque signal is oscillatory. This causes similar variations in velocity and position of the motor/inertia, and essentially an unstable system. This is unstable in the sense that the desired equilibrium is never reached. In summary, the results in Figure 6.10 show an example of not following the guidelines of Equation (6-2).

The previous example also points out the need to consider the time constant of the Entach filter when contemplating changes in torque station parameters. Chapter 5 mentioned that a possible variation considered for the next generation assembly cell was to decrease the inertia,  $J_{MF}$ . This is beneficial for part tightening since the damping is increased. However, the effect on rundown speed control must also be considered because  $\tau_m$  is decreased. The time constant of the Entach filter may have to be decreased accordingly.

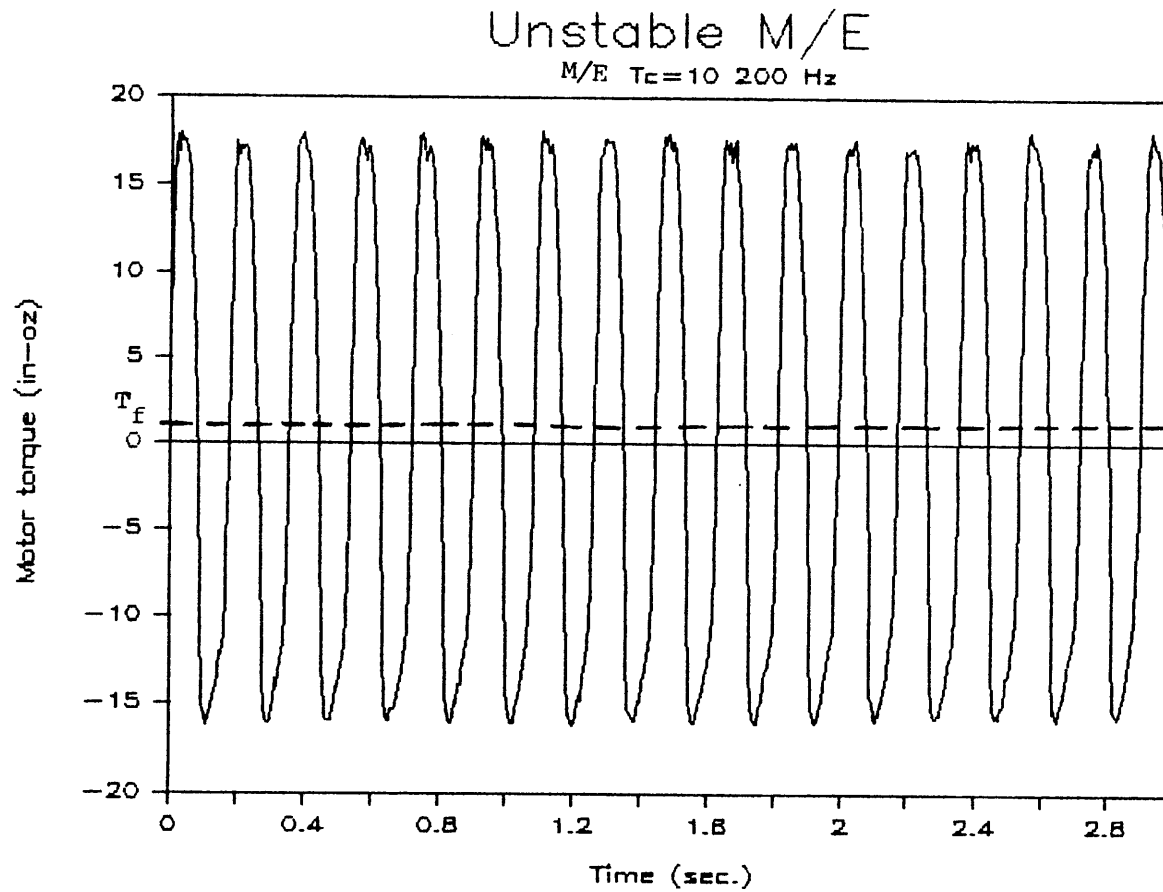


Figure 6.10 Measured Motor Torque for M/E with  $G_T = 1/1000$   
and  $\tau_f = 40$  msec showing oscillatory instability.  
Desired motor output is horizontal line at 1.25 in.-oz.

## 6.2 Alteration of Control Scheme

In the assembly sequence of the automated assembly cell, the current feedback method of torque control is utilized by using a single torque command to perform both the rundown and tightening phases. The torque command functions as a velocity command during rundown. When bottoming occurs and the torque due to part mating increases, the torque in the motor increases until the motor stalls and a final torque value is reached. How fast the parts are torqued depends on the physical parameters of the torque station, parts, and tool/collet/RCC assembly, and the amount of electrical damping that is added by velocity feedback. Once an assembly cell or other automation system is constructed, the only gain that can be varied is  $G_T$ . If a variety of threaded parts are to be assembled, the controller must be able to provide an overdamped tightening response for each one. The velocity feedback gain can theoretically be adjusted to provide enough damping so that this can occur. However, in the case of the control circuit used in this research, it was seen that the magnitude of the feedback gain, when adjusted to very high values, had a detrimental effect on the current control loop. It is not known by this author whether or not this problem could be alleviated by alternate circuit designs, but it is known that high feedback gains do produce greater sensitivity to measurement noise in a closed loop system. An alternate utilization of the current feedback method of torque control is now presented which provides an additional degree of freedom to the method, and allows less reliance on electrical damping.

This proposed modification is based in part on the manual assembly procedure. In this procedure, the threads are started and run down by hand, and lightly bottomed. A torque watch is then used for tightening to the desired level. In a sener, rundown and tightening are performed with different "tools". An alternate procedure for the torque controller is as follows:

1. Use the original procedure to perform rundown with a small torque command. A fraction above the rundown torque is suggested.
2. Stop and reduce the command to zero.



3. Issue the desired final torque command, but put it through a time-dependent function or filter to change the command from a step input to a ramp input or some other function.

The first two steps are self-explanatory. Care must be taken to use a low torque but also to assure bottoming. Use of this scheme with parts requiring a final torque that is a small percentage above rundown may not be possible.

Filtering the input command does not change the closed loop dynamics but does have the effect of slowing down the speed at which motor torque is increased by adding feedforward dynamics. Because the overall response is dependent on the motor torque, the speed at which the parts are tightened is reduced. This allows the velocity feedback gain to be reduced which improves the current loop performance (if the feedback resistor was affecting its response). Electrical damping cannot be totally abandoned, though. It still has the greatest effect on the system response. A large reduction may require the use of separate gains for steps 1 and 3 in the scheme.

Several possible methods can be used to "delay" the input. Either analog or digital filters could be used to operate on the step command. Figure 6.11 shows three possible functions. The modified input is represented by  $T_i$ . In general

$$T_i = f(T_c, t) \quad (6-7)$$

This scheme was not implemented for threading. An experiment was performed to examine a first-cut attempt at implementation. Using the control computer, a ramp function was generated in software as a staircase function with 0.1 in.-oz increments in torque command from 0 to 10 in.-oz. To be able to observe the dynamics visually, the spring of the torque watch was used which had a windup over a period of several seconds in previous experiments. The velocity gain was reduced to  $G_T = 1/1000$  and various total times,  $\Delta T$ , for the ramp function were used. As  $\Delta T$  decreased, the rise time of the response also decreased as expected, and overshoot eventually resulted.

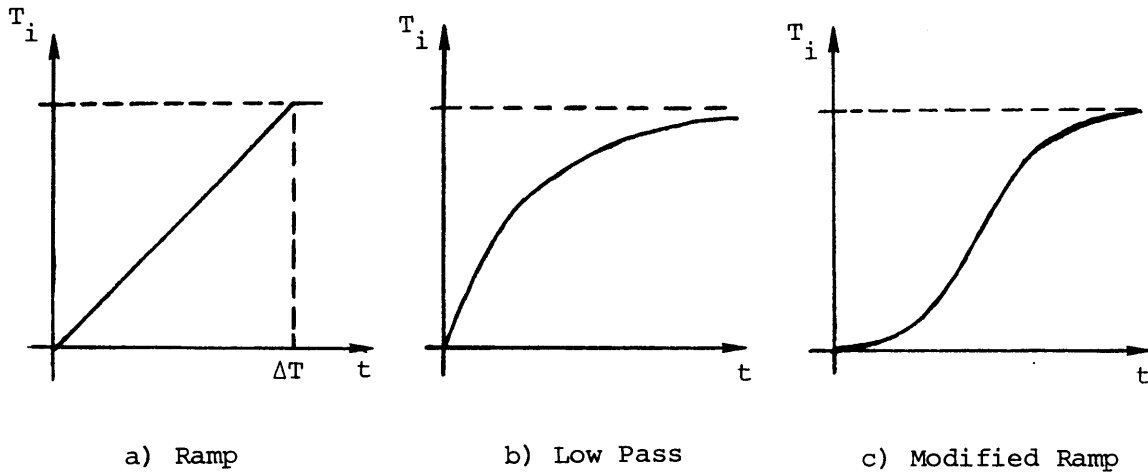


Figure 6.11 Input Modification Functions

This was not an all-encompassing experiment but did illustrate that the input modification scheme is feasible. It requires more sophistication in the input and a possible need for two different velocity feedback gains. However, this increased complexity does offer a solution to the problem of a small feedback resistor in the control circuit.

## CHAPTER 7

### TORQUE SENSOR FEEDBACK TORQUE CONTROL

This chapter discusses several issues relating to the use of torque sensor feedback torque control for threaded part mating. Using torque (sensor) feedback in addition to (motor) current feedback provides the control system with additional information about the part mating process. Conceivably, more information implies that better control is possible. The issues of implementing torque feedback include torque sensor design, sensor placement, choice of control strategy, and assembly cell interfacing. Also important is whether or not using additional feedback results in actual improvement of process control.

#### 7.1 Torque Feedback Objectives

The previous experimental and analytical results show that the current feedback method does work, but has limitations. These limitations are centered around uncertainties in output torque due to motor friction, and a heavy reliance on actuator and process models. The latter can be minimized by taking a conservative approach to the model, and employing a large amount of electrical damping. However, the performance of the assembly cell control circuit revealed that there may be a limit to the magnitude of electrical damping that can be used without affecting the system performance.

A look back at the threaded part mating process reveals that it has two phases with drastically different dynamics. The transition between these phases is difficult to predict. Therefore, a control system that smoothly adapts to time-varying parameter changes is necessary. The current feedback method with electrical damping does adapt to these changes. However, the tightening transient response depends on the parameters and dynamics of the specific parts being assembled. A torque station may have to assemble several different threaded part assemblies. Modeling each assembly may not be desirable, nor accurate. Also, especially with analog control, using a

different velocity feedback gain for each set of parts is undesirable. In the spirit of flexible automation systems, the torque station controller should allow assembly of different parts and reasonably different torque levels.

In light of these considerations, the major objective of the addition of torque feedback is to lessen the reliance on the process model and actual dynamics, and still achieve the desired results. Other objectives include lessening the effect of actuator friction on the torque command, and allowing for calibration of the system with a configuration that has dynamics that are close to those of the system during threaded part mating. The current feedback method uses torque watch windup for calibration. This method is acceptable but has much slower and more damped dynamics than threading. Also, it cannot be done when the assembly cell is closed off from the outside environment. Monitoring the motor torque can be done remotely, but an additional sensor would improve the reliability of the system.

## 7.2 Torque Sensor Design and Placement

Adding a torque sensor to the assembly cell requires that it be compatible with cell operation. Figure 4.4 shows possible placement of the device on either side of the part mating process. The choice and/or design of a sensor depends on this placement. During the course of this research, this author investigated commercially available devices and found none that were good candidates for precision threaded part mating control. In most cases, the low torque level requirement was not met. In others, the devices were essentially black boxes with unknown parameters. Stiffness could be found from calibration, but devices capable of rotation had friction whose location relative to the sensing element was unknown. Since the elimination of losses between the sensor element and the process was an objective, these devices are undesirable. In all cases, size prevented adaptation to the existing cell. This may or may not be a problem in another cell design. Several ideas for custom sensor design and implementation are now presented.

### 7.2.1 Design Principles

Before specific designs are presented, it is necessary to consider several principles of torque sensing. Two methods that are used to measure torque are 1) using position sensors to measure the relative angle between the two ends of an elastic element in torsion; and 2) using strain gauges to measure the strain of the element. The strain gauge method is normally used for large levels of torque. Using this method for low torque levels such as the 10 in.-oz specification of the wheel assembly would result in elements that were too fragile for assembly cell operation. Therefore, the first method is more feasible for low level measurement. Selection of the stiffness of the sensing element should consider the control system requirements and the available resolution of the position sensors. The resolution of a torque sensor is defined by

$$dT = K_s d\theta \quad (7-1)$$

where  $K_s$  is the sensor stiffness, and  $d\theta$  is the smallest change in angular deflection that can be measured.

A lesson can be learned from torque watch design. The midrange deflection of the device is chosen so that the measured torque creates a change in angle that an operator can easily control. These changes in angle depend on the smallest angle that an operator can detect on a dial indicator, and also how much damping he can apply to his turning motion at the applied torque level. Surely, position sensors are available to detect changes smaller than can be done with the human eye. However, matching the damping capability is also necessary when using sensor output in a control system.

### 7.2.2 In-Line Torque Sensor Design

Placing a torque sensor between the motor and the torque adapter which holds the rotating threaded part is now referred to as an "in-line" sensor implementation. An in-line sensor must have a compliant sensing element which is capable of continuous rotation. It is part of the drive train. Measuring the deflection of the compliant element must allow for this rotation. Slip

rings are required if the detector used must be attached to the compliant element. This would be the case with strain gauges. Slip rings add friction and also have electrical noise and reliability problems. Therefore, a method should be used that does not require this method of signal transfer.

A proposed in-line torque sensor is shown in Figure 7.1. It was conceived with the existing assembly cell torque station in mind, but the general principle could be used for other applications. The figure shows the drive shaft separated into two pieces and a spiral torsion spring placed in between these two pieces.

One end of this configuration is rigidly connected to the motor shaft. The other is contained in a set of duplex bearings for lateral support. The motor is connected to an encoder which measures the position of the input end of the torque sensor. The output shaft of the torque sensor is passed through another encoder and is ultimately connected to the torque adapter. This encoder measures the angle of the output. A torque value is generated by multiplying the stiffness of the sensor by the difference in the angles measured by the encoders

$$T_s = K_s (\theta_m - \theta_f) \quad (7-2)$$

where  $K_s$  is the stiffness, and  $\theta_m$  and  $\theta_f$  are the measured angles of the motor (input) and fixture (output) ends of the spring. The only loss in torque between the spring and the rotating part in the threaded part mating process is the friction torque of the duplex bearings. This torque can be made to be much less than the friction torque of the motor. Calibration can be performed on the torque sensor without using torque from the motor.

The advantage of the dual encoder architecture is that position information for both the motor and torque adapter is provided in addition to a torque signal. This information may be necessary if the torque station would require position control to orient the torque adapter.

In the present assembly cell, this positioning is done by the air cylinders and hard stops. However, future designs may require position control instead. Positioning may also be necessary for other assembly tasks.

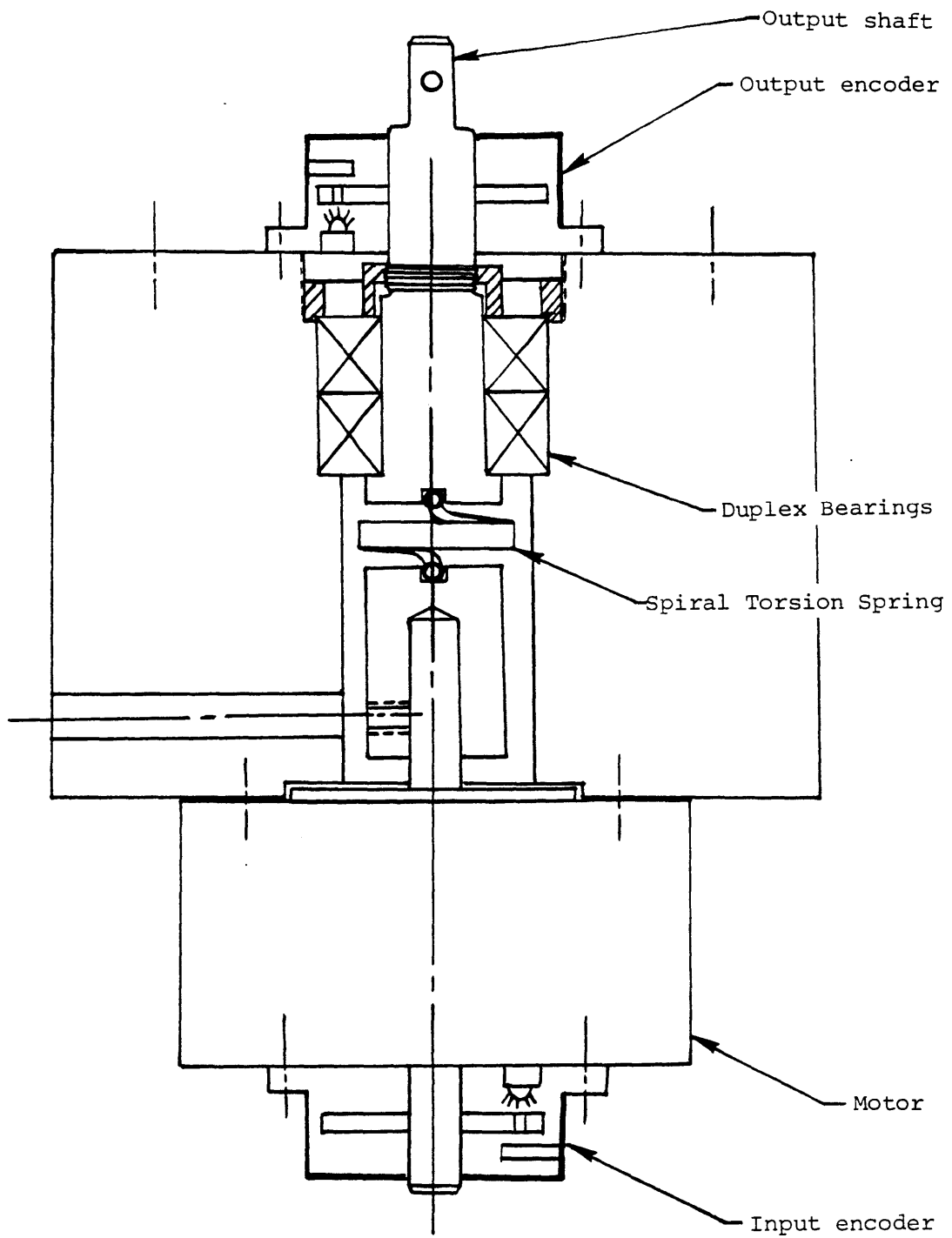


Figure 7.1 Proposed In-line Torque Sensor  
(shown with motor)

### 7.2.3 Use of the RCC as a Torque Sensor

Placing the torque sensor on the tool side of the process presents several problems. First, the robot arm performs tasks other than threading. Therefore, adding a torque sensor must not compromise the performance of the ARCT assembly for these tasks. Second, the size and weight of a torque sensor would require additional length for the ARCT assembly and require a stronger arm. For these reasons, placing a new torque sensor assembly on the arm is not considered to be feasible. However, the experimental apparatus used to determine the stiffness of the RCC and measure its dynamic deflection during threading showed that using the RCC as a torque sensor was somewhat feasible. The experimental data obtained indicated that there was a linear correlation between the deflection and torque in the RCC.

The experimental apparatus could detect changes in angle of  $0.05^\circ$  through digital sampling and an even finer resolution with analog measurement. From the range of stiffnesses found, this corresponds to a torque resolution of 0.14 to 0.18 in.-oz. This resolution is as good or better than can be obtained using a torque watch. If this device were to be used, initial calibration should be performed without the motor as the torque source since its friction causes a hysteresis effect on the torque vs deflection curve.

Unfortunately, using this apparatus in its present form in the assembly cell is not feasible. It interferes with the tool changing operations of the robot arm. A sensor that fits inside the outer diameter of the arm is necessary. The existing RCC is only instrumented for XY translation, but plans are being made to provide sensing for all five degrees of freedom in the next generation assembly cell design. The experimental apparatus had the advantage of a lever arm greater than the radius of the robot arm to improve resolution. This is not possible with an interior sensor. Therefore, resolution may not be as good.

### 7.3 Torque Feedback Control Concepts

Torque feedback control was not implemented in hardware by this research. Several concepts for actual implementation were considered, and are now presented. Force/torque feedback has been successfully used for many automated tasks, but each of these tasks has characteristics that influence how the feedback is to be applied in a control system. Both the placement and parameters of the torque sensor influence the control strategy to be used.



### 7.3.1 Sensor Parameters

The design concepts for torque sensors did mention that the stiffness of the elastic element influences the resolution, but no mention was made of the effect of the stiffness on system dynamics. A strategy employed in force/torque feedback control system design that is indicated in the literature is to 1) keep the sensor stiffness less than that of the process and the robot arm; and 2) minimize the mass/inertia between the sensing element and the process for which torque is to be controlled. This strategy is employed to minimize any dynamic interaction between the sensor and process stiffnesses, and to slow down the overall system dynamics because bandwidth is often a problem.

The general design guidelines presented in Chapter 5 showed that if the stiffness of the threading process was much greater than that of the RCC, it could be ignored. The system dynamics would be totally controlled by the RCC stiffness. Note that this refers to the tightening phase.

A simple experiment was performed to illustrate this fact. The torque watch windup test was repeated by adding the wheel assembly parts to the procedure. One part was held by the torque watch and the other by the torque station. The parts were initially placed and aligned, and then threading was performed with the torque watch in place of the ARCT. Data was collected for motor torque and velocity, and no difference was found between these results and those of a regular torque watch windup test.

A very soft in-line spring would also have a similar effect. However, additional dynamics are created because a third inertia/compliance pair is added to the system.

Thus, choosing a soft spring for the torque sensor seems to be the answer to the objective of lessening the effect of process dynamics on the torque control system. However, other factors must be considered. The stiffness of the RCC cannot be arbitrarily reduced because it must perform a series of other tasks such as peg-in-hole insertions. A very soft RCC would also be more prone to damage, and may require some form of damping.

Another parameter to be chosen is the inertia between the sensor element and the process. Clearly, in the RCC case this choice is limited by the fact that the RCC must support a tool, the collet, and a threaded part. For the in-line torque sensor, the inertia must include the torque adapter, an assembly fixture, and a threaded part. Inertia combines with stiffness to determine the natural frequency and amount of deflection in the device when it is not connected to the process, and during rundown.

Although a soft spring is desirable for the tightening phase, this may not be the case for rundown. During this phase, the part stiffness is essentially zero. Therefore, oscillation of the inertia attached to the spring in the torque sensor may be a problem. Its natural frequency is reduced with a softer spring. The experimental results in Chapter 5 showed that these oscillations can occur, but are not a problem if their magnitude is small and frequency large. For an in-line sensor, a soft spring could create an oscillation of the torque adapter and the tool. Examination of torque watch use reveals that the device is not normally used for rundown. Bottoming and tightening could be affected by an oscillation of the part caused by the soft torque watch spring.

### 7.3.2 Influence of Torque Feedback on System Dynamics

A brief review of the current feedback control method is used to set the stage for the addition of torque feedback. The current feedback controller is essentially a velocity controller during rundown. The steady-state speed is effected by the rundown torque and the amount of electrical damping or electrical velocity feedback that is used. Thus the controller functions well for this phase. When bottoming occurs, the controller changes to a position controller due to the addition of mechanical position feedback in the form of an actual position-dependent torque being exerted on the system. The mechanical position feedback causes the system to reach a steady-state position, zero velocity, and final motor torque. The threaded part mating process itself signals the controller to change from velocity to position control. Tightening transient dynamics are controlled by the equivalent inertia and stiffness of the system, and the amount of electrical damping that

is used. The error signal that is made to go to zero is at the mechanical side of the motor. This is a summing of actual torques. Thus the steady-state command to the motor is not zero. Also, the steady-state error in position (actually torque) is zero assuming that an adjustment to the command has been made for friction.

When torque feedback is added, an electrical signal proportional to the sensed torque, or difference in position, is summed with the torque command, or difference in position command, to close an additional position loop for the controller. Using the equivalent second order representation for the threaded part mating process presented in Chapter 5, Figure 7.2 shows a simplified block diagram representation of the addition of torque feedback. This is a simplified form to illustrate the concept, not to totally explain the system dynamics.

In the figure, the equivalent process parameters are  $J_{EQ}$  and  $K_{EQ}$ . The symbol  $\theta_p$  represents a vector of the positions within the process. This vector and  $\theta_m$  determine the difference in position that produces both the mechanical torque feedback, and the input to the torque sensor. The output of the torque sensor is the sensed torque,  $T_s$ . The gain of the torque sensor is  $G_s$ . The overall velocity feedback gain is  $G_w$ . Two inputs are shown -- one for velocity and one for torque/position. A torque feedback compensator is represented by  $H_T(s)$ .

Application of the block diagram to the threading process begins with consideration of tightening phase control. The control strategy for this phase is to control the deflection in the torque sensor to produce the desired applied torque. A comparison of the block diagram of this system with that of a simple position control system reveals that the equivalent torque control system is similar to a damped position control loop with a disturbance torque. Such a system has a steady-state error when proportional control is used, and zero steady-state error if proportional-plus-integral (PI) control is used. The desired steady-state relationship for the generalized threading controller in Figure 7.2 is

$$\frac{\Delta\theta_s}{T_c} = \frac{1}{G_s} \quad (7-3)$$

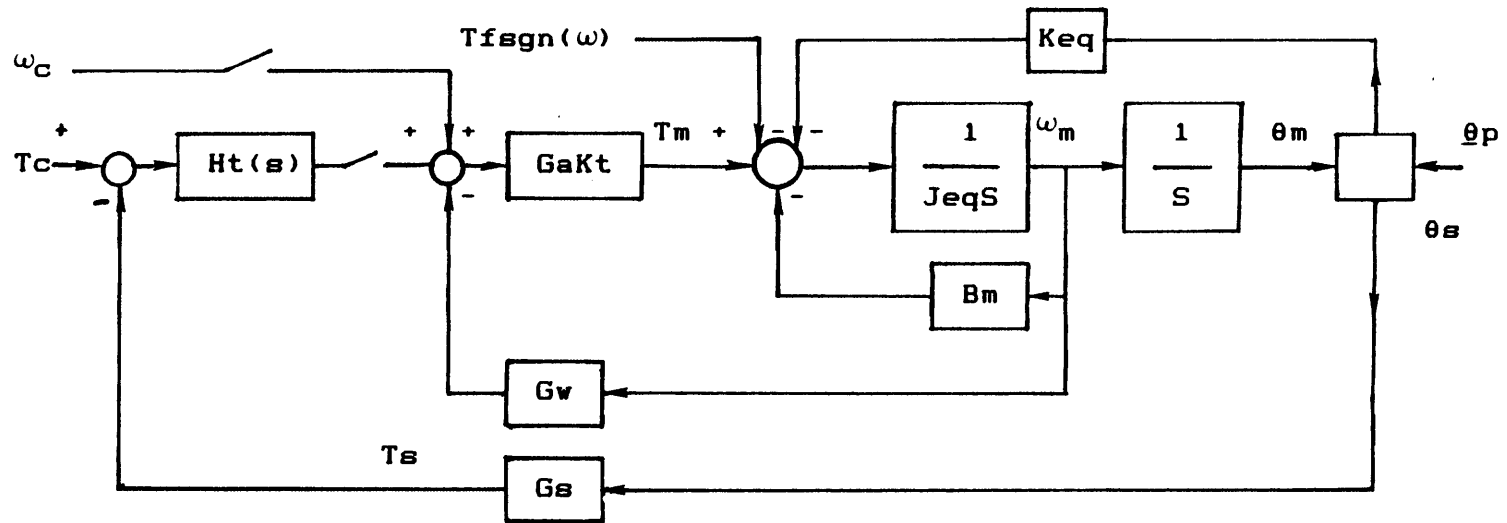


Figure 7.2 Generalized Torque Sensor Feedback Diagram

Treating the equivalent system as linear and second-order, the use of proportional control yields

$$H_T(s) = H_p \quad (7-4)$$

$$\frac{\Delta\theta_s}{T_c} = \frac{K_P G_A K_T}{J_{EQ} s^2 + B_T s + (H_p G_A K_T G_S + K_{EQ})} \quad (7-5)$$

The steady-state relationship is

$$\frac{\Delta\theta_s}{T_c} = \frac{K_P G_A K_T}{H_p G_A K_T G_S + K_{EQ}} \quad (7-6)$$

Therefore, there is a steady-state error. This can be minimized by increasing  $H_p$ . However, comparison of the new characteristic equation with that of the current feedback method given in Equation (5-49) reveals that adding torque feedback has increased the natural frequency and decreased the damping ratio. This is due to the  $H_p G_A K_T G_S$  term. Therefore, increasing the controller gain may result in overshoot. Also, friction has not been considered. It adds to the steady-state error since it is also a disturbance torque.

Use of PI control yields

$$H_T(s) = H_p + \frac{H_I}{s} \quad (7-7)$$

$$\frac{\Delta\theta_s}{T_c} = \frac{G_A K_T (H_p s + H_I)}{J s^3 + B_T s^2 + (H_p G_A K_T G_S + K_{EQ}) s + (H_I G_A K_T G_S)} \quad (7-8)$$

The steady-state relationship is

$$\frac{\Delta\theta_s}{T_c} = \frac{1}{G_S} \quad (7-9)$$

Therefore, PI control reduces the steady-state error to zero. The compensation adds a pole at the origin. Therefore its zero should be chosen between the compensator pole and the slowest real pole from the current feedback system dynamics. A set of gains is chosen to keep the overdamped response. This assumes that a real compensator can be built to match these gains. Therefore, in theory, a PI compensator is preferred over a proportional compensator for tightening.

The additional velocity command input shown in Figure 7.2 is provided for the rundown phase. If the PI torque feedback controller were used during this phase, an input torque command is meaningless. The error signal from the torque command and feedback would be integrated by the compensator and large velocities could occur if enough damping was not provided.

Thus the torque controller can be switched off during rundown, and the speed control of the current feedback control method used. Switching from one command to another can be accomplished by using the output of the torque sensor to trigger the transition when bottoming occurs, and the sensed torque rises above a threshold.

### 7.3.3 In-Line Torque Sensor Use

The simplified model used for torque feedback control illustrates the basic principles of the method, but must be increased in complexity for actual controller design. This is especially true for the addition of an in-line torque sensor. The equivalent second-order model is not valid since the order of the system is increased by the addition of another inertia/compliance pair. From the modal analogy used to describe the current control method dynamics, it was seen that two modes existed. One, the chain mode, could be controlled and had to be overdamped. The other was a part mode which was not controllable, but also not really present in the actual and nonlinear simulation results. With the addition of an in-line torque sensor, another oscillatory mode is added that probably does show up. It is the oscillation of the torque adapter, parts, and collet between the RCC and the sensor spring. If  $K_c \gg K_s$ , this may not be a problem. If not, some more sophisticated elastic system control scheme might be necessary.

#### 7.3.4 RCC Torque Sensor Use

Employing the RCC as a torque sensor does not change the physical dynamics of the system. This is advantageous for complexity reasons since other robot tasks are not adversely affected. The rundown phase is performed smoothly since a proven velocity controller can be used. No additional compensation must be made for the physical dynamics of the torque station. However, the relatively fixed stiffness of the RCC removes a design parameter for the controller. As was seen in the parts used by this thesis, the RCC and part stiffnesses are of the same order of magnitude. Thus the process model is still very important.

What does set the RCC based sensor apart from the in-line sensor is that the scheme allows torque to be measured on both sides of the part mating process. In order to verify that overshoot was not present, the RCC deflection was measured in the current feedback torque control experiments. The simulations showed a better correlation between part torque overshoot and RCC overshoot than motor torque overshoot. Verifying the in-line torque sensor method also requires RCC position information.

Of importance to all torque control methods is that the part torque is never directly measured and used for control. To do this would require forming a torque feedback signal based on the relative position of the parts. Clearly this is not desirable because the angle is so small and very minute errors in detecting the bottoming point would cause large errors in part torque. This approach would essentially be the turn-of-the-nut method of part assembly used in a dynamic situation.

Knowing the time history of the positions of the two parts is beneficial to verifying the process and system models, though. The actual tightening angle could be determined with this information. Of interest is whether or not these time histories are repeatable from assembly to assembly. Being able to measure all of the variables plotted in the simulation would be beneficial even if the information was not actively used in the control system.

Use of the RCC as a torque feedback signal generator does provide direct correlation between current feedback and torque feedback control. Both methods can be implemented with the same physical hardware and then compared for performance. This is the final judgement for choosing between the two

methods.

#### 7.4 Evaluation of the Torque Feedback Method

Addition of torque feedback can result in improved performance. The torque measured and used for control is less contaminated by losses between the sensor and the process than the motor torque. The feedback signal is also generated by a sensor which can be calibrated independently of the actuator. Actual deflection is measured rather than motor current. Since the threading process involves the dynamics of the RCC, basing the torque feedback there offers the advantage of knowing torques on both sides of the process. However, torque feedback requires that additional sensing and complexity be added to the system. This can affect performance of other assembly tasks.

Torque feedback also requires additional electrical damping since an additional position loop is closed and the transient dynamics are less damped. The possible need to switch between the rundown and tightening controllers requires additional logic in the control strategy, and may be easier said than done.



## Chapter 8

### Conclusion and Recommendations

Control of the process of threaded part mating in an automated assembly cell designed and implemented for precision assembly has been examined. The assembly cell can properly position the parts to initiate the part mating process. Therefore, the efforts of this thesis concentrated on the control of the threading torque.

Perhaps the most important lesson learned from this research was that torque control of a process must consider a model of that process. Blindly exerting a torque on the process can create dynamics that yield undesirable results. In the case of threaded part mating, no overshoot in torque applied to the parts is allowed. Since both parts have dynamics in an automated assembly system, several torque levels are present in the process. These are the net motor output torque, the part torque, and the RCC torque. It is necessary to control all of these torques to meet the assembly specifications.

In order to do this, the control system must be designed to control the level of torque that its actuator applies as well as the transient dynamics that this torque causes. The controller must also adapt to changes in the process dynamics. This need is seen in threaded part mating for the transition from rundown to tightening at the bottoming point.

This thesis proposed a dynamic part mating model to be incorporated with the current feedback torque control method to evaluate existing hardware performance, as well as to formulate guidelines for generalized part mating controller design. The total control system model was used to illustrate the strategy necessary to achieve controlled speed rundown and controlled torque tightening. Experimental results and observations added to the analytical tools provided from modeling by revealing some of the limitations of real hardware.

## 8.1 Threaded Part Mating Model

The dynamic part mating model presented by this thesis in Chapter 3 is based on experimental results that characterize the process. A torque vs angle curve was defined to indicate the torque required to change the relative position of the two parts. This curve is the basis for the model. Two dynamic models were formulated. The piecewise linear model separates the process into linearized parts to describe rundown and tightening. Its accuracy for describing the steady-state level of the part torque is limited by its linearization, but it allows an accurate prediction of the control system transients using well understood linear analysis methods. A more complete description is provided by the non-linear model that combined the coulomb friction and spring-like characteristics of the process. This model predicts both the steady-state and transient nature of the process.

The non-linear CFS model is a first attempt at characterizing the threaded part mating process with a dynamic model. The model is admittedly a simplification. Reflecting the TVA curve about the position axis as shown in figure 3.10 was not totally experimentally justified. Determining what the negative side of the curve really looks like is recommended as an area of future investigation.

The data collected to define the TVA curve was taken statically using a torque watch. An apparatus should be designed to allow this data to be taken in a dynamic situation. This could be done by creating an experimental torque station and tool apparatus with instrumentation for the position and velocity of both of the threaded parts. The dependence on relative velocity as well as on relative position of the TVA curve is another unknown that should be investigated.

Only one example of a precision assembly was considered by this research. It is recommended that a series of assemblies be compared for size, assembly torque levels, tolerances, and experimental TVA curve data. Guidelines for automated precision assembly cannot be considered complete until a better numerical representation of the properties of precision assembly is formulated. One problem in this area is the limited availability of precision parts for process modeling experiments.

Other recommendations for the CFS model are now presented as part of the concluding discussion of the current feedback control method.

## 8.2 Current Feedback Torque Control

The control method presented by modeling, hardware implementation, and experimental verification in this thesis was based on the use of DC motor current feedback for torque control. The method is adapted for specific use to control threaded part mating by incorporating velocity feedback to provide damping for rundown speed control and tightening transient response control.

The control system dynamics were described by a control system model which incorporated the linear and CFS models of the process. Analysis of this model was used to simulate the response of the system as well as to investigate the effect of changes in system parameters.

This thesis made an attempt at providing additional tools to investigate controller parameters by using the linear model to predict the actual and non-linear model results. A description of the system using the linear model was considered in Chapter 5 by developing the concept of a chain mode and a part mode. It was shown that achieving an overdamped torque response for all three process torques required that the eigenvalues corresponding to the chain mode be real. For the range of values simulated in this research, the part mode was found to be of higher frequency than, and dominated by, the chain mode. The part mode is really an artifact of the model since the parts are actually a "one-way" spring.

This concept appears to be reasonably valid. It is recommended that it be evaluated by exploring more comparisons between the predictions of this model and actual results. The concept may break down when the extremes of parameters are considered. For example, if the torque station inertia were much less than that of the tool/collet, the part mode may play a greater role in the dynamics since its frequency is reduced with respect to that of the chain mode.

The non-linear simulations of the system dynamics provided a good representation of the actual dynamics seen in the experimental data taken in this research. However, this data was somewhat clouded by circuit problems. It is recommended that further correlation of this model and actual results be performed for variation of the velocity feedback gain and the torque station inertia. These two parameters may be the only ones available to the controller designer for variation.

This thesis used a linear fit to the tightening portion of the TVA curve in the CFS model. Curves with other shapes should be investigated further with non-linear simulation. Parts that are tightened to a greater degree than the wheel assembly may exhibit a rise in the slope of the TVA curve. This may alter the tightening response.

The hardware lessons learned for actual implementation of the current feedback torque control method complement the analytical efforts. A designer using this method of control may assume that he can solve all of his problems by increasing the velocity feedback gain to high levels that positively assure an overdamped tightening response. However, this reasoning is flawed because the actual control circuit may not be able to utilize such high gains without degraded performance. Also, the torque station may turn so slowly that the assembly process takes an unreasonable amount of time. At very low speeds, friction also plays a role in speed control.

The particular control circuit used in this research that is shown in figure 5.2 suffered from a dependence of the current loop on the velocity feedback resistor. Improvement of this circuit is a topic for further investigation. This circuit can also be used in the force/torque control of other processes, and its merits and limitations should be quantified. The

incorporation of an encoder-based tachometer presented in Chapter 6 seemed to alleviate the circuit problem. However, it should be fully tested for threaded part assembly. Results of these tests may indicate that another iteration of the first-order approach to "Entach" design is necessary. We suggest a microprocessor-based digital filter be tried.

Overall, the current feedback torque control method is judged to be an acceptable approach to the control of threaded part mating. It is necessary to complement the method with experiments such as RCC deflection measurements to provide an indication of the actual dynamics. The method is most limited by friction in the motor and drive. Friction can be calibrated out as long as it is a fraction of the final torque. The final torque to friction torque ratio of the wheel assembly parts was 10:1. There is a lower limit on this ratio that should be investigated with further experimentation. The variability of the friction at low speeds and torque commands is of particular interest. Scaling of the hardware to different torque levels may or may not be possible. The method is critically dependent on the precise linear current to torque conversion capability of the DC motor. There appears to be a range of 1 to 200 in-oz of output torque that is covered by motors in the "precision motor" category. Exceeding these limits with the current feedback method may not be possible.

### 8.3 Part Mating Controller Design Guidelines

The various guidelines presented by this thesis for estimation of the process control dynamics are now summarized. They are based on the models developed in this thesis and the hardware employed by the assembly cell for threaded part assembly. Utilization of these guidelines should be accompanied by good engineering judgement. Adapting them to different hardware configurations may require modifications to the models used. For example, modeling an automation system employing a shear pad instead of wire RCC would require that damping be added to the model of the RCC.

Various degrees of complexity are represented by the guidelines. They present different ways of analyzing the problem. An aim of the guidelines is to allow the controller designer to estimate the system dynamics and determine the hardware that is needed before an actual automated system is constructed.

Remembering that the aim of the controller is to achieve controlled speed rundown and an overdamped application of torque to the threaded joint during tightening, the guidelines are:

1. Estimate the desired rundown speed by comparing the kinetic energy of the rotating torque station with the area under the TVA curve. This area indicates the energy that can be absorbed by the parts. If detailed TVA experiments are not possible, at least estimate the total tightening angle. This comparison provides an indication of the parts' ability to stop the inertia of the torque station by themselves. A term must also be added to the kinetic energy equal to the product of the torque applied by the torque station during rundown and the tightening angle. This is additional energy added by the motor.

2. Estimate equivalent parameters for the parts/tool/collet/RCC chain to form a second order representation for the process. An equivalent stiffness,  $K_{EQ}$ , can be found by summing the torque station and tool/collet inertias. This is a conservative approach. Add the equivalent parameters to the basic performance model of the controller to form a closed loop system which has a characteristic equation in the following form:

$$J_{EQ}s^2 + B_Ts + K_{EQ} = 0 \quad (8-1)$$

Estimate the necessary damping,  $B_T$ , by assuring real roots for this equation. To do this the equivalent damping ratio must be greater than 1.

$$\zeta_{EQ} = B_T / (J_{EQ}K_{EQ})^{1/2} > 1 \quad (8-2)$$

This is about the limit of sophistication that can be used without requiring assistance from a computer. This second order representation is a tool for estimating whether or not a proposed physical design of the torque

station and ARCT assembly is feasible before it is finalized and built. If the amount of confidence in the calculated stiffness is of concern, the value can be increased to provide additional assurance. If several sets of parts are to be assembled, it is necessary to use the largest part stiffness, or assume an infinite stiffness, and use only the RCC stiffness.

3. Create a fourth-order piecewise linear model for the parts and the control system, which, from equation 5.34 has a characteristic equation in the form

$$s^4 + C_1s^3 + C_2s^2 + C_3s + C_0 = 0 \quad (8-3)$$

The roots of this equation and the eigenvectors of the matrix representation of the model describe two modes-- the chain mode and the part mode. Of greatest interest is the former. The desired response for this system is to choose parameters to create a pair of real poles (underdamped) that correspond to the chain mode, and dominate a pair of underdamped poles that correspond to the part mode. The part mode should be of a frequency that is much higher than the chain mode for this to take place. The part mode is actually an artifact of the piecewise linear model but cannot be completely ignored. It does have some effect on the response since the non-linear simulation and actual data exhibit some dynamics that are superimposed on the overall overdamped response.

4. Perform a piecewise linear simulation of equations 5.30 to 5.33 using the chosen parameters. Make sure to include the rundown velocity of the torque station inertia as an initial condition. In the results, examine the overall trend of the transient response and ignore the high frequency dynamics.

5. Perform a non-linear simulation of equations 5.35-5.45 using the chosen parameters and a representation for the TVA curve based on experimental results. This simulation will show the transient response as well as overshoot in the part torque, if present. Of importance with this model is to examine not the exact value of any overshoot in part torque, but when it starts to occur as a function of the parameters used. The sensitivity to parameter

changes should be investigated. For example, an extreme sensitivity to variation in a control resistor of just a few ohms may indicate that the control circuit and gains should be modified.

6. If an encoder-based tachometer is to be used, determine a representation for its transfer function and determine the effect on the system. If there is a time constant involved with the tach, a good rule of thumb is to keep

$$\tau_f \ll \tau_m \quad (8-4)$$

where  $\tau_f$  is the tach time constant, and  $\tau_m$  is the mechanical time constant of the velocity controller.

7. If the motor, tach, and control circuit are available before the automation system is completed, perform torque watch windup and speed control tests, and compare the results to calculated values. Establish any dependence of stall torque on velocity feedback gain.

These steps have been presented as guidelines for the design of a torque control system for the threaded part mating process. They are geared to the precision assembly realm of automation, but are also general principles for any type of threaded part assembly.

Evaluation of these guidelines can only be made when they are applied to an actual design. It is recommended that they be used as a first attempt to provide a design methodology and be improved upon with use.

#### 8.4 Further recommendations

Chapter 7 presented a preliminary picture and analytical description for the addition of a mechanical torque sensor to the control system hardware. We suggest that this possibility be further investigated by building an in-line



or RCC-based torque sensor for the 1-30 in-oz range. It is recommended that torque feedback be used to complement current feedback and not to replace it. The torque sensor output should be used to fine tune the level of torque applied.

Considering the other tasks that an assembly cell must perform, the RCC-based implementation of a torque sensor appears to be the best choice. It allows indication of torque on both sides of the process. It also does not interfere with rundown. Since the stiffness of the RCC probably cannot be decreased, closing a torque feedback loop with its sensor output will require as much damping or more than current feedback alone.

Use of torque sensor feedback can improve the confidence in the torque level applied to the parts because losses between the sensor and one end of the process are removed. A final thought is the use of a torque sensor to provide remote calibration for the current feedback method. In this case the sensor output signal is only used to measure the performance of the current feedback method, and is not used in the control loop itself. This provides a sort of monitor for the controller-- an independent evaluation of the threaded part assembly process. Thus an on-line calibration of the control system can be performed. Reliability is increased by this fault-tolerant type of approach. This can also be thought of as a form of long-term feedback to provide information about the quality of the assembly that is being performed by an assembly cell.

## APPENDIX A

### HARDWARE MODELS

This appendix presents the models that are used to represent the hardware utilized in operation and control of the torque station. The information presented here can be found in other sources but the particular issues of modeling that affect control of threaded part mating are discussed. Transfer functions for DC permanent magnet motors, power amplifiers, and DC tachometers are provided. A discussion of the methods of representing friction is also included.

#### A.1 DC Permanent Magnet Motors

DC motors are made in many shapes and sizes, and have various architectures. This section considers only DC permanent magnet motors (DCPMM). The construction, method of input, and particular application of a DCPMM affect its nominal transfer function. This nominal function is only an ideal model and deviations from this model should be considered.

##### A.1.1 Motor Construction and Operation

The basic architecture of a DCPMM is shown in Figure A.1. The three basic parts numbered in the figure are:

1. Rotating armature containing circuits that carry current.
2. Permanent magnet field.
3. Commutator containing slip rings to switch current in the armature circuits.

The motor is just an electromagnetic device which uses the force generated by having an electric current pass through a magnetic field be applied with a lever arm to create a torque. This torque causes rotation of the armature. Because the magnetic field has stationary poles, the

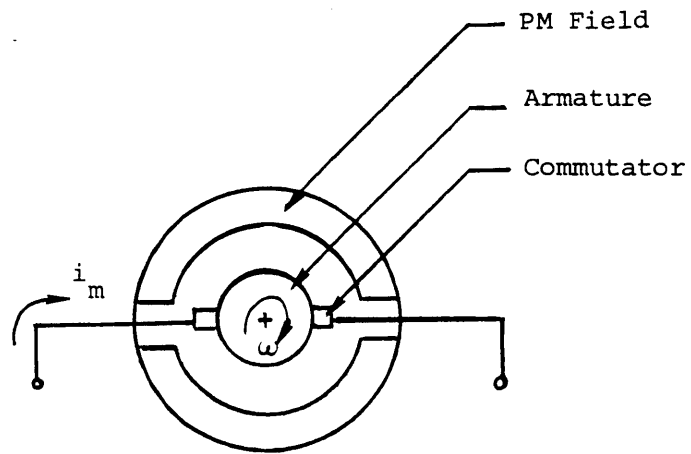


Figure A.1 DC PM Motor

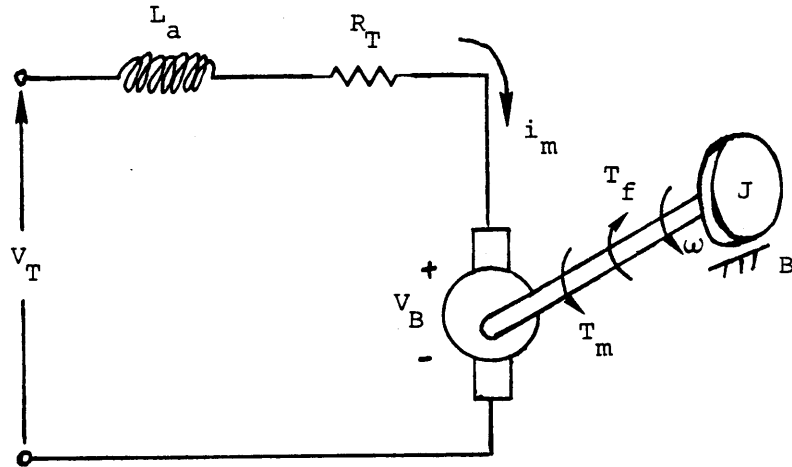


Figure A.2 Equivalent DC PM Motor Schematic

current in the armature must be continually switched to create proper orientation of the current to the magnetic field as the motor rotates. This switching is done by the mechanical slip rings, or brushes, of the commutator.

The armature is connected to a shaft held in bearings to maintain the necessary axial and radial alignment of the motor parts.

A DCPMM is a power transducer. It transforms electric power into mechanical power. It therefore has both electrical and mechanical connections. These connections determine its operation.

#### A.1.2 Model

A DCPMM is modeled as an ideal electromechanical transducer. Magnetic and thermal losses are ignored. Electrical losses are confined to power drops through resistances. Mechanical losses are lumped into coulomb friction and viscous damping. The nominal model of a DCPMM developed by Whipple<sup>[19]</sup> and others is derived from the equivalent electrical circuit, and lumped mechanical model of Figure A.2. The symbols used are defined in the List of Symbols.

The DC PM motor has the following transducer relationships

$$T_m = K_T i_m \quad (A-1)$$

$$V_B = K_B \omega_m \quad (A-2)$$

The torque generated is proportional to the current in the armature; and the voltage generated by passing an electrical conductor through a magnetic field is proportional to the angular velocity. The motor torque constant is  $K_T$  and the generator voltage constant is  $K_B$ . Using the lumped model of Figure A.2, equations are written for the electrical and mechanical "sides" of the motor.

The equivalent electric circuit of the armature is a series LR circuit with two voltage sources. One is the input voltage and the other is the back EMF generated by the motor. The latter has the polarity shown. The voltage of the armature circuit is

$$V_M = V_T - V_B \quad (A-3)$$

$$V_M = La \frac{di_m}{dt} + R_T i_m \quad (A-4)$$

Expressing Equation (A-4) in terms of its Laplace transform

$$V_M(s) = (La s + R_T) i_m(s) \quad (A-5)$$

$$i_m(s) = \frac{1/R_T}{\tau_e s + 1} \quad (A-6)$$

where  $\tau_e = La/R_T$ . This is the electrical time constant of the armature.

The steady-state relationship is

$$\frac{i_m}{V_M} = \frac{1}{R_T} \quad (A-7)$$

The equivalent mechanical side of the motor is a lumped inertia,  $J$ , with viscous damping,  $B$ , and friction torque,  $T_f$ . The quantities must include the values of the motor as well as anything connected to the output shaft. If gearing is employed, reflection through the gear ratio must be included. The friction includes that of the motor bearings and commutator brushes.

Summing torques on the total inertia

$$T_m - T_f - B\omega = J\dot{\omega} \quad (A-8)$$

$$\omega(s) = \frac{1}{Js + B} (T_m - T_f) \quad (A-9)$$

From Equations (A-1) through (A-9), the transfer function of the motor and load can be formulated. The transfer function depends on whether or not the voltage,  $V_T$ , or the current,  $i_m$ , is used as input to the motor.

i) Voltage Input

Combining the motor equations as shown in the block diagram of Figure A.3a, the transfer function is

$$\frac{\omega}{V_T} = \frac{K_T}{(L_a J)s^2 + (J R_T + B L_a)s + (B R_T + K_E K_T)} \quad (A-10)$$

The characteristic equation has two real poles for the parameters of all practical motors. In most cases, the natural or mechanical damping is quite small and the characteristic equation can be reduced to the form

$$(\tau_e s + 1)(\tau_m s + 1) = 0$$

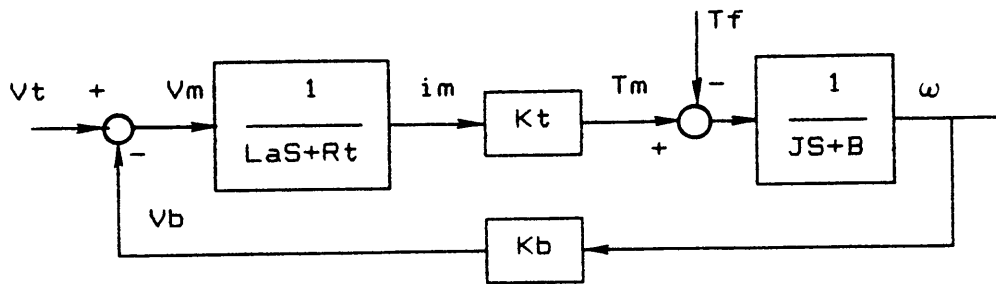
where

$$\tau_e = \frac{L_a}{R_t} \quad (A-11)$$

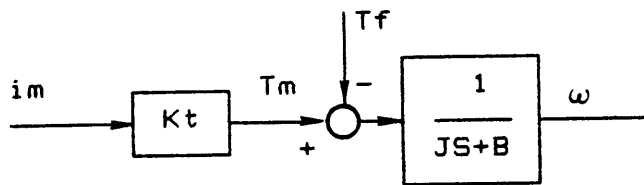
is the same electrical time constant as the LR armature circuit, and

$$\tau_m = \frac{R_t J}{K_B K_T} \quad (A-12)$$

is the mechanical time constant. Normally the electrical dynamics are much faster than the mechanical dynamics and can be neglected.



a) Voltage Input



b) Current Input

Figure A.3 DC Motor Transfer Functions

## ii) Current Input

When the electrical input to the motor is a current through the armature, the motor equations combine to form the block diagram in Figure A.3b. The transfer function becomes

$$\frac{\omega}{I_M} = \frac{K_T}{Js + B} \quad (A-13)$$

Note that the electrical dynamics are not present in this case. The time constants become

$$\tau_E = 0 \quad \tau_m = \frac{J}{B} \quad (A-14)$$

This implies that the source that provides the current can deliver an infinite voltage,  $V_T$ , when a step change in current occurs, and that the voltage can also overcome the back EMF in the motor. Obviously, this cannot happen. Consideration of the amplifier must be made in this case. Note also that the mechanical time constant depends only on mechanical quantities. If the damping is small, the time constant is large. Thus the motor is slowed down mechanically and sped up electrically compared to the voltage input.

Overall, the motor transfer function depends not only on the motor itself, but also on connections to its electrical and mechanical sides. It is only the "middle man" of the system's energy domains.

### A.1.3 Torque Output

The transfer functions shown do not address the friction torque of the motor and its effect on the torque output. In this thesis, this output is a controlled variable so anything that affects it must be considered. The effect of friction in the motor must be considered when it becomes a sizable percentage of the desired motor torque. The internal motor torque,  $T_m$ , is

$$T_m = K_T i_m$$



For any motion to occur in the motor,  $T_m$  must be greater than the friction torque,  $T_f$ . If  $T_L$  is defined as the output motor torque, then

$$T_L = T_M - T_f = K_T i_m - T_F \quad (A-15)$$

Figure A.4 shows a plot of  $T_m$  and  $T_L$  vs  $i_m$ .

This figure shows that a current is required before the motor can exert any net torque. This current is

$$i_s = T_f / K_t \quad (A-16)$$

A description of the net torque is therefore a linear relation, but with an offset added. This offset may or may not be constant. It may be a function of the motor position and velocity. Ways of representing the friction torque are presented in Appendix A.6.

#### A.1.4 Variations from the Ideal Model

The curve shown in Figure A.4 shows a perfectly linear relationship between  $i_m$  and  $T_m$ , or a constant  $K_T$ . This is the ideal case. To thoroughly investigate variations from the ideal requires electromagnetic analysis beyond the scope of this thesis. Briefly, variations in  $K_T$  and the motor torque can be caused by several factors. The two most important are: 1) cogging torque, and 2) ripple torque.<sup>[2,4,7,19]</sup>

Armature construction of DC PM motors often is done by wrapping conductors around an iron core to form the necessary circuits. This creates a finite number of magnetically polarized positions in the armature. Combining this with the fixed magnetic poles of the stator creates a finite number of preferred positions for the armature. When the armature is not in one of these positions, cogging torque results. At low speeds, this torque can cause a motor to "cog" around, hence the name. Cogging torque can be eliminated by certain methods of construction.

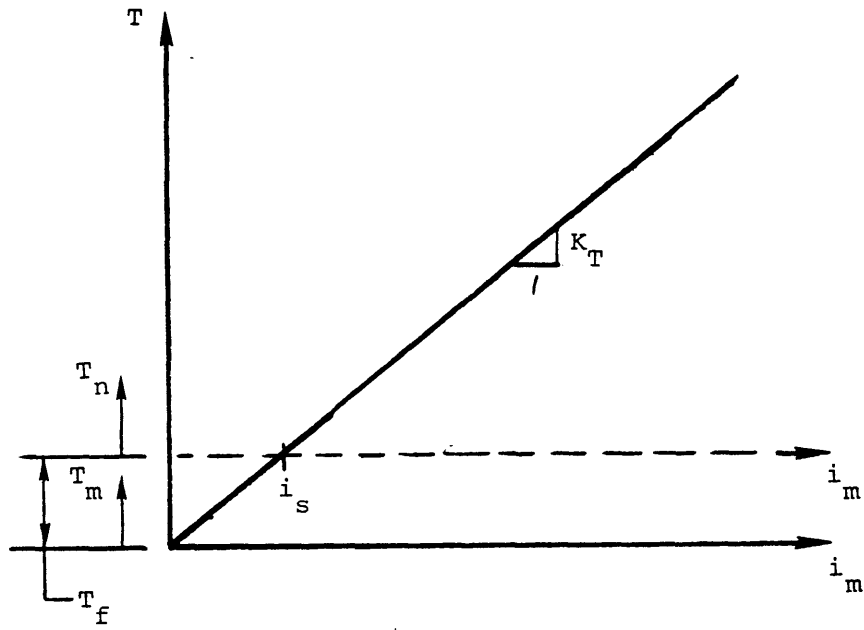


Figure A.4 Motor Torque vs Current

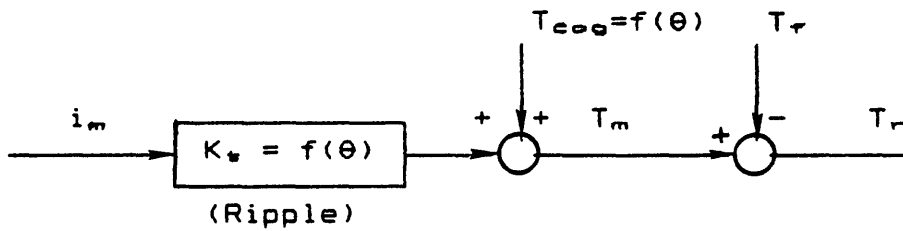


Figure A.5 Effect of Cogging and Ripple

Ripple torque is caused by magnetic variations in the motor and by commutation of the armature. It is a variation in the torque constant that is position dependent. Variations in the magnets cause change in  $K_T$  because of variations in magnetic field strength. Commutation causes variation in  $K_T$  because of the constant switching of current from one circuit to another. The action of the brushes causes small changes in resistance of the circuits at each commutator bar or switch. This effect is reduced by using a large number of commutations per revolution. Increasing the number decreases the magnitude of the variation and increases the frequency as a function of motor speed.

The effect of cogging and ripple on a system employing a motor is illustrated in Figure A.5. Torque ripple is a position-dependent variation in the torque constant or gain of the motor. It modulates the system gain as the motor is rotated and thus affects the frequency response and bandwidth. Cogging is a position-dependent torque disturbance that is summed with the motor torque. It adds to the effect of friction and load torques in the system.

Another modulation of the torque constant can be caused by variations in the temperature of the motor. Normally, increased temperature results in a lowering of the torque constant.

#### A.1.5 Choice of DC PM Motor Type

Motors of today perform much closer to the ideal model than they did 20 years ago. However, elimination of the causes of model deviations has created a series of specialized motors. These motors are optimized for specific types of uses. Choice of a motor is based upon this optimization.

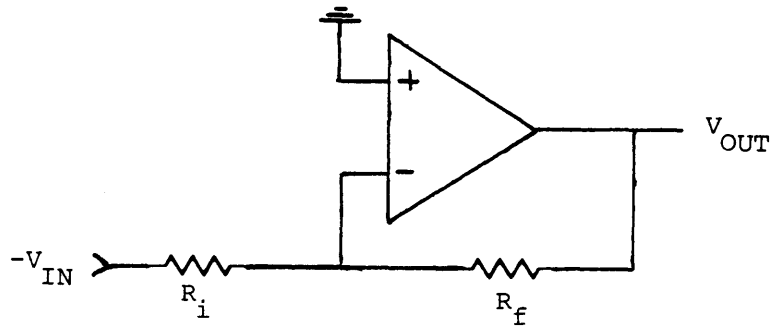
This research attempts to utilize a motor for precise current-to-torque conversion slow speed control, and electrical input as current rather than voltage. A high degree of precision is necessary. The chosen motor is a "printed circuit" DC PM motor. It has zero cogging torque because the armature has no iron in it. Its inductance is very low. This provides a fast electrical response and eases the burden of instantly changing current through the inductance. The precision of the magnetic elements of the motor and a large number of commutations reduce the ripple variation in  $K_T$  to less than 3%. The commutation does cause a friction torque that is not negligible for precision threaded part assembly, though.

A new type of motor is becoming available for practical use called a brushless DC PM motor. In this motor the permanent magnets are placed in the rotor and the armature circuits in the stator. The mechanical commutation of current is replaced by a combination of position sensors and electronic switches. The obvious advantage is the elimination of the commutator brushes which are a troublesome source of friction and electrical noise. For a clean room environment, the benefit is less debris generated. The motors are often sold in pieces so that the motor can be directly mounted into a system and its bearings. The motor suffers from nonlinearity in the torque constant. To achieve high linearity, brush-type motors use a large number of armature circuits and therefore many commutations. For brushless motors to do this, a large number of position sensors must be crammed into the circumference of the motor. Current technology limits this number. However, as time progresses, this may be the universal motor of choice.

## A.2 Power Operational Amplifiers

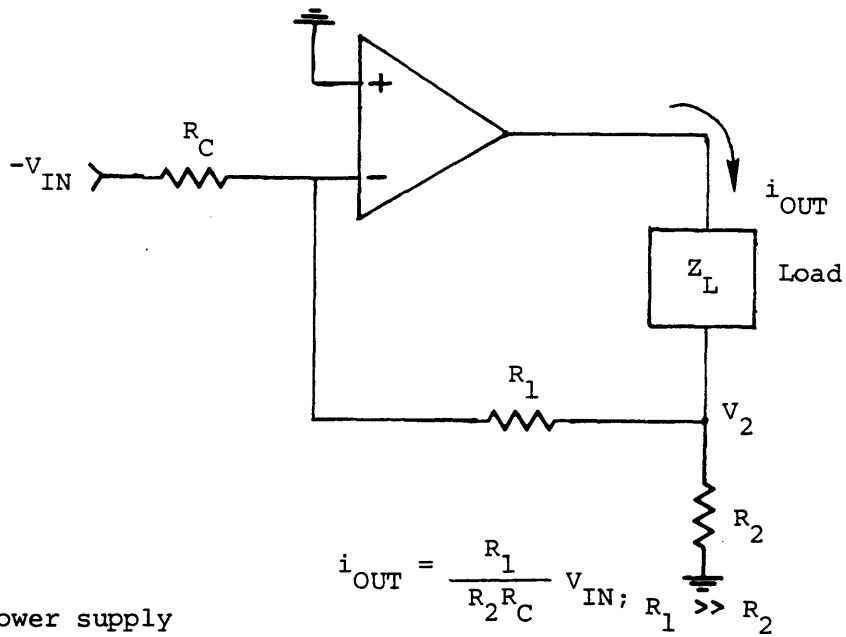
To provide electrical input to a DC PM motor, amplification of the power of the command signal is necessary. This section describes the configurations that can be used with a power operational amplifier to achieve this amplification. This research utilized a single component amplifier in the control circuitry. Often more complicated servo amplifiers are used which result in a transfer function which is closer to the ideal model that is presented here.

A power operational amplifier is identical to a common instrumentation amplifier except that it has significantly higher output current and power capabilities. Since it is an op amp it can be used to sum signals, and output a current or voltage. The amp can be used in the two configurations shown in Figure A.6. Additional inputs can be added to these configurations for summing operations. The transfer functions are also illustrated in the figure.



$$V_{OUT} = \frac{R_f}{R_i} V_{IN}$$

a) Voltage Output



$$i_{OUT} = \frac{R_1}{R_2 R_C} V_{IN}; R_1 \gg R_2$$

Note: Amp power supply not shown.

b) Current Output

Figure A.6 Operational Amplifier Configurations

For voltage output

$$\frac{V_{OUT}}{V_{IN}} = \frac{R_f}{R_i} = G_V \quad (A-17)$$

For current output

$$\frac{i_{OUT}}{V_{IN}} = \frac{R_1}{R_2 R_C} = G_A$$

$$R_1 \gg R_2 \quad (A-18)$$

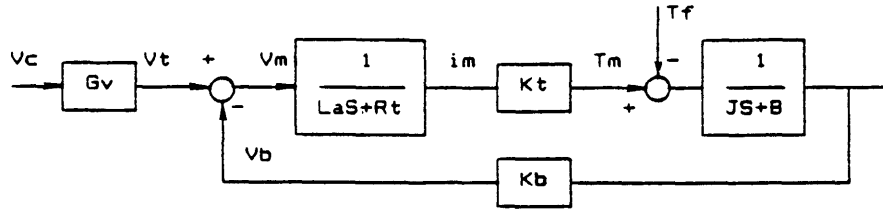
### A.3 Motor/Amp Interaction

This section examines the use of a generalized power operational amplifier to drive the electrical side of a DC motor. Separate transfer functions have been presented for motors and amplifiers with no real mention of the effect of one upon the other. Closer analysis of the two elements shows that they must be analyzed together [17]. This is especially true in the case of a current amplifier driven motor.

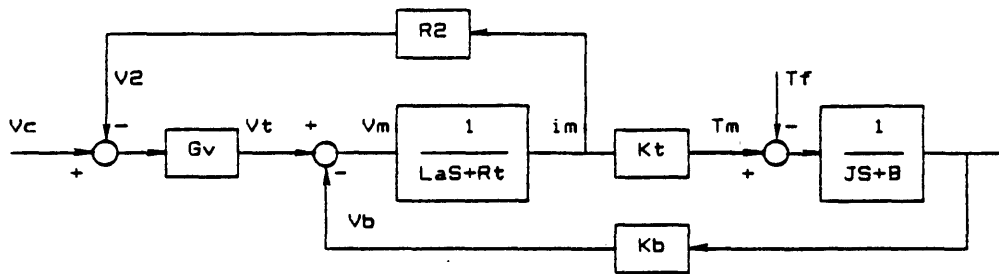
When it is desired to control the input voltage to the motor, the voltage output configuration of Figure A.6a is used. Figure A.7a shows the combined motor/amp block diagram. The overall steady-state loop gain becomes  $G_V K_T / (B R_T + K_B K_T)$ . The system poles remain the same. For practical motors, they are

$$s_1 = -\frac{1}{\tau_e} = -\frac{R_t}{L_a} \quad (A-19)$$

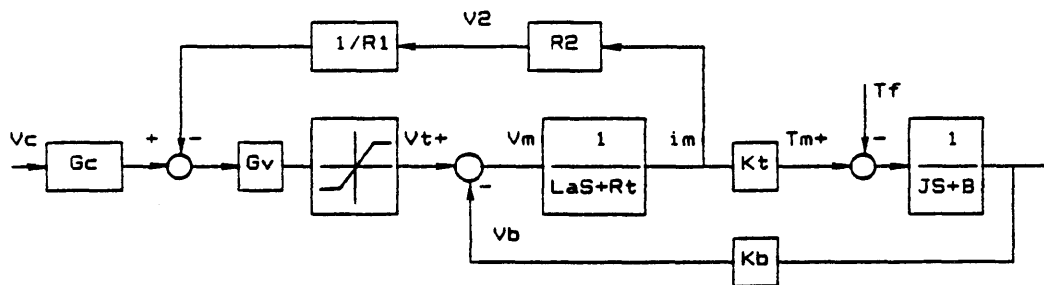
$$s_2 = -\frac{1}{\tau_m} = -\frac{K_B K_T}{J R_t} \quad (A-20)$$



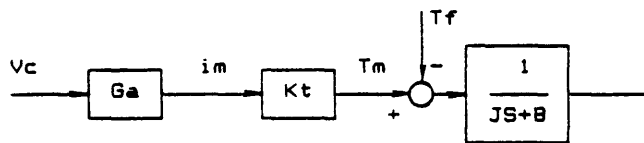
a) Voltage Motor/Amp Control



b) Voltage Control with Current Feedback



c) Current Motor/Amp Control



d) Reduced current control diagram

Figure A.7 DC Motor/Amplifier Configurations

In this configuration, the interaction is confined to the amplifier's capability to supply the necessary current and voltage. No dynamics of the amp itself are shown. In reality, there is a time constant associated with the amp response. For available amplifiers, this is normally in the microsecond range -- much faster than the motor time constants. Voltage control is the most commonly used motor/amp configuration and is the reason why the elements are normally modeled independently.

A variation on the voltage control configuration is shown in Figure A.7b. In this case, the magnitude of the motor current is tapped with a small resistor to ground and provides a voltage to alter the system dynamics. The new transfer function becomes

$$\frac{\omega}{V_c} = \frac{G_V K_T}{(LaJ)s^2 + (JR_t + BLa + JG_V R_2)s + (BG_V R_2 + K_T K_B)} \quad (A-21)$$

Comparing this result with Equation (A-10), it is seen that the characteristic equation and system poles are changed. For the same case of low damping, the poles of Equations (A-19) and (A-20) become

$$S_1' = S_1 (1 + \beta) \quad (A-22)$$

$$S_2' = \frac{S_2}{1 + \beta} \quad (A-23)$$

where  $\beta = (G_V R_2)/R_t$ .

The effect is to move the poles farther apart. The electrical dynamics become faster, and the mechanical time constant becomes slower.  $R_t$  remains fixed in the motor and  $R_2$  must remain small to minimize its loading on the circuit. Therefore  $G_V$  is used to regulate the feedback effect.

A special use of voltage control with current feedback is pure current control. When the current feedback gain,  $\beta \rightarrow \infty$ , the current in the motor is controlled instead of the input voltage. Figure A.7c shows the summing of  $V_c$  and  $V_2$  modified to change their relative gain. Also shown is a saturation element at the output of the amplifier. Since infinite voltage gain implies



infinite output voltage, this must be considered.

The model of Figure A.7c can be reduced to that of Figure A.7d to show proportional current control by neglecting the saturation effect, and by imposing the restriction  $R_1 \gg R_2$  and  $R_C \gg R_2$ . The transfer function becomes

$$\frac{\omega}{V_C} = \frac{G_A K_T}{J s + B} \quad (\text{A-24})$$

where  $G_A$  remains unchanged from Equation (A-18). The poles are identical to Equation (A-14).

Neglecting the saturation is largely dependent on the rate of change in motor current that is desired. If the saturation voltage of the amp is  $V_{MAX}$ , then the maximum rate of change in current is

$$\left. \frac{di}{dt} \right|_{\max} = \frac{1}{L_a} [V_{MAX} - (R_t + R_2)i - V_B] \quad (\text{A-25})$$

The  $R_{2i}$  term is included because the motor is not directly grounded. For small velocities or stall,  $V_B$  can be ignored. Equation (A-25) points out that a motor with low inductance should be used with current feedback in order to maximize the response capability of the amplifier.

The basis for torque control of a motor by current feedback is this specialized case of voltage control with current feedback. The voltage  $V_2$  is directly proportional to the torque of the motor. It is important to remember the need to consider the amp as well as the motor for this implementation. How the implementation works out in the actual application of threaded part mating is the basis for the analytical and experimental efforts of this thesis discussed in Chapter 5.

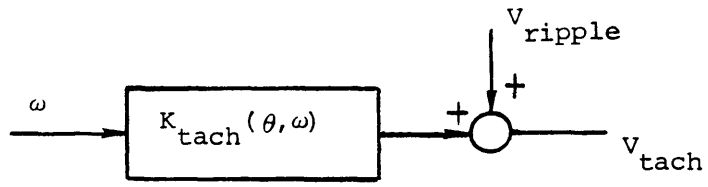
#### A.4 DC PM Tachometers

A DC PM tachometer is essentially a motor reversed in function to provide the back EMF as the output, and angular velocity as input. Many considerations in modeling and implementation of the device are similar to those of a motor. The tachometer is used to provide a feedback signal in the form of a voltage. The ideal transfer function is

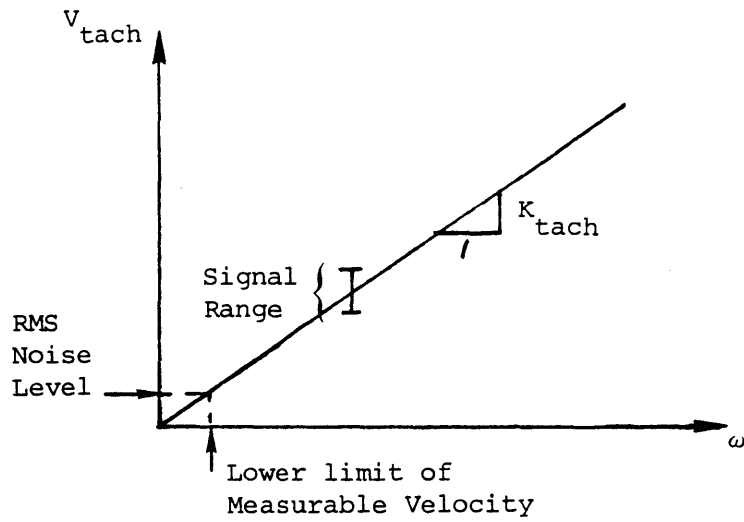
$$\frac{V_{TACH}}{\omega} = K_{TACH} \quad (A-26)$$

The tachometer also has characteristics that make its output deviate from its ideal model. Its output has a component of ripple similar to that of the motor torque. This is due to brush noise, commutation, and magnetic imperfections. It is manifested in the tach model both as a modulation in the gain and as an additive disturbance, or noise, in the output signal. This is shown in Figure A.8a. At a given velocity, the output signal may vary within a range about the nominal value. This is exaggerated in Figure A.8b.

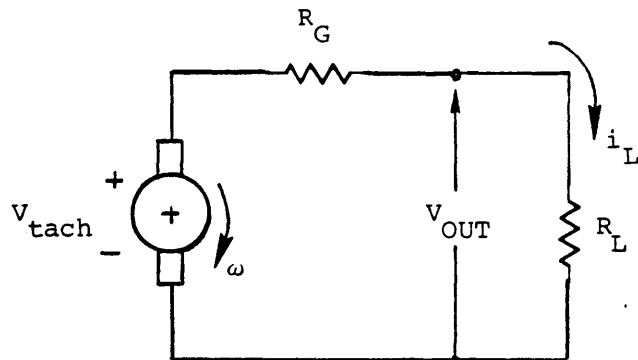
Since the voltage output is proportional to the input velocity, it decreases in value as the speed decreases. However, the magnitude of the noise level does not, and may even increase near zero velocity. Thus there exists a lower limit on velocity that is distinguishable from noise. If the output of the tach is used in a high gain servo loop this may be of



a) Block Diagram



b) Tach voltage vs velocity



c) Output and Load Impedance

Figure A.8 DC Tachometer Characteristics

concern. Compensation of this problem by filtering may only be successful if the filtering dynamics are much faster than those of the closed loop system.

Figure A.8c shows an equivalent electric circuit for the tachometer output. The tach signal is normally measured or utilized by a device with a certain impedance. The magnitude of this impedance would not be of concern if the tach did not have its own output impedance. If the voltages around the circuit in the figure are summed

$$V_{TACH} = K_{TACH}\omega = R_G i_L + R_L i_L \quad (A-27)$$

where the resistances are those of the tach and load, respectively. Solving for the actual output voltage

$$V_{OUT} = \frac{R_L}{R_G + R_L} K_{TACH}\omega \quad (A-28)$$

Therefore the effective generator constant becomes

$$K_{eff} = \frac{R_L}{R_G + R_L} K_{TACH} \quad (A-29)$$

If  $R_L \gg R_G$ , then  $K_{eff} = K_{TACH}$ . If this is not the case then the effect of the tach output impedance must be considered.

A possible solution to the small signal at low velocity problem would seem to be choosing a tach with a larger generator constant. However, tachometers with larger generator constants are also physically larger and thus have greater output impedance and brush friction. The friction is undesirable. A larger signal only results if the load impedance is increased accordingly. Often this isn't possible.

#### A.5 Friction Modeling

Precision threaded part mating requires high accuracy in the torque delivered to the parts. A source of contamination to the magnitude of the applied torque is friction. Friction acts as a disturbance torque on a system. Its effects are not easily included in linear transfer function

form. The classical model of coulomb friction is a constant torque which always acts in a direction that opposes motion. It is described by

$$T_f = |T_f| \operatorname{sgn}(\omega) \quad (\text{A-30})$$

where

$$\operatorname{sgn}(\omega) = \begin{cases} 1 & \omega > 0 \\ 0 & \omega = 0 \\ -1 & \omega < 0 \end{cases}$$

Equation (A-30) is represented in block diagram form as shown in Figure A.9. If the velocity is known to only occur in one direction, then friction acts as a constant disturbance, but its direction must be reversed with sign changes in velocity.

The classical model has its limitations. The most obvious is the assumption that the magnitude of the friction does not change with velocity. It is known that starting friction, that present at zero or small velocities, is normally greater than running friction, that present at larger velocities. A typical figure used is  $T_{st} = 2T_f$  where the starting function is  $T_{st}$  and the sliding friction  $T_{sl}$ . A more subtle point is that the friction torque is only as large as the net torque applied to an inertia at rest. For example, if the starting friction is 1 in.-oz and 0.5 in.-oz is applied to a stationary inertia, then the friction torque is only 0.5 in.-oz. Raibert and Craig [13] have adopted a compact notation to describe this

$$T_f = \begin{cases} \operatorname{sgn}(\omega) \cdot \min[T_{st}, T_{\text{applied}}] & \text{for small } \omega \\ \operatorname{sgn}(\omega) \cdot T_{sl} & \text{otherwise} \end{cases} \quad (\text{A-31})$$

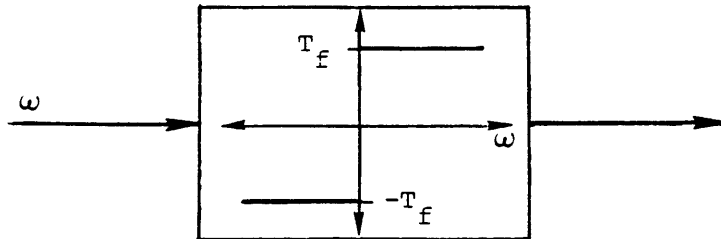


Figure A.9 Coulomb Friction Element

In modeling and simulation, friction is often ignored. It is just considered an unmodeled disturbance and controllers are designed to account for it. For low speed torque control, this may not be the case. This thesis attempts to control the net torque of a DC motor with friction and must include the friction in system modeling and calibration. In the design of a torque sensor the effect is also critical.

## APPENDIX B

### OPTICAL ENCODER-BASED VELOCITY SIGNAL GENERATION

This appendix presents the method used by this research to generate an angular velocity signal from the output of an incremental optical encoder. Velocity signals can be used for many purposes including feedback of the controlled variable in speed control loops, added damping in position and torque control loops, and collection of velocity data. Choice of a device to generate the required signal depends upon how it is to be used, and what type of hardware is available to interface with it.

#### B.1 Objectives

Use of a velocity signal in the control of the threaded part mating process considered in this thesis requires a method of generating the signal that satisfies several objectives. They are:

1. Good low speed performance (1-30 rpm).
2. Zero output signal at zero speed.
3. Highest gain possible without compromising performance.
4. Small size, clean room compatible.

Note that the objectives do not include a requirement for exact speed control. During rundown the speed should be reasonably constant. What is most important is the average level. Variations of  $\pm 10\%$  of nominal are acceptable. For example, if the desired speed was 10 rpm, a level of 9-10 rpm would suffice, but not 90-100 rpm. The average speed during rundown indicates the level of damping which is important to the tightening phase dynamics.

## B.2 Incremental Optical Encoders

Briefly, an incremental optical encoder is a digital position sensing device. It has a rotating disk which is attached to a shaft when the device is installed in a system. Normally, there are two rows of slots around the circumference of the disk. Two optical sensors are focused on the slots and are positioned one-half slot width apart. When a slot passes by the sensor, light shining through the slot from a source on the opposite side of the disk activates the sensor output. The two sensors are normally referred to as channels A and B. Due to the offset in sensor positions, the output of channel B is 90 degrees out of phase with channel A. Channel A leads B in one direction of rotation and B leads A in the opposite direction.

The sensor outputs can either be in a square wave quadrature form, or in a sinusoidal wave form. The latter is similar to the output of a resolver. This discussion only considers the first form of output.

The frequency of cycles in the output is proportional to the angular velocity of the shaft rotation. The number of cycles indicates the amount of angular travel. An encoder with N "counts" per revolution can detect an angular change of  $360/N$  degrees of rotation. The number of slots, N, also effects the resolution of angular velocity that can be detected. A larger value of N creates a greater number of transitions in the output per unit time.

## B.3 Methods of Velocity Signal Generation

A position signal is derived from an encoder output by counting the number of transitions of the output channels. This count is directly proportional to the change in angular position. Direction information is obtained by keeping track of whether A is leading B or vice-versa. The resolution can also be increased by a factor of 4 since there are actually 4 transitions per count of the output. Each channel of the quadrature square wave has both an UP and DOWN transition, and all 4 transitions occur at different times.



Deriving a velocity signal from an encoder output is more complicated. There are several ways to accomplish the task [14]. Choice of the method depends on the purpose for which the generated signal is to be used, and the hardware that is available. Each is essentially a variation of measuring the frequency or the period of the transitions of the encoder output. The methods are:

1. Count the number of encoder counts in a given time period. This number is proportional to the velocity.
2. Measure the period between the counts. This value is inversely proportional to the velocity. The measurement can be done with an analog integrator, or by digitally counting the number of high speed clock pulses between the encoder counts to form a "digital integrator".
3. Generate a pulse train of known pulse width and magnitude as the output of a one-shot, or monostable device, whose firing is controlled by the frequency of the encoder counts. Low pass filter the pulse train to form an analog signal whose average value is proportional to the angular velocity.
4. Implement a digital control system and create an observer for the velocity state using a digital filter on the value of the position signal at each update rate.

#### B.4 Low Pass Filtering of a Pulse Train Method

The third method mentioned above was implemented for use in this research. It is perhaps the simplest method and a "first-order" approach compared to the others. However, the encoder is basically a digital device, and the best methods of converting its position information to velocity information require digital signal processing hardware. The controller used in the torque station is entirely analog except for the command generation. Therefore, the chosen method is easily interfaced with the control circuit, and requires no major change in the control strategy.

Figure B.1 shows the method in schematic form. The input to the encoder is a shaft rotation and the output is a quadrature square wave. A digital logic circuit operates on this output to determine when a transition occurs, and keeps track of direction. In this figure, A is

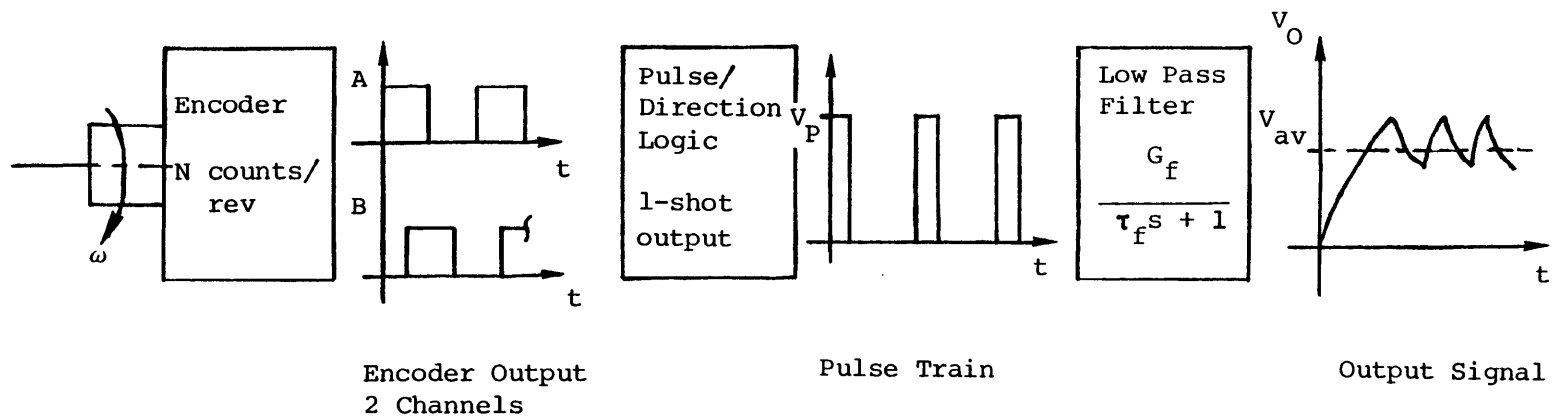


Figure B.1 Low Pass Filtering of a Pulse Train Method

leading B, and this is considered a positive velocity. The output of the digital logic circuit is two UP or DOWN counts per encoder cycle. These directions correspond to positive and negative velocity. The UP and DOWN counts are generated as pulses by a "one-shot" device, and are of a prescribed magnitude and width. The polarity depends on the direction of the input velocity. The pulses can be used to drive up/down counters for position information. They are utilized by this velocity signal generation method as the input to a low-pass filter.

The filter used in this implementation was first-order with time constant,  $T_f$ , and also had a DC gain,  $G_f$ . The output signal shown in Figure B.1 is the result of filtering the pulse train with a low pass filter. At startup, there is an initial transient with a time constant which is due to the filter. If the velocity is constant, the steady-state output signal is as shown in the figure. There is a rise and fall of the output during and between the one-shot pulses, respectively. Figure B.2 shows an enlarged view of this rise and fall. The signal rises during an input pulse, and then decays until the next pulse arrives. For a steady-state speed the result is the rise and fall of the output voltage,  $V_o$ , about some average level. The magnitude of this "ripple" is determined by the angular velocity, and width and magnitude of the one-shot pulses. In Figure B.1, the startup transient is shown without ripple to illustrate the dependence on  $T_f$ . It can include a ripple also.

The period between one-shot pulses is

$$t_p = \frac{60}{2N\omega} \quad (\text{sec, rpm}) \quad (\text{B-1})$$

A pulse width,  $t_w$ , for the pulses is chosen based on Equation (B-1). For  $\omega = 0$ ,  $t_p = \infty$ , and  $V_o = V_{AV} = 0$ . For  $t_p \leq t_w$ , a new pulse comes before the previous one is finished and the one-shot is saturated at the pulse magnitude,  $V_p$ . Thus the maximum velocity before saturation is

$$\omega_{\max} = \frac{60}{2Nt_w} \quad (\text{B-2})$$

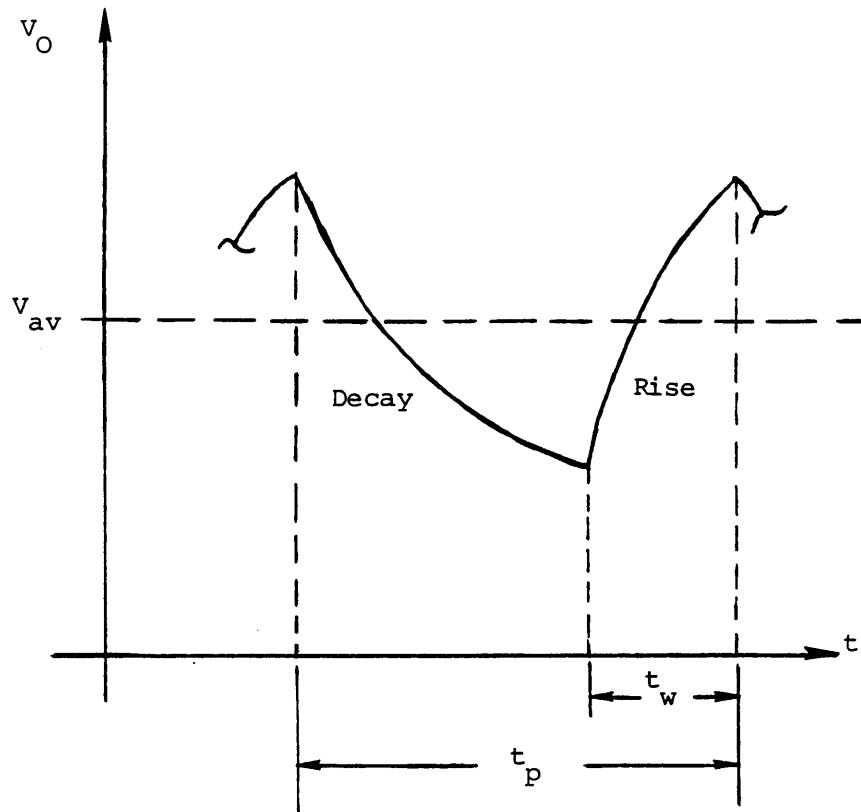


Figure B.2 Rise and Decay of Filter Output

Therefore the pulse width must be chosen based on the maximum desired velocity. The encoder used for this research has a resolution of  $N = 1024$  counts/rev. So for  $t_w = 1$  msec,  $\omega_{\max} = 29.3$  rpm, for  $t_w = 0.1$  msec,  $\omega_{\max} = 293$  rpm, and so on.

The average value of the filter is proportional to the ratio of the pulse width and pulse period, or the duty cycle of the pulse train. In general

$$\begin{aligned}
 V_{av} &= \frac{t_w}{t_p} V_p G_f \\
 &= \frac{2Nt_w V_p G_f}{60} \omega
 \end{aligned}
 \tag{B-3}$$

The average output signal is proportional to the velocity. Thus the "gain" of the signal can be adjusted using the gain of the low pass filter. However, this also increases the magnitude of the ripple.

The output voltage,  $V_o$ , is utilized as an analog signal for velocity feedback in this implementation. The signal can be smoothed by increasing the value of  $T_f$  but this can result in a detrimental effect on the control system. Some filtering is needed especially for  $t_w \ll t_p$ , or small velocities with respect to the chosen maximum.

The use of this implementation of deriving a velocity signal from an optical encoder in the torque station control circuit is presented in Chapter 6. The effect of the ripple in the output voltage on the velocity controller is experimentally determined as well as the effect of the pulse filter time constant.

## LIST OF REFERENCES

- [1] Blaer, I.E., "Reliable Automatic Starting of Threaded Parts," Russian Engineering Journal, Vol. 42 No. 12, 1962.
- [2] DC Motors, Speed Controls, Servo Systems, 5th ed., Engineering Handbook, Electrocraft Corp., 1980.
- [3] Dean, D.L., Jr., "Design of a Robotic End-Effector for Automated Bolting," Master's Thesis, MIT Department of Mechanical Engineering, 1985.
- [4] Direct Drive DC Motors, Inland Motor Specialty Products Corp., April 1982.
- [5] Drake, S.H., "Using Compliance in Lieu of Sensory Feedback for Automatic Assembly," Doctor of Science Thesis, MIT Department of Mechanical Engineering, 1977.
- [6] Hartley, J., Robots at Work, IFS (Publications) Ltd., UK, 1983.
- [7] Jacobs, S.R., and H.O. Tyler, "Sensitivity Analysis of a Rate Control System Applied to a Centrifuge," Motion, Vol. 1 No. 2, Third Qtr. 1985.
- [8] Kondoleon, A.S., "Screw Cross Threading," C.S. Draper Laboratory Internal Memo MAT-368, Feb. 1976.
- [9] Koren, Y., Robotics for Engineers, McGraw-Hill, 1985.
- [10] Luh, J.Y.S., W.D. Fisher, and R.P.C. Paul, "Joint Torque Control by Direct Feedback for Industrial Robots," IEEE Trans. on Automatic Control, Vol. AC-28, No. 2, Feb. 1983.
- [11] Mason, M.T., "Compliance and Force Control for Computer Controlled Manipulators," IEEE Trans. on Systems, Man, and Cybernetics, Vol. SMC-11, No. 6, June 1981.
- [12] Nevins, J.L., and D.E. Whitney, "Computer-Controlled Assembly," Scientific American, Vol. 238, No. 2, Feb. 1978.
- [13] Raibert, M.H., and J.J. Craig, "Hybrid Position/Force Control of Manipulators," Trans. of ASME J. of Systems, Measurement, and Control, Vol. 102, June 1981.

- [14] Rangan, K.V., "Position and Velocity Measurement Using Optical Shaft Encoders," The Robotics Institute, Carnegie-Mellon Univ. Report No. CMU-RI-TR-82-8, June 1982.
- [15] Rourke, J.M., and D.S. Seltzer, "Precision Automated Assembly in a Clean Room Environment," C.S. Draper Laboratory Report No. P-2622, Oct. 1985.
- [16] Simons, J., and H. Van Brussel, "Force Control Schemes For Robot Assembly," Robotic Assembly, K. Rathmill, Ed., IFS (Publications) Ltd., UK, 1985.
- [17] Tal, J., "The Effect of Amplifiers on Control Systems," Servo Trends, Vol. II, No. 1, Galil Motion Control, Inc., Jan. 1986.
- [18] Treer, K.R., "Tensioning Threaded Fasteners," Automated Assembly, SME, 1979.
- [19] Whipple, D.G., "Direct Drive DC Torquers with Permanent-Magnet-Field Excitation," MIT Instrumentation Laboratory (C.S. Draper Laboratory) Report No. E-667, Oct. 1957.
- [20] Whitney, D.E., and J.L. Nevins, "What is the Remote Center Compliance (RCC) and What Can It Do?," C.S. Draper Laboratory Report No. P-728, Nov. 1978.